SUMO-mediated protein homeostasis in Candida glabrata

Thesis submitted for the degree of **Doctor of Philosophy**

work carried out by

Dipika Gupta Reg.no.18LBPH01

under the supervision of

Prof. Krishnaveni Mishra



DEPARTMENT OF BIOCHEMISTRY
SCHOOL OF LIFE SCIENCES
UNIVERSITY OF HYDERABAD
HYDERABAD – 500 046
INDIA



UNIVERSITY OF HYDERABAD SCHOOL OF LIFE SCIENCES DEPARTMENT OF BIOCHEMISTRY

DECLARATION

I, Dipika Gupta, hereby declare that this thesis entitled "SUMO-mediated protein homeostasis in Candida glabrata" submitted by me under the guidance and supervision of Prof. Krishnaveni Mishra, is an original and independent piece of research work. I also declare that it has not been submitted previously in part or in full to this University or any other University or Institution for the award of any degree or diploma.

Date: 16/4/24

Name: Dipika Gupta

Reg. No. 18LBPH01

Dipika huffa Signature of the student



CERTIFICATE

This is to certify that the thesis entitled "SUMO-mediated protein homeostasis in Candida glabrata" submitted by Dipika Gupta bearing registration number 18LBPH01 in partial fulfilment of the requirements for award of Doctor of Philosophy in the School of Life Sciences is a bonafide work carried out by her under my supervision and guidance.

The thesis is free from plagiarism and has not been submitted previously in part or in full to this or any other University or Institution for the award of any degree or diploma.

The student has following publications prior to submission:

Gupta, D.; Garapati, H. S.; Kakumanu, A. V. S.; Shukla, R.; Mishra, K. SUMOylation in Fungi: A Potential Target for Intervention. Comput Struct Biotechnol J 2020, 18, 3484–3493. https://doi.org/10.1016/j.csbj.2020.10.037.

Part of this work has been presented in the following conferences:

- "EMBO Workshop-Protein quality control: From molecular mechanisms to therapeutic intervention", May 2023, Srebreno-Dubrovnik, Croatia, Europe.
- "Yeast India-2023", March 2023, IISER, Mohali, India.
- "18th National Research Scholar's Meet (NSRM-2022)", December 2022, ACTREC, Tata Memorial Centre, Navi Mumbai, India (Best Poster Award).
- "International Conference on Frontier Areas of Science and Technology (ICFAST-2022)", September 2022, University of Hyderabad (UoH), Hyderabad, India (Best Poster Award).
- "Hy-Sci 2022", May 2022, Centre for DNA Fingerprinting and Diagnostics (CDFD), Hyderabad, India.

Further the student has passed the following courses towards fulfilment of coursework requirement for Ph.D.

Course code	Name	Credits	Pass/Fail
S801	Research Methodology/ Analytical Techniques	4	Pass
S802	Research Ethics, Biosafety, Data Analysis	4	Pass
S803	Research Proposal and Scientific Writing	4	Pass

Prof. KRISHNAVENI MISHRA Department of Biochemistry School of Life Sciences University of Hyderabad Hyderabad-500046. (TS), INDIA

SV. Naun 13-Head of the Department जीवरसायनविभाग / Department of Biochemistry

जीवविज्ञान राकाय / School of Life Sciences

हैदराबाद / Hyderabad-500046. INDIA

Dean of the School

संकाय अध्यक्ष / Dean जावावज्ञान सकाव / School of Life Sciences हैदराबाद विश्वदिद्यालय / University of Hyderabad जीव विज्ञान संकाय / School of Life Sciences हैदराबाद विश्वविद्यालय / University of Hyderabad हैदराबाद / Hyderabad-500 046.

SI No. 2522 Notification No. 1

हैदराबाद विश्वविद्यालय

UNIVERSITY OF HYDERABAD

(A Central University Established by an Act of Parliament)

P.O. CENTRAL UNIVERSITY, GACHIBOWLI, HYDERABAD - 500 046 (INDIA)

SEMESTER GRADE TRANSCRIPT

REGULAR EXAMINATION

REG. NO. 18LBPH01

NAME OF THE STUDENT DIPIKA GUPTA

MONTH AND YEAR OF NOV 2018 SEMESTER 1

COURSE Ph.D. BIOCHEMISTRY

PARENT'S NAME NULL / NULL

COURSE NO	TITLE OF THE COURSE	CREDITS	RESULTS
S801	RESEARCH METHODOLOGY/ ANALYTICAL TECHNIQUES	4	PASS
S802	RESEARCH ETHICS, BIOSAFETY, DATA ANALYSIS	4	PASS
S803	RESEARCH PROPOSAL AND SCIENTIFIC WRITING	4	PASS

SEMESTER GRADE POINT AVERAGE (SGPA):10.0

(In words) :TEN POINT ZERO

DEPUTY REGISTRAR (ACAD & EXAMS)

Date Of Result Notification : Jan 5, 2019

Date Of Download: Mar 7, 2024

This is system generated certificate issued by O/o The Controller of Examinations, University of Hyderabad

CONTENTS

	Page No
Acknowledgement	9
List of Abbreviations used	11
List of Figures	17
List of Tables	19
Chapter 1 Introduction	20-35
1.1 The burden of fungal infections	20
1.2 Antifungal drug resistance	21
1.3 Candida glabrata	23
1.4 SUMOYLATION: A POTENTIAL ANTIFUNGAL TARGET	25
1.4.1 Mechanism of SUMO conjugation	26
1.4.2 Mono- and polySUMOylation	27
1.4.3 SUMOylation motif	28
1.4.4 SUMO Interacting Motifs (SIM)	29
1.4.5 SUMO deconjugating enzymes	30
1.4.6 SUMOylation in pathogenic fungi	31
1.4.7 SUMO-dependent Ubiquitination mediated protein degradation	34
1.5 Specific objectives of the current study	34
Chapter 2 Materials and Methods	36-55
2.1 Molecular biology methods	36
2.1.1. Polymerase Chain Reaction	36
2.1.2. Molecular cloning	37
2.1.2.1. Ultracompetent cells preparation	37
2.1.2.2. DNA transformation into bacterial cells	37
2.1.2.3. Plasmid isolation	38
2.1.2.4. Screening of the clones by restriction digestion	38

2.1.3. Site-directed mutagenesis	39
2.1.4. cDNA synthesis and Quantitative Real-Time PCR	39
2.2 Yeast growth and mutant strain generation	40
2.2.1. Genomic DNA isolation	40
2.2.2. Yeast transformation	41
2.2.3. Gene disruption in C. glabrata strains	42
2.2.4. Plate-based growth assay	43
2.2.5. Biofilm formation	43
2.2.6. Yeast two-hybrid screen	43
2.3 Protein and related biochemical techniques	44
2.3.1. Whole cell protein extract from yeast cells by Trichloroacetic acid	44
2.3.2. SDS-PAGE and Western blot	44
2.3.3. Quantification of the western blot	45
2.3.4. Protein expression and purification	45
2.3.5. Invitro pull-down assay	47
2.3.6. CgUlp2 binding assay	47
2.3.7. CgUlp2 protease activity	47
2.3.8. Pull down of SUMOylated proteins	48
2.4. Cell culture	49
2.4.1. Preparation of THP-1 Macrophage monolayer	49
2.4.2. Infection of C. glabrata in THP-1 cells	50
2.5 Tandem mass tag (TMT)-based quantitative total proteomics analysis	50
2.5.1. Sample preparation	50
2.5.2. TMT labeling and mass spectrometry	51
2.5.3. Analysis of gene ontology	51
2.6 Imaging mitochondria in C. glabrata cells by confocal microscopy	52
2.7 Computer-aided drug design	52

2.7.1 Homology modeling	52
2.7.2 Protein-protein docking	53
2.7.3 Determination of active site on the protein	53
2.7.4 Pharmacophore mapping and virtual screening for ligands	53
2.7.5 Protein-ligand docking	54
2.7.6 Binding energy calculations	54
2.7.7 Molecular dynamic simulation	54
2.8 Statistics	55
Chapter 3 Perturbation of SUMOylation affect the homeostasis of proteins essen	tial for the
establishment of successful infection	56-75
3.1 Introduction	56
3.2 Results	57
Identification of SUMO-targeted ubiquitin ligases in Candida glabrata	57
STUbLs in the physiology and pathology of Candida glabrata	61
STUbLs are essential for the survival of <i>C. glabrata</i> within the macrophage	67
STUbL mutants in C. glabrata have differential SUMOylation pattern	69
CgUls1 protein is upregulated in STUbL mutants	71
Loss of proteins and reduced growth of STUbL mutants is due to enhanced prodegradation	oroteasomal 72
3.3 Summary	75
Chapter 4 Identification of targets of deSUMOylase CgUlp2 and STUbLs	76-91
4.1 Introduction	76
4.2 Results	76
Identification of global proteome of $Cgulp2\Delta$, $Cgslx8\Delta$, $Cguls1\Delta$, $Cgulp2\Delta Cgulp2\Delta Cgulp2\Delta Cguls1\Delta$ deletion strains in comparison with wild type	gs <i>lx8</i> ∆ and 76
Purine biosynthetic pathway is compromised in <i>Cgulp2</i> Δ <i>Cgslx8</i> Δ	83
Mitochondria function is compromised in $Cgulp2\Delta$ and $Cgulp2\Delta Cgslx8\Delta$	87

4.3 Summary	90
Chapter 5 Establishment of a method to enrich for SUMOylated proteins	92-95
5.1 Introduction	92
5.2 Results	92
5.3 Summary	95
Chapter 6 Determination of atomic resolution structure of key enzymes in	protein
SUMOylation to design drugs that target them	96-127
6.1 Introduction	96
6.2 Results	96
SUMO protease CgUlp2 was identified as least conserved with human	96
Expression and purification of CgUlp2 protein	97
Secondary structure prediction of CgUlp2 protein	99
Crystallization of the catalytic domain of CgUlp2 (CD_CgUlp2) protein	100
Biophysical characterization of the SUMO protease CgUlp2 protein	101
Secondary structure characterization of CD_CgUlp2 protein by Circular dichroise spectroscopy	m (CD) 103
Homology model of the catalytic domain of Ulp2 protein of various pathogenic fungi	105
CgUlp2 protein has conserved catalytic triad residues	108
CgUlp2 interacted with CgSmt3 (SUMO) protein directly via SUMO-interacting motifs	110
Functional characterization of SUMO protease CgUlp2	114
Structure of the SUMO protease CgUlp2 full length with 6x-SUMO protein complex rev Negative stain electron microscopy (EM)	ealed by 117
Pharmacophore-based virtual screening of CD_CgUlp2-CgSmt3 protein complex for molecule inhibitors (ligands)	or small 119
6.3 Summary	127
Chapter 7 Discussion	128-131
8 FutureProspects	132

9	Appendix 13	3-177
	9.1 List of plasmids used in the study	134
	9.2 List of primers used in the study	137
	9.3 List of strains used in the study	140
	9.4 Schematic representation of the single deletion strains generated for this study	y 141
	9.5 Details of recombinant DNA constructs generated for this study	142
	9.6 List of significant proteins identified by quantitative mass spectrometry for	
ea	ch mutant	156
	9.7 List of publications	176
10	References	177

ACKNOWLEDGEMENT

My doctoral journey was made possible with the support and encouragement of several people. Finally, I would like to express my gratitude to all my friends and well-wishers for their involvement in my success.

I am deeply indebted to my supervisor Prof. Krishnaveni Mishra for encouraging, supporting, and pushed me to higher thinking. Thanks to her for providing a degree of freedom to carry on my research work peacefully and for her constructive suggestions. She has been kind and patient to me throughout my PhD. It was a great opportunity to do my doctoral program under her guidance and to benefit from her expertise despite her incredibly busy schedule because she always made herself available to clarify my doubts.

I am grateful to my Doctoral Committee members Prof. Naresh Babu V. Sepuri (UoH) and Dr. Rupinder Kaur (CDFD) for assessing my research work and for the useful suggestions.

I would like to acknowledge Prof. Naresh Babu V. Sepuri, Head, Department of Biochemistry, and former Heads Prof. Krishnaveni Mishra, and Prof. Mrinal Kanti Bhattacharyya for making my research feasible with excellent infrastructure and lab facilities. I also thank Prof. N. Siva Kumar, Dean, School of Life Sciences, and former Deans Prof. Dayananda Siddavattam and Prof. K.V.A. Ramaiah for providing the general facilities of the school.

I would like to extend my sincere gratitude to Dr. Radha Chauhan (NCCS) for her continuous support, guidance, cooperation, encouragement and for facilitating all the requirements for my structural studies-related work.

I thank Chary Sir and Prabhu Sir for helping in the processing of bills and official documents at the earliest. I also thank non-teaching staff members of the Department of Biochemistry and the School of Life Sciences for their kind assistance and cooperation.

I thank all past and present members of my lab Dr. Hita, Dr. Gurrana, Dr. Pallavi, Dr. Renu, Kathir, Chhaya, Hitakshi, Bhaskar, Vidya, Sirisha, Reema, Manikandan, Mavuniya, Sowmya, Sukriti, Rajlaxmi, Dr. Niraja, and All Master student for their help during my Ph.D. I also thank Dr. Radha Chauhan group members Dr. Ekta, Dr. Pankaj, Dr. Priyanka, Jyostna, Aswathy,

Bheem, Lalit, and Venketash, for their help during my work at the National Centre for Cell Science (NCCS), Pune. I thank Anil Bhaiyaa for all the daily basis work in the lab that enabled us to carry out our experiments efficiently. I thank Srinivas for making the paperwork hasslefree.

Special thanks to Dr. Renu Shukla for her simple and caring nature and for helping me throughout my PhD. Her invaluable contribution to this project, particularly in RT-PCR, cell culture, and Y2H screening is deeply acknowledged. Special thanks to Sowmya for her help and support for the bioinformatics work.

I thank all the funding bodies DST-COE, IOE-UOH, UGC, DBT-SERB, CSIR, and School facilities for providing proper infrastructure for my research work and I am deeply grateful to the Council of Scientific and Industrial Research, India for the financial support. I thank the University of Hyderabad for its excellent Infrastructure and School facilities.

I specially express my gratitude to my dear best friend and supporter Dr. Kannan Balakrishnan who was always there for me in all my ups and downs. I value his considerate help and prayers throughout my PhD.

I also thank my friends Subha, Venketash, Sriram, Chhaya, Vipul, Manna, and Namita who were with me in all difficult phases of my life and always extended their much-needed support whenever required.

In the end, today I could achieve all this because of my family for their constant support. I have been blessed throughout my life with love, encouragement, and inspiration from my Papa and Mummy. I also thank Chacha, Chachi, Rohit, Dinesh bhai, Pinki Bhabi, and all my family members for believing in me and supporting me. I thank my nephew Yogesh and niece Bhakti for easing all my tensions. Thanks to the Almighty for keeping everything on track through his grace and mercy

Dipika Gupta



LIST OF ABBREVIATIONS USED

AOS Activation of Smt3p

AIDS Acquired immunodeficiency syndrome

ABPA Allergic bronchopulmonary aspergillosis

AIR Aminoimidazole ribonucleotide

ANOVA Analysis of variance

ASP Arabidopsis SUMO protease

ABC ATP binding cassette

BLAST Basic local alignment search tool

Beta mercaptoethanol

CO₂ Carbon dioxide

CAA Casamino acid

CD Catalytic domain

CWI Cell wall integrity

CPA Chronic pulmonary aspergillosis

CD Circular dichroism

CFU Colony forming unit

CP Core particle

CTD C-terminal domain

DAVID Database for annotation, visualization, and integrated discovery

DeSI DeSUMOylating isopeptidase

DNA Deoxyribonucleic acid

dNTP Deoxyribonucleotide

DMSO Dimethyl sulfoxide

DTT Dithiothreitol

EM Electron microscopy

ETC Electron transport chain

ERAD Endoplasmic reticulum-associated protein degradation

ECL Enhanced chemiluminescence

EPA Epithelial adhesion

ERG Ergosterol gene

EDTA Ethylene-diamine-tetra acetic acid

EMBOSS European molecular biology open software suite

FDR False discovery rate

FBS Fetal bovine serum

FLP Flippase

FRP Flippase recognition target

FDA Food and drug administration

FGAR Formylglycinamide ribonucleotide

FPPL Fungal priority pathogens list

GO Gene ontology

GAA Glacial Acetic Acid

GST Glutathione S-transferase

GAR Glycineamideribonucleotide

HPLC High-performance liquid chromatography

HIS Histidine

HRP Histone deacetylase

HDAC Horse-radish peroxidase

h Hour(s)

HIV Human immunodeficiency virus

H₂O₂ Hydrogen peroxide

HEPES 4-(2-hydroxyethyl)-1-piperazineethanesulfonic acid

HU Hydroxyurea

IBS Illustrator for biological sequences

IMP Inosine 5'-monophosphate

ICU Intensive care unit

ISBN International standard book number

IPA Invasive pulmonary aspergillosis

IPTG Isopropyl β-D-1-thiogalactopyranoside

LiAc Lithium Acetate

L Litre

LCMS Liquid- chromatography mass spectrometry

LB Luria-Bertani broth

MS Mass spectrometry

MMS Methylmethanesulfonate sensitivity

μ Micro

m Mili

MitoSOX Mitochondrial superoxide

M Molar

MD Molecular dynamics

MM/GBSA Molecular mechanics with generalized born and surface area

MeV Multiple experiment viewer

NAC N-acetylcysteine

n Nano

NCBI National center for biotechnology information

NEM N-ethylmaleimide

NEB New England Biolabs

Ni-NTA Nickel-nitrilotriacetic acid

NAT Nourseothricin acetyltransferase

NTD N-terminal domain

NPC Nuclear pore complex

NUP Nucleoporin

ORFs Open reading frames

OD Optical density

OPLS Optimized potentials for liquid simulations

OTS Overly Tolerant to Salt

PMSF Phenylmethylsulfonyl flouride

PMA phorbol 12-myristate 13-acetate

PBS Phosphate buffered saline

PGK Phosphoglycerate kinase

PRA phosphoribosylamine

PRPP 5-phosphoribosyl-1-pyrophosphate

PIPES Piperazine-1,4-bis(2-Ethanesulphonic Acid)

PAGE Polyacrylamide gel electrophoresis

PEG Polyethylene glycol

PCR Polymerase chain reaction

PVDF Polyvinylidene fluoride

pH Potential hydrogen

PCA Principal component analysis

PDB Protein data bank

PHYRE Protein homology/analogy recognition engine

PIAS protein inhibitor of activated STAT

RAD Radiation sensitive

RCP Ramachandran plot

RANBP Ran-binding protein

ROS Reactive oxygen species

RING Really interesting new gene

RP Regulatory particle(s)

RNA Ribonucleic acid

RNF Ring finger protein

RT Room temperature

RMSD Root mean square deviation

RPM Rotations per minute

SGD Saccharomyces Genome Database

SRplot Science and research online plot

sec Second(s)

SENP Sentrin/SUMO-specific protease

STAT Signal transducer and activator of transcription

SIR2 Silent information regulator 2

SPA Simple pulmonary aspergilloma

ssDNA Single-stranded DNA

SEC-MALS Size exclusion chromatography-multiangle light scattering

SUMO Small ubiquitin-like modifier

SDS Sodium dodecyl sulphate

SD Standard deviation

SG Stress granules

SIM SUMO interaction motif

STUbLs SUMO-targeted ubiquitin ligases

SOB Super optimal broth

SMT Supressor of mif two

SLX Synthetic Lethal of unknown [X] function

TMT Tandem mass tag

3D Three-dimensional

TCA Trichloro acetic acid

TEABC	Triethylammonium bicarbonate
TFA	Trifluoroacetic acid
TBST	Tris-buffered saline with 0.1% Tween20 detergent
2D	Two-dimensional
UBA	Ubiquitin activating
UBC	Ubiquitin-conjugating
ULS	Ubiquitin ligase for SUMO conjugates
ULP	Ubiquitin-like proteases
UPS	Ubiquitin-proteasome system
UV	Ultraviolet
WT	Wild type
WHO	World health organization
XTT	2,3-bis-(2-methoxy-4-nitro-5-sulfophenyl)-2H-tetrazolium-5-carboxanilide
YPD	Yeast extract peptone dextrose
YNB	Yeast nitrogen base
Y2H	yeast two-hybrid

LIST OF FIGURES

Figures Pa	age No
Figure 1. Classification of antifungals along with their mode of actions	22
Figure 2. Schematic representation of various physiological processes that are regula	ated by
SUMOylation	26
Figure 3. Schematic depiction of the SUMOylation pathway	27
Figure 4. Schematic illustration of the role of SUMOylation pathway in the pathogen	iesis of
various fungi	33
Figure 5. Schematic representation of orthologs of the S. cerevisiae STUbL proteins Slx	:5,
Slx8, Uls1 in Candida glabrata	61
Figure 6. STUbL genes are crucial in the maintenance of cellular homeostasis	63
Figure 7. Biofilm in C. glabrata mutants	66
Figure 8. Reduced survival and replication inside macrophage by STUbL mutants of C.	
glabrata	68
Figure 9. Differential SUMOylation pattern was shown by STUbL mutants of C. glabra	ta 70
Figure 10. Upregulation of CgUls1 protein in STUbL mutant	72
Figure 11. Loss of proteins and reduced growth of STUbL mutants is due to enhanced	
proteasomal degradation	73
Figure 12. Pathways that are differentially affected in each mutant	77
Figure 13. Graph shows the proteins involved in various transport that were downregular	ated in
Cgulp 2Δ , Cgulp 2Δ Cgsl $x8\Delta$, and upregulated in Cgulp 2Δ Cguls 1Δ mutant	78
Figure 14. Heat map illustrating the differences in protein levels of ribosomal proteins	80
Figure 15. Heat map illustrating the altered levels of components of proteosome-m	ediated
ubiquitin-dependent pathway in mutants	82
Figure 16. Loss of proteins and reduced growth of $Cgulp2\Delta Cgslx8\Delta$ double mutant is	due to
the altered proteins involved in the purine biosynthetic pathway	85
Figure 17. Mitochondrial functions were affected in Cgulp2 Δ and Cgulp2 Δ Cgslx8 Δ	88
Figure 18. Molecular basis for the phenotypes of loss of deSUMOylase CgUlp2 and S	TUbLs
in C. glabrata	91
Figure 19. Schematic representation of SIM-based SUMOylated protein enrichment in glabrata	C. 93

Figure 20. Purification of SUMO-interacting motif (SIM) in C. glabrata	94
Figure 21. Enrichment of SUMOylated proteins in SUMO protease and STUbL mutants	s in C
glabrata	95
Figure 22. Purification of the CgUlp2 protein	96
Figure 23. Diagrammatic representation of the CgUlp2 protein secondary structure as	shown
in PDBsum	99
Figure 24. Purification and crystallization screening of the catalytic domain of C	gUlp2
protein	100
Figure 25. SEC-MALS profile showing the molecular weight of catalytic domain of C	gUlp2
protein	101
Figure 26. Fluorescence spectrum of the catalytic domain of CgUlp2	103
Figure 27. Secondary structure characterization of catalytic domain of CgUlp2 protein	104
Figure 28. Homology model of CD_CgUlp2 protein	106
Figure 29. Homology modeling of the catalytic domain of Ulp2 protein of various patho	ogenic
fungi	107
Figure 30. Conserved catalytic triad residues (His-Asp-Cys) of CgUlp2 protein	109
Figure 31. Interaction studies of SUMO protease CgUlp2 and SUMO protein	111
Figure 32. Interaction of domains of CgUlp2 protein with CgSmt3 protein	112
Figure 33. A. CgUlp2 interacted with CgSmt3 by SUMO-interacting motifs	113
Figure 34. Longer linear SUMO chains are the preferred binding partners of the C	gUlp2
protein	115
Figure 35. The SUMO protease activity of CgUlp2 targeting linear SUMO cha	ins is
encouraged by the CgUlp2 SIM	116
Figure 36. Negative staining EM analysis of CgUlp2•6xSUMO complex complex	118
Figure 37. Active site of the CD_CgUlp2_CgSmt3 protein complex	119
Figure 38. Pharmacophore map of CD_CgUlp2_CgSmt3 protein complex	120
Figure 39. Molecular docking of a CD_CgUlp2-CgSmt3 protein complex with small l silymarin, and honokiol	igand, 123
Figure 40. MD simulation of CD_CgUlp2-CDSmt3 protein complex	125
Figure 41. MD simulation of CD_CgUlp2-CDSmt3 protein complex with 3 lead molecule	es 126

LIST OF TABLES

Tables	Page No
Table 1. Setting up the PCR reaction	36
Table 2. Setting up restriction digestion	39
Table 3. Reaction mixture for cDNA synthesis	40
Table 4. Components of the transformation mixture	41
Table 5. Orthologs of SUMO-targeted Ubiquitin Ligases (STUbLs) across fungi	59
Table 6. Orthologs of the S. cerevisiae STUbL proteins Slx5, Slx8, Uls1 in C. glabrata	60
Table 7. SUMO protease CgUlp2 showed the least conservation with its human homology	og 97
Table 8. Ramachandran plot statistics for the homology model of CD_CgUlp2 protein	106
Table 9: Coordinates (X, Y, and Z) of pharmacophores for the CD_CgUlp2-CgSmt3	3 protein
complex	120
Table 10. Top hits of lead molecules identified through virtual screening of the CD_	CgUlp2-
CgSmt3 protein from the small molecules database	121
Table 11. Top hits of lead molecules identified through virtual screening of the CD_	CgUlp2-
CgSmt3 protein from the FDA database	122
Table 12. List of the amino acid residues of CD_CgUlp2 (chain A) and CgSmt3 (chain I	3) protein
complex interacted with lead molecules along with the distance and type of interaction	124

CHAPTER 1 INTRODUCTION

1.1 THE BURDEN OF FUNGAL INFECTIONS

Infections, caused by fungi pose a significant risk and threat to public health due to their widespread effect on diverse populations. Fungal infections or mycosis are harmful not only to humans but also to plants and animals. Fungal infections range from systemic infections like aspergillosis and candidiasis that can be serious, to common superficial infections like ringworm and athlete's foot ^{1–3}.

Pathogenic fungi include Aspergillus species, Magnaporthe oryzae (primarily infects plants), Candida species, and Cryptococcus neoformans. Diseases like pulmonary aspergilloma, aspergillosis, candidiasis, and cryptococcal meningoencephalitis are commonly caused by these pathogenic fungi ^{4,5}. A significant surge in fungal infection, including approximately 1.5 million deaths, has been recorded in the recent past. Individuals with poor immune systems, including those with HIV/AIDS, organ transplant recipients, individuals undergoing chemotherapy, or patients with prolonged stay in the Intensive Care Unit (ICU) are at higher risk of severe fungal infections⁶⁻⁹. In fact, the fungal burden on humans was traditionally underestimated and therefore research was underfunded. However recently, WHO released a first-ever Fungal priority pathogens list (FPPL), bringing into focus the importance of fungal infections and antifungal resistance (ISBN 978-92-4-006024-1). Agriculture faces challenges from fungal attacks on staple crops like rice, wheat, corn, and soybeans, resulting in potential crop losses of up to 70% and impacting food security ^{10,11}. Plant pathogenic fungi like Magnoporthe oryzea cause rice blast disease, posing a major threat to agriculture ¹². Rust fungi species, including Puccinia graminis and Puccinia striiformis cause rust diseases in wheat, leading to reduced crop yields. Emerging fungal pathogens present new challenges to agriculture and forestry ^{13–15}. Moreover, aspergillosis affects various animal species, including birds and mammals, causing respiratory distress and systemic illness. Among animals, especially in livestock, fungal infections result in economic losses in the agricultural sector, while wildlife populations are affected, impacting biodiversity and overall ecosystem health ^{3,16–18}.

1.2 ANTIFUNGAL DRUGS

Antifungal drugs are commonly used to treat fungal infections in both plants and animals. These drugs exhibit a considerable level of specificity, offering protection against disease and aiding in the recovery process for the affected individuals¹⁹. The three main classes of antifungals that are commonly used are azoles, echinocandins, and polyenes. The targets of these drugs and common means of resistance are described below.

Azoles: A class of antifungals known as azoles (Ketoconazole, Fluconazole, Itraconazole, Miconazole, and Voriconazole) prevents the synthesis of ergosterol, which is an essential component of the fungal cell membranes. Azole drugs are highly potent and often used to treat fungal infections as ergosterol is not produced in plants or animals and therefore in fungus specific. Resistance to azoles has now been seen in many fungi. There are several ways in which azole resistance can arise: a) Overexpression of efflux pump: the expression of efflux pumps, like ABC transporters, can be upregulated by fungi. These pumps actively remove azole drugs from fungal cells, preventing their accumulation to harmful levels. b) Target site alterations: Alterations in lanosterol 14α -demethylase, the target enzyme (encoded by the ERG11 gene), can decrease the enzyme's affinity for azole medications, consequently decreasing their efficacy (Figure 1) 8,20,21 .

Echinocandins: Echinocandins prevent the production of β -(1,3)-D-glucan, an essential component of the fungal cell wall by targeting the glucan synthases. The following mechanisms can lead to resistance to echinocandins: a) Mutations in the FKS genes: The β -(1,3)-D-glucan synthase subunits are encoded by the FKS genes (*FKS1*, *FKS2*, and *FKS3*), which are the target of echinocandins. These genes can be mutated to change the structure of the enzyme, which lowers the echinocandins' affinity for binding. b) Activation of compensatory pathways: By triggering compensatory pathways like the cell wall integrity (CWI) pathway, certain fungi can preserve cell wall integrity even with the compromised glucan synthesis and counteract the effects of echinocandins (Figure 1) 8,22,23 .

Polyene: In the fungal cell membrane, ergosterol binds to polyenes like amphotericin B, leading to the creation of pores that cause leakage of cellular contents (Figure 1). There are several

mechanisms by which resistance to polyenes can arise: a) Decreased ergosterol content: in order to decrease the number of target sites available for polyene binding, fungi may lower the amount of ergosterol in their cell membranes b) Alterations in membrane composition: the composition of lipids in membranes can be altered by fungi, leading to the reduction of polyene binding affinity through the addition of substitute sterols ^{20,21,24}.

Apart from these specific drugs, nucleoside analogues like Flu Cytosine which interferes with fungal DNA synthesis, and Griseofulvin that damages the mitotic spindle are also used (Figure 1) ^{19,21,24}.

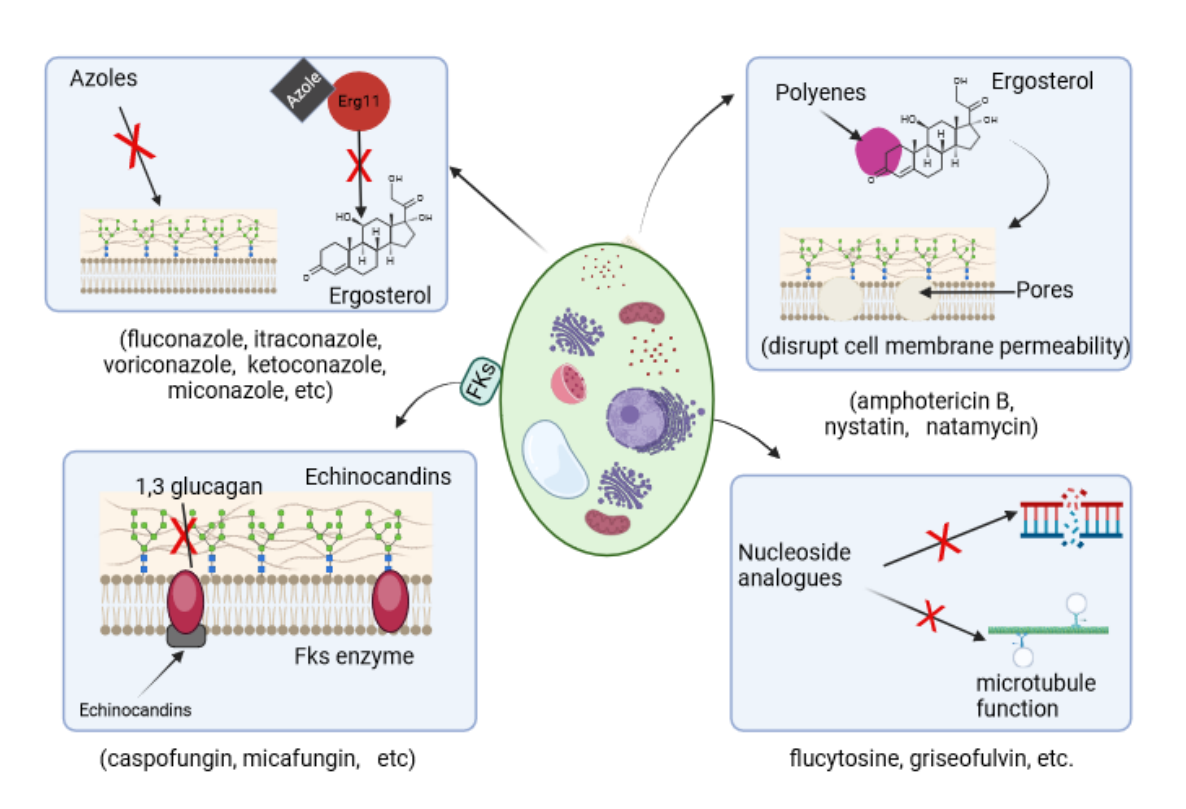


Figure 1. Classification of antifungals along with their mode of actions

However, the overuse of these antifungals, particularly azoles, has resulted in multidrug resistance.

Drug resistance is one of the most common causes of high mortality in fungal infections. Fungi are underappreciated as pathogens, and research on them receives far less funding than other illnesses with similar death tolls, such as malaria ^{2,25}. As a result, new antifungals haven't been introduced in a long time. It is essential to identify novel targets for the development of

antifungals as currently only two targets, that is, biosynthesis of the cell wall and cell membrane have been targeted. Since fungi are eukaryotes and also are closely related to mammals (as they both belong to the same group Opisthokonts), there aren't as many sufficiently different targets available. A successful target should be a) existing in the pathogen; b) essential for pathogenesis; c) druggable; and d) either completely absent from the host or sufficiently different from the pathogen target.

This thesis is an attempt to establish the SUMO-mediated protein homeostasis pathway as a potential target for antifungal drug development in the pathogenic yeast *Candida glabrata*.

1.3 Candida glabrata

Candida glabrata, a haploid, pathogenic yeast belonging to the ascomycetous genus Candida is commonly found in the human microbiota, including the oral cavity, vaginal tract, and intestinal tract. In a healthy individual, *C. glabrata* coexists with other human microbiota bacteria without posing any threat; however, it can infect patients with compromised immune systems, including those with AIDS, those who have received organ transplants, and those who stay in the intensive care unit for an extended period. Hence it is an opportunistic pathogen ^{9,26}. Compared to Candida albicans, a human pathogenic yeast in the same genus, it is more closely related to Saccharomyces cerevisiae ²⁷. The pathogenicity of Candida glabrata is governed by various virulence factors, some of which are outlined below:

- 1. Adhesion and Biofilm Formation: Adhesins located on the cell surface of *Candida glabrata* play a vital role in its ability to adhere to host tissues, a critical initial step in the onset of infections. Proteins like Epa1 and Awp2 facilitate this adherence process. Additionally, the capability to form biofilms enhances its persistence on both biotic and abiotic surfaces ^{27–30}. This feature increases resistance to host defenses and antifungal treatments, underscoring its significance in the pathogenicity of *Candida glabrata*.
- 2. Immunoevasion and Immune Modulation: *Candida glabrata* has the capacity to control the host immune response, which allows for immune system evasion. The yeast can use mechanisms that interfere with phagocytosis and intracellular killing processes to reduce the effectiveness of phagocytes, such as neutrophils and macrophages. It is also possible

- for the organism to control the production of cytokines, which will impact the inflammatory response of the host ^{29,31}.
- 3. Iron Acquisition: Iron, an essential micronutrient, is indispensable for both the survival and pathogenicity of *C. glabrata*. It can obtain iron from the host environment through various mechanisms such as secreting siderophores (e.g., triacetylfusarinine C) and using host iron-binding protein (e.g., transferrin) ^{26,27}.
- 4. Cell Wall Composition: The structure of the fungal cell wall plays a pivotal role in interactions with the host. In the case of *C. glabrata*, its unique cell wall composition, featuring mannoproteins and beta-glucans, is essential for its pathogenicity. These components actively participate in immune recognition, adhesion processes, and the evasion of host defences ²⁶.

There are other pathogenic factors in C. glabrata that play an essential role in its ability to cause infections, influencing the establishment, persistence, and severity of infections. These factors include: a) morphological plasticity: In contrast to C. albicans, C. glabrata typically does not form true hyphae. Nevertheless, it has the potential to display a pseudohyphal growth form, and this morphological flexibility may play a role in its capacity to invade host tissues ^{32,33}, b) hemolytic activity- C. glabrata exhibits hemolytic activity, inducing the breakdown of red blood cells. This activity may contribute to tissue damage and the spread of infection, c) osmotic stress response- C. glabrata has a robust osmotic stress response, enabling it to survive in various osmotic conditions encountered within the host. This adaptability is critical for colonizing different host niches, d) Candida drug efflux pumps- C. glabrata is known for its high expression of drug efflux pumps, enhancing its resistance to antifungal agents. These pumps actively remove drugs from the fungal cell, reducing their effectiveness and posing challenges to treatment, e) sterol biosynthesis pathway- alterations in the sterol biosynthesis pathway, including changes in ergosterol production, can impact the susceptibility of C. glabrata to antifungal drugs. Disruptions in this pathway may contribute to antifungal resistance, f) protease activity- C. glabrata produces various proteases capable of degrading host proteins. This proteolytic activity may contribute to tissue invasion and immune evasion ^{26,27,34}.

The progression of the *Candida glabrata* infection involves a series of sequential steps, encompassing adherence, immune evasion, tissue invasion, and systemic dissemination. The

initiation of infection by this organism involves adhering to the host surfaces, facilitated by adhesins, particularly EPA (epithelial adhesin) proteins, which promote the attachment of yeast to mucosal surfaces for effective colonization. Evading the host immune system is a strategic aspect of *C. glabrata* infection process, demonstrated by its resistance to phagocytosis by neutrophils and macrophages, ability to survive within phagocytes, and inhibition of immune signaling pathways. Subsequent to adherence and colonization, *C. glabrata* can invade host tissues, causing localized damage. In individuals with compromised immune systems, the yeast may disseminate systemically, resulting in more severe infections ^{26,27}.

One such prevalent and critical fungal infection in humans is Candidemia which plays an essential role in invasive candidiasis. This infection poses a severe threat due to its rapid progression and significant impact on major organs, resulting in a high fatality rate. Various *Candida* species contribute to invasive candidiasis including *Candida albicans*, *Candida glabrata*, and *Candida tropicalis*. Notably, *Candida glabrata* has emerged as the second leading cause of mortality associated with candidiasis ²⁶. Its multidrug-resistant nature, particularly its resistance to antifungal drugs such as azoles and echinocandins, intensifies the challenge in fungal treatment ³⁵. The high mortality rate, ranging from 40-60%, underscores the urgent need to discover new antifungals to treat fungal infections. To address this challenge, we are exploring the protein SUMOylation pathway in *Candida glabrata* as a potential target for identifying novel antifungals.

1.4 SUMOYLATION: A POTENTIAL ANTIFUNGAL TARGET

During SUMOylation, a post-translational modification process, a small ubiquitin-like protein (SUMO) is covalently attached to the target protein, enabling it to interact with other proteins. In yeast, the SUMO protein is coded by the *SMT3* gene. SUMOylation of target proteins can lead to multiple consequences (Figure 2). SUMOylation could lead to changes in protein subcellular localization, the interaction of one protein with another, and alteration in catalytic functions. In multiple cellular physiological pathways like DNA repair, intracellular transport, cell cycle progression, transcription, and immune response, SUMOylation is known to play an important regulatory role ³⁶. Also, SUMOylation has been found to play a crucial role in adaptation to

stress conditions, cell division, and growth, making it a suitable target for the development of antifungals.

A cascade of enzymatic actions leads to SUMOylation of targets. While basic machinery appears conserved in all organisms studied so far, the SUMOylation system has expanded in some organisms. For instance, there are potentially 8 isoforms of the SUMO gene in *Arabidopsis thaliana*; humans possess 4 SUMO isoforms, *viz*, SUMO-1, -2, -3, and -4, while *S. cerevisiae* expresses a single SUMO paralogue, called Smt3p ³⁷.

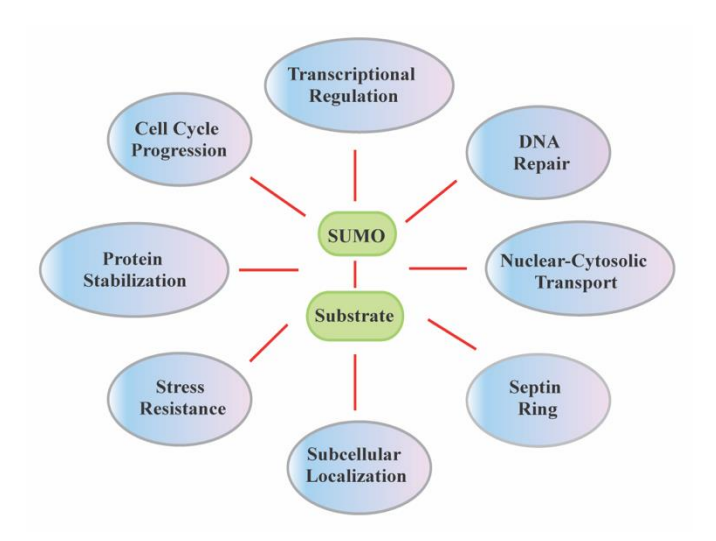


Figure 2. Schematic representation of various physiological processes that are regulated by SUMOylation.

1.4.1 Mechanism of SUMOylation

The process of SUMOylation involves multiple steps. SUMO first undergoes proteolytic processing that involves the removal of a few C-terminal amino acids, revealing a diglycine motif at the C-terminus to become mature SUMO. The ubiquitin-like proteases (Ulp) family of proteases in yeast catalyzes SUMO maturation. An E1 activating enzyme, an E2 conjugating enzyme, and one of several SUMO E3 ligases are required for SUMO conjugation. In step one of SUMO conjugation, ATP-dependent E1 activating enzyme (Aos1/Uba2 in yeast), forms a high-energy thioester bond with the SUMO C-terminus ^{38,39}. This step requires ATP hydrolysis. Then the transfer of SUMO from the E1 activating enzyme to the SUMO conjugating enzyme involves the formation of a thioester linkage between the C-terminal glycine of SUMO and the catalytic

active site of a cysteine residue of the E2 conjugating enzyme. In yeast, the single E2 conjugating enzyme is encoded by Ubc9 and is responsible for catalyzing conjugation reactions. Subsequently, the SUMO moiety attaches to the target protein by forming an isopeptide bond between the C-terminal glycine of SUMO and \(\mathcal{E}\)- amino group of lysine residue of the target protein \(^{40,41}\) (Figure 3). While *in vivo* E3 ligases aid in the process of transferring SUMO to the target, *in vitro* the E2 enzyme is adequate for conjugating SUMO to a lysine residue in the substrate \(^{42}\).

In contrast to many E2 conjugation enzymes involved in ubiquitination, Ubc9 is the sole SUMO-conjugating E2 enzyme found in eukaryotes. *UBC9* is essential in *S. cerevisiae*, just like many other SUMOylation components, including Smt3, Aos1, and Uba2 ^{43,44}. In vivo, E3 ligases are involved in the transfer of SUMO from Ubc9 to the target proteins. Various E3 ligases contribute to the substrate range and specificity in the SUMOylation process. So far, identified SUMO E3 proteins which mainly comprise members of PIAS (protein inhibitor of activated STAT) proteins possessing the SP-RING domain are Siz1, Siz2, Mms21, and Zip3 in *S. cerevisiae*. On the other hand, RANBP2 (Ran-binding protein 2), a component of the nuclear pore complex, functions as a SUMO ligase despite lacking the canonical RING domain for catalytic activity ^{45–48}. Moreover, histone deacetylase 4 (HDAC4), KRAB-associated protein 1 (KPA1), Pc2, and Topors, have also been identified as potential SUMO ligases ³⁷.

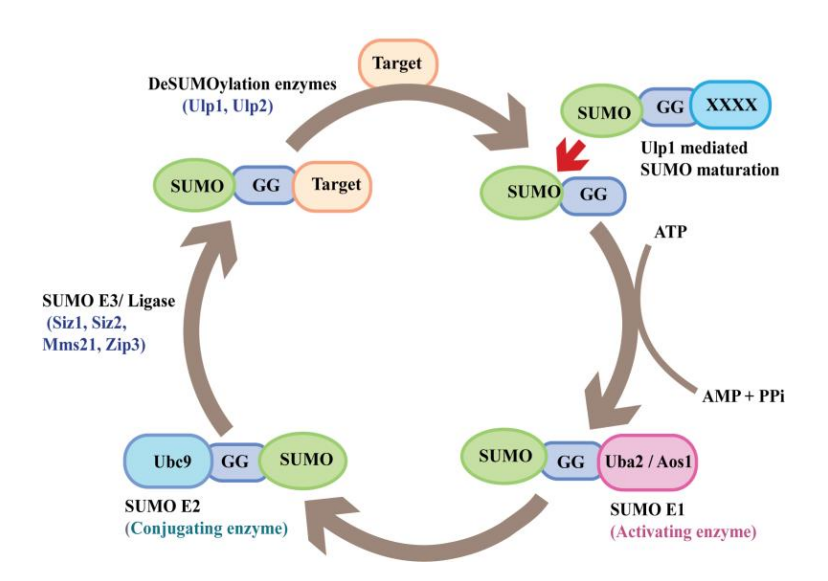


Figure 3. Schematic depiction of the SUMOylation pathway.

1.4.2 Mono- and polySUMOylation

MonoSUMOylation occurs when a single SUMO protein becomes covalently bound to a target protein. It can regulate the activity, stability, and localization of the target protein. This modification exerts significant influence over diverse cellular functions, such as transcription, DNA repair, and cell cycle progression and also modulating protein-protein interactions ^{40,49}. For example, monoSUMOylation of Rad52 (a key player in homologous recombination) is critical in its role in DNA repair and may influence its interactions with other repair factors ⁵⁰. Similarly, Sir2 monoSUMOylation regulates its translocation from the telomere to the nucleolus ⁵¹.

In contrast, polySUMOylation involves the sequential addition of multiple SUMO proteins to a substrate, resulting in the formation of SUMO chains. The SUMO-conjugating enzyme (E2) and the SUMO ligase (E3) carry out this modification. Specific SUMO E3 ligases are involved in prompting polySUMOylation, ensuring the efficient transfer of SUMO from the E2 enzyme to the target protein. The specific lysine residue on the target protein undergoing polySUMOylation can vary, as SUMO can be attached to multiple lysines within the target protein. For example, in yeast, Smt3 can be conjugated to lysines via positions 11,15, and 19 while in humans, SUMO2/3 are known to form polymeric chains on lysine 11 ^{52–56}.

The consequences of polySUMOylation are diverse, impacting various cellular processes. Notably, polySUMOylation of nucleoporins is crucial for the proper functioning of the nuclear pore complex, regulating nucleocytoplasmic transport ^{48,57}. Additionally, it is involved in DNA repair mechanisms, influencing the recruitment of repair factors to damaged sites and contributing to genome stability. It also contributes to regulating the cell cycle and mitosis by affecting the stability and activity of key cell cycle regulators. This modification also regulates the turnover of the target protein ^{58–62}. PolySUMOylation dynamics is regulated by the deSUMOylases, such as Ulp in fungi and SENP in higher organisms that can cleave SUMO from target proteins thus protecting the protein from ubiquitination and consequent degradation.

Moreover, polySUMOylation serves as a signal for recognition by the ubiquitinating machinery. These polySUMOylated proteins are polyubiquitinated and degraded in the proteasome. This

intricate interplay between SUMOylation and ubiquitination contributes to the dynamic regulation of cellular processes and protein homeostasis.

1.4.3 SUMOylation motif

Short amino acid sequences known as "SUMOylation motifs" are recognized by the enzymes that facilitate the covalent attachment of Small Ubiquitin-like Modifier (SUMO) proteins to target proteins. The SUMOylation machinery is guided by these motifs to particular lysine residues in the target proteins. The consensus SUMOylation motif is commonly identified by a core of ψ KxE/D, where ψ represents a hydrophobic amino acid, K is the lysine that is SUMOylated, x can be any amino acid, and E/D can be either glutamic or aspartic acid 36,49,63 . Notably, the most highly conserved position is glutamate 64,65 . Ψ KxE serves as the E2 Ubc9 recognition site, and the conjugation process depends on the interaction between the motif and the enzyme $^{66-68}$. Even though this motif is present in one-third of the proteins, to achieve precise SUMOylation, other factors, such as the steric environment in SUMO attachment signals are also important 69 .

Apart from the core sequence, additional variations around this motif also influence the site of SUMOylation. These mainly include negatively charged amino acid-dependent SUMOylation motifs (NDSMs), as well as phosphorylation-dependent SUMOylation motifs (PDSMs). The clusters of residues downstream of the ΨKxE core exhibit strong interactions with both the substrate and Ubc9, hence enhancing SUMO conjugation ^{70–72}. Moreover, the inverted motif [(E/D)xKΨ] has been reported to be SUMOylated ⁷³. In sum, the precise combination of factors that determine SUMOylation is still obscure.

1.4.4 SUMO interacting motif

SUMO interaction motif (SIM) refers to the short amino acid sequences that are involved in the non-covalent binding of SUMO proteins to target proteins. The first conserved SUMO interacting motifs were defined in the year 2000 ⁷⁴. SIMs are typically characterized by a hydrophobic core, often composed with valine (V), leusine (L), or isoleucine (I) residues, flanked by acidic or polar amino acids. The consensus sequence for SIMs is usually V/L/I-x-V/L/I, where "x" represents any amino acid^{74–76}. SIMs are frequently found in areas of unstructured regions. The presence of negatively charged residues can play a crucial role in

determining the SUMO/SIM interaction affinity, polarity, and paralogue specificity, probably through salt bridges and hydrogen bonding with conserved basic residues on the surface of SUMO ^{75,77}. There are currently three different types of SIMs that have been identified: SIMa (ΨΨxΨAcn), SIMb (ΨΨDLT), and SIMr (AcnΨxΨΨ) ^{78,79}. In these SIMs, Ψ represents a hydrophobic residue (V, I, or L), n is a number between two and five, and Ac stands for Asp, Glu, or Ser. Ser, while not being an acidic amino acid, is frequently present in SIMs, most likely because it is a phosphorylation target ⁷⁹. In comparison to ubiquitin-binding domains, there is a limited number of SIMs are known ⁸⁰. This could imply that more forms of SIMs have yet to be discovered.

1.4.5 SUMO deconjugating enzymes

The process of SUMOylation is dynamic and reversible. De-conjugases or deSUMOylating enzymes or SUMO-specific proteases cleave the SUMO protein from the target protein. Ulp1 and Ulp2 (ubiquitin-like proteases) are two SUMO proteases found in yeast. These are isopeptidase-related enzymes that sever the isopeptide bond between the target protein and SUMO. Ulp1 is present at the nuclear pore complex (NPC) and is required for cleaving both the SUMO precursor and also SUMO conjugates from target proteins. Ulp1 also plays a critical role in the regulation of cell division by deSUMOylating several components of the septin ring. Ulp2, which is found in the nucleoplasm ⁸¹, is important for dismantling polySUMO chains apart from also deSUMOylating monoSUMO from nucleolar and nuclear proteins ⁸². The two proteins also appear to deSUMOylate a distinct set of SUMO conjugates ⁸¹. Ulps (SENPs in higher eukaryotes) share a conserved ~200-amino-acid catalytic domain that is typically found near their C-terminus.

In plants and animals, there is an expansion in the SUMOylation machinery. SUMO isoforms are abundant in higher animals and plants. SUMO isopeptidases and ligases have also expanded. In these organisms, the SUMO isopeptidase and SUMO ligase both seem to be at least somewhat selective for the SUMO isoform. Mammals have at least six SENPs, including SENPs 1, 2, 3, 5, 6, and 7. While SENP6 and SENP7 are more Ulp2-like, SENP1-3 and SENP5 are more Ulp1-like ⁸³. SENP proteins can be grouped into three major families. The first family, which consists of SENP-1 and SENP-2, is effective at eliminating all the mammalian SUMO isoforms (SUMO-1–3). The second family contains SENP-3 and SENP-5, which selectively remove SUMO-2/3

from substrates. Additionally, SUMO-2/3 is selectively removed from substrates by SENP-6 and SENP-7 ⁸⁴. In contrast to SENPs, which are primarily found in the nucleus, two new types of SUMO proteases have also recently been discovered. Dimer DeSI1 (DeSUMOylating isopeptidase 1), which is found in both the cytosol and the nucleus, and DeSI2, which is primarily found in the cytoplasm ^{85,86}. DeSI1 may deconjugate SUMO-1 and SUMO-2/3 and exhibit isopeptidase activity ⁸⁵. Seven SUMO-specific proteases have been found in the *Arabidopsis* genome. These are categorized as ULP1-like SUMO proteases, including ULP1a/ELS1 (Ub-like protease 1A/ESD4 like SUMO protease 1), ULP1b, ULP1c/OTS2 (Overly Tolerant to Salt2), ULP1d/OTS1 (Overly Tolerant to Salt1), and ESD4 (Early in Short Days 4). SUMO proteases that are similar to ULP2 are known as ULP2a and ULP2b/ASP1 (Arabidopsis SUMO protease1). Additionally, phylogenetic analysis of ULP1d/OTS1 and ULP1c/OTS2 shows that they are more similar to yeast ScUlp2 ^{87–89}. These findings highlight how higher eukaryotes have a more complex SUMOylation pathway than yeast.

1.4.6 SUMOvlation in pathogenic fungi

While research on *S. cerevisiae* has uncovered the mechanisms underlying SUMOylation as well as its functional consequences, several labs have recently looked at SUMOylation in pathogenic fungi. These studies have revealed that SUMOylation has a substantial impact on physiology and fungal pathogenicity. I briefly outline some of the findings on SUMOylation in pathogenic fungi below ⁴¹.

In both *C. albicans* and *C. glabrata*, protein SUMOylation has been investigated. The SUMO gene, *SMT3*, is required for survival of *C. glabrata*. Changes in SUMOylation have an impact on the potential for growth, stress resistance, and DNA repair in *C. glabrata*. Ulp2 was discovered to be necessary for virulence, adhesion, and biofilm formation and its deletion in *C. glabrata* increased sensitivity to stress (Figure 4) ⁹⁰. *SMT3* is not required for survival in *C. albicans*, however, *smt3* mutants have slow growth that is exacerbated by stressful environments, making them sensitive to a wide variety of perturbations, such as temperature, oxidative, and cell wall stressors ⁹¹. *SMT3* inactivation in *C. albicans* results in a heterogeneous population of slowly expanding, elongating cells that resemble pseudohyphae (Figure 4) ⁹¹. Loss of SUMO ligases also resulted in an increase in hyphal production in *C. albicans*, potentially increasing its

virulence ⁹². These mutants were also vulnerable to genotoxic, thermal, and cell wall stressors, which may indicate that SUMO conjugation is crucial for differentiation and combating stress.

The species of Aspergillus and Cryptococcus are toxic to both plants and animals. Invasive pulmonary aspergillosis (IPA), chronic pulmonary aspergillosis (CPA), simple pulmonary aspergilloma (SPA), and allergic bronchopulmonary aspergillosis (ABPA) are all caused by Aspergillus infections 4,93 . Both pulmonary cryptococcosis and cryptococcal meningoencephalitis have been linked to the Cryptococcus. An opportunistic human pathogenic fungus called Cryptococcus neoformans primarily targets immunocompromised individuals 94,95 . Infections caused by Cryptococcus have a significant mortality rate and exhibit resistance to many widely used antifungal drugs. In Cryptococcus, SUMOylation has not been specifically studied 96 . However, a large-scale investigation that looked for a potential therapeutic molecule for C. neoformans discovered that SUMO activating enzyme ($\Delta aos 1$) ortholog knockouts reduced the growth of C. neoformans capsules and biofilms on medical equipment (Figure 4) 97 . The virulence of C. neoformans is decreased by the loss of capsule formation. In this investigation, numerous other proteasomal elements as well as NEDD (an additional ubiquitin-like molecule) were discovered to be crucial for capsule formation. This implies that in the absence of these pathways, the pathogen's virulence traits may be reduced.

The three *Aspergillus* species that produce aflatoxin most frequently are *A. fumigatus*, *A. flavus*, and *A. carcinogen*. A prominent source of food contamination is aflatoxin, which is present in foods like almonds. Studies on *A. flavus* revealed that SUMO-conjugated protein accumulated at higher temperatures, but the deletion of the SUMO gene negatively impacted the pathogenicity and capacity for colony formation ⁹⁴. The entire SUMOylation machinery in *A. nidulans* has been found and described. *A. nidulans* has a single gene SumO, that encodes SUMO and also contains the E3 ligases SizA, SizB, and MmsU ^{98,99}. SumO protein is necessary for cellular differentiation in this fungus even though it is not required for fungal vegetative development. *A. nidulans* Δ*sumO* cells exhibit enhanced susceptibility to the DNA-damaging chemical methyl methanesulfonate (MMS) and the DNA synthesis inhibitor hydroxyurea (HU) in addition to impaired conidiation ¹⁰⁰. Additionally, Δ*sumO* cells exhibit self-sterility, indicating that SUMOylation of important targets is necessary for the production of viable meiotic progeny in *A. nidulans*. Proteins were tagged using a method called "SUMOlock" to identify 149

SUMOylated proteins (SUMOylome) ⁹⁹. This study demonstrated that a significant portion of the SUMOylated proteins was involved in DNA repair, RNA processing, and transcription regulation. It's interesting to note that the deletion of UlpB or all three SUMO ligases together had very severe effects on conidiation and growth (Figure 4). Another intriguing finding from this research was that although *sumO* deletion was generally well tolerated, deletion of *ulpB* was not, indicating that deSUMOylation of key substrates is required for growth.

The plant pathogen *Magnaporthe oryzae* causes rice blast disease. It is a filamentous ascomycete. Deletion of the SUMO (smt3), E1 (aos1, uba2), and E2 enzymes in *M. oryzae* caused a variety of abnormalities, including defects in septum formation, conidiation, sensitivity to stress, mycelial development, and pathogenicity ^{12,101}. It has been shown that at least four septins are SUMOylated, and any alterations to the consensus SUMOylation sites in each septin cause the septins to separate in the appressoria and impair virulence ⁶⁰. These mutants developed obtrusively and with delayed host penetration. Additionally, compared to the wild type, SUMO pathway mutants (smt3, aos1, uba2, and ubc9) showed increased sensitivity to DNA damaging stress. (Figure 4) ¹².

These results collectively show that although SUMOylation is not necessary for survival in pathogenic fungi (except in *C. glabrata*), it is required for stress response, differentiation, and pathogenicity in all fungi so far investigated ⁴¹.

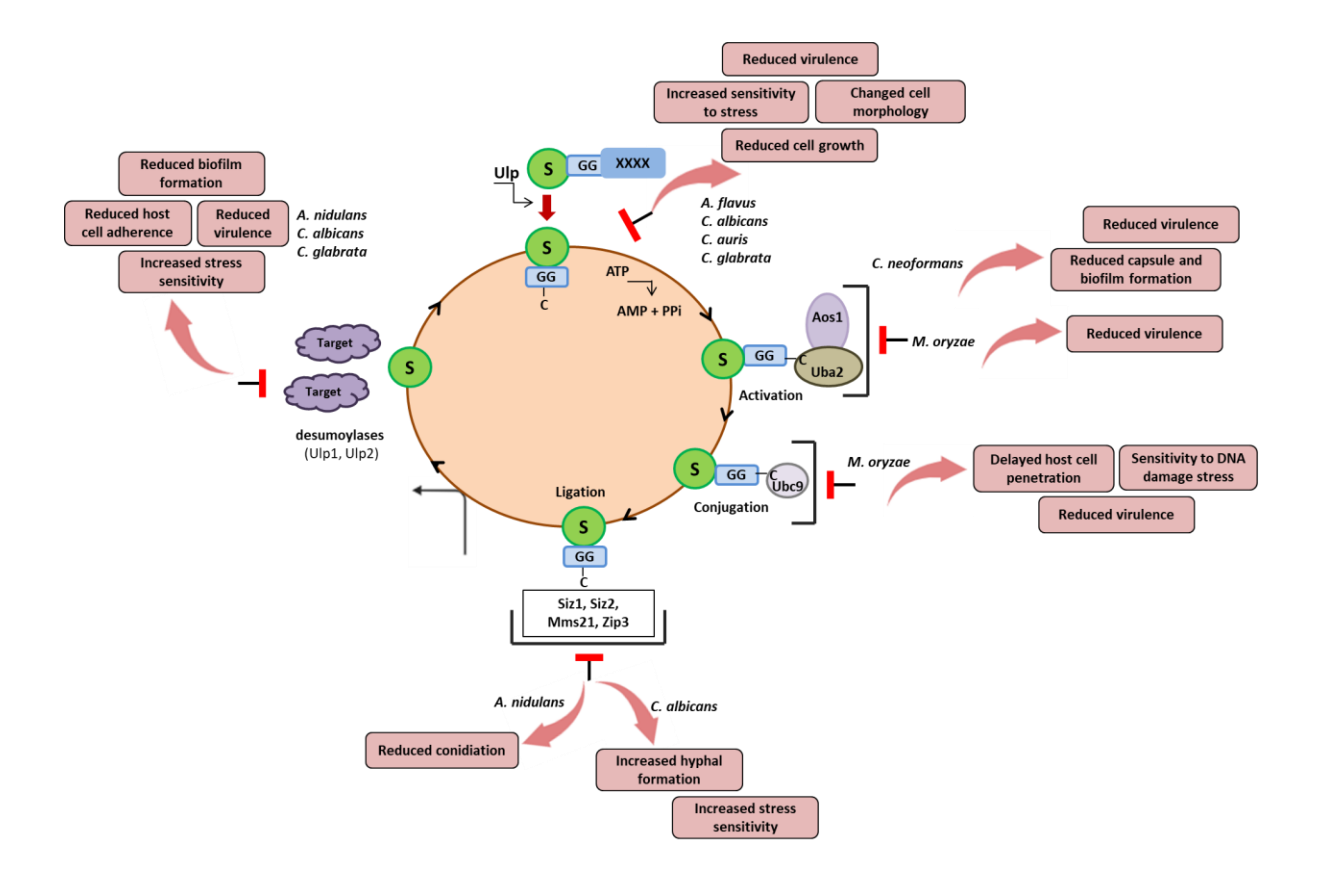


Figure 4. Schematic illustration of the role of SUMOylation pathway in the pathogenesis of various fungi.

1.4.7 SUMO-dependent Ubiquitination mediated protein degradation

There exists a significant interplay between the SUMO and ubiquitin pathways, facilitated by a class of E3 ubiquitin ligase known as SUMO-targeted ubiquitin ligases (STUbLs). These enzymes specifically target polySUMOylated proteins marking them for degradation by the 26S proteasome. Over the past decades, identification of STUbLs has relied on various indicators such as the presence of SUMO-interacting motifs (SIMs), interactions with SUMO, and homology studies. ^{102–107}. STUbLs are characterized by two essential features. First, they possess the RING-finger domain which facilitates protein-protein interactions and specifically interacts with ubiquitin-conjugating enzymes. Second, STUbLs contain multiple SIMs, enabling effective interaction with SUMO ^{108,109}. The presence of multiple SIMs enables STUbLs to selectively ubiquitinate proteins carrying poly-SUMO chains ^{63,102–105,110–112}. At present, two STUbLs, Uls1 and Uls2, have been discovered in *S. cerevisiae*. Uls1 (*aka* Dis1, Ris1, and Tid4) is a 1612-amino acid protein featuring a RING finger motif, a Swi2/Snf2-like translocase domain, and four

putative SIMs ^{79,110,111}. On the other hand, Uls2 forms a heterodimer composed of Slx5 and Slx8. Slx5, also known as Hex3 possesses two SIMs and a RING finger domain ^{105,111,113}. In humans, RNF4 (Ring Finger Protein 4) is the only studied STUbL. It has been implicated in the regulation of diverse cellular processes, including DNA repair, transcriptional regulation, and stress response. Anomalies in RNF4 levels have been linked to a variety of illnesses, including cancer ^{114,115}. This emphasizes the relevance of STUbLs in cellular homeostasis. By connecting the ubiquitin and SUMO pathways, STUbLs provide an additional regulatory mechanism for controlling the levels of SUMOylated substrate forms.

1.5 SPECIFIC OBJECTIVES OF THE CURRENT STUDY

As discussed above, SUMOylation plays a significant role in regulating fungal development, differentiation, and virulence, and appears to be critical for the pathogenesis of various fungi. Our laboratory had identified the SUMOylation machinery in *C. glabrata* and demonstrated that the SUMOylation pathway was required to combat stresses like high temperature and DNA damage. We also showed that CgUlp2 was required for virulence of *C. glabrata* ⁹⁰. Based on these studies we wondered if SUMOylation could serve as a good target of intervention for fungal infection. Since SUMOylation appeared to be critical for survival or combating stress or for virulence in many fungi ^{41,90,91,116}, it could serve as a pathway for targeting antifungals. We, therefore, followed up our previous observations. As we had seen that loss of CgUlp2 led to reduced protein SUMOylation, we had hypothesized that this reduced protein SUMOylation was due to increased degradation of polySUMOylated proteins. If that were true, then the STUbL pathway was operational in *C. glabrata*. Therefore, in this thesis, we set out to

- 1) Identify and characterize the STUbLs and STUbL-mediated protein homeostasis in *C. glabrata*.
- 2) Since the loss of CgUlp2 leads to reduced capacity for survival in macrophages and systemic candidiasis, we attempted to decipher the structure of the CgUlp2-SUMO complex to design specific drugs that can disrupt this interaction.

CHAPTER 2 MATERIALS AND METHODS

2.1 MOLECULAR BIOLOGY METHODS

2.1.1. Polymerase Chain Reaction

The polymerase chain reaction (PCR) was performed using Vent DNA Polymerase to ensure the error-free amplification for cloning, generation of mutants, and protein expression studies whereas Taq DNA polymerase was used for screening purposes. Both the polymerases were supplied by New England Biolabs (NEB). The following was the setup for the PCR reaction used for amplification. For Taq Polymerase, standard Taq Buffer was utilized, and for Vent Polymerase, ThermoPol Buffer was employed.

Table 1. Setting up the PCR reaction

Component	Volume
10X buffer	2.5 μl
10mM forward primer	0.5 μ1
10mM reverse primer	0.5 μ1
10mM dNTPs	0.5 μ1
Template DNA 100ng	1 μ1
Polymerase	0.125 μl
MiliQ	19.875 μ1

The PCR reaction was conducted in the manner described below:

Initial denaturation		95°C
Denaturation		95°C
Annealing	30 cycles	55-65°C
Extension		72°C
Final extension		72°C
Hold		4°C

The product was amplified using an Eppendorf thermal cycler. The PCR products were resolved and verified via agarose gel electrophoresis. If necessary, a Qiagen gel extraction kit was used to purify the separated products.

2.1.2. Molecular cloning

2.1.2.1. Ultracompetent cells preparation

The Inoue method, as outlined in Sambrook and Russell (2006), was employed to prepare ultra-competent cells of the DH5α strain of *Escherichia coli* ¹¹⁷. Initially, a single colony of bacteria was inoculated in SOB broth and allowed to grow for 16 hours at 37°C to make the primary culture. The next day, a secondary culture was initiated by transferring 1/100th volume of primary culture in 100mL of SOB broth, followed by incubation at 18°C with shaking at 180 rpm until the OD600 reached 0.4-0.5. After cooling the flask with ice, the cells were quickly extracted using centrifugation at 12,000 rpm for 10 minutes at 4°C. The supernatant was carefully discarded, and the cell pellet was washed with cold, distilled water before being resuspended in 80 mL of Inoue transformation mix (containing 50mM MnCl₂.4H₂O, 15mM CaCl₂.2H₂O, 250mM KCl, 500mM PIPES pH6.7). The suspension was centrifuged again for ten minutes at 4°C at 12,000 rpm, and the supernatant was discarded with caution to avoid disturbing the pellet. The cells were then resuspended in 20 mL of ice-cold Inoue buffer, supplemented with 1.5 mL of DMSO, and the mixture was gently rotated. After allowing the cell suspension to rest on ice for ten minutes, it was divided into 100 μl aliquots and then snap-frozen in liquid nitrogen. Further, the tubes containing aliquots were maintained at -80°C until use.

2.1.2.2. DNA transformation into bacterial cells

100 μ l of ultracompetent DH5 α cells of *E. coli* were retrieved from from -80°C storage and thawed on ice. Following this, 2 μ l of plasmid DNA was added to the cells, and the mixture was allowed to stand on ice for 20 minutes. Subsequently, the cells underwent a heat shock treatment at 42°C for 90 seconds, after which the tube was promptly returned to ice for a further five minutes. Upon completion of the heat shock, 900 μ L of LB broth was added to the cells, and the mixture was incubated in a thermomixer set at 37°C for 40 minutes with gentle agitation. Following this incubation period, 100 μ L of the cell suspension was spread onto a LB plate with appropriate antibiotics, which was then incubated in a 37°C for 14-16 hours for further analysis.

Instead of using LB media, 900µl of SOB was utilized to transform the ligated DNA construct. Additionally, the cells were given a 60-minute recovery period at 37°C. The cell suspension was spun for one minute at 13000 rpm. After removing 900µl of the supernatant, the cells were resuspended in the residual media and distributed on LB plates containing the relevant antibiotics.

2.1.2.3. Plasmid isolation

The alkaline lysis method was used to isolate plasmids from bacteria. In 3 mL of LB broth with the proper antibiotic for selection, a single colony of bacteria was inoculated. The culture was grown overnight at 37°C and 180 rpm of continuous shaking. Next, by centrifuging at 13,000 rpm for one minute, the culture was harvested and pelleted. The excess liquid was then removed by decanting the media and inverting the tube onto a piece of tissue. The pellet was mixed with 200µl of ice-cold Solution-I (25 mM Tris-Cl pH 8.0, 10 mM EDTA pH 8.0), and dissolved by pipetting or vigorously vortexing the tube for 10 seconds. Solution-II (0.2 % NaOH, 0.2 % SDS) was added (200µl), and the tube was gently inverted to mix. After that, 200µl of Solution-III (3 M potassium acetate, 11.5 % glacial acetic acid) was added, and the mixture was gently mixed by repeatedly inverting the tube four to five times. The tube was then instantly kept on ice for five minutes. Subsequently, the tubes were spun for 10 minutes at 4°C at 13,000 rpm. After collecting the supernatant carefully in a new Eppendorf tube (without disturbing the pellet) 420ul of isopropanol (0.7 volumes) was added to it. In order to mix, the tube was inverted four or five times and then centrifuged it to precipitated the DNA at 13,000 rpm for ten minutes at room temperature. The resulting pellet was washed with 70% ethanol and allowed to air dry in order to get rid of any remaining alcohol. Finally, the plasmid DNA was resuspended in 40µl of TE-RNase (10 mM Tris-Cl pH 7.4, 1 mM EDTA pH 8.0, 0.1 mg/mL of DNase free RNase) and allowed to incubate for 30 minutes at 37°C. Routinely, the plasmid concentration and purity were assessed using agarose gel electrophoresis.

2.1.2.4. Screening of the clones by restriction digestion

The above-described procedure was used to isolate the plasmids, and restriction digestion was used to verify that the insert was present. Via agarose gel electrophoresis, the recombinants were distinguished by size differences between the insert-carrying and empty vectors. In order to

verify the clones, subclone the insert into a different vector, and digest the PCR product flanking restriction sites, restriction digestions were carried out. The reaction mixture was made in the following manner for a 10 µl reaction in order to facilitate DNA digestion using high-fidelity restriction enzymes from NEB. At 37°C, those reaction mixtures were incubated for a minimum of one hour. Subsequently, the digested samples were subjected to agarose gel to determine the presence of DNA and isolated for further use if required.

Table 2. Setting up restriction digestion

Component	Volume
10X CutSmart Buffer	1 μ1
DNA (1-2μg)	2-4 μl (depending on concentration)
Enzyme (4 units)	0.2 μl
MiliQ water	4.8-6.8 μl

2.1.3. Site-directed mutagenesis

Point mutations in the *CgULP2* gene were created by site-directed mutagenesis. For the PCR reaction, the high-fidelity KOD polymerase was employed. Following the reaction, DpnI was used to digest the product. Since DpnI only cleaves at methylated sites, the PCR product remains intact while the template plasmid is consumed. This step is crucial as it prevents the proliferation of colonies derived from the parental template, considering the significantly higher transformation efficiency of circular template plasmids compared to linear PCR products. Following digestion, 10 μl was transformed with ultracompetent cells and incubated for 16 hours at 37°C to form colonies. The primers used to produce the *CgULP2* mutations are listed in Appendix 8.2.

2.1.4. cDNA synthesis and Quantitative Real-Time PCR

C. glabrata cells were grown in YPD at 30°C for 16 hours, it was sub-cultured till it reached an OD₆₀₀ of 1. Cells were treated with DNA damaging agent (0.04% MMS), and hydroxyurea (100mM) and allowed to grow for additional 2 hours. For thermal stress, C. glabrata cells were

shifted to 42°C and incubated for 2 hours. The cultures were then pelleted down and stored at -80°C for RNA extraction.

For RNA extraction, the Ribo Pure kit from Invitrogen was used, followed by cDNA conversion using the SuperScript III First-strand Synthesis System for RT-PCR (Invitrogen) with 1 µg RNA as a template. SYBR green master mix (Invitrogen) was employed for quantitative reverse transcriptase PCR. *Cg-Act-1* was used to normalize RNA levels and also served as endogenous control.

Table 3. Reaction mixture for cDNA synthesis

Component	Volume
5X cDNA synthesis Buffer	4μl
5mM dNTP Mix	2µl
RNA Primer	1µl
RT enhancer	1µl
Verso Enzyme Mix	1µl
Template (RNA)	1-5μ1
Nuclease free water	to 20µ1
Total Volume	20µ1

Before cDNA preparation, the RNA preparations were routinely tested for DNA contamination by performing Act1 PCR. Only DNA-free RNA preparations were used for expression studies. qRT-PCR was used to measure the transcript levels. The fold change was computed using the $\Delta\Delta$ Ct method.

2.2 YEAST GROWTH AND MUTANT STRAIN GENERATION

2.2.1. Genomic DNA isolation

In 5 mL of YPD broth, a single colony of *C. glabrata* was grown for 16 hours. The cells were extracted using a 5-minutes, 3000 rpm centrifugation. Subsequently, 500 µl of breaking buffer (10 mM Tris-Cl pH8.0, 1 mM EDTA pH8.0, 100 mM NaCl, 2% TritonX-100, 1% SDS) was used to resuspend the cell pellet. A 2.0 mL microfuge tube that had been roughly filled with

glass beads to the 200µl mark was then filled with the cell suspension. 200µl of a Phenol: Chloroform: Isoamyl alcohol (25:24:1) solution was mixed to this. After wrapping the tubes with parafilm tape, they were vortexed for two minutes at a high speed. Then, the same tube was filled with 200µl of TE-pH8.0, and it was quickly vortexed for 30 seconds. After five minutes of centrifuging at 13,000 rpm, the top aqueous layer containing DNA was carefully transferred to a sterile microfuge tube. Subsequently, 1 mL of 100% ethanol was added to the tube, and the contents were thoroughly mixed by inversion. The mixture was centrifuged again at 13,000 rpm for five minutes, resulting in the formation of a DNA pellet. The pellet of DNA was left to air dry while the supernatant was disposed off. 40 µl of TE with RNase was used to resuspend the pellet. The DNA quality and concentration were evaluated by agarose gel electrophoresis.

2.2.2. Yeast transformation

The yeast colony was grown overnight in 5 mL of YPD after being inoculated. Cells were harvested by centrifuging them for 5 minutes at 3000 rpm. During the next step, cells were resuspended in sterile double distilled water and pelleted after discarding the supernatant. Further, cells were resuspended in 100mM LiAc and pelleted down again. This pellet was then given 350µl of the transformation mixture.

Table 4. Components of the transformation mixture

Components	Volumes
PEG 3500 50% w/v	240 μ1
LiAc 1 M	36 µl
Single stranded DNA (2mg/ml)	50 μ1
Plasmid DNA 1µg + Double distilled water	24 μ1
The total volume of the transformation mixture	350 μ1

After vortexing the cells to resuspend them, the mixture was put in a thermomixer and incubated it for 40 minutes at 42°C. After centrifuging the cells for 5 minutes at 3000 rpm, the supernatants were removed by pipetting. After being redissolved in 100 µl of distilled water, the pellet was spread out onto a selection plate. After air-drying the plates in a laminar hood, they were incubated at 30°C for two or three days.

2.2.3. Gene disruption in *C. glabrata* strains

The ORFs in *C. glabrata* were disrupted by homologous recombination using a cassette containing the nourseothricin acetyltransferase (*NAT1*) gene, which provides resistance to nourseothricin. This cassette was flanked by 5'- and 3'-UTR regions of the target gene (schematic in appendix 8.4). To initiate this process, the 5'- and 3'-UTRs (about 600 bps) of the target gene were amplified from wild-type genomic DNA . Simultaneously, the *NAT1* gene was amplified from a plasmid with one-half of each of the 5'- and 3'-UTR fused to it. 300–350 bp complementary regions were shared by the two *NAT1*-amplified fragments. After cotransforming the fused PCR products into the wild-type strain, and the transformants were plated onto YPD. Following a 12–16 hour incubation at 30°C to promote homologous recombination between the *NAT1* fragments and the genomic loci, cells were replica-plated onto YPD plates supplemented with 200 mg/ml nourseothricin. These plates were then incubated for an additional 24 hours at 30°C. Colonies resistant to nourseothricin were isolated, and PCR was used to test for gene disruption caused by homologous recombination.

To obtain double deletions, the parental single-deletion strain was subjected to transformation with a plasmid carrying the FLP flippase gene. Transformants exhibiting uracil prototrophy in the CAA medium was selected. The *NAT1* resistance cassette excision is made possible by the flippase enzyme at FRT (Flippase recognition target) sites flanking the *NAT1* gene. The transformants that were sensitive to nourseothricin were isolated and subjected to curing of the FLP flippase-encoding plasmid after four to five passages in a non-selective YPD medium. This was further confirmed in CAA plates for the loss of URA. Cells were then transformed using a linearized segment of the second target gene, which carried the sequence 5'-untranslated region (5'-UTR)-*NAT1* cassette-3'-untranslated region (3'-UTR), and had been PCR amplified from the genomic DNA of a single deletion strain. Colonies that were resistant to nourseothricin were isolated, and a PCR was used to check for target gene disruption.

For complementation assays, the genes for *CgSLX5* (1.52 kb), *CgSLX8* (633bps), and *CgULS1* (4.22 kb) were amplified by PCR from wild-type genomic DNA using the high-fidelity Vent polymerase. Then, at the BamHI-XhoI restriction enzyme sites, these genes were cloned into the pGRB2.2 plasmid, which is located downstream of the PGK1 promoter. The recombinant

plasmids were then transformed into the appropriate deletion mutants for the complementation assay, and the phenotypes were scored.

2.2.4. Plate-based growth assay

C. glabrata wild type and deletion strains were grown in YPD/CAA medium at 30°C until reaching an O.D of 1.0 at A₆₀₀. Then 10-fold serial dilutions were made in 96 well plates. 2-3µl of diluted cell suspensions were spotted onto appropriate plates and incubated for 2-4 days at the required temperatures to evaluate the cell growth.

2.2.5. Biofilm formation

Biofilm formation was performed on a flat-bottomed 24-well polystyrene plate. YPD-grown *C. glabrata* cells in the exponential phase were added to the plate and incubated at 37°C with mild rotation (75 rpm) for 90 minutes. Wells were then washed twice using PBS, followed by the addition of 1ml of RPMI-1640 complete media to each well. The plate was then incubated at 37°C with 75 rpm, for another 24 hours to promote biofilm formation. The next day, 500µl of used media was pipetted out and fresh 500µl RPMI containing 10% FBS was added. The plate was further incubated for 48 to 72 hours. During incubation, every day 500µl of fresh media was replaced to provide continuous nutrients for the growing biofilm. After 72 hours, the plate was washed with PBS to eliminate all the planktonic cells. Cells were then collected in PBS, pelleted down, and stored at -80°C for RNA isolation. XTT assay was used to quantify biofilm formation in wild type and various deletion strains of *C. glabrata*, after 72 hours of biofilm formation, the plate was washed thrice with PBS to remove unattached cells. 100µl of 1x XTT solution was added, and the plate was incubated in the dark for one hour. Absorbance at 492nm was measured, RPMI-1640 complete medium serving as a negative control, and the absorbance of the *Candida*-grown wells was subtracted from this value.

2.2.6. Yeast two-hybrid assay

Yeast two-hybrid assay was used to test and confirm CgUlp2-CgSUMO interaction. The 'bait' which is denoted by *CgULP2* and 'prey', represented by *CgSMT3* were cloned in the pGBDU-C1 and pGAD-C1 vectors respectively. The integrity of both constructs was confirmed by sequencing. The constructs were also checked and evaluated for their GAL4 self-activation

possibilities. Both the constructs containing 'bait' and 'prey' plasmids were then co-transformed in a reporter strain. The reporter strain (PJ694-A) used in the study is equipped with *HIS3* and *ADE2* as reporter genes. Transformants were then selectively cultured on SC-Leu-Ura medium plates and subsequently patched onto SC-Leu-Ura-His and SC-Leu-Ura-Ade plates to confirm the interaction between CgUlp2 and CgSmt3.

2.3. PROTEIN AND RELATED BIOCHEMICAL TECHNIQUES

2.3.1. Whole cell protein extracts from yeast cells by Trichloroacetic acid (TCA)

The TCA method of protein precipitation was used to extract the proteins. *C. glabrata* cells were cultured in the appropriate medium until they reached the exponential phase. Cultures were spun down at 3000 rpm for 5 minutes and glass beads were added to the cell pellet along with 200µl of 20% TCA, and the mixture was vortexed at a high speed for three minutes to lyse the cells. Lysates were collected in a new 1.5 ml Eppendorf tube. Then, two washes of 5% TCA were applied to the tube containing glass beads, followed by three minutes of vortexing, and the lysates were pooled and centrifuged for 10 minutes at 13000 rpm. As a final step, 200µl of Laemmli buffer was used to resuspend the pellet after the supernatant was removed. Then a drop of 2M Tris (unpHed) was added to the buffer till it turned blue to neutralize the acid. To denature proteins, the extracts in Laemmli buffer were boiled at 95°C for five minutes, followed by centrifugation at 3000 rpm for five minutes. The supernatant was then carefully collected in fresh Eppendorf tubes. Protein quality was assessed by running 8-15% SDS-PAGE followed by Coomassie brilliant blue staining for at least an hour and then destaining.

Composition of solutions used:

4X SDS loading dye (Laemmli buffer): 200 mM Tris-HCl pH 6.8, 8% SDS w/v, 40% Glycerol v/v, 6 mM Bromophenol Blue, 4 % β-mercaptoethanol

Coomassie staining solution: Coomassie Brilliant Blue-250- 0.25 g, Methanol-45 ml, Glacial acetic acid (GAA)-10 ml, Water- 45 ml

destaining solution: Methanol-45 ml, Glacial acetic acid-5 ml, Water- 50 ml

2.3.2. SDS- PAGE and Western blot

A standard protocol was followed for casting the gels for SDS-PAGE. A 4% stacking gel was used, and depending on the molecular weight of the targeted protein being examined, the resolving gel ranged from 8 to 15%. Electrophoresis was carried out at 75–80V for the stacking gel and 100–120V once the proteins entered the resolving gel. To monitor the migration, the samples were loaded with pre-stained molecular weight markers. Western blotting was performed using a conventional semi-dry transfer technique to the PVDF membrane after SDS-PAGE. 5% skim milk powder was then used to block the membrane for one hour with. Following blocking, it was incubated with α -flag primary antibody (Sigma, 1:10,000) for 14-16 hours. Further, the membrane was washed thrice with TBST for 10 minutes each before being exposed to a mouse HRP-conjugated secondary antibody (Abcam, 1:20,000) for 1 hour. Following three TBST washes, the blot was developed using Biorad western ECL substrate i.e., luminol and peroxide reagent, and imaged using the ChemiDoc Imaging system to detect the signal through chemiluminescence. Blots were further reprobed with α -tubulin for the loading control.

Ponceau Staining solution was used to stain PVDF membranes to assess the total protein as well as examine the transfer of proteins to the membrane.

Composition of Ponceau Staining solution (100 mL): Ponceau S -100 mg, Water- 95 ml, Glacial acetic acid-5 ml.

2.3.3. Quantification of the western blot

ImageJ/FIJI's Gel Analyzer option was used to perform a densitometric analysis of the chemiluminescence readout following a western blot. The loading control for protein expression, which is typically an antibody to a housekeeping gene-expressed protein, was used to normalize protein expression. Western blots from at least three separate experiments were quantified for protein expression.

2.3.4. Protein expression and purification

We cloned *CgULP2* and *CgSMT3* in both pET28a and pGEX4T1 vectors, which have 6x-Histidine and Glutathione S-transferase (GST) tags. For protein expression, the recombinant plasmids were then transformed into the BL21(DE3)RIL bacterial strain. A single colony was then inoculated in an appropriate volume of LB broth containing the necessary antibiotics and was incubated for 14–16 hours at 37°C and 180 rpm. One percent of the primary culture was then transferred to a secondary culture and incubated at 37°C until it reached an O.D-0.6. Then 1 ml of culture was set aside in a 1.5 ml microfuge tube for further use as a control (uninduced culture) and the remaining culture was induced to overexpress the target recombinant protein using 0.4 mM IPTG. Both induced and uninduced cultures were incubated at 22°C and 180 rpm for 16 hours. Following induction, 1 ml of each induced and uninduced culture was placed in a 1.5 ml microfuge tube and centrifuged at room temperature for one minute at 13,000 rpm. The resulting pellet was resuspended in 100 ul of 1x SDS loading dye and vortexed for one minute at high speed. The samples were boiled at 95°C for 10 minutes. Afterward, protein expression was checked by analyzing both induced and uninduced samples using 8-15% SDS-PAGE with a molecular mass ladder, followed by Coomassie Blue G-250 staining.

Following protein expression analysis, we lysed the cell pellet in lysis buffer, sonicated it for 3 minutes with a 3-second 'on' and 7-second 'off' cycle. The lysate was then centrifuged at 15,000 rpm for an hour to obtain the protein supernatant. The supernatant containing the protein was then incubated with Ni-NTA or glutathione resin for two hours at 4°C. Following incubation, the flow through was discarded, and the resin-bound proteins were washed with wash buffer to remove impurities. Elution of the bound proteins was carried out using elution buffer. The quality of the affinity-purified proteins was assessed using 8–15% SDS-PAGE with an unstained protein marker, followed by Coomassie Blue G-250 staining.

Buffers for purification of 6xHIS-tagged proteins:

Lysis buffer- 25 mM Tris (pH7.5), 350 mM NaCl, 1 mM β ME, 5 mM Imidazole, 0.1% IGEPAL CA-630, and 1 mM PMSF

Wash buffer- 25 mM Tris (pH7.5), 250 mM NaCl, 1 mM βME, and 50 mM Imidazole

Elution buffer- 25 mM Tris (pH7.5), 250 mM NaCl, 1 mM β ME, 1 mM EDTA, 10% glycerol, and 300 mM of imidazole

Buffers for purification of GST-tagged proteins:

Lysis buffer- 25 mM Tris (pH7.5), 350 mM NaCl, 1 mM β ME, 0.1% IGEPAL CA-630, and 1 mM PMSF

Wash buffer- 25 mM Tris (pH7.5), 250 mM NaCl, and 1 mM βME

Elution buffer- 25 mM Tris (pH 7.5), 250 mM NaCl, 1 mM βME, 1 mM EDTA, 10% glycerol, and 10 mM reduced glutathione.

Gel filtration, or size exclusion chromatography, was carried out using SEC buffer containing 25 mM Tris-HCl, pH 7.5, 250 mM NaCl, 1 mM EDTA, 2% glycerol, and 1 mM DTT. This step aimed to eliminate the non-specific proteins that were detected after affinity purification. To separate the purified proteins, approximately 500 μl of the protein sample at a concentration of 2–3 mg/ml was loaded onto a Superdex 200 10/300 GL column (GE Healthcare) that had been pre-equilibrated with the SEC buffer. The purified proteins were separated into fractions, which were then analyzed using 8-15% SDS-PAGE to visualize the protein of interest. The purified proteins obtained from this process were used for the biophysical and functional characterization of the CgUlp2 protein.

2.3.5. Invitro pull-down assay

Invitro pull-down was carried out using Ni-NTA resin beads. Initially, pellets from 1-litre cultures each of bacteria expressing two distinct proteins with two different tags (6xHIS and GST) were co-lysed, combining the cell pellets in 20ml of lysis buffer for each culture. After sonication, the cell lysate was spun at 15,000 rpm for an hour at 4°C. The supernatant was separated and kept for binding with an equilibrated 1ml Ni-NTA column for 2-3 hours at 4°C. Following the incubation, the flow through was removed, and the resin was thoroughly washed with 40 ml of wash buffer to remove nonspecifically bound proteins. Then the bound proteins were eluted from the resin using 1 ml of elution buffer containing 300 mM imidazole (3 times). To test for the interaction of the two proteins, the eluted proteins were separated by SDS-PAGE, followed by western blot analysis using both α -GST and α -His antibodies.

2.3.6. CgUlp2 binding assay

We transformed various constructs of CgUlp2 protein and constructs of various lengths of linear SUMO chains in BL21(DE3)RIL bacterial strain which were expressed and purified as described in the sections above. To investigate the interaction, we incubated 100µg of 1x-SUMO, 2x-SUMO, and 6x-SUMO protein individually, as well as a combination of linear poly-SUMO chains containing these proteins, with 10µl CgUlp2 protein-coupled glutathione resin in 100µl of PBS buffer at 4°C for two hours. Following the incubation period, the beads were subjected to three washes with 200 µl of PBS each to remove any nonspecifically bound proteins. Subsequently, proteins bound to the resin wereeluted by boiling beads at 95°C in 50µl of 1x SDS loading dye. The eluted proteins, as well as the input and flow-through samples, were analyzed using Coomassie staining on a 12% SDS-PAGE gel to visualize the protein interactions.

2.3.7. CgUlp2 protease activity

For testing the protease activity of CgUlp2, WT and SIM mutant of CgUlp2 protein was expressed and purified from bacteria. Additinally, 2x-SUMO and 6x-SUMO substrates were purified from bacteria for use in the assay. In this experiment, 100 µg of each protein construct, whether it was in dimer or hexamer, was mixed with 50 µl of PBS containing 1 mM DTT and 1 µg of either CgUlp2 (WT) or its SIM mutant variant. The reactione were conducted at room temperature, and aliquots of 10 µl were taken at 0, 15, 30, and 60 minute interval after the addition of protein construct. These aliquots were subjected to SDS-PAGE analysis by loading them onto a 12% SDS-PAGE gel. Visualization of the proteins was achieved using Coomassie staining.

2.3.8. Pull down of SUMOylated proteins

To isolate proteins SUMOylated in vivo from *C. glabrata* extracts, a protocol was derived using SUMO-interacting motifs. This method was adapted from M.S. Rodriguez lab ¹¹⁸. SUMO Interacting Motif was cloned tandemly in the pET28a bacterial expression vector, which has a 6xHIS tag at the N-terminus. Initially, we annealed the forward and reverse primers that contained sequences for 2 SIM peptides and utilized them as a template for PCR. In the first PCR round, the forward primer incorporated Nde1, and the reverse primer included a BamH1 site. Following successful PCR amplification, indicative of the presence of the 2 SIM peptide, the

product was digested with Nde1 and BamH1 for direct cloning into the pET28a vector. After confirming the presence of the 2 SIM peptide in the pET28a vector through sequencing, this construct was employed as a template to introduce an additional 2 SIM peptide. This step involved using a forward primer with a BamH1 site and a reverse primer with a Sac1 site. The presence of the resulting 4 SIM peptide was confirmed through sequencing, and the 4 SIM-pET28a construct served as the template for the subsequent round. In the final PCR round, a forward primer with a Sac1 site and a reverse primer with a HindIII site was utilized to generate the next set of 4 SIM peptides. The successful cloning resulted in the tandem incorporation of 8 SIM peptides into the pET28a vector. Following the transformation of these motifs in the BL21(DE3)RIL bacterial strain, they were expressed and purified using the previously described Ni-NTA affinity purification method.

To employ the SIM motif as affinity traps for the pull-down of SUMOylated protein, *C. glabrata* yeast strains containing 3xFLAG-tagged SUMO were cultured at 30°C until they reached O.D-1.4. The cells were then collected by centrifugation at 3000 rpm for 5 minutes at 4°C. The cell pellet was promptly snap-frozen in liquid nitrogen and kept at -80°C until needed. The pellet was first mixed with freshly made, chilled lysis buffer containing protease inhibitors, and the tube was then put in the ice for two minutes. Next, the cell suspension was moved to a 2 mL microfuge tube that had been chilled beforehand and had been filled to about 500 µl with glass beads. A bead beater was used to lyse the cells, with six cycles of a 30-second pulse and a 1-minute ice rest in between to prevent the lysate from overheating. The lysate was spun for 40 minutes at 4°C at 13000 rpm. After collecting the supernatant, the pH of the lysate was assessed, and if it measured below 8, 1 M Tris (unadjusted pH) was employed to bring it to the desired level. A total of 5% of the whole cell lysate was utilized as input; it was then boiled with 1x SDS loading dye and kept at -20°C until needed.

After pre-washing 100µl of Ni-NTA SIM immobilized beads in lysis buffer free of protease inhibitors, the lysate was incubated for 6 hours at 4°C in an end-over-end rotator. The tube was spun at 1000 rpm for five minutes at 4°C to collect the beads. The beads were washed thrice with wash buffer at 1000rpm for two minutes at 4°C. For elution of potentially SUMOylated proteins, beads were incubated in an elution buffer in an end-over-end rotator at 4°C for 10 minutes. The eluates were mixed with 2xSDS-loading dye and subjected to boiling at 95°C for 5 minutes to

denature the proteins. The proteins were then separated on a 10% SDS-PAGE and western blots with anti-FLAG antibody were done to visualize the enrichment of SUMOylated proteins.

Composition of the buffers used:

Lysis buffer- 25 mM Tris (pH7.5), 250 mM NaCl, 0.1% IGEPAL CA-630, 25 mM NEM, and 1x protease inhibitor (complete mini, EDTA-free)

Wash buffer- 25 mM Tris (pH7.5), and 250 mM NaCl

Elution buffer- 25 mM Tris (pH7.5), 250 mM NaCl, and 300 mM of imidazole

Precautions:

All the buffers should be freshly prepared and pre-chilled before use.

All the steps should be performed on ice or 4°C.

2.4. CELL CULTURE

2.4.1. Preparation of THP-1 Macrophage monolayer

Human monocyte, THP-1 cells were seeded in a 25mm culture flask in RPMI-1640 medium supplemented with 10% FBS, 2 mM glutamine, and an antibiotic cocktail, and kept at 37°C in a humidified 5% CO₂. Cells were allowed to grow until a monolayer was formed. Cell density was maintained at 2.5 x 10⁵ cells/ml by counting with a hemocytometer and 1µl of 160mM PMA (prepared in DMSO) was added to 10ml THP-1 cell suspension, resulting in a final concentration of 16nM to stop the cells from further division and to differentiate them into macrophages. After 12 hours of incubation, the old medium containing PMA was replaced with fresh prewarmed RPMI-1640 complete medium. The cells were then allowed to recover for another 12 hours under the same incubation conditions. These macrophage cells were checked under an inverted microscope for their flattened, spindle-shaped, and adherent morphology.

2.4.2. Infection of *C. glabrata* in THP-1 cells

C. glabrata strains were cultured in liquid YPD media at 30°C with 180 rpm of agitation. A cell density of 2.5 x 10⁶ cells/ml was used to infect the cells, maintaining a multiplicity of infection of 1:10. C. glabrata cells were co-cultured with THP-1 macrophages for 2 hours, followed by gently washing several times (3-6 times) using 1 ml of sterile PBS to ensure the complete

elimination of the non-phagocytosed yeast pathogen. Cells were then incubated for 8, 12, and 24 hours to examine the *C. glabrata* cell survival/proliferation.

To quantify internalized yeast, macrophage internalized *C. glabrata* cells were washed and lysed using 1ml of sterile water for 2-3 minutes in the culture plate. Cells were scraped softly and cell lysate was collected. The cells were then serially diluted to 100 folds and 100µl of it was plated on a solid YPD medium followed by incubation at 30°C for 1-2 days. Colonies that appeared on YPD plates, were counted manually, and CFU (colony forming units) was calculated by multiplying with the dilution factor.

2.5. TANDEM MASS TAG (TMT)-BASED QUANTITATIVE TOTAL PROTEOMICS ANALYSIS

2.5.1. Sample preparation

For proteome analysis, exponential phase YPD grown *C. glabrata* cells were pelleted at 3000 rpm, washed once with MiliQ, and suspended in a lysis buffer composed of 50 mM HEPES pH 8.2, 8 M Urea, 50 mM NaCl, and EDTA-free protease inhibitors. Cell lysis was achieved using a Bead-beater in microfuge tubes for six cycles of 30-second duration each, with 1-minute interval between cycles to prevent lysate overheating. Lysates were cleared by centrifugation at 15,000 rpm for 30 minutes at 4°C. The protein concentration was then determined using the Lowry method and 200µg of proteins were run on a 10% SDS-PAGE to check the protein quality which was then sent to Mass Spectrometry (MS) facilities, Institute of Bioinformatics, Bangalore, India. At the MS facility, proteins were acetone precipitated, alkylated, and digested with trypsin.

2.5.2. TMT labeling and mass spectrometry

For TMT labeling, the 12 channels from the TMT pro-16 plex kit were used for labeling the respective samples. Each TMT channel reagent was solubilized in 200µl of anhydrous acetonitrile and allowed to incubate for 5 minutes. Then, 40 ul of respective TMT reagent was added to 80ug of each of the 12 sample peptide mix (dissolved in 40mM TEABC buffer), incubated for 60 mins at RT (after mixing) and the labeling reaction was stopped by adding 5% methylamine solution. An aliquot (5µl) of each of the labeled samples was quenched by adding 8 µl of 5% hydroxylamine, pooled, dried, reconstituted in 0.1% TFA, cleaned up using C18 stage

tip, dried and re-dissolved in LCMS grade water (containing 0.1% TFA and 3% acetonitrile) for labeling efficiency check. After the C18 stage tip clean-up, the sample was dried and dissolved in water (containing 0.1% TFA and 3% acetonitrile) for LCMS analysis to check the labeling efficiency. The labeling efficiency (>95 %) and reporter ion intensity normalization were performed. After the labeling efficiency check, the reaction was quenched using 5% hydroxylamine (for 15 min, at RT). Based on the reporter ion intensity values, each of the labeled samples was pooled, dried, and fractionated using basic pH Reverse phase HPLC into 96 fractions and concatenated into 12 fractions. The final LCMS run was performed (in triplicates) after dissolving the (desalted) 12 fractions in water (containing 0.1% TFA and 3% acetonitrile) and loading 1µg equivalent peptide to the mass spectrometer.

The LCMS analysis was performed using Q Exactive HF-X (Thermo Scientific, Bremen, Germany) interfaced with Dionex Ultimate 3000 nanoflow liquid chromatography system. The acquired mass spectrometry data was analyzed against *C. glabrata* reference proteome (downloaded from the UniProt database) using the SEQUEST search algorithm on the Proteome Discoverer platform (version 2.4, Thermo Scientific). Data was filtered with a 0.01% false discovery rate (FDR) based on the decoy search.

2.5.3. Analysis of gene ontology

The corresponding systematic ORF (CAGL IDs) of *C. glabrata* were achieved from the UniProt database using the accession numbers obtained from the proteins identified through mass spectrometry analysis. These proteins were then mapped to CAGL IDs in the Candida Genome Database. Subsequently, functional enrichment analysis, encompassing biological processes, cellular components, and molecular functions, was conducted using the DAVID tools. The resulting data were visualized through graphs generated using GraphPad Prism and SRplot software.

2.6. Imaging mitochondria in *C. glabrata* cells by confocal microscopy

To study the mitochondrial morphology and reactive oxygen species (mtROS) in wild-type and deletion strains of *C. glabrata*, MitoTracker Green dye (Invitrogen, M7514) and MitoSOX Red (Invitrogen, M36008) were used respectively. Exponential phase cells grown in YPD medium (1.0 A600) were harvested, and the pellet was washed thrice with 1x PBS to get rid of any

remaining YPD medium. After that, cells were treated with 200 nM MitoTracker Green and 1 μM MitoSOX Red in 250μl PBS and allowed to incubate for 20 minutes at 30°C. Following incubation, cells were rinsed with PBSand resuspended in PBS without MitoTracker Green and MitoSOX Red.

Cells resuspended in PBS were placed on a 35mm cover glass bottom dish that had been coated with 0.1% solution of concanavalin A to facilitate imaging. Images were captured using a Leica TCS SP8 confocal microscope equipped with an HC PL APO CS2 63x/1.40 OIL objective. The microscopy data was processed and analyzed using Fiji Software.

2.7. COMPUTER-AIDED DRUG DESIGN

2.7.1 Homology modeling

The crystal structure of the catalytic domain of Ulp2 (PDB Id: 5LNB) and the Smt3 protein (PDB Id: 1EUV) of *S. cerevisiae* were obtained from the Protein Data Bank (PDB). These structures served as a template for homology modeling of the *C. glabrata* proteins Ulp2 and Smt3 using SWISS MODEL. CgUlp2 protein has a sequence identity of 58.57 percent and 96 percent sequence coverage whereas CgSmt3 protein has a sequence identity of 87.88 percent and 92 percent sequence coverage with *S. cerevisiae* counterparts. The models were refined and their energy was minimized using GalaxyWeb and PROCHECK. On PDBsum, the models were evaluated for quality and rated using Ramachandran plots. The identification of key catalytic triad residues in the model was determined through a sequence alignment with those of *S. cerevisiae* and *H. sapiens*.

2.7.2 Protein-protein docking

Protein-protein docking was conducted utilizing the homology-modeled catalytic domain of CgUlp2 and CgSmt3 protein. The ClusPro 2.0 web server generated 22 docked models, which were subsequently ranked based on their weighted scores. From these, the top 10 ranking docked complexes were manually visualized. Models demonstrating direct interactions between CD_CgUlp2 and CgSmt3 via SUMO interacting motif were selected for active site prediction in order to perform pharmacophore-based virtual screening.

2.7.3 Determination of active site on the protein

The active site on CD_CgUlp2-CgSmt3 protein was determined using the DoGSiteScorer application¹¹⁹. It estimates various physicochemical characteristics and predicts active site pockets on the protein. It returns a druggability score between 1-0. Pockets showing the highest druggability score were chosen as active site pockets.

2.7.4 Pharmacophore mapping and virtual screening for ligands

In order to design a suitable ligand, that can fit into the given active site pocket, along with the location and its residues, we need to know the binding nature of the active site pocket. The pharmacophore map of protein gives us the required molecular definitions and structural features, of the pocket. A ligand complementing such features can be virtually screened which will act as a ligand.

The pharmacophore map for the given protein was designed using the 'Phase' module of Schrodinger suite ¹²⁰. Molecular features in terms of placement of aromatic ring, hydrogen bond density electron density are determined. Coordinates of these pharmacophore features were used to screen for ligands using the Pharmit website ¹²¹. It screened ligands from CHEMBL32, Molport, ChemDiv, ChemSpace, MCULE, PubChem, ZINC, LabNetwork, NCI open repository, and 2000 FDA drugs. Lead molecules were screened out of thousands of molecules based on RMSD score (less than 0.5) and MM/GBSA score (less than 0.002).

2.7.5 Protein-ligand docking

Molecular docking for all top 10 ligands was performed with CD_CgUlp2-CgSmt3 protein using the Flare suite of CressetUk software (https://www.cresset-group.com/software/flare/). Protein was prepared by removing excess water molecules and neutralizing ions, following molecular docking at a pre-determined receptor site. Top 10 hits were shortlisted based on docking scores (less than -9.0).

2.7.6 Binding energy calculations

After docking, relative binding energies between ligand and protein are calculated by Average Molecular mechanics generalized by the Born surface area (MM/GBSA) technique. MM/GBSA

calculations in Schrodinger (Prime, version 2.1, Schrodinger, LLC, New York 2022) were used for these calculations ¹²². The binding energy is given by:

$$\Delta G_{bind} = \Delta G_{pL} - (\Delta G_p + \Delta G_{L})$$

here, Protein(P), and ligand (L) form a complex (PL). Protein-ligand complexes from molecular docking were used for the calculation of MM/GBSA. Local optimization feature was used to minimize protein-ligand poses and the OPLS-2005 force field was used in the generalized -Born/Surface Area continuum solvent model for the calculation of the energies of complexes. Complex giving the lowest MM/GBSA score were further shortlisted.

2.7.7 Molecular dynamics simulation

Molecular dynamics (MD) simulation for 10ns was performed for the top 4 hits using the GROMACS simulation program. MD simulation for protein complex (CD_CgUlp2-CgSmt3) and top 3 protein-ligand complexes for 10ns in TIP3P water using CHARMM36 force field was performed. The system was solvated in a truncated octahedral boxes using TIP3P water, with the protein centered within the simulation container, ensuring a minimum distance to the box area of 1 nm to satisfy the minimum image convention. For neutralization of the overall system, NaCl ions were delivered, followed by minimization steps of 5000 using the Steepest Descent algorithm, achieving convergence within the force threshold of 1000 KJ⁻¹ nm⁻¹ to resolve any steric conflict. NVT and NPT ensembles were employed for 100ps and 1000ps at 300K temperature to equilibrize the system and ensure the system is entirely converged for production. The Particle Mesh Ewald (PME) technique was used to compute electrostatic interactions nad forces. Finally, production was executed for 10ns. The generated output was further processed for the calculation of RMSD.

2.8. STATISTICAL ANALYSIS

Using GraphPad Prism software, the data was analyzed using the student's t-test and one-way analysis of variance (ANOVA) with Tukey's test. A statistical significant threshold was set at a p-value of ≤ 0.05 .

Chapter 3 Perturbation of SUMOylation affects the homeostasis of proteins essential for the establishment of successful infection

3.1 INTRODUCTION

Earlier work in our laboratory has established the role of SUMOylation machinery, particularly the *CgULP2* gene, for the pathogenicity of *Candida glabrata*. Deletion of deSUMOylase *ULP2* in *C. glabrata* was shown to be defective in infection and reduces virulence in mice models as well ^{90,116}. Our biochemical studies indicated that loss of *CgULP2* reduced the accumulation of polySUMOylated proteins. We had reasoned that the accumulation of polySUMOylated proteins in *CgULP2* deletion may have led to protein degradation via the SUMO-dependent ubiquitin-mediated protein degradation. This led to our hypothesis that *ULP2* reduces the pathogenicity of the *C. glabrata* due to perturbed protein homeostasis and that is mediated through the STUbL pathway.

In the budding yeast *S. cerevisiae*, accumulation of higher molecular weight polySUMOylated proteins was detected in strains lacking the heterodimer *SLX5* and *SLX8*. These strains also showed sensitivity towards DNA-damaging agents ^{76,113}. They are known as STUbLs because they ubiquitinate the SUMOylated substrate and are found in *Drosophila*, *Schizosaccharomyces pombe*, and mammals. In a SUMO-independent mechanism, the Slx5-Slx8 complex is found to ubiquitinate the target proteins, but SUMOylation can also stimulate the ubiquitylation of some proteins ¹²³. Additionally, damaged DNA in *S. cerevisiae* is shunted to the nuclear pore and repaired through a process involving Nup84 and Slx5/Slx8, highlighting the functional involvement of STUbL in DNA maintenance and repair ¹²⁴.

ULS1 on the other hand is not much explored as STUbL in yeast but the presence of multiple SIM motifs on it suggests its possible role as STUbL. Growth defects were observed in the cells lacking ULS1. In comparison to single mutants of $slx5\Delta$ and $uls1\Delta$, double mutant strains of $uls1\Delta slx5\Delta$ displayed a greater accumulation of SUMOylated proteins. Furthermore, studies have shown the physical and genetic interaction of Uls1 with Slx5-Slx8, where the loss of Uls1 resulted in a decrease in the SUMOylation of Slx5 111,125 . It is also known that human STUbL, RNF4, depleted cells are sensitive to DNA damage and also showed an accumulation of stress granules (SG particles) in the cytoplasm 126 .

STUbLs have not been studied in pathogenic fungi, including *C. glabrata*. We have identified STUbLs in various pathogenic fungi using a computational approach and have experimentally interrogated the importance of STUbLs in the normal physiology and pathogenesis of *C. glabrata*.

3.2 RESULTS

Identification of SUMO-targeted ubiquitin ligases in Candida glabrata

In our previous work, we identified the homologs of the components of SUMOylation pathway in fungi ⁹⁰. Here, we identified the SUMO-targeted ubiquitin ligases (STUbLs) pathway across fungi. To identify orthologs in selected fungi, we retrieved the sequences of STUbL proteins, namely Slx5, Slx8, and Uls1, in *Saccharomyces cerevisiae* from the Saccharomyces Genome Database (SGD). Fungal organisms representing the five major phyla (Ascomycota, Basidiomycota, Chytridiomycota, Mucoromycota, and Microsporidia) were selected for analysis. For each protein, homologs were obtained by performing BLASTp against the NCBI nr database restricted to each of the organisms considered ¹²⁷. The top hits (RefSeq hits) obtained in the BLASTp analysis were then assessed by using reciprocal BLAST analysis (BLASTp restricted to *S. cerevisiae* S288c sequences) to identify true orthologs. Only the hits that returned the *Saccharomyces cerevisiae* query protein as the top hit were considered true orthologs. The sequences that did not give the *S. cerevisiae* protein in the rBLAST were excluded. In some cases where no orthologs were identified using *S. cerevisiae*, we used sequences from *S. pombe*, or *C. albicans* to identify orthologs.

This pathway is highly conserved in fungi and homologs of Slx5, Slx8, and Uls1 proteins could be identified. Slx5 and Slx8 were identified in a few organisms using *S. cerevisiae* sequences. For some fungal organisms, Slx8 orthologs could be detected using *C. albicans* and *S. pombe*. Few of them were found to have multiple Slx8 orthologs with *S. commune* having 4 orthologs, *C. dubliniensis* having 3 orthologs, and *L. maculans*, *C. graminicola*, *C. albicans*, *C. tropicalis*, *C. orthopsilosis*, *K. phaffii*, *C. neoformans and P. graminis* having 2 orthologs each (Table 5).

A single Uls1 ortholog is present in most of the organisms except in *B. cinerea*, *S. pombe*, *S. punctatus* which have two orthologs. In Microsporidia, Slx8 orthologs were identified in *E. intestinalis*, *E. hellem* and *O. colligate* and two orthologs of Slx8 were detected in *E. intestinalis* and *O. colligate* using *C. albicans* sequence. Interestingly, though Uls1 orthologs are more widespread across fungi, no ortholog could be identified in any of the Microsporidia shortlisted in our study. To summarise, all fungi have at least one and often both of the STUbLs, Uls1 and Slx8. Slx5 seems to be less conserved than Slx8 and Uls1 and is restricted to a few classes only (Table 5).

To further characterize the SUMO-targeted ubiquitin ligases (STUbLs) in *C. glabrata*, we compared homologies between the *S. cerevisiae and C. glabrata proteins*. Table 6 displays their percent similarity across the complete protein sequence. Uls1 is the most conserved of them, having a 60% similarity between *C. glabrata* and *S. cerevisiae* (Table 6). Both the Slx5 and Slx8 share over 45% protein sequence similarity between *C. glabrata* and *S. cerevisiae*, respectively. Additionally, STUbLs have conserved RING domains. Slx5 and Slx8 lack the "SNF2-like translocase" domain, which Uls1, a large protein with 1408 amino acids, has in addition to the SIM motif and RING domain (Figure 5).

Table 5. Orthologs of SUMO targeted Ubiquitin Ligases (STUbLs) across fungi.

Phylum	Class	Fungal Organisms	Slx5	Slx8	Uls1
Ascomycota	Eurotiomycetes	Aspergillus fischeri			
Ascomycota	Eurotiomycetes	Aspergillus nidulans			
Ascomycota	Eurotiomycetes	Microsporum canis			
Ascomycota	Dothideomycetes	Leptosphaeria maculans			
Ascomycota	Dothideomycetes	Parastagonospora nodorum			
Ascomycota	Leotiomycetes	Botrytis cinerea			
Ascomycota	Leotiomycetes	Sclerotinia sclerotiorum			
Ascomycota	Sordariomycetes	Fusarium graminearum			
Ascomycota	Sordariomycetes	Colletotrichum graminicola			
Ascomycota	Sordariomycetes	Chaetomium globosum			
Ascomycota	Sordariomycetes	Thielavia terrestris			
Ascomycota	Sordariomycetes	Neurospora crassa			
Ascomycota	Sordariomycetes	Magnaporthe oryzae			
Ascomycota	Pezizomycetes	Tuber melanosporum			
Ascomycota	Saccharomycetes	Candida albicans			
Ascomycota	Saccharomycetes	Candida dubliniensis			
Ascomycota	Saccharomycetes	Candida tropicalis			
Ascomycota	Saccharomycetes	Candida parapsilosis			
Ascomycota	Saccharomycetes	Candida orthopsilosis			
Ascomycota	Saccharomycetes	Candida auris			
Ascomycota	Saccharomycetes	Candida glabrata			
Ascomycota	Saccharomycetes	Saccharomyces cerevisiae			
Ascomycota	Saccharomycetes	Zygosaccharomyces rouxii			
Ascomycota	Saccharomycetes	Kluyveromyces lactis			
Ascomycota	Saccharomycetes	Eremothecium gossypii			
Ascomycota	Saccharomycetes	Komagataella phaffii			
Ascomycota	Schizosaccharomycetes	Schizosaccharomyces pombe			
Basidiomycota	Agaricomycetes	Trametes versicolor			
Basidiomycota	Agaricomycetes	Schizophyllum commune			
Basidiomycota	Agaricomycetes	Agaricus bisporus			
Basidiomycota	Tremellomycetes	Cryptococcus neoformans			
Basidiomycota	Ustilaginomycetes	Ustilago maydis			
Basidiomycota	Pucciniomycetes	Puccinia graminis			
Mucoromycota	Glomeromycetes	Rhizophagus irregularis			
Chytridiomycota	Chytridiomycetes	Spizellomyces punctatus			
Chytridiomycota	Chytridiomycetes	Batrachochytrium			
		dendrobatidis			
Microsporidia	Microsporidia	Encephalitozoon intestinalis			
Microsporidia	Microsporidia	Encephalitozoon cuniculi			
Microsporidia	Microsporidia	Encephalitozoon hellem			
Microsporidia	Ordosporidae	Ordospora colligate			
Microsporidia	Nosematidae	Nosema ce <u>r</u> anae			
		als are in red font nathogenic			

The organisms that are pathogenic to animals are in red font, pathogenic to plants are in green font and those that are pathogenic to both animals and plants are in yellow font. The presence

and absence of orthologs identified for proteins are shown. Light green-filled rectangles represent the presence of a single ortholog and red-filled rectangles represent the absence of an ortholog. Likewise, dark green filled rectangles represent the presence of 2 orthologs, light blue represents 3 orthologs, and dark blue represents 4 orthologs.

Table 6. Orthologs of the S. cerevisiae STUbL proteins Slx5, Slx8, Uls1 in Candida glabrata.

Saccharomyces cerevisiae	Candida glabrata	% similarity	% Identity
SLX5 (619) RING domain : 527-604 SIM : 24-28, 93-97, 116-119, 155-159, 476-479	CAGL0K01881g (506) RING domain: 431-460 SIM: 10-13, 34-38, 140-143, 309-312	49.4	35.3
SLX8 (274) RING domain : 206-250 SIM : 178-181	CAGL0G03553g (210) RING domain: 146-194 SIM: 24-27, 124-127	48.6	34.4
ULS1 (1619) RING domain: 1330-1386 SIM: 7-10, 371-374, 470-473, 540-543 SNF2: 956-1157 Helicase C: 1428-1605	CAGL0G09493g (1408) RING domain : 1118-1176 SIM : 216-219, 253-256, 836- 839, 1325-1328, 1368-1371 SNF2 : 736-1070 Helicase C : 1232-1348	60.0	46.5

The Saccharomyces Genome Database was used to collect *S. cerevisiae* proteins, and Blastp was used to determine which *C. glabrata* proteins served as orthologs. Pfam was used to search the protein sequences for annotated domains. The EMBOSS Stretcher (pairwise sequence alignment) tool was used to calculate the percentages of identity and similarity.

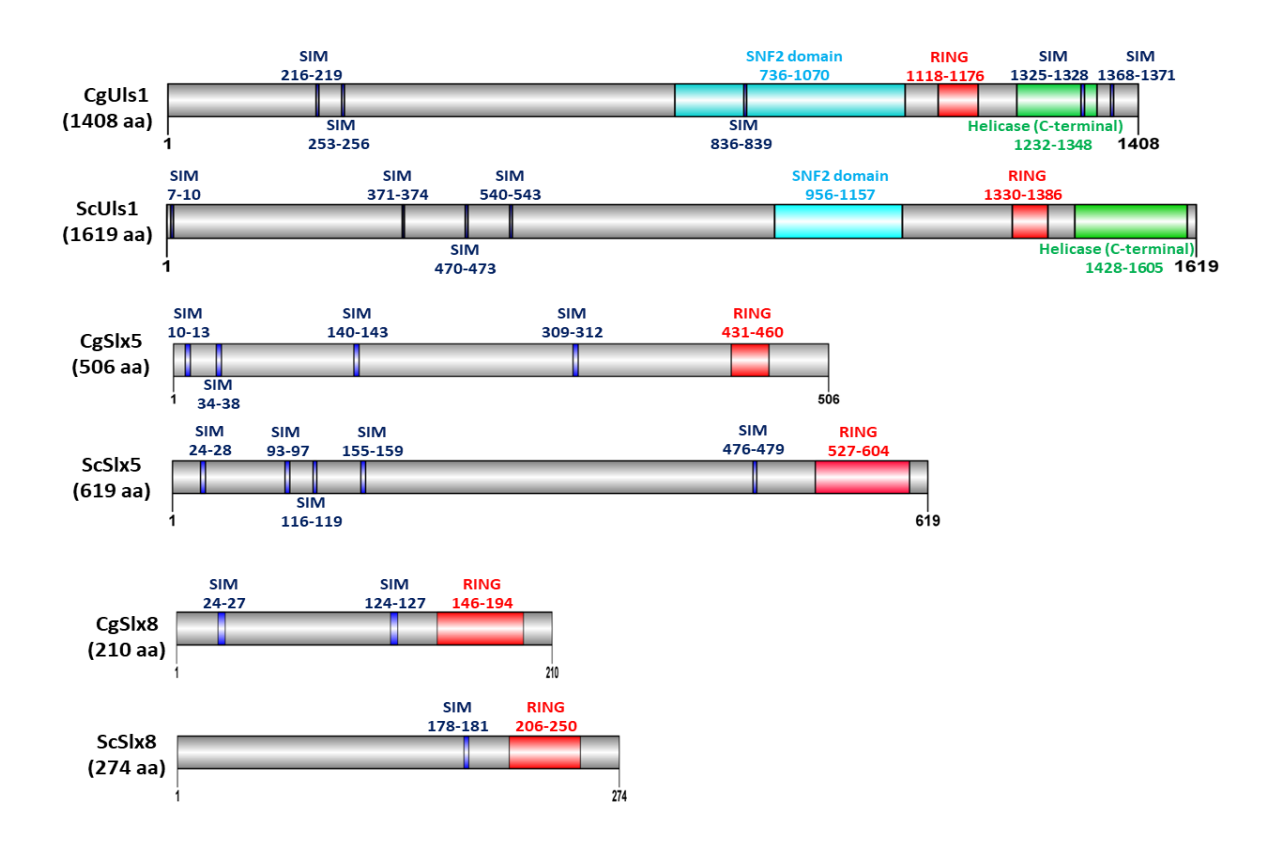


Figure 5. Schematic representation of orthologs of the *S. cerevisiae* STUbL proteins Slx5, Slx8, Uls1 in *Candida glabrata*. Using IBS 1.0, maps of proteins and their domains were produced.

STUbLs in the physiology and pathology of C. glabrata

We generated STUbL-deficient strains of C. glabrata to study the impact of STUbL disruption on the physiology and pathogenicity of the organism. Using a fusion PCR and homologous recombination-based method, we were able to create deletion strains for the CgSLX5, CgSLX8, and CgULS1 genes. In order to better understand inter-STUbL interactions and STUbL interaction with CgULP2 in the pathobiology of C. glabrata, we also created double deletion strains of STUbLs and STUbLs with CgULP2. In this context, while we could create all combinations of these double mutants, we could not obtain $Cgslx8\Delta Cguls1\Delta$ double mutant despite several attempts. We believe that the loss of both the conserved STUbLs may be lethal to the cell. As shown in Table 5, all fungi have at least one of these two STUbLs, underscoring the importance of this pathway for survival.

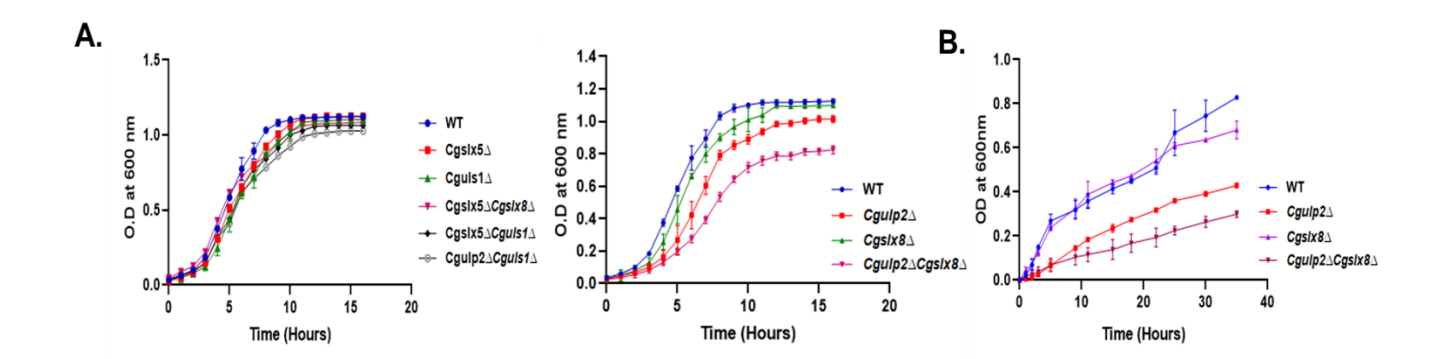
We first performed the phenotypic characterization of the STUbL mutants in C. glabrata to study the role of SUMO-targeted ubiquitin ligases in cell physiology. Growth analysis of single deletion strains of $Cgulp2\Delta$, $Cgslx5\Delta$, $Cgslx5\Delta$, $Cgslx8\Delta$, and $Cguls1\Delta$, as well as double deletion strains of $Cgslx5\Delta Cgslx8\Delta$, $Cgslx5\Delta Cguls1\Delta$, $Cgulp2\Delta Cgslx8\Delta$, and $Cgulp2\Delta Cguls1\Delta$, confirmed that the mutant strains of $Cgulp2\Delta$ grew slower than the wild-type (WT). In addition to that, $Cgulp2\Delta Cgslx8\Delta$ double mutant grew much slower as compared to WT and $Cgulp2\Delta$ in both YPD and RPMI complete medium even at conducive temperatures (Figure 6A-B). All other strains did not have any growth defects in these conditions.

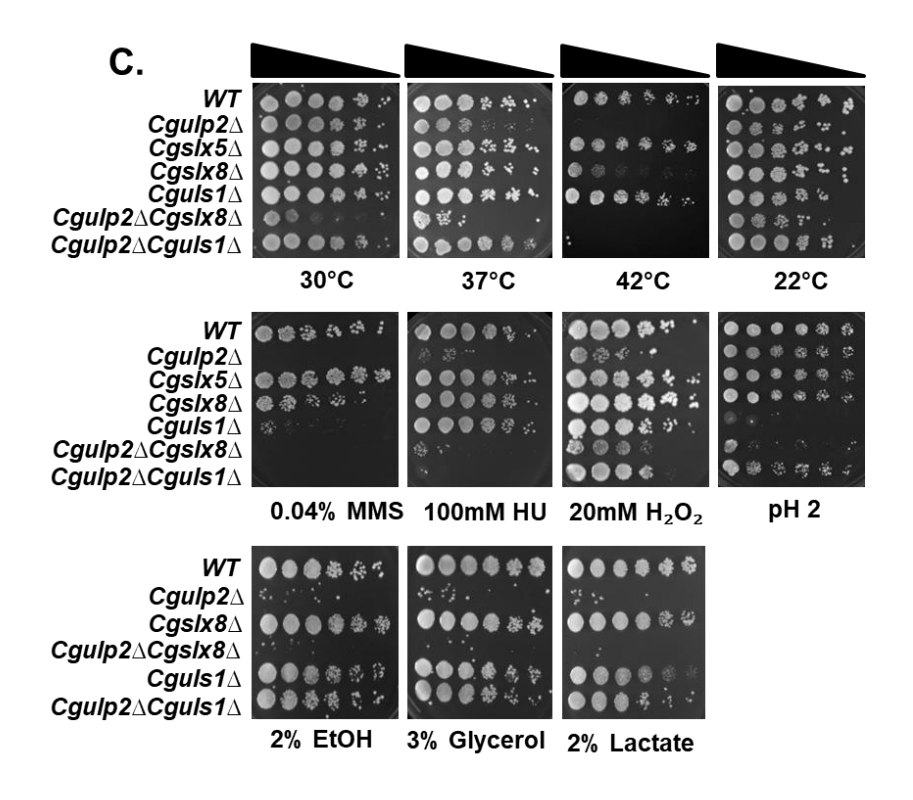
Earlier studies have shown that $Cgulp 2\Delta$ mutant grew slowly at 42°C and was vulnerable to the DNA-alkylating agent methyl methanesulfonate (MMS), replication fork staller hydroxyurea, and oxidative stress-inducing agent hydrogen peroxide (Gujjula et al., 2016). In this study, compared to WT cells, Cguls 1\Delta showed more sensitivity to DNA-damaging stress conditions (0.04% MMS) and $Cgslx8\Delta$ was sensitive to a higher temperature (42°C) which could be rescued by ectopic expression of CgULS1 and CgSLX8, respectively (Figure 6C-E). Contrary to both the mutants, the growth of the $Cgslx5\Delta$ mutant remains unaffected under diverse stress conditions. In addition, both $Cgslx5\Delta Cguls1\Delta$ and $Cgulp2\Delta Cguls1\Delta$ double mutants were temperaturesensitive for growth at 42°C and were more sensitive to 0.04% MMS when compared with WT but similar to the single $Cguls 1\Delta$ (Figure 6D). Interestingly, $Cgulp 2\Delta Cguls 1\Delta$ double mutants suppressed the phenotype of $Cgulp2\Delta$ single mutant in oxidative stress (20 mm H_2O_2), nonfermentable carbon sources (2% ethanol, 3% glycerol, 2% lactate, and 2% sodium acetate) and DNA damage (0.03% MMS) respectively. Cgulp2\Delta Cgslx8\Delta grows poorly even at 30°C compared to either single mutants while at low temperature (22°C), it appears to grow better than at 30°C. But it still grows poorly compared to all other strains at 22°C (Figure 6C-D). Cguls 1\Delta, $Cgslx5\Delta Cgslx8\Delta$, $Cgslx5\Delta Cguls 1\Delta$, and $Cgulp2\Delta Cgslx8\Delta$ were sensitive to acidic pH as well (Figure 6D).

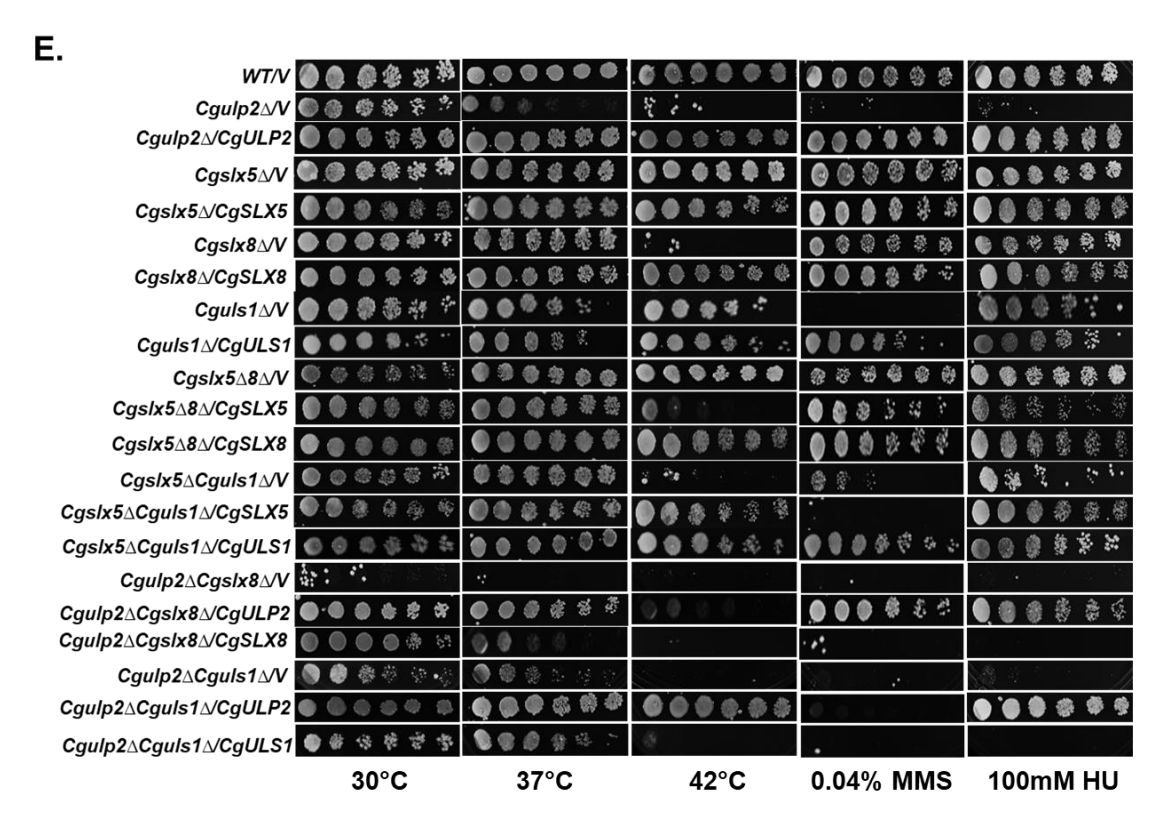
S. cerevisiae strains with $slx5\Delta$ and $slx8\Delta$ deletion are sensitive to cell membrane stress (0.03% SDS) ¹²⁸. However, unlike S. cerevisiae, neither the single nor the double mutants of STUbLs of C. glabrata were sensitive to SDS. The phenotypes of increased sensitivity of single and double deletion strains of SUMO-targeted ubiquitin ligases to various stress conditions were rescued by ectopic expression of either CgULP2 and STUbL genes, indicating,

indeed, the phenotypes observed are due to loss of STUbLs (Figure 6E). In summary, these data show that the loss of slx5 has minimal effect on the various conditions tested here; $slx8\Delta$ exacerbates multiple phenotypes of $ulp2\Delta$ and $uls1\Delta$ suppresses the sensitivity of $ulp2\Delta$ to several stress conditions.

As the loss of STUbLs had differential sensitivities to various stress conditions tested here, it is possible that they are specifically required to combat these conditions. Therefore, we analyzed the expression of the SUMO protease CgULP2 and STUbL genes under thermal stress (42°C), DNA-alkylating agent methyl methanesulfonate (0.04% MMS), and replication fork staller hydroxyurea (100mM HU). In the aforementioned stress conditions, the lack of CgULP2 caused significant growth anomalies and we found that the expression of CgULP2 was increased in wild-type cells under these conditions (Figure 6F). Similarly, CgSLX8 was upregulated at high temperatures and CgULS1 was upregulated when exposed to MMS, again conditions in which loss of these genes showed poor growth. CgSLX5, CgSLX8, and CgULS1 genes were down-regulated in response to hydroxyurea treatment and no phenotype was seen upon treatment in deletion of these genes. (Figure 6F). These findings collectively suggest that specific SUMO-targeted ubiquitin ligases are essential for resistance to heat and DNA damage.







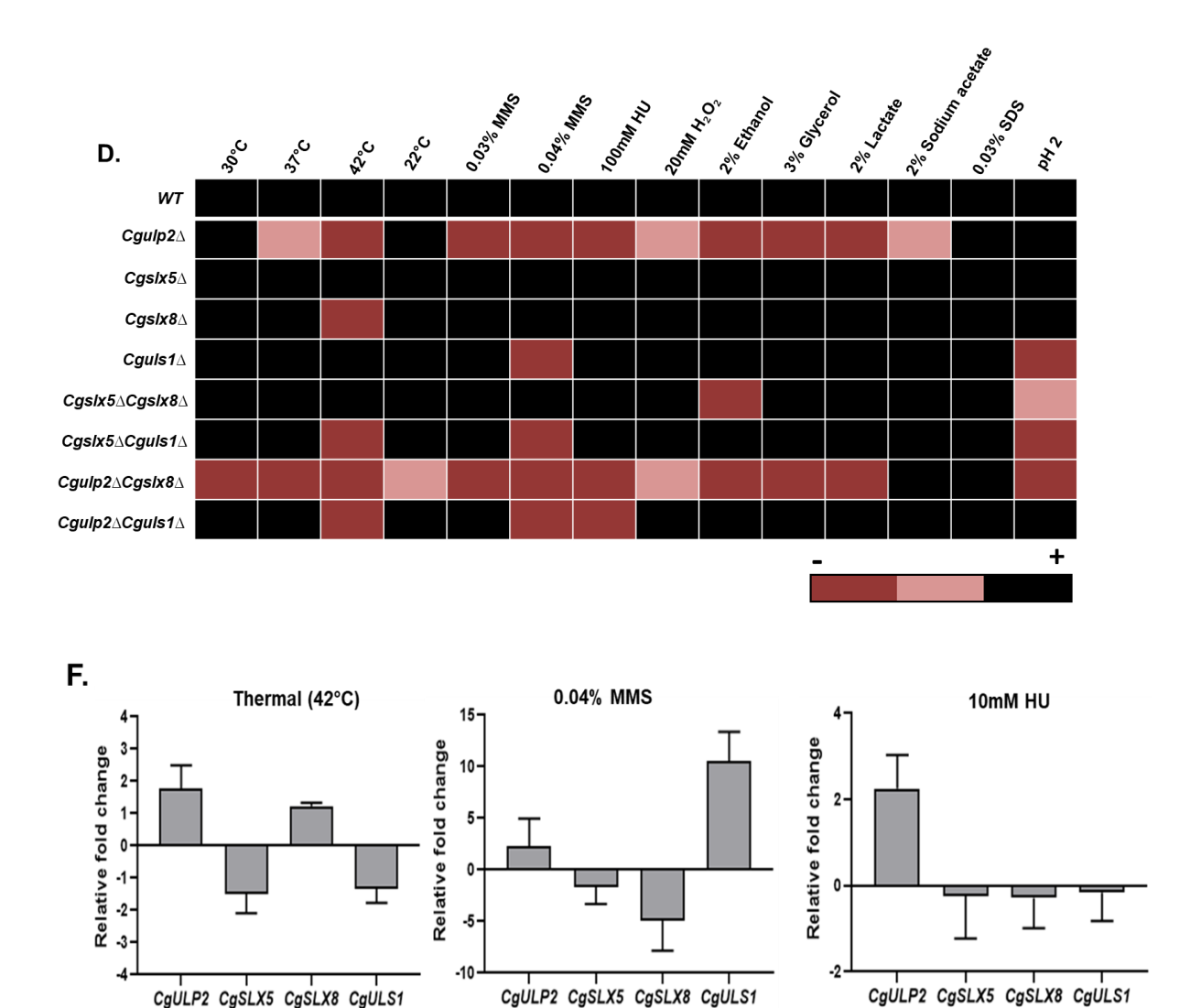


Figure 6. STUbL genes are crucial in the maintenance of cellular homeostasis. Analysis of growth of STUbL deletion strains. Overnight grown cultures of indicated *C. glabrata* strains were inoculated in (A) YPD and (B) RPMI complete medium to an initial A600 of 0.1. Absorbance at 600nm was measured. Data represent the mean of triplicates. C. Sensitivity of the STUbL deletion strains under various stress conditions. 3μl of ten-fold serial dilutions of overnight grown cultures were spotted on indicated plates and images were taken after 2-4 days of incubation. D. Heat map illustrating cell growth of STUbL mutants in the presence of diverse stress-causing agents. The sensitivity of STUbL mutants of *C. glabrata* to various treatments is represented as a heat map with black color (not sensitive; full growth) and different shades of red color (dark red indicates a high level of sensitivity and light red indicates a low level of sensitivity). E. Complementation assay of STUbL mutants where strains were transformed with

plasmids encoding the indicated genes and plated on appropriate plates **F.** Expression of SUMO protease and STUbL genes under selected stress conditions, namely, 42°C, 0.04% MMS, 10mM HU, was examined by performing qRT-PCR. Data was normalized with untreated wild-type cells. Data represents the mean and standard deviation of three independent experiments.

Biofilm formation by *C. glabrata* on the biotic (body tissue) and abiotic (plastic and medical devices) surfaces are major virulence factors ¹²⁹. We therefore tested the ability of these mutants to form biofilm and compared them with wild-type strains. Interestingly, all single mutants of STUbLs had reduced capacity to form biofilms, and the double mutants of $Cgulp2\Delta Cgslx8\Delta$ were more compromised than either single mutant (Figure 7A). $Cgulp2\Delta Cguls1\Delta$ on the other hand formed a biofilm similar to that of WT. This follows the same trend we have observed for stress conditions tested and discussed above that $Cgulp2\Delta Cguls1\Delta$ tends to mitigate the effects of $Cgulp2\Delta$.

Further, to assess if these phenotypes indicated the requirement of these gene products for biofilm formation, we checked the expression of deSUMOylating enzyme CgULP2 and STUbL (CgSLX5, CgSLX8, and CgULS1) genes in biofilms. CgULS1 was found to be highly upregulated which was followed by CgULP2 (Figure 7B). This observation was in correlation with the biofilm formation assay where a single mutant of $Cgulp2\Delta$, $Cgslx5\Delta$, $Cgslx8\Delta$, and $Cguls1\Delta$ showed reduced biofilm formation, suggesting that deSUMOylase CgULP2 and STUbLs function is important for biofilm formation.

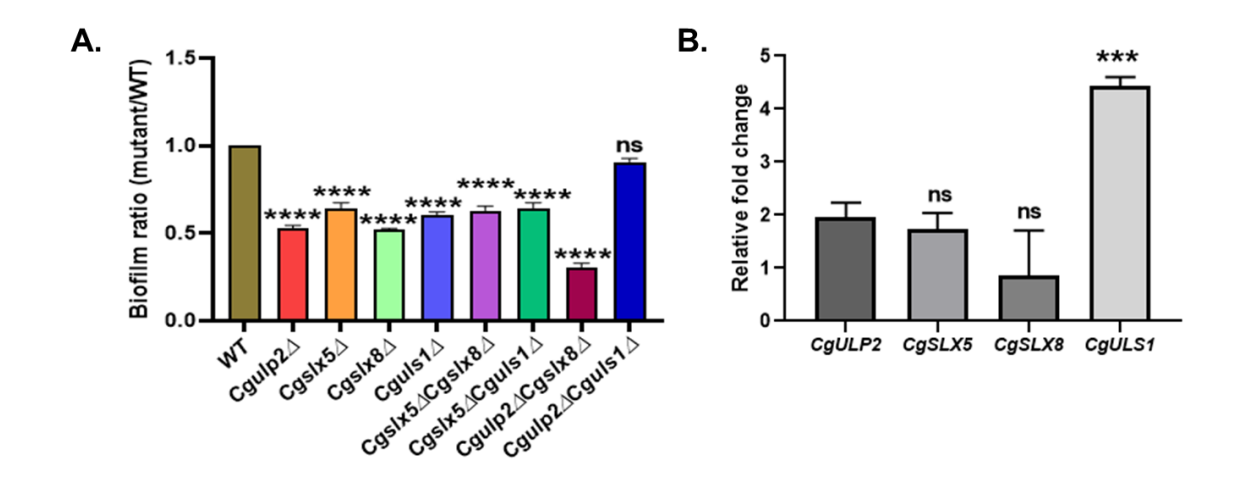


Figure 7. Biofilm in *C. glabrata* mutants. A. Biofilm formation was recorded for *C. glabrata* mutants vs wild type using XTT assay. Data represent the mean and SD of three independent experiments and significance was calculated with respect to WT (****, $p \le 0.0001$; ns, non-significant, two-tailed unpaired Student's t-test). B. Biofilm formation from the wild-type cells was used for RNA isolation and cDNA conversion. RT-PCR was then performed to check the expression level of SUMO protease CgULP2 and STUbL genes. The experiment was done in triplicate and the mean was plotted. The error bar shows the standard deviation of the mean and statistical significance was obtained using one-way ANOVA (****, p < 0.0005).

STUbLs are essential for the survival of *C. glabrata* within the macrophage

The studies described above suggest a crucial role for STUbLs in the physiology of *C. glabrata*. We wanted to ask now if survival in host cells also required STUbL function. To study this, we investigated the survival of STUbL mutants in macrophages using the colony-forming unit (CFU) assay. In parallel, we also investigated growth in the RPMI medium, which is closer to the human physiologic milieu than YPD. Except for $Cgulp2\Delta$ and $Cgulp2\Delta Cgslx8\Delta$, mutants were replicating as like WT when grown in YPD as expected. In contrast, growth in RPMI medium was 6 to 8 fold lower than in YPD medium for $Cgulp2\Delta$ and all the STUbL single and double mutants as compared to the wild type (Figure 8A-D).

To test for survival in macrophages, cultured human THP-1 macrophages were infected with equal numbers of wild-type, $Cgulp2\Delta$, and STUbL mutants. Internalized C. glabrata were then extracted from the macrophages at the indicated time points and plated on a YPD solid medium to obtain the live cell count. Based on our previous studies, we know that after 8 hours, C. glabrata cells start to divide and multiply in numbers and this was captured in the WT infections in this experiment as well. However, we observed that the survival and replication of all the internalized STUbL mutants of C. glabrata were much less than the wild type (Figure 8E-F). The reason for the reduced propagation of C. glabrata cells in macrophages might be due to the cell's inability to grow in culture conditions or vulnerability towards oxidative stress.

The above data indicate that CgULP2 and STUbLs may be required for replication in the macrophages. So we tested if these genes were induced upon infection, which could be an indication of their importance in these conditions. The expression of deSUMOylating enzyme

CgULP2 along with STUbL genes CgSLX5, CgSLX8, and CgULS1 was measured by qRT-PCR at different time points after adding yeast cells to macrophage culture. Figure 8G shows the time course of changes in expression during the infection condition. As can be seen, the expression of CgULP2 is upregulated as early as 2 hours of infection, which remained high up to 24 hours. Importantly, expression of CgSLX5, CgSLX8, and CgULS1 was also found to be induced; while the CgSLX5 and CgSLX8 transcripts show a modest increase, CgULS1 had higher levels of expression (Figure 8G). Notably, these findings are also corroborated with the prior CFU assay, which revealed that a single mutant of $Cgulp2\Delta$, $Cgslx5\Delta$, $Cgslx8\Delta$, and $Cguls1\Delta$ had reduced intracellular proliferation and had a low CFU count (Figure 8E-F). This outcome indicates the key role played by CgULP2 and STUbLs during infection. In other words, it supports the notion that CgULP2, CgSLX5, CgSLX8, and CgULS1 are involved in the survival and proliferation of the pathogen in the host cells.

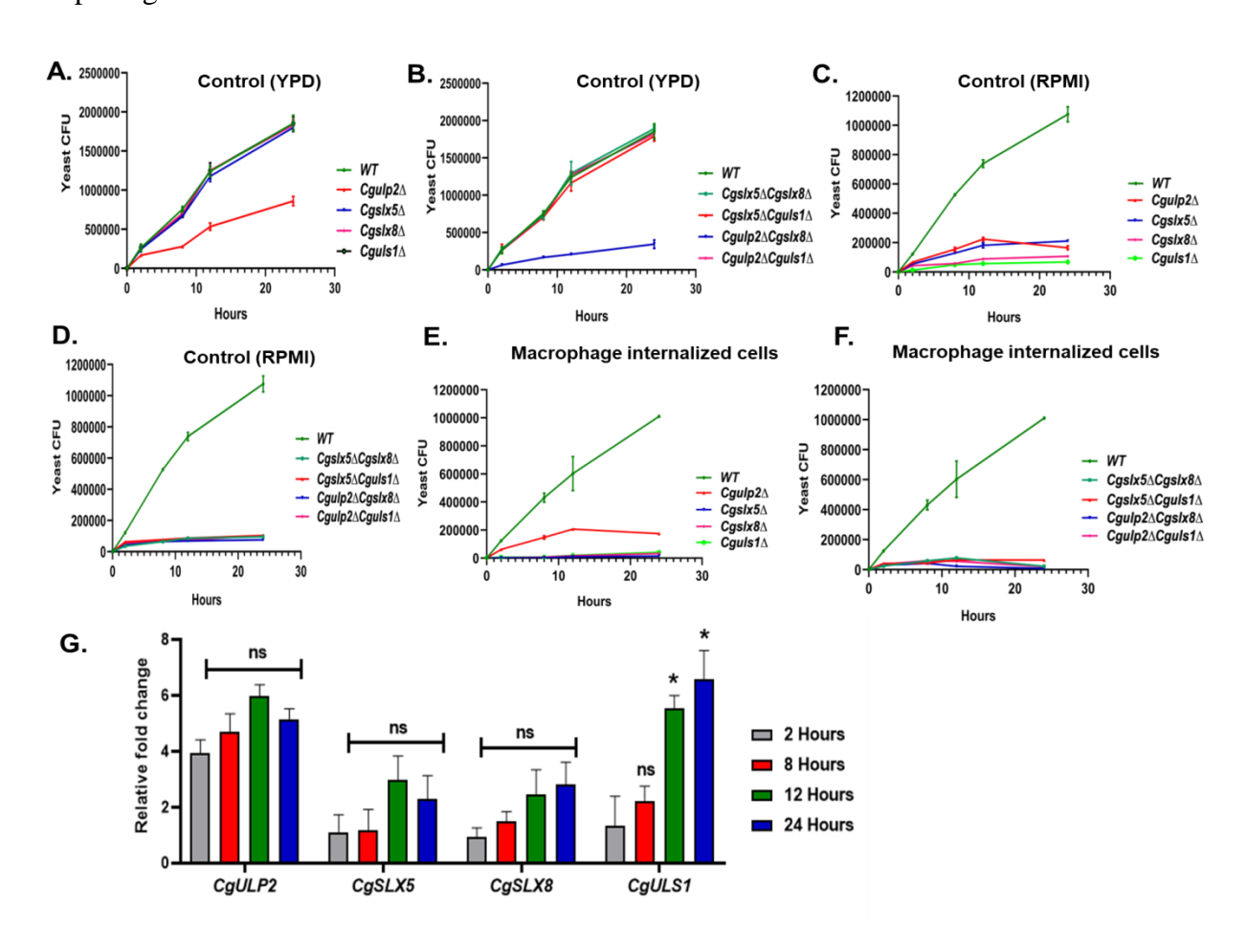


Figure 8. Reduced survival and replication inside macrophage by STUbL mutants of C. glabrata. A, B, C, and D. CFU assay was used to assess cell proliferation of the indicated C. glabrata strains in YPD and RPMI-1640 medium containing 10% FBS (fetal bovine serum). E. and F. 2.5*10^6 C. glabrata strains were added to phorbol 12-myristate 13-acetate-differentiated THP1 cells in a 24-well plate, and non-phagocytosed C. glabrata cells were removed after 2 hours. Intracellular yeast cells were recovered at the indicated time intervals by lysing THP-1 cells in water and plating appropriate dilutions of lysates on the YPD medium. After 24 - 48 hours of incubation at 30 °C, yeast colonies were counted. Data represents the mean and SD of three independent experiments. G. Expression of STUbL genes in internalized C. glabrata cells by qRT-PCR. RNA was extracted from C. glabrata isolated from macrophages at the indicated time intervals, cDNA prepared and expression of CgULP2 and STUbLs was measured. Data represent the mean and standard deviation of three independent experiments (*, p \leq 0.01; ns, non-significant, two-tailed unpaired Student's t-test).

STUbL mutants in C. glabrata have differential SUMOvlation pattern

Loss of function of CgUlp2 was earlier shown to reduce the amount of SUMOylated proteins 90. We had reasoned that accumulation of polySUMOylated protein led to increased degradation of proteins via the SUMO-targeted Ubiquitin ligases, and that is why lower levels of SUMOylated protein were detected. Therefore, we hypothesized that double deletion strain of both Cgulp2 and STUbLs will lead to the retention of higher levels of polySUMOylated proteins. In order to determine the SUMO proteome in each of the STUbL mutants, we used an anti-FLAG antibody to perform western blots on whole cell lysates from the C. glabrata STUbL mutants augmented with dual tagged CgSmt3 protein (carrying His6 and FLAG epitopes at the N-terminus). The lack of higher molecular weight SUMOylated proteins in the Cgulp2Δ mutant was confirmed (Figure 9). Whereas in the case of STUbL single mutants, only $Cgslx5\Delta$ was found to have higher molecular weight SUMOylated protein (Figure 9). In principle, STUbL deletion strains should accumulate higher molecular weight polySUMOylated proteins as polySUMOylated proteins cannot be degraded ⁷⁹. The absence of such a prominent accumulation of polySUMOyalted proteins suggests that in the absence of one of the STUbLs, another might compensate. This could be the reason for the absence of polySUMOylated proteins in the $Cgslx8\Delta$ and $Cguls1\Delta$ single mutants. Interestingly, accumulation of polySUMOylated

proteins was seen in the double mutants of $Cgulp2\Delta Cguls1\Delta$, and $Cgslx5\Delta Cguls1\Delta$ (Figure 9, Lane 7 and 9). This suggests that Uls1 could be the primary ubiquitin-ligase for many of the SUMOylated proteins that escape deSUMOylation in the absence of CgUlp2. Of note, we have demonstrated that $Cgulp2\Delta Cguls1\Delta$ double mutant was able to restore $Cgulp2\Delta$ mutant growth under a variety of stress conditions (Figure 6C-D) and interpret the appearance of these SUMOylated proteins as a reason for the restoration of growth in the double mutant. Importantly, the $Cgulp2\Delta Cgslx8\Delta$, which had exacerbated the $Cgulp2\Delta$ phenotypes, not only grew very slowly, but it also had the least amount of SUMOylated protein, suggesting enhanced degradation of proteins.

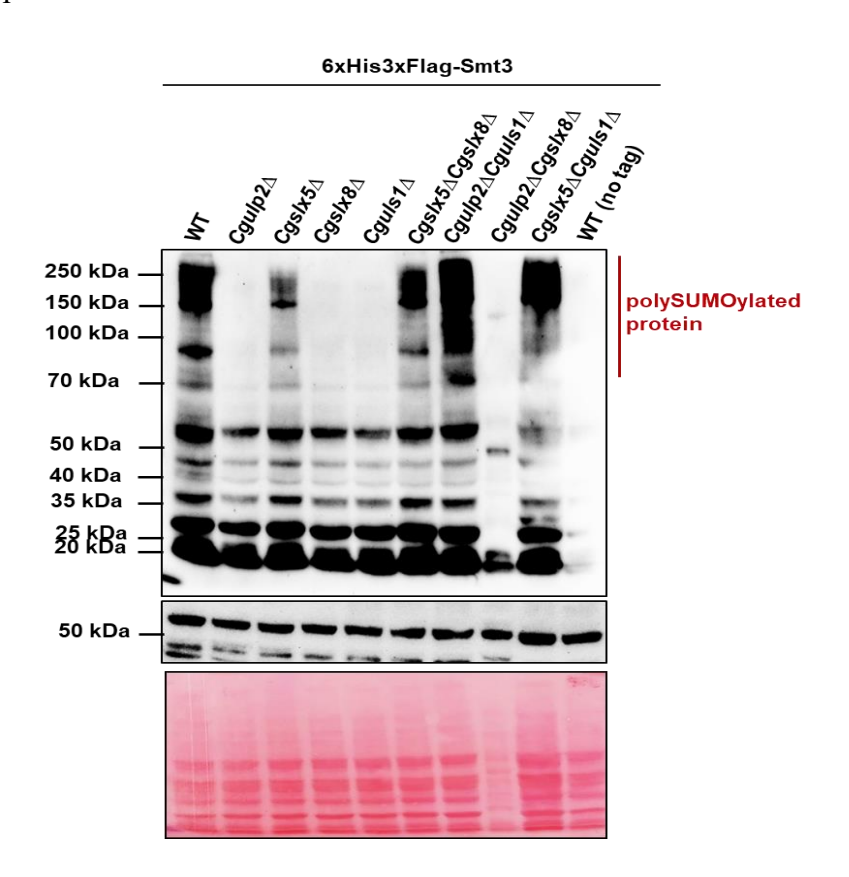


Figure 9. Differential SUMOylation pattern was shown by STUbL mutants of C. glabrata. Strains were grown in a YPD medium and an equal number of cells were taken for whole-cell extracts. Tubulin was used as a loading control. Blot stained with Ponceau S to show the level of protein degradation in $Cgulp2\Delta Cgslx8\Delta$ double mutant in comparison to WT and other mutants.

Each of these enzymes affects growth phenotypes and polySUMOylated products differently. Based on these observations, we reason that because the polySUMOylated proteins are not degraded when Cguls1 is lost in the $Cgulp2\Delta$ mutants, the $Cgulp2\Delta$ growth phenotype is suppressed. On the other hand, $Cgulp2Cgslx8\Delta$ cells lose more protein as seen in the western blot, and get sicker (Figure 9). Based on this and the observation that single mutants of STUbLs do not accumulate polySUMOylated proteins, we hypothesize that Cgslx8 deletion possibly upregulates CgUls1 activity and leads to increased protein degradation. An alternative explanation is that CgUls1 is the main STUbL, however, several essential proteins required for strong growth may be degraded in the $Cgslx8\Delta$ mutant leading to compromised growth in this double mutant.

CgUls1 protein is upregulated in STUbL mutants

To test whether CgUls1 is upregulated in Cgslx8 deletion, we created a construct of dual-tagged 6xHIS-3xFLAG-CgULS1 (HF-CgULS1) under its promoter and confirmed the expression of CgUls1 protein in the $Cguls1\Delta$ mutant by western blot using an α -flag antibody. As shown in Figure 7C, $Cguls1\Delta$ is sensitive to DNA-damaging agents (0.04%MMS). We tested the ability of HF-CgULS1 to complement the MMS sensitivity of $Cguls1\Delta$ mutant and we found that expression of HF-CgULS1 restored the phenotype of the $Cguls1\Delta$ mutant (Figure 10A).

When we checked the level of expression of CgUls1 protein in WT, $Cgulp2\Delta$, $Cguls1\Delta$, $Cgslx8\Delta$, and $Cgulp2\Delta Cgslx8\Delta$ deletion strain, a two-fold higher expression of CgUls1 protein in $Cgulp2\Delta Cgslx8\Delta$ double deletion mutant was seen in comparison with wild type and $Cgulp2\Delta$, $Cgslx8\Delta$ single mutants (Figure 10B-C). Further, to test if this increased levels of protein is a result of increased transcription, we tested the expression of the CgULS1 gene in these deletion strains. We observed that RNA levels of CgULS1 in $Cgulp2\Delta Cgslx8\Delta$ were higher than in $Cgulp2\Delta$ and $Cgslx8\Delta$ single mutants (Figure 10D). Together, these findings show that there is increased CgUls1 protein (and potentially increased activity) in the $Cgulp2\Delta Cgslx8\Delta$ mutant and this leads to elevated loss of proteins.

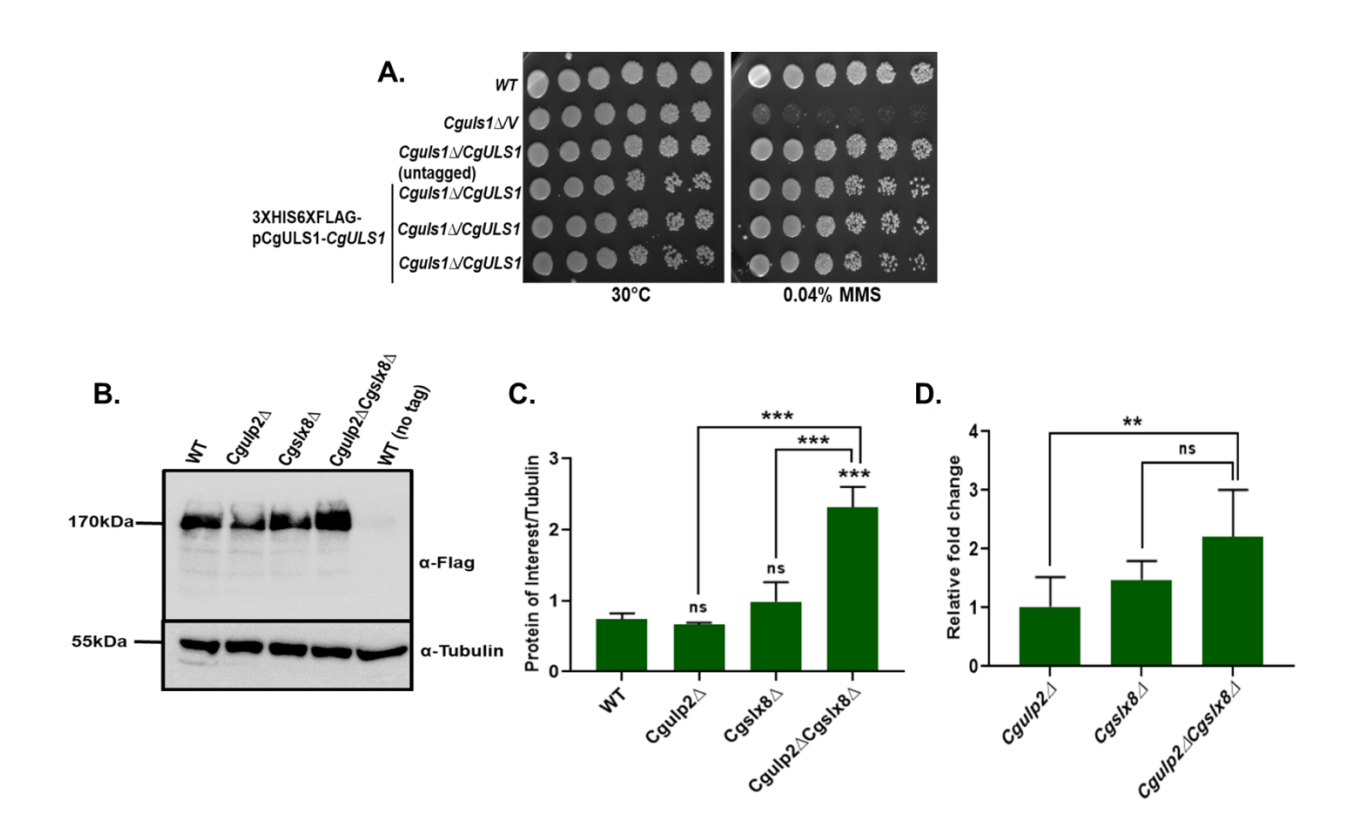
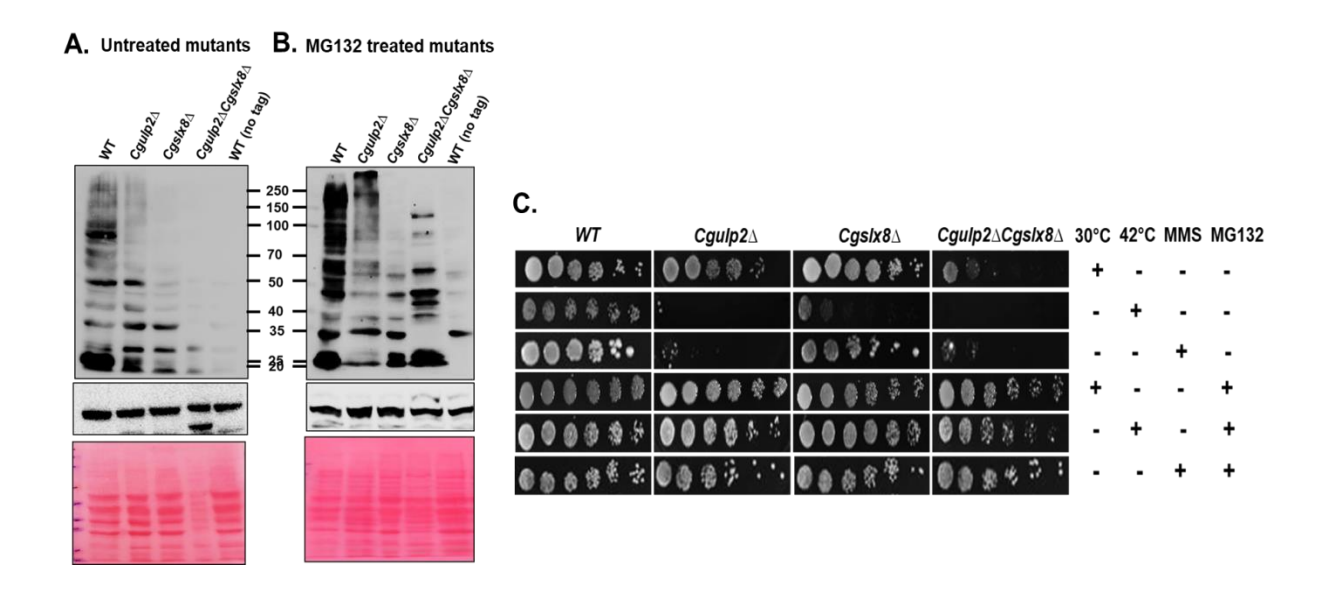


Figure 10. Upregulation of CgUls1 protein in STUbL mutant. A. Complementation of $Cguls1\Delta$ mutant with HF-CgUls1 was tested by growth at 30°C and in 0.04% MMS. 3µl of 10-fold serial dilutions of cultures of C. glabrata strains were spotted on indicated plates. Images were taken after 2-3 days of incubation **B.** Western blot analysis with anti-FLAG antibody to check the expression of CgUls1 protein in the STUbL mutant strains. Tubulin was used as a loading control. **C.** Quantification of the western blot. **D.** RNA was isolated from YPD-grown wild-type, $Cgulp2\Delta$, $Cgslx8\Delta$, and $Cgulp2\Delta Cgslx8\Delta$ cells and qRT-PCR was performed to check the expression of the CgULS1 gene. Data represents the mean and standard deviation of three independent experiments. Statistical significance was obtained using one-way ANOVA (****: p \leq 0.0005; **, p < 0.005; ns: non-significant).

Loss of proteins and reduced growth of STUbL mutants is due to enhanced proteasomal degradation

We examined the SUMOylation pattern in $Cgulp2\Delta$, $Cgslx8\Delta$, and $Cgulp2\Delta Cgslx8\Delta$ cells treated with the proteasome inhibitor MG132 to test the possibility that an increase in the accumulation of polySUMOylated proteins in these mutants results in their degradation by the ubiquitin-

proteasome pathway. To test this, we used the proteasome inhibitor, MG132. Whole-cell protein extracts were prepared from cultures that were treated with MG132 for 2 hours and tested for the presence of SUMOylated proteins by western blots. Higher molecular weight proteins could be detected in the MG132-treated $Cgulp2\Delta$ single mutants (Figure 11B, Lane 2) as compared to the untreated mutant strain (Figure 11A, Lane 2) indicating that the degradation of polySUMOylated proteins was prevented. Fewer changes were seen in the $Cgslx\delta\Delta$ consistent with the phenotypes seen for this mutant. Most interestingly, in the double mutant of $Cgulp2\Delta Cgslx8\Delta$, with MG132, higher molecular weight proteins appeared suggesting prevention of degradation of proteins (Figure 11B, Lane 4) compared to the untreated mutant (Figure 11A, Lane 4) and we could also recover more protein from this strain when treated with MG132. Furthermore, the reappearance of higher molecular weight proteins is accompanied by the restoration of growth of these mutants (Figure 11C-G). Also, MG132 treatment could overcome the thermal and MMS sensitivity of the $Cgulp2\Delta$, $Cgslx8\Delta$, and $Cguls1\Delta$ single mutant (Figure 11C-G). These findings strongly imply that the reason for slow growth at 30°C and increased stress sensitivity of $Cgulp2\Delta Cgslx8\Delta$ double mutant was due to excess proteasomal degradation. Together these results support our hypothesis that loss of Ulp2 leads to the accumulation of increased polySUMOylated proteins that are degraded by proteasome via the STUbL pathway.



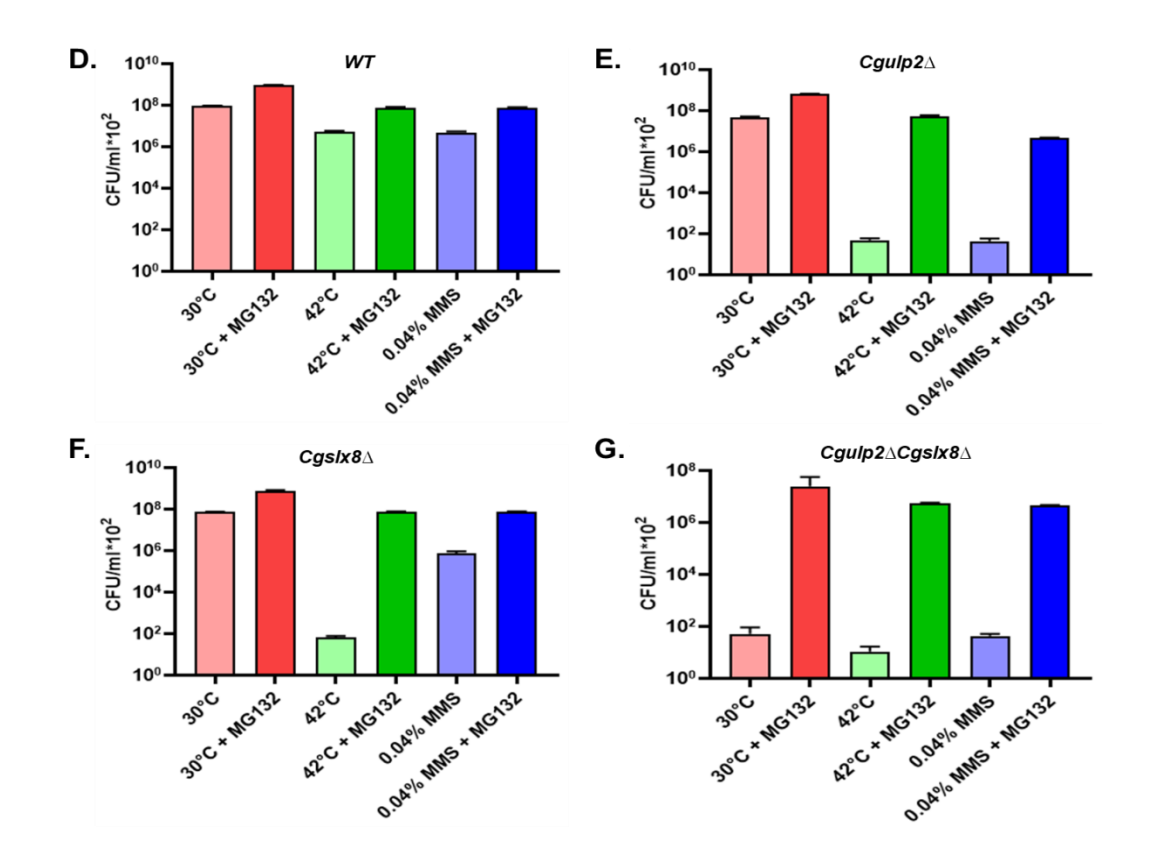


Figure 11. Loss of proteins and reduced growth of STUbL mutants is due to enhanced proteasomal degradation. *C. glabrata* strains were grown overnight in YNB medium at 30°C and 180 rpm with 0.1% proline serving as the only nitrogen source. After cell harvesting, a fresh medium containing 0.003% SDS was used to adjust the A600 to 0.5, and the cells were then grown for 4 hours. A. Cells without MG132 treatment were used as a control. B. Cultures were placed in a 2 ml microcentrifuge tube with 1 ml of YNB-proline media and 200μM MG132, and they were then incubated for two hours at 30°C and 180 rpm. Whole-cell extracts were prepared and analyzed by western blot using α-Flag antibody. Tubulin was used as a loading control. Blots stained with Ponceau S are shown for comparison of total proteins in *Cgulp2*Δ*Cgslx8*Δ in treated versus untreated cells. C. MMS (0.045%) was added to the media and grown for 3 hours after MG132 treatment. Similarly, thermal treatment was given to the cultures for 3 hours. After that, cultures were serially diluted 10-fold, and a 2 μl volume was spotted on the YPD medium. Images of the plates were taken following 2-3 days of incubation at desired temperatures. D-G. Quantification of growth of STUbL mutants in various stress conditions with and without MG132 treatment. Data represents the mean and SD from at least three independent experiments.

3.3 SUMMARY

We have identified STUbLs in multiple pathogenic fungi including *C. glabrata* using sequence comparisons. We created deletions of the STUbL components in *C. glabrata* and examined the effect on both the physiology and pathogenesis of *C. glabrata*. In the absence of STUbLs, this pathogen showed reduced biofilm formation and survival inside macrophages. Loss of STUbLs reduced the capacity of *C. glabrata* to combat stress. Additionally, we have shown here that, CgUls1 activity is increased in the strain lacking both deSUMOylating enzyme *Cgulp2* and a STUbL *Cgslx8*, resulting in enhanced protein degradation. This study also establishes that loss of protein homeostasis is the key reason for stress sensitivity observed in the STUbL mutants. Overall, we demonstrate here that STUbLs are important modulators of protein homeostasis and along with CgUlp2 play a vital role in *C. glabrata* pathogenesis.

Chapter 4 Identification of targets of deSUMOylase CgUlp2 and STUbLs

4.1 INTRODUCTION

The results shown in Chapter 3 indicate that the loss of a single STUbL has minimal effect on growth and the capacity of the organism to combat stress. However, when the deSUMOylase is also inactive, there is an excess accumulation of polySUMOylated proteins, which activates the STUbL pathway leading to the degradation of a large number of the polySUMOylated proteins. This affects the overall protein homeostasis. In order to determine if proteins that are part of critical growth pathways are particularly degraded in the STUbL double mutant $(Cgulp2\Delta Cgslx8\Delta)$ and restored in $Cgulp2\Delta Cguls1\Delta$, we conducted tandem mass tag (TMT) labeled quantitative mass spectrophotometry analyses.

4.2 RESULTS

Identification of global proteome of $Cgulp2\Delta$, $Cgslx8\Delta$, $Cguls1\Delta$, $Cgulp2\Delta Cgslx8\Delta$ and $Cgulp2\Delta Cguls1\Delta$ deletion strains in comparison with wild type

We analyzed the proteins of log-phase grown cells of WT, $Cgulp2\Delta$, $Cgslx8\Delta$, $Cguls1\Delta$ single mutants, $Cgulp2\Delta Cgslx8\Delta$, and $Cgulp2\Delta Cguls1\Delta$ double mutants using a tandem mass tag (TMT) labeled quantitative mass spectrophotometry. The samples were sent to the Institute of Bioinformatics (IoB) in Bangalore for analysis by mass spectrometry. Through the TMT-labeled mass spectrometry, a comprehensive dataset of 3281 proteins was obtained. Following Principal Component Analysis (PCA), 2194 proteins were retained, excluding those exhibiting variations between biological replicates and those not consistently present across all mutants. Based on the abundance value of the proteins, we calculated the p-value for each mutant by using MeV_4.9.0 software and took a threshold of 0.05 for a significant p-value. We identified 107, 87, 148, 277, and 300 proteins that were significantly upregulated, and 90, 130, 241, 184, and 134 proteins were significantly downregulated in $Cgulp2\Delta$, $Cgslx8\Delta$, $Cguls1\Delta$ single mutants, $Cgulp2\Delta Cgslx8\Delta$, and $Cgulp2\Delta Cguls1\Delta$ double mutants respectively. All the significantly upregulated and downregulated proteins for each mutant are shown in Appendix 9.6.

We used the DAVID database to perform Gene Ontology (GO) to identify the pathways of the upregulated and downregulated proteins for each mutant in comparison with WT. The pathways were then represented as horizontal bar graphs using SR plot software (Figure 12). We have seen proteins from multiple pathways that were differentially affected in these mutants. These include components of metabolic processes, biosynthetic processes, intracellular transport, ribosomal biogenesis, translation, proteasomal protein-mediated degradation, and many more.

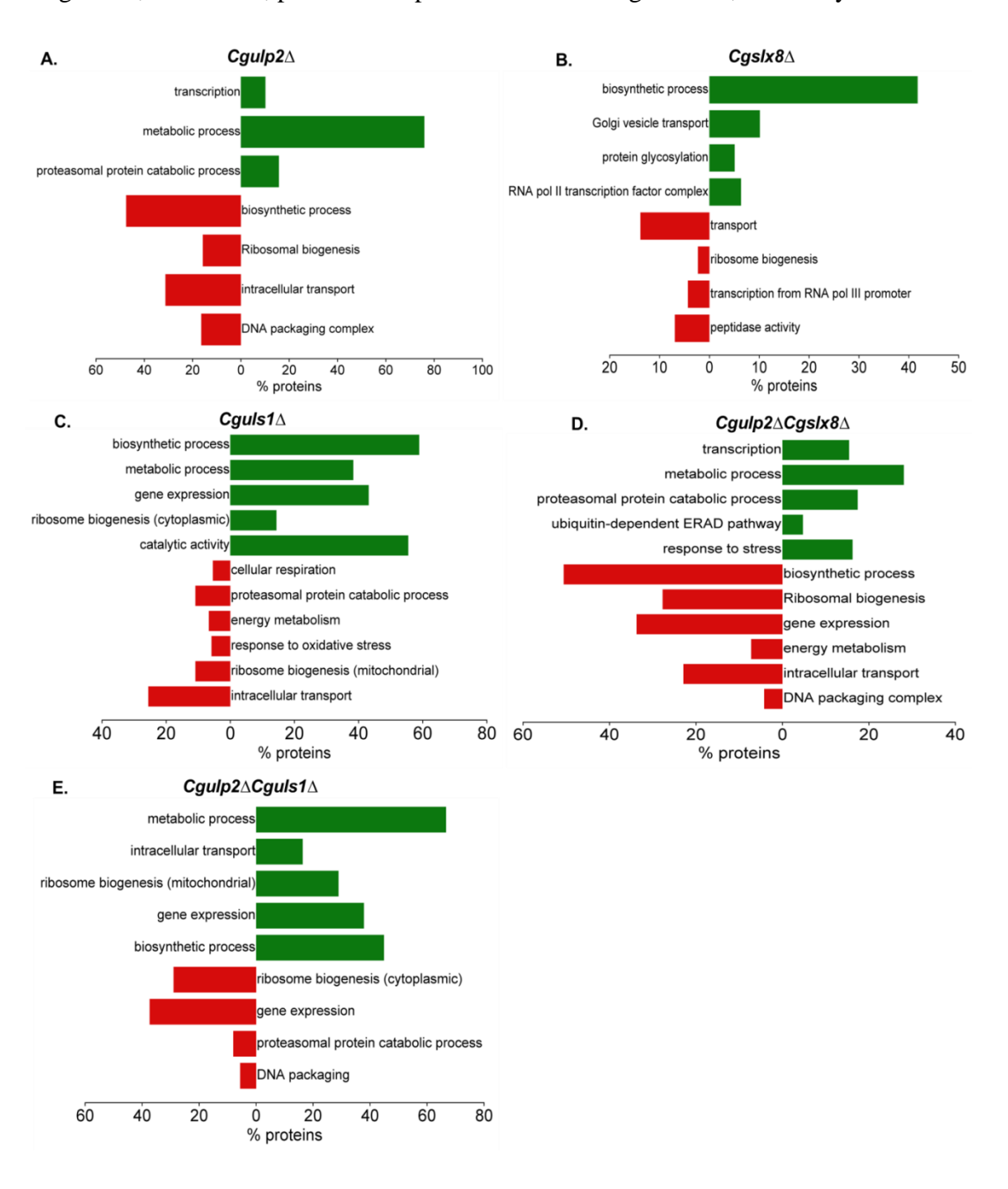
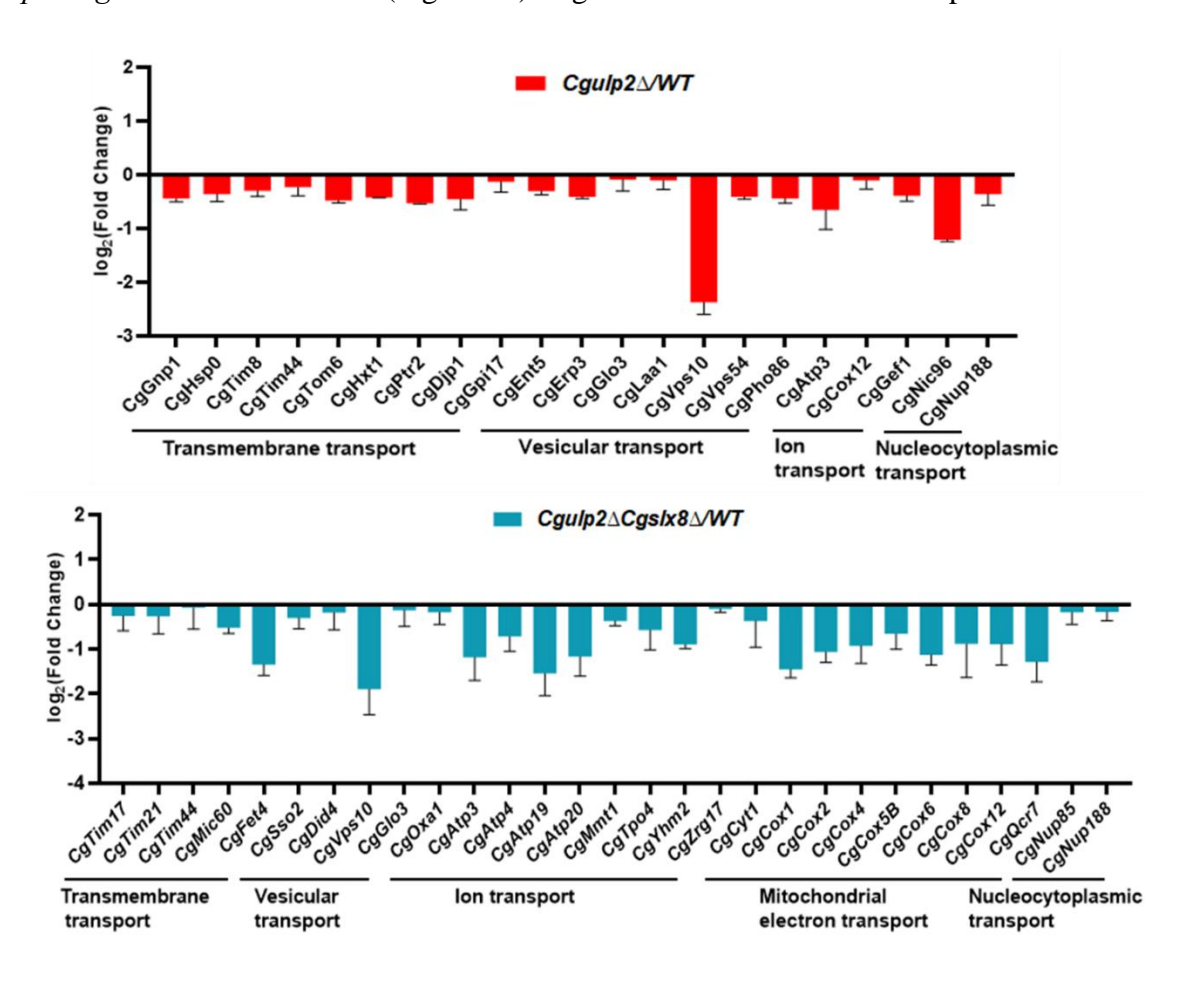


Figure 12. Pathways that are differentially affected in each mutant. The horizontal bar graph shows the pathways in A) $Cgulp2\Delta$, B) $Cgslx8\Delta$, C) $Cguls1\Delta$ D) $Cgulp2\Delta Cgslx8\Delta$, and E) $Cgulp2\Delta Cguls1\Delta$ mutant in comparison to WT. The green bar represents pathways with proteins that are higher and the dark red bar represents those that are lower than wild type.

Analyzing the data from proteomics suggested some key pathways that were particularly affected and also differentially affected in the mutants. It also could potentially provide a reason for the differential phenotypes observed. In this chapter, we describe some key observations made and a few follow-up experiments to validate these observations.

a) Intracellular transport: In our study, proteins involved in intracellular transport, particularly mitochondrial electron transport, transmembrane transport, and other ion transport were downregulated in $Cgulp2\Delta$, $Cgslx8\Delta$, $Cguls1\Delta$, and $Cgulp2\Delta Cgslx8\Delta$, but upregulated in $Cgulp2\Delta Cguls1\Delta$ double mutant (Figure 12). Figure 13 shows some of these proteins.



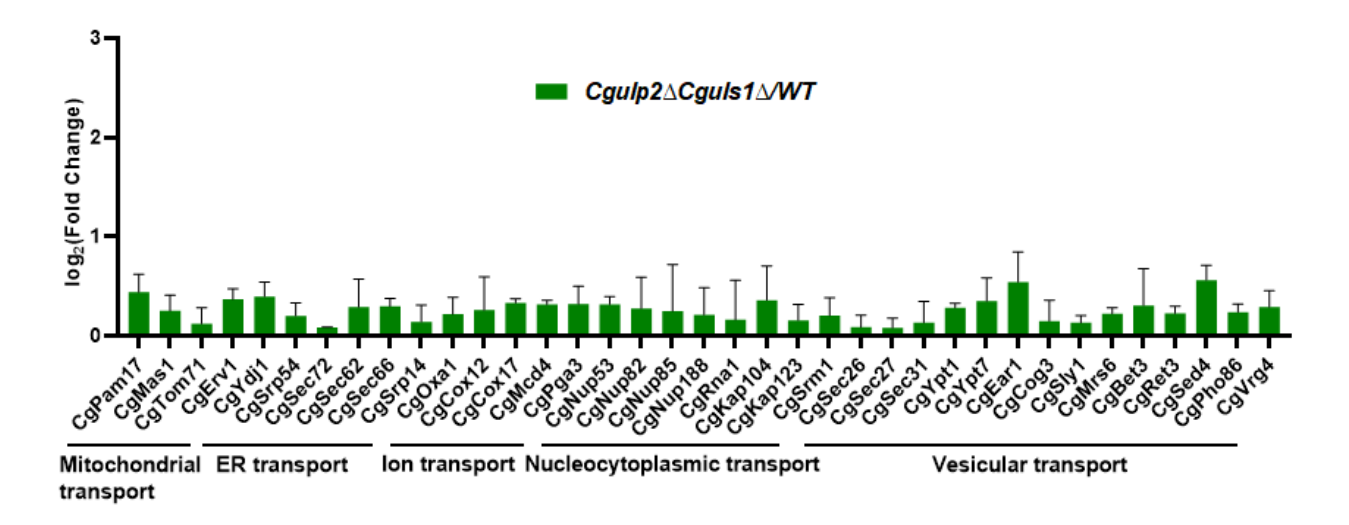


Figure 13. Graph shows the proteins involved in various transport that were downregulated in $Cgulp2\Delta$, $Cgulp2\Delta Cgslx8\Delta$, and upregulated in $Cgulp2\Delta Cguls1\Delta$ mutant. The error bar represents the log_2 standard deviation.

b) Ribosomal biogenesis and translation: Ribosomes are required for protein synthesis and therefore are essential for cellular survival, growth, and proliferation. Ribosome biogenesis includes ribosomal RNA synthesis and processing, ribosomal protein assembly, transport to the cytoplasm, and ribosomal subunit association. A few cytoplasmic and mitochondrial proteins involved in biogenesis were found to be downregulated in the $Cgulp 2\Delta$ and $Cgslx 8\Delta$ single mutant. In $Cguls 1\Delta$, we found that while the mitochondrial ribosomal proteins were reduced, there was an increase in cytoplasmic ribosome subunit levels (Figure 14). However, in the $Cgulp2\Delta Cgslx8\Delta$ double mutant, ribosomal subunits of both the cytoplasmic and mitochondrial translation were low. This could lead to an overall lower translation and could contribute the reduced protein levels this seen in mutant. Although the $Cgulp 2\Delta Cguls 1\Delta$ double mutant had increased levels of mitochondrial ribosomal proteins of both large and small subunits, the majority of cytoplasmic ribosomal proteins were lower than wild type (Figure 14). This suggests that perhaps mitochondrial translation is required for suppressing the $Cgulp2\Delta$ single mutant phenotype by the $Cgulp2\Delta Cguls1\Delta$ double mutant.

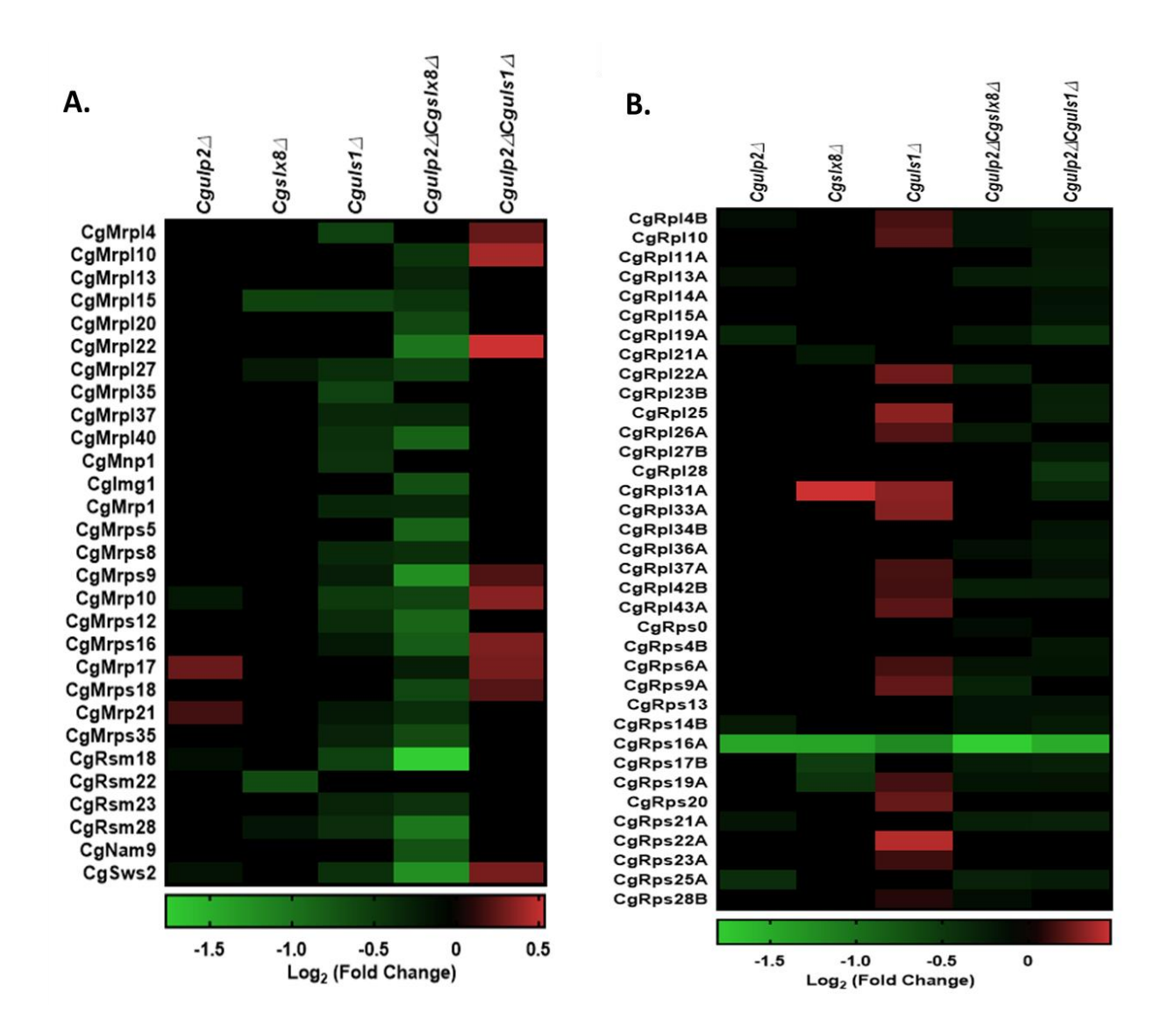


Figure 14. Heat map illustrating the differences in protein levels of ribosomal proteins. A. Heat map of mitochondrial ribosomal proteins and B. cytoplasmic ribosomal proteins of large and small subunits in $Cgulp2\Delta$, $Cgslx8\Delta$, $Cguls1\Delta$ single mutants, $Cgulp2\Delta Cgslx8\Delta$ and $Cgulp2\Delta Cguls1\Delta$ double mutant in comparison with WT. Heat maps were generated for the increased (different shades of red color) and decreased (different shades of green color) levels proteins for each mutant compared to the wild type.

c) Proteasomal mediated ubiquitin-dependent protein catabolic process: The massive protein complex known as the proteasome uses metabolic energy to break down intracellular proteins. The ubiquitin-proteasome system (UPS) is responsible for regulating a wide array of fundamental physiological functions by targeting short-lived regulatory or structurally abnormal

proteins for degradation. These functions encompass crucial processes such as signal transduction, cell cycle progression, cell death, metabolism, immunological responses, protein quality control, and development. The two subcomplexes that make up the proteasome are the catalytic core particle (CP), also referred to as the 20S proteasome, and one or more terminal 19S regulatory particle(s) (RP), which act as proteasome activators ¹³⁰. In this study, the $Cgulp2\Delta$ single mutant was found to have elevated levels of a small number of proteins that belong to both subcomplexes. The majority of the proteins in the 26S proteasomal complex and those involved in endoplasmic reticulum degradation (ERAD) which include CgKar2, CgCdc48, CgHlj1, CgHrd3, CgJem1, CgUbr1, and CgUfd1 were also substantially elevated in the $Cgulp2\Delta Cgslx8\Delta$ double mutant (Figure 15), suggesting that this increased protein degradation components could be responsible for the significantly elevated levels of protein degradation occurring in this double mutant. The proteasome-mediated ubiquitin degradation pathway proteins were reduced in $Cguls1\Delta$ and $Cgulp2\Delta Cguls1\Delta$ mutants (Figure 15) and this correlates with increased protein levels in these mutants. In summary, the decreased translation and increased degradation collectively contribute to reduced protein levels in the $Cgulp2\Delta Cgslx8\Delta$ double mutant.

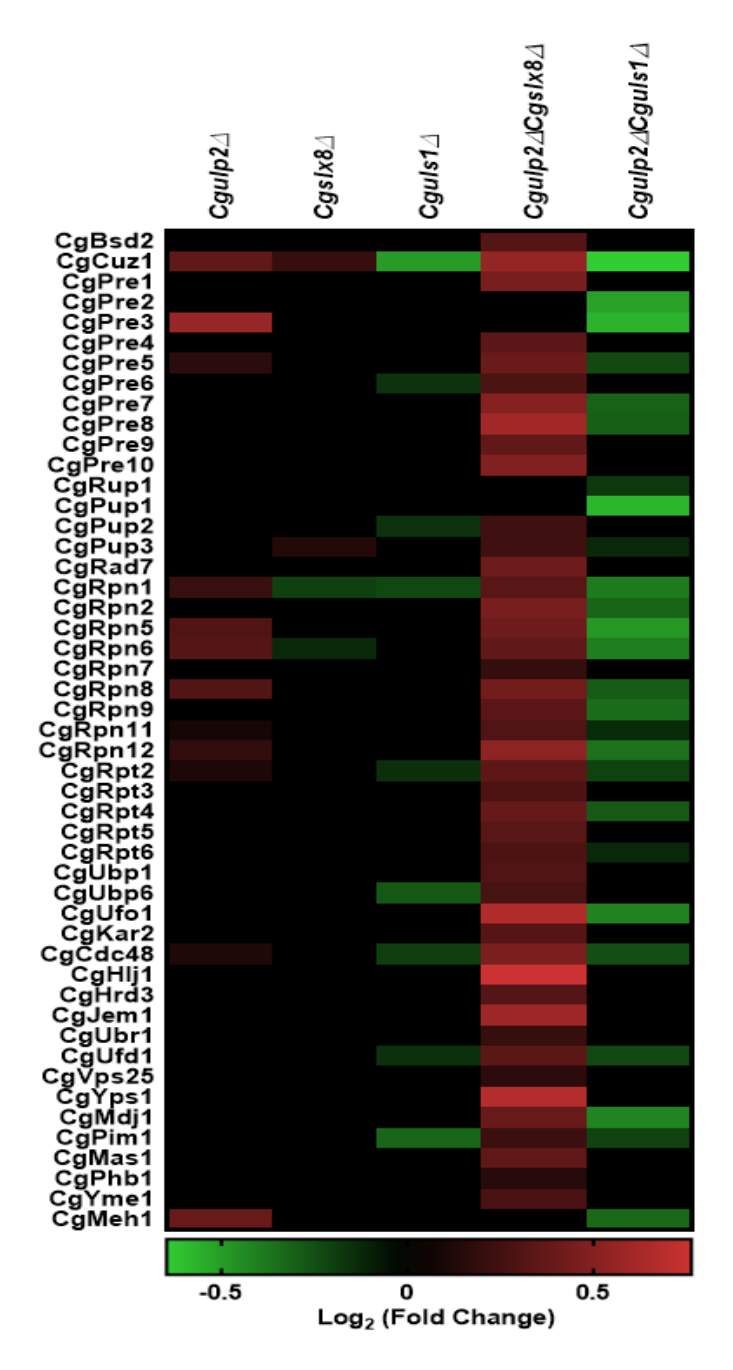


Figure 15. Heat map illustrating the altered levels of components of proteosome-mediated ubiquitin-dependent pathway in $Cgulp2\Delta$, $Cgslx8\Delta$, $Cguls1\Delta$ single mutants, $Cgulp2\Delta Cgslx8\Delta$ and $Cgulp2\Delta Cguls1\Delta$ double mutant in comparison with WT. A heat map of the elevated (different shades of red color) and diminished (different shades of green color) proteins for each mutant.

Purine biosynthetic pathway is compromised in $Cgulp2\Delta Cgslx8\Delta$

The process of biosynthesis involves multiple steps that are catalyzed by enzymes to transform substrates into increasingly complex products. These include biosynthesis of lipids, nitrogen compounds, amino acids, nucleotides, secondary metabolites, and more. The biosynthetic pathways were differentially affected in $Cgulp2\Delta$, $Cgslx8\Delta$, $Cgulps1\Delta$, $Cgulp2\Delta Cgslx8\Delta$, and $Cgulp2\Delta Cguls1\Delta$ mutants. One key observation was that components of the ATP biosynthesis process were reduced in $Cgulp2\Delta Cgslx8\Delta$ (Figure 17). It suggests that energy metabolism was impacted in these mutants and could be one contributing reason why $Cgulp2\Delta Cgslx8\Delta$ mutant cells might become sick at 30°C.

Among the biosynthetic gene products that were reduced in the $Cgulp2\Delta Cgslx8\Delta$, we noticed that there were several enzymes of the de novo purine biosynthetic pathway (Figure 16A, B). Purine nucleotide biosynthesis, as shown in Figure 16A, begins with 5-phosphoribosyl-1pyrophosphate (PRPP), which is then converted through a sequence of reactions into inosine 5'monophosphate (IMP). After that, IMP may go through various processes that produce either GMP or AMP, which are subsequently transformed into ADP and GDP, respectively ^{131,132}. Based on the mass spectrometry data, the $Cgulp2\Delta Cgslx8\Delta$ double mutant had reduced levels of most of the proteins involved in this biosynthesis. These included CgAde57 which was also found to be elevated in the $Cgulp2\Delta Cguls1\Delta$ double mutant and reduced in the $Cgulp2\Delta$ and Cgulp2ΔCgslx8Δ double mutant (Figure 16B). Since this change in CgAde57 reflected the altered growth phenotypes observed, we investigated whether CgADE57 overexpression could restore the Cgulp2\Delta Cgslx8\Delta double mutant growth at 30°C. In order to accomplish this, we constructed a plasmid encoding CgADE57 gene in the pGRB2.2 C. glabrata expression vector (carrying 3x-FLAG at the N-terminus), and we used an α -flag antibody to confirm the expression of CgAdeE57 protein in the WT, $Cgulp2\Delta$, $Cgslx8\Delta$, $Cguls1\Delta$, $Cgulp2\Delta Cgslx8\Delta$, and $Cgulp 2\Delta Cguls 1\Delta$ mutants through western blot. All these mutants showed the same levels of expression of the ectopically expressed CgAde57 protein (Figure 16C). In comparison to controls, the overexpression of the CgADE57 gene resulted in some degree of improved growth in the cells of the WT and mutants at 30°C and 42°C (Figure 16D). Significantly, we found that overexpressing the CgADE57 gene allowed the $Cgulp2\Delta Cgslx8\Delta$ double mutant to partially

recover its growth at 30°C and 42°C (Figure 16D-F) suggesting reduced levels of this protein could be a major contribution to the poor growth of the mutant.

Since these results suggested that the purine biosynthesis pathway is particularly compromised, we further tested this idea using inhibitors of this pathway. If some strains are already compromised in this biosynthetic pathway, they will be more sensitive to inhibitors of this pathway. We used three inhibitors- azaserine, pemetrexed, and isatin that inhibit specific enzymes of the purine biosynthesis pathway to examine growth inhibitions in WT and mutants. The initial, rate-limiting step involves the conversion of PPRP to PRA, which is catalyzed by PRPP amidotransferase. azaserine, an antifungal agent, inhibits this step ^{131,132}. An anticancer drug called pemetrexed prevents GAR transformylase from converting GAR to FGAR in the third step. The process by which the enzyme AIR carboxylase converts AIR to CAIR is inhibited by isatin, an antifungal agent. In this study, we observed 40-50% inhibition and reduced growth in WT cells upon the addition of 2mM azaserine, 6mM pemetrexed, and 4mM isatin in comparison to vehicle control. 80% inhibition was seen in the case of $Cgulp2\Delta$ and Cgulp2ΔCgslx8Δ mutants when treated with 2 mM azaserine, and 55% inhibition was observed with 6 mM pemetrexed and 4 mM isatin. In contrast, the $Cgslx\delta\Delta$, $Cgulsl\Delta$, and $Cgulp2\Delta Cguls1\Delta$ mutants showed similar levels of inhibitions to those of WT (Figure 16G-J). When these inhibitors were added, we found that both $Cgulp2\Delta$ and $Cgulp2\Delta Cgslx8\Delta$ were more sensitive to the drug. The doubling time of the WT, $Cgslx\delta\Delta$, $Cgulsl\Delta$, and $Cgulp2\Delta Cgulsl\Delta$ mutants ranged between 2-3 hours, whereas the $Cgulp2\Delta$ and $Cgulp2\Delta Cgslx8\Delta$ mutants displayed a prolonged doubling time of around 9-10 hours, especially in the presence of 2mM This could be the reason for the slow growth exhibited by $Cgulp2\Delta$ and azaserine. $Cgulp2\Delta Cgslx8\Delta$ mutants in the presence of the inhibitors. Altogether, this data suggests that purine nucleotide biosynthesis was one of the key factors for the compromised growth of $Cgulp2\Delta Cgslx8\Delta$ mutant, and cell growth was restored in $Cgulp2\Delta Cguls1\Delta$ double mutant.

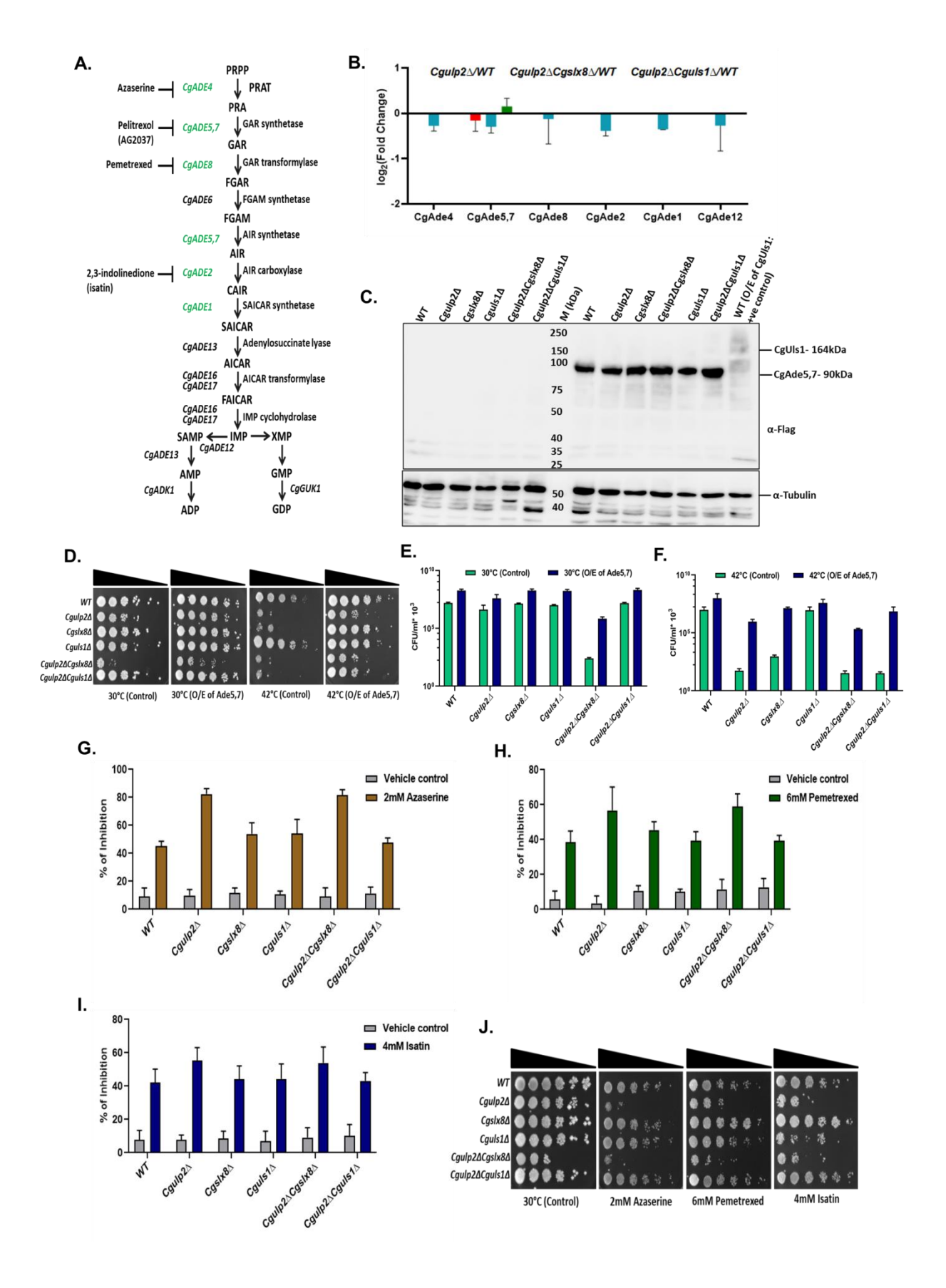


Figure 16. Loss of proteins and reduced growth of $Cgulp2\Delta Cgslx8\Delta$ double mutant is due to the altered proteins involved in the purine biosynthetic pathway. A. de novo pathway of purine nucleotide biosynthesis. Proteins labeled in green color were displayed in mass spectrometry data. A few inhibitors (Azaserine, pemetrexed, and isatin) that were carried out in this study were mentioned in a particular reaction step. Abbreviation: PRPP- 5-phosphoribosyl-1- pyrophosphate, PRAT- phosphoribosylamidotransferase, PRA- phosphoribosylamine, GARglycineamide ribonucleotide, FGAR- N-formylglycinamide ribonucleotide, FGAM- Nformylglycinamidine ribonucleotide, AIR- 5-aminoimidazole ribonucleotide, CAIR- AIR carboxamide, SAICAR- N-succino-5-aminoimidazole-4-carboxamide ribonucleotide, AICARaminoimidazole-4-carboxamide ribonucleotide, FAICAR- 5-formyl-AICAR, IMP, SAMPadenylosuccinate, AMP- adenosine monophosphate, ADP- adenosine diphosphate, XMPxanthosine monophosphate, GMP- guanosine monophosphate, GDP- guanosine diphosphate, ADK1-adenylate kinase 1, GUK1- guanylate kinase 1. B. Bar graph shows the upregulation and downregulation of the proteins involved in this pathway for $Cgulp2\Delta$, $Cgulp2\Delta Cgslx8\Delta$, and $Cgulp2\Delta Cguls1\Delta$. The error bar represents the log_2 standard deviation. C. Western blot was performed to check the expression of CgAde57 protein in WT and mutants by using an α-flag antibody. Before the protein marker, there are negative controls of WT and mutants (no tag). Overexpression of CgUls1 protein in WT cells acts as a positive control. Tubulin is used as a loading control. **D**. Overexpression of CgADE57 in STUbL mutants. To test the growth upon overexpressing CgADE57, a serial dilution-spotting assay was used. 3 µl of 10-fold serial dilutions of exponential phase (1.0 A600) grown cultures of C. glabrata strains were spotted in media lacking uracil. Plate images were taken after 1-3 days of incubation at 30°C and 42°C, respectively. E and F. Bar graphs showed the quantification of cell growth of each mutant upon overexpressing the CgADE57 gene. G-I. Inhibition assay in STUbL mutants. Overnight grown cultures of indicated C. glabrata strains were inoculated in YPD medium to an initial A600 of 0.2. 100µl of C. glabrata cell suspension were added to the wells. Azaserine, Pemetrexed, and Isatin inhibitors were added in the concentration of 2mM, 6mM, and 4mM to the cell suspension, and the final volume of 200ul for each well was maintained by adding YPD-rich media. YPD medium and cell suspension (100ul) without inhibitors were used as a control. Inoculum was incubated at 30°C for 24-48 hr with 300 rpm agitation. Absorbance at 600nm was measured at the relevant time intervals. Data represent the mean of triplicates and the error bar represents the

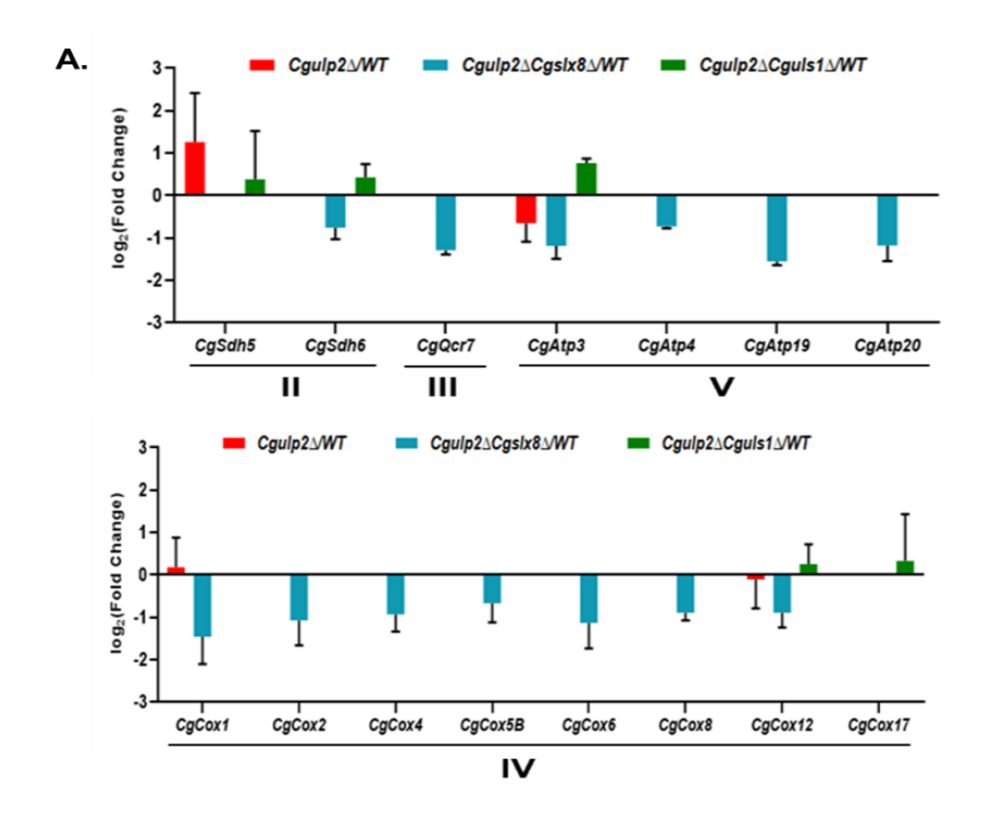
standard deviation. **J.** Plate assay shows the inhibition of cell growth of WT and mutants at 30°C by adding 2mM azaserine, 6mM pemetrexed, and 4mM isatin. 2 µl of 5-fold serial dilutions of logarithmic phase grown culture of WT and mutants were spotted on YPD medium. Plate images were captured after 48 hours of incubation at 30°C.

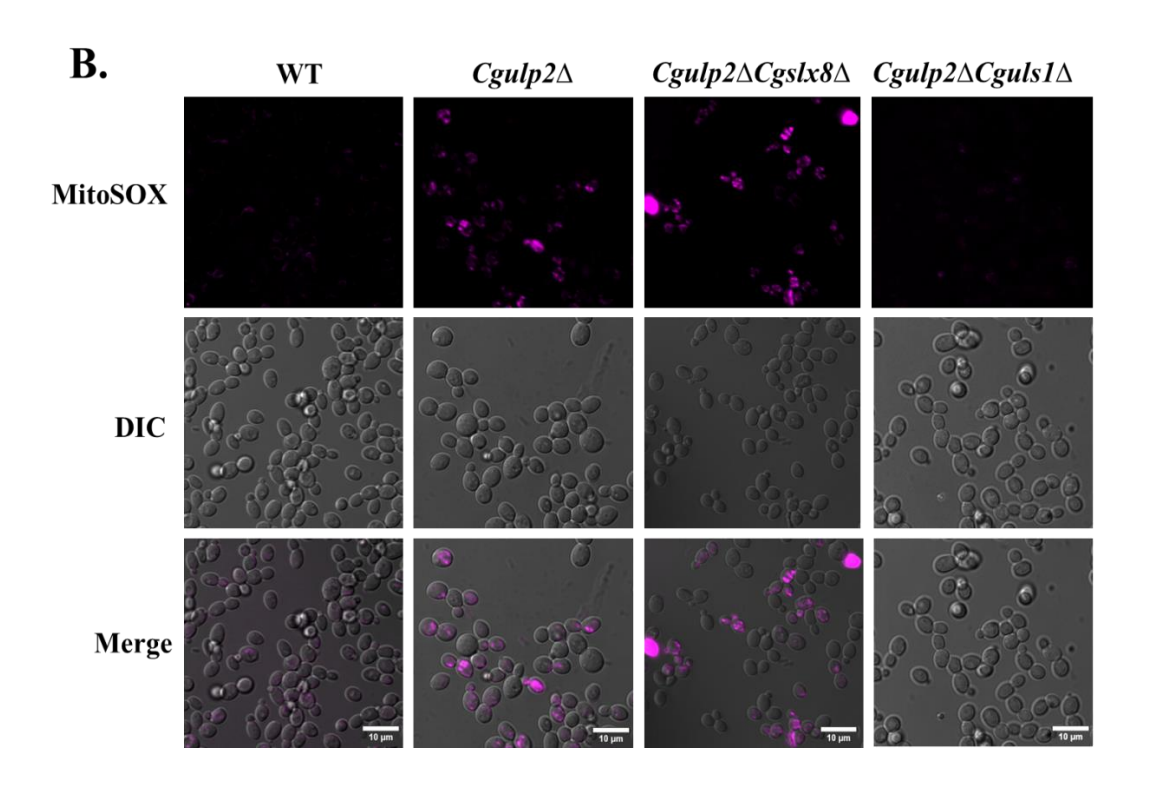
Mitochondria function is compromised in $Cgulp2\Delta$ and $Cgulp2\Delta Cgslx8\Delta$

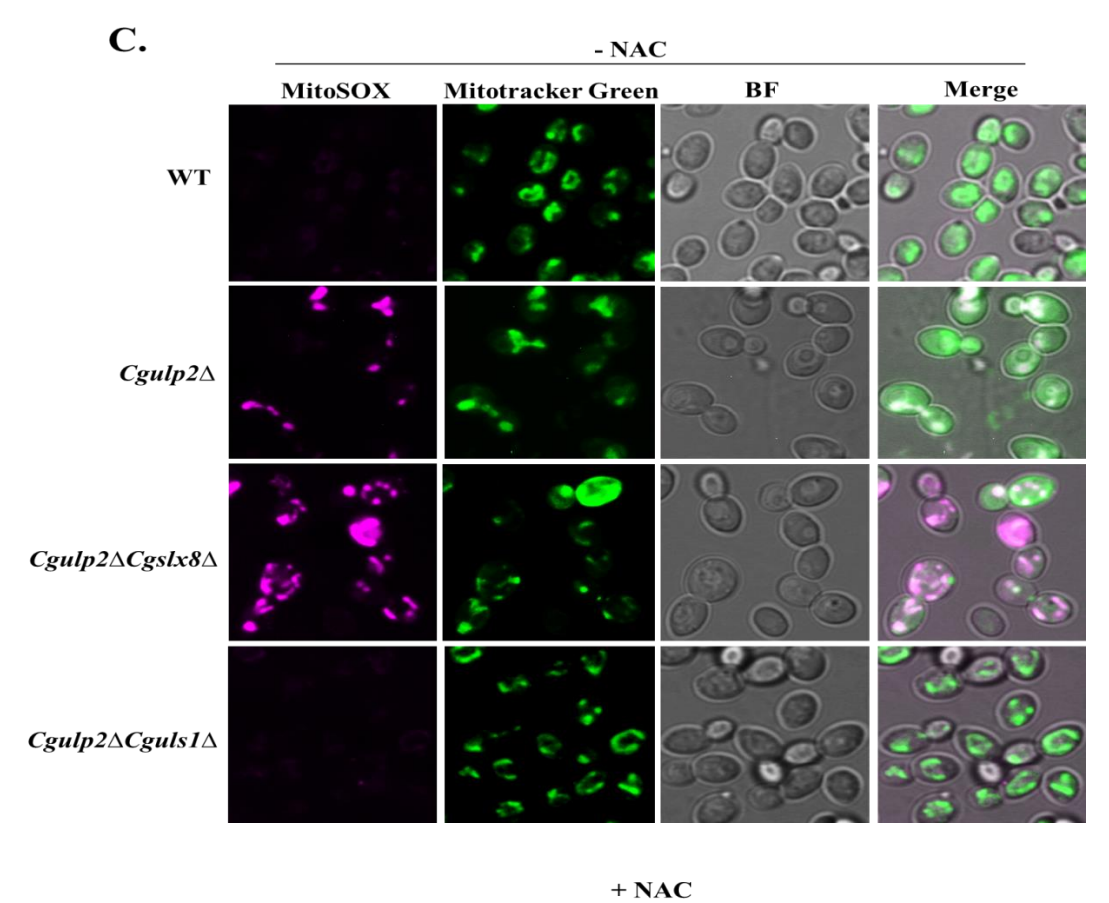
The electron transport chain (ETC) complex was another pathway that was critically affected by $Cgulp2\Delta Cgslx8\Delta$ double mutant as complex II, III, IV, and V were highly reduced in $Cgulp2\Delta Cgslx8\Delta$ suggesting mitochondrial metabolism was severely affected. In the case of $Cgulp2\Delta$, there was no clear down-regulation, with few components being present in larger or lesser levels than the wild type. In addition, proteins associated with these complexes were either upregulated or up to the level of WT in the $Cgulp2\Delta Cguls1\Delta$ double mutant (Figure 17A).

Dysregulation of mitochondria has several consequences such as ATP depletion, ROS generation, oxidative stress, etc. Also, $Cgulp2\Delta$ and $Cgulp2\Delta Cgslx8\Delta$ were shown to have reduced growth in non-fermentable carbon sources like 2% ethanol, 3% glycerol, and 2% lactate, and $Cgulp2\Delta Cguls1\Delta$ appeared to suppress the defects seen in the single mutant $Cgulp2\Delta$ (Chapter 3, Figure 6D).

To test if these mutants had compromised mitochondrial function, we examined mitochondrial morphology and reactive oxygen species in the mutants. The wild-type cells exhibited a tubular mitochondrial morphology, while $Cgulp2\Delta Cgslx8\Delta$, and $Cgulp2\Delta$ displayed fragmented mitochondria. Interestingly, $Cgulp2\Delta Cguls1\Delta$ retained tubular mitochondria similar to the wild-type cells (Figure 17C). To assess reactive oxygen species (ROS) levels, we stained WT and C. glabrata mutants with MitoSOX, a mitochondria superoxide indicator. $Cgulp2\Delta Cgslx8\Delta$ cells showed elevated ROS levels, with a stronger fluorescent signal followed by $Cgulp2\Delta$ mutant. $Cgulp2\Delta Cguls1\Delta$ and WT had no or very little amount of ROS (Figure 17B-C). Further to validate that the increased signal in $Cgulp2\Delta$ and $Cgulp2\Delta Cgslx8\Delta$ cells is due to enhanced mtROS production, we treated these cells with N-acetylcysteine (NAC), an antioxidant known to scavenge ROS. NAC treatment significantly decreased fluorescent signals in both $Cgulp2\Delta$ and $Cgulp2\Delta Cgslx8\Delta$ cells compared to untreated cells (Figure 17C). These data together suggest a compromised mitochondrial function in $Cgulp2\Delta Cgslx8\Delta$ and $Cgulp2\Delta$.







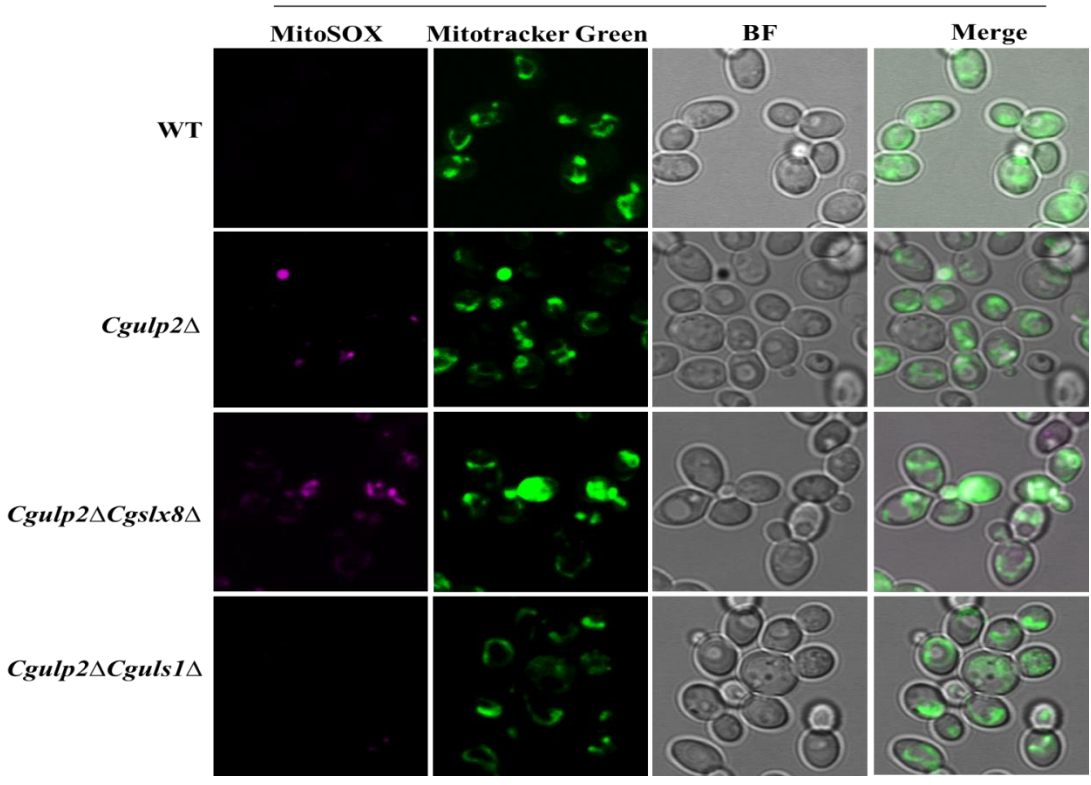


Figure 17. Mitochondrial functions were affected in $Cgulp2\Delta$ and $Cgulp2\Delta Cgslx8\Delta$. A. Bar graph shows the upregulation and downregulation of the proteins involved in the mitochondrial complexes of the ETC pathway for $Cgulp2\Delta$, $Cgulp2\Delta Cgslx8\Delta$, and $Cgulp2\Delta Cguls1\Delta$. The error bar represents the standard deviation. B. Confocal microscopic images of the WT, $Cgulp2\Delta$, $Cgulp2\Delta Cgslx8\Delta$, and $Cgulp2\Delta Cguls1\Delta$ that showed the level of ROS generation. Scale bar- 10 μm. C. Cells were grown in YPD medium with (+ NAC) or without 10mM NAC (- NAC) at 30°C for 12 hours and then stained with MitoTracker Green and MitoSOX. Images were captured in confocal microscopy. Scale bar- 5 μm

4.3 SUMMARY

From the quantitative mass spectrometry, we have identified multiple pathways that were differentially affected in the mutants of C. glabrata (Figure 12). Pathways such as intracellular transport, biosynthetic process, ribosomal biogenesis, mitochondrial, and proteasomal pathways were severely affected in $Cgulp2\Delta Cgslx8\Delta$. However, upon validating the pathways experimentally that were directly correlating with the phenotypes of the mutants, the de novo pathway of purine biosynthesis was found to be one of the key factors for the slow growth of $Cgulp2\Delta Cgslx8\Delta$ double mutant. In addition, mitochondrial function was compromised in $Cgulp2\Delta Cgslx8\Delta$ double mutant. Both these pathways were partly restored to WT levels (or higher in some cases) in the $Cgulp2\Delta Cguls1\Delta$ double mutant. These molecular data correlate with the phenotypic observations presented in the previous chapter. While these two pathways could contribute significantly, based on the proteomics data, it is clear that multiple pathways are compromised and could also contribute to the phenotype.

The major findings from Chapters 3 and 4 are schematically summarized in Figure 18. In the presence of CgUlp2, SUMO chains are removed from the target protein whereas, in its absence, polySUMOylated proteins were accumulated and targeted for protein degradation via STUbL CgUls1. This is a key contributor to the homeostasis of the target proteins. As more polySUMOylated protein accumulates in the absence of CgUlp2, due to the lack of CgUls1, it is not degraded. The double mutant $Cgulp2\Delta Cgslx8\Delta$ exhibits an increased level of protein degradation possibly because of upregulated activity of Uls1. Following MG132 treatment, degradation of proteins was prevented and SUMOylated proteins appeared in $Cgulp2\Delta$ and $Cgulp2\Delta Cgslx8\Delta$ mutants and so did the improved growth. Based on the experimental validation

of quantitative mass spectrometry data, ubiquitin-proteosome pathway, purine nucleotide biosynthesis pathway, and mitochondrial function were found to be significantly impacted in $Cgulp2\Delta Cgslx8\Delta$ double mutant. This was followed by the $Cgulp2\Delta$ single mutant. We propose that these are the primary causes of the increased protein loss and slow growth of $Cgulp2\Delta Cgslx8\Delta$ cells at 30°C. On the other hand, the level of the components of these pathways was opposite in $Cgulp2\Delta Cguls1\Delta$ double mutant. The ubiquitin-proteosome pathway had decreased level whereas purine nucleotide biosynthesis pathway and mitochondrial function had increased level due to which restoration of growth and accumulation of polySUMOylated protein was seen in $Cgulp2\Delta Cguls1\Delta$ mutant.

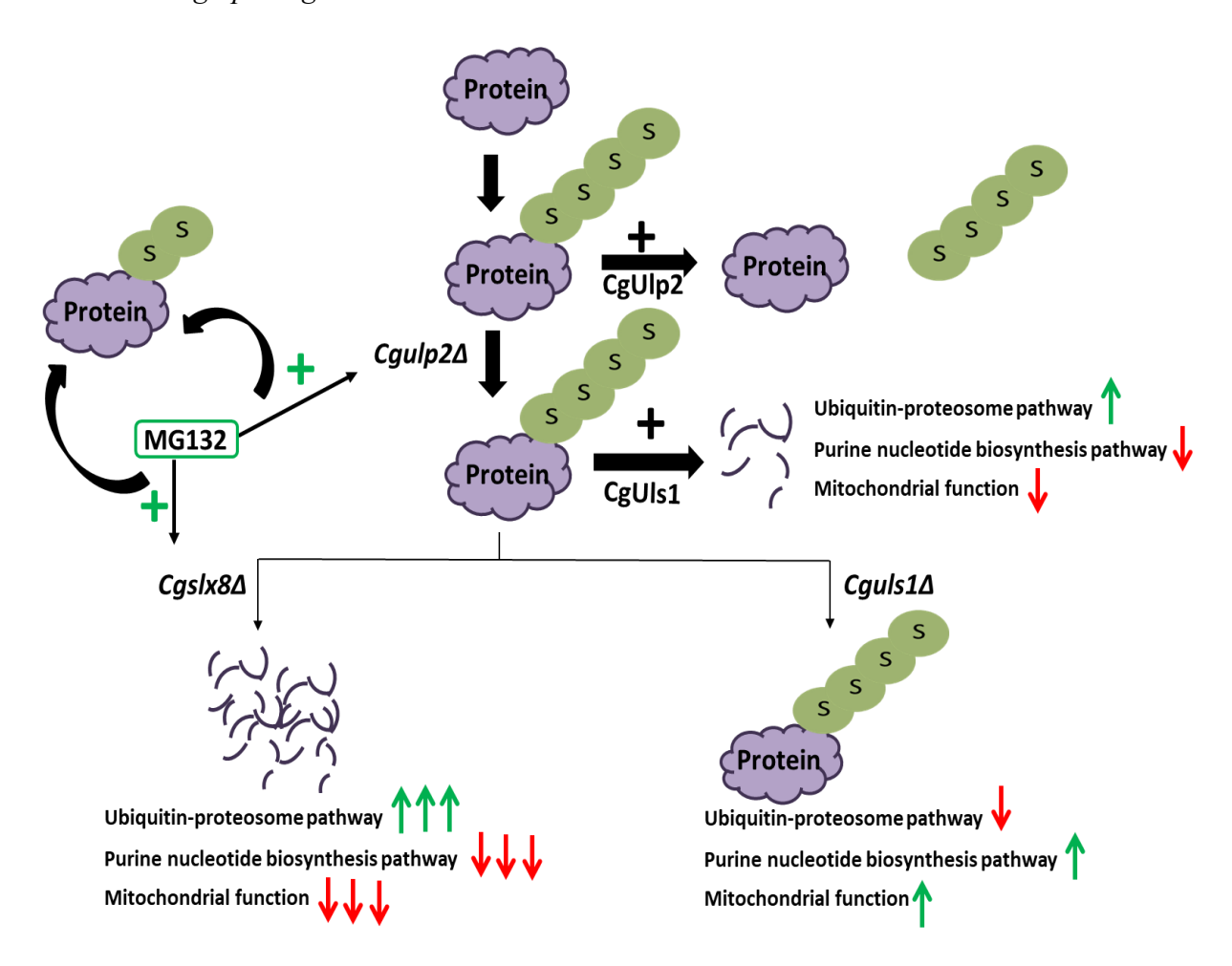


Figure 18. Molecular basis for the phenotypes of loss of deSUMOylase CgUlp2 and STUbLs in *C. glabrata*. Description in text.

Chapter 5 Establishment of a method to enrich for SUMOylated proteins

5.1 INTRODUCTION

In the majority of pathogenic fungi investigated, the SUMO pathway is found to be indispensable for either survival or virulence. In *Candida glabrata*, for instance, the gene encoding for SUMO, *CgSMT3*, is essential and disruption of SUMOylation leads to increases stress sensitivity and diminished virulence in the pathogenic fungi ^{41,90,116}. Of note, deletion of Cg*ulp2* results in decreased cell survival and reduced adhesion, underscoring the significance of SUMOylation in fungal physiology and pathogenesis. In Chapter 3, we have shown that STUbL mutants have reduced cell survivability under various stress conditions. So we aim to identify the target proteins that are SUMOylated and whose SUMOylation or levels in the cell affect the response of *C. glabrata* to these stress conditions. In order to do this, we have to pull down the SUMOylated proteins and do mass spectrometry to identify the targets.

5.2 RESULTS

For the pull-down protocol for SUMOylated proteins, there are multiple methods available for SUMOylated proteins in *S. cerevisiae* and in mammalian cell lines. We tried several of these, including methods previously published in our laboratory for *S. cerevisiae* ⁵¹. However, while most worked well in *S. cerevisiae*, they did not work efficiently with *C. glabrata*. After several attempts with different modifications to the procedure, we set out to develop an alternate method which is described below.

We standardized SUMO proteome isolation in *C. glabrata* using tandem SUMO interacting motifs (SIM), inspired by a similar method developed in the laboratory of M.S. Rodriguez ¹¹⁸. The protocol for SIM-based enrichment of SUMOylated proteins is schematically presented in Figure 19. SIM consisits of a sequence comprising four hydrophobic amino acids surrounded by acidic amino acids. SIM was identified in the Uls1 protein of *S. cerevisiae*. By sequence alignment of the Uls1 proteins from *S. cerevisiae* and *C. glabrata*, we identified the putative sequence of SIM as "VVIVD" spanning amino acid 1325 to 1329 in *C. glabrata* (Figure 20A). At first, we cloned 8 SIM tandemly in the pET28a bacterial expression vector, and subsequently

proceeded with the expression and purification of the tandem SIMs using Ni-NTA affinity purification. We could detect a 20kDa peptide representing the tandem SIM motif (Figure 20B-E). Then the Ni-NTA column bound SIM was incubated with the *C. glabrata* cell extracts for 6 hours. It was then washed several times to remove non-specifically bound proteins and eluted with 300mM imidazole to pull SUMOylated proteins along with the 8xSIM peptide and analyzed by western blot using anti-FLAG antibody (Figure 21).

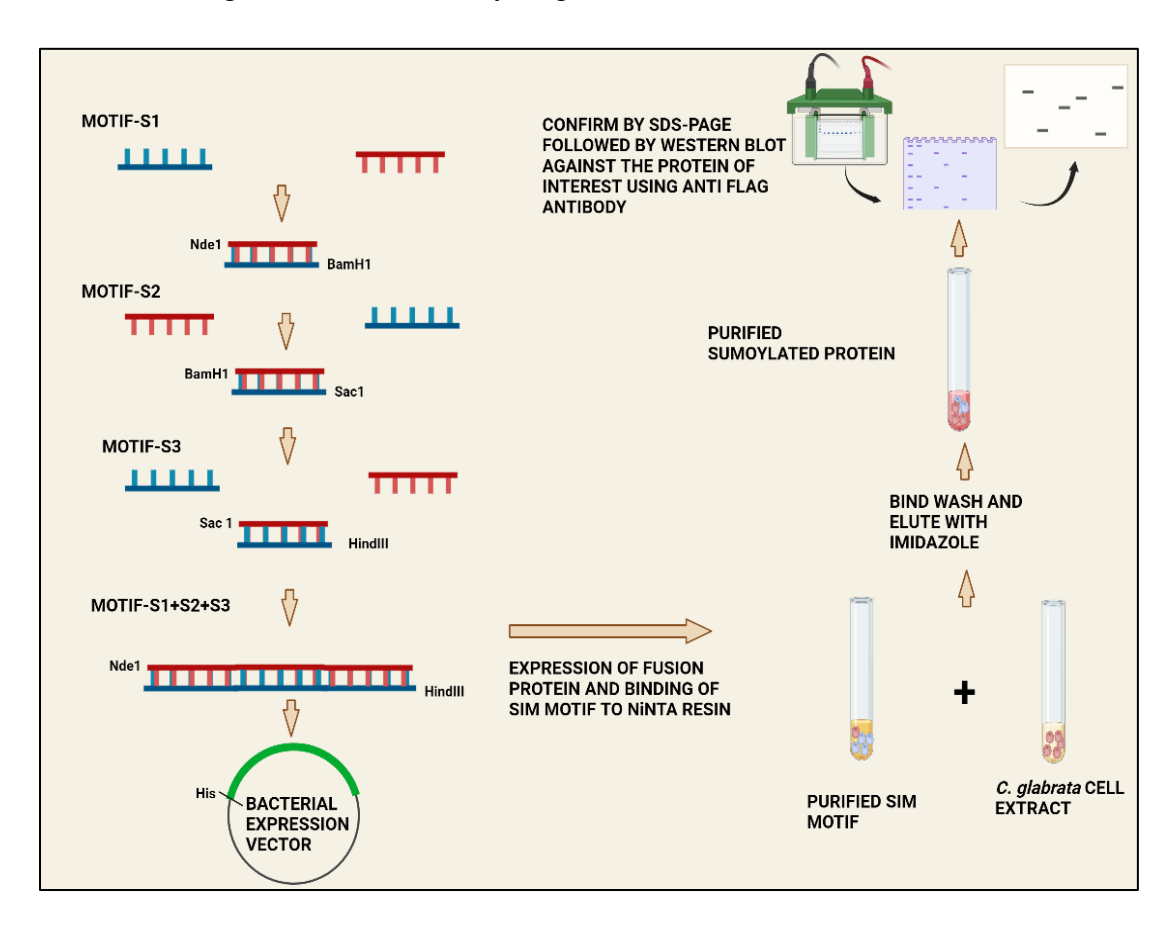
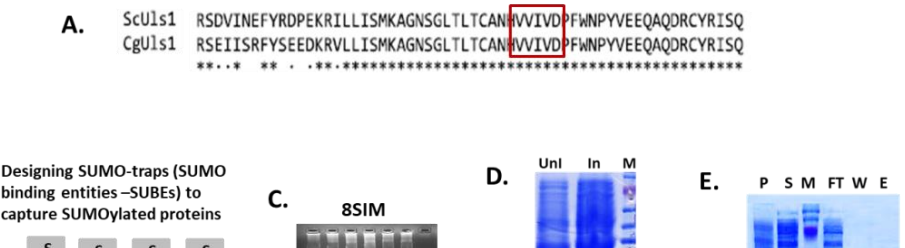


Figure 19. Schematic representation of SIM-based SUMOylated protein enrichment in *C. glabrata*.



SIM

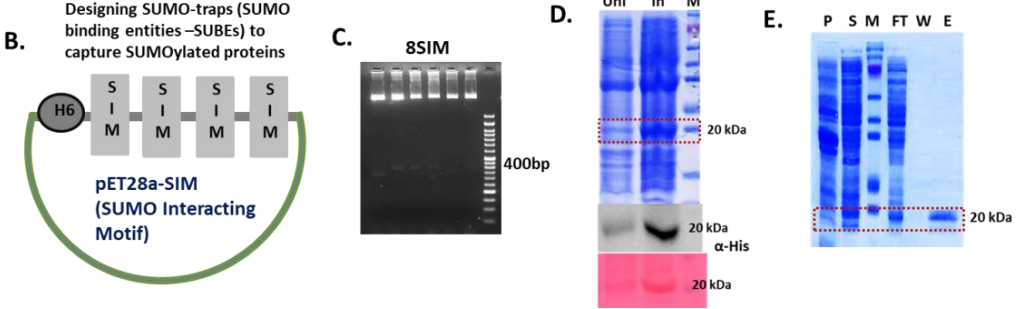


Figure 20. Purification of SUMO-interacting motif (SIM) in *C. glabrata*. A. Putative sequence of SIM in *C. glabrata* by sequence alignment of *ULS1* of *S. cerevisiae* and *C. glabrata*. B. Schematic representation of SIM cloned tandemly in the bacterial expression vector (pET28a). C. 1% agarose gel shows the SIM cloned in the pET28a vector. D. Protein expression of SIM motifs and E. purification of SIM motifs. UnI-Uninduced protein, In-induced protein, P and S-pellet, and supernatant after sonication, FT- Flow through, W- Wash after binding of protein to Ni-NTA beads, and E- purified protein elution.

In objective 3, we have shown that loss of Cguls1 suppresses the growth phenotype of Cgulp2 mutant due to accumulation/lack of degradation of the polySUMOylated proteins in the absence of Cguls1. Therefore, we performed the above-mentioned protocol in dual-tagged CgSmt3 expressed in wildtype, $Cgulp2\Delta$, $Cguls1\Delta$ single mutant, and $Cgulp2\Delta Cguls1\Delta$ double mutant strain. Also, a wild-type strain lacking dual-tagged CgSmt3 served as a negative control to check the specificity of SUMO enrichment. Notably, slower-moving bands were absent in this strain, suggesting that the proteins eluted from this column are likely to be specific. When we performed a pull-down assay with these mutants, as expected, higher molecular weight SUMOylated protein bands (above 25kDa) were observed in the wild type strain and also several prominent polySUMOylated protein bands in $Cgulp2\Delta Cguls1\Delta$ double mutant compared with negative control when probed with anti-FLAG antibody (Figure 21). In the absence of a deSUMOylase, we were unable to detect any higher molecular weight (potentially polySUMOylated) proteins as in the western blots

performed with whole cell extracts earlier. Together, these data establish that tandem SIM motifs could be a viable means of enriching SUMOylated proteins in *C. glabrata*.

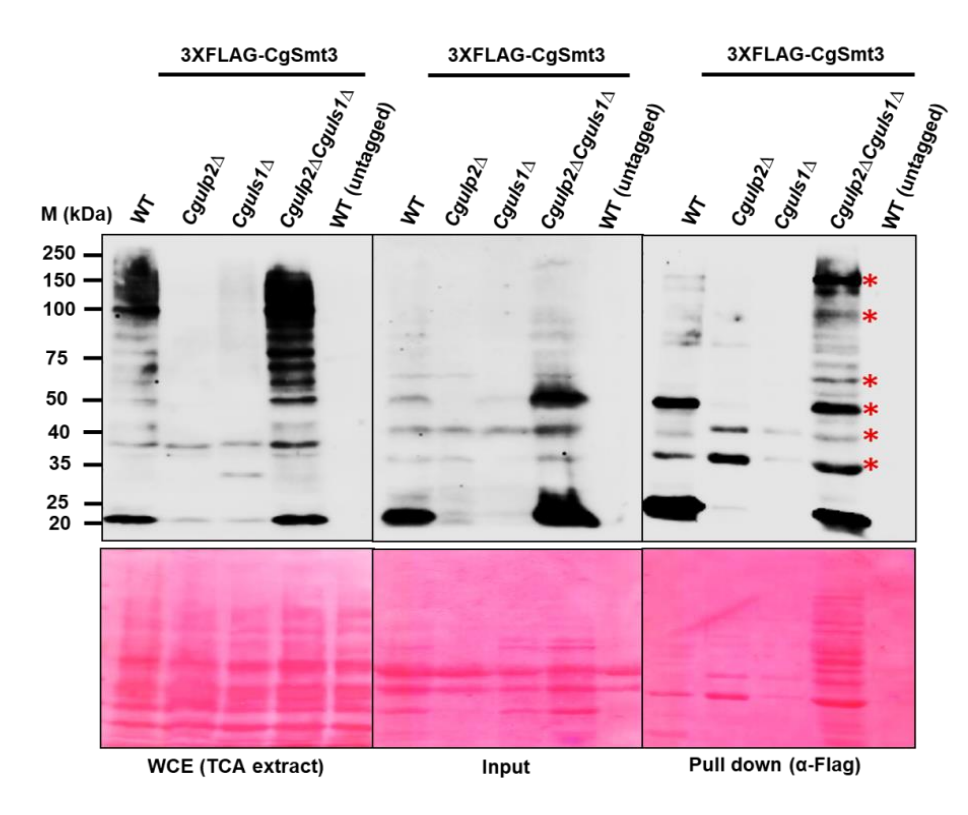


Figure 21. Enrichment of SUMOylated proteins in SUMO protease and STUbL mutants in *C. glabrata.* * indicates SUMOylated proteins.

5.3 SUMMARY

We have established tandem SUMO-interacting motifs (SIMs) based enrichment of SUMOylated proteins in *C. glabrata*. This can be used to determine the SUMOylation targets that impact infections in this organism.

Chapter 6 Determination of atomic resolution structure of key enzymes in protein SUMOylation to design drugs that target them

6.1 INTRODUCTION

In yeast *S. cerevisiae*, both Ulp1 and Ulp2 are responsible for removing monoSUMOylation from proteins, while Ulp2 specifically targets the removal SUMO from polySUMOylated target proteins ^{82,116}. As a result, this enzymatic activity ensures the reversibility of protein SUMOylation and maintains a pool of free SUMO within the cell to continue the SUMOylation cycle. Ulp1 is also involved in the initial step of SUMOylation, maturating SUMO precursors. In our laboratory, previous and current work has shown these pathways are likely to be conserved in *C. glabrata* as both *ULP1* and *SMT3* are essential in both yeasts. Perturbations to the SUMO pathway affect the pathobiology of *Candida glabrata*. Ulp2 exhibits high selectivity as a deSUMOylase, targeting specific protein complexes involved in crucial cellular processes such as DNA replication, ribosomal DNA maintenance, and chromosomal segregation in *S. cerevisiae*. Consequently, our primary objective in studying SUMOylation in *C. glabrata* is to explore the potential fro targeting this pathway for intervention since perturbing SUMOylation will adversely affect several essential processes. Given the limited availability of drugs inhibiting SUMOylation (e.g., Ginkgolic acid), our aim is to design inhibitors targeting this pathway.

In chapters 3 and 4, we have established that protein homeostasis via deSUMOylase CgUlp2 is a critical factor and also identified downstream pathway, so we planned to target Ulp2 as loss of Ulp2 has been shown to affect the virulence of multiple pathogenic fungi. In addition, the components of the SUMO pathway in various fungi were compared with humans to identify the least conserved protein that will define the better target.

6.2 RESULTS

SUMO protease CgUlp2 was identified as least conserved with human

Based on sequence homology, we have identified the orthologs of components of the SUMOylation pathway in multiple pathogenic fungi and identified the level of conservation of the proteins involved. We found that many proteins of this pathway share a very high level of similarity with human orthologs, with Ubc9 sharing maximum similarity. The full length of Siz1,

Ulp1, and Ulp2 proteins share the least similarity (Table 7A). On comparing the catalytic domains, the SUMO proteases Ulp1 and Ulp2 share lesser similarity with their human counterparts (Table 7B). Among them, the SUMO protease Ulp2 orthologs exhibit the lowest similarity with the human protein, making it most suitable for a potential drug target. **Peptidase C48**, spanning amino acid residues 450-675, represents the catalytic domain in the CgUlp2 protein.

A.								B.			
SUMO	Saccharomyces	Candida	Candida	Cryptococcus	Magnaporthe	Aspergillus	Candida	Candida	Ното	Full length	Catalytic Domain
pathway	cerevisiae	glabrata	albicans	neoformans	oryzae	nidulans	parapsilosis	glabrata	sapiens	(% similarity)	(% similarity)
genes								CgSIZ1	PIAS1	39.7	58.6
SMT3	57.4	54.7	51.6	48.1	50.0	51.7	39.2	CgSIZ1	PIAS2	39.1	57.9
								CgSIZ1	PIAS3	38.6	56.1
AOS1	52.8	50.4	46.0	48.5	43.7	47.0	46.5	CgSIZ1	PLAS4	33.3	60.3
UBA2	50.4	51.0	51.5	51.6	51.7	54.3	50.0	CgSIZ1	ZMIZ1	35.5	56.1
UBC9	69.9	70.8	51.5	75.1	73.3	67.0	68.0	CgSIZ1	ZMIZ2	35.6	56.1
								CgULP1	SENP1	41.0	49.1
MMS21	40.1	40.7	40.3	43.6	36.6	32.8	-	CgULP1	SENP2	40.2	47.9
SIZ1	24.6	27.4	17.5	26.1	39.5	31.2	21.9	CgULP1	SENP3	38.8	45.0
ULP1	39.3	40.5	47.4	46.0	23.6	30.8	44.0	CgULP1	SENP5	39.8	47.9
	22.0			200				CgULP2	SENP6	37.5	31.1
ULP2	38.9	38.7	38.2	34.1	37.9	36.4	36.8	CgULP2	SENP7	38.7	32.0

Table 7. SUMO protease CgUlp2 showed the least conservation with its human homolog. A.

Comparison of the percentage similarity of full-length *H. sapiens* ortholog with the orthologs identified in selected fungi. **B.** Comparison of the percentage similarity of the full-length protein and only the catalytic domains of the SIZ2, ULP1, and ULP2 orthologs in *C. glabrata* and *H. sapiens*. CgUlp2 is highlighted with a red color box.

Full-length Ulp2 structure is not available at high resolution in any organism. Therefore, our objective is to express and purify significant quantities of CgUlp2 for structural studies.

Expression and purification of CgUlp2 protein

CgUlp2 protein was cloned in the pET28a vector followed by checking the expression of the CgUlp2 protein. We observed a low level of expression of pET28a encoded CgUlp2 (105kDa) protein (Data not shown). Since our attempts to improve the expression were unsuccessful, we cloned, expressed, and purified parts of CgUlp2 protein in the pET28a vector (Figure 22A). We generated constructs for the N-terminal domain (NTD), catalytic domain (CD), and C-terminal

domain (CTD) encompassing amino acid residues 1-478, 405-710, and 590-917, respectively (Figure 22A) in pET28a vector and expressed in BL21(DE3)RIL bacterial strain. Further, the full length and the domains of CgUlp2 protein were purified using Ni-NTA resin and we found that these constructs were affinity purified with non-specific protein bands. Also, the full length of CgUlp2 protein had a very low yield upon purification (Figure 22B).

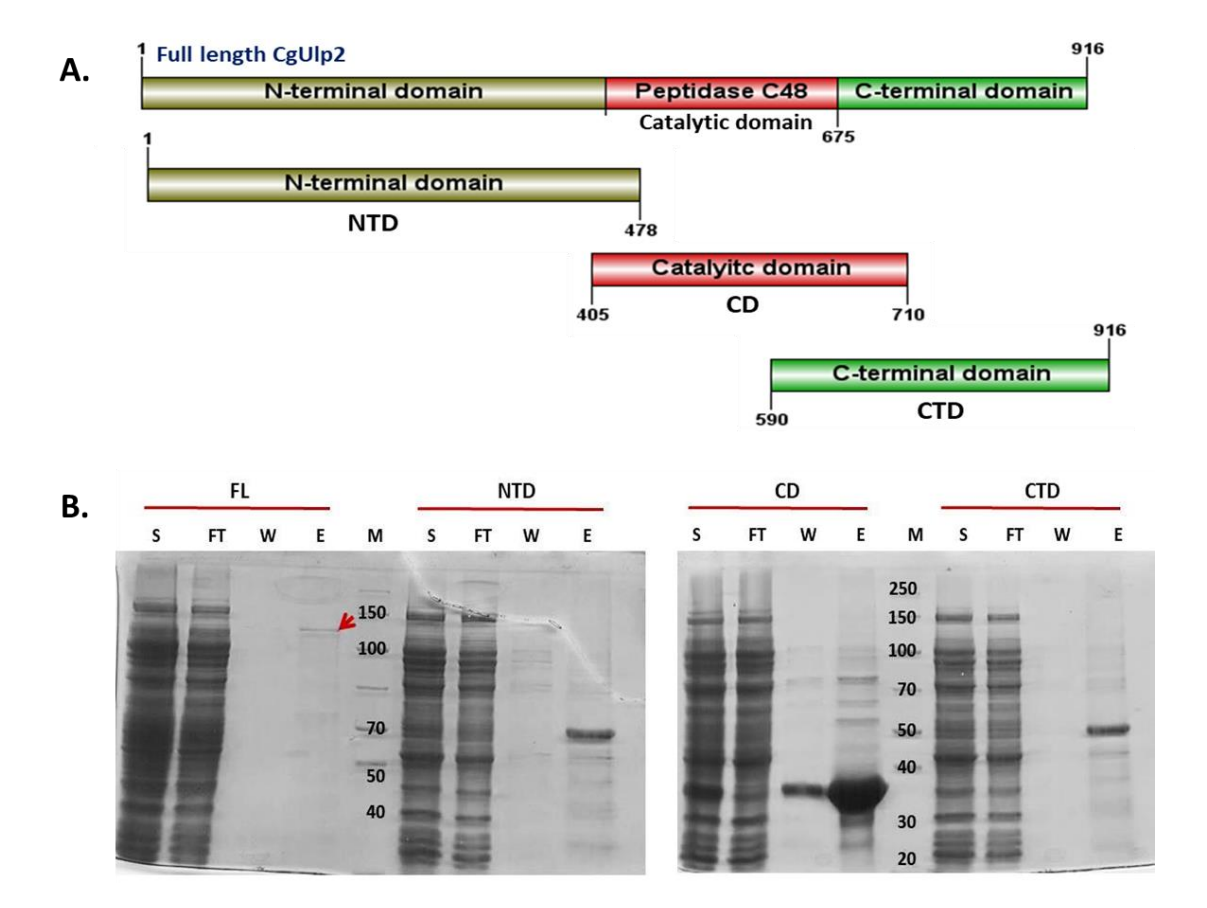


Figure 22. Purification of the CgUlp2 protein. A. Schematic representation of full-length CgUlp2 showing three individual domains: N-terminal domain (NTD-50kDa), Catalytic domain (CD-37kDa), and C-terminal domain (CTD-50kDa). **B.** Affinity purification of the CgUlp2 protein. S- supernatant form after sonication, FT- Flow through, W- Wash after binding of protein to Ni-NTA beads, E- purified protein elution, and M-protein marker.

To remove the non-specific proteins that were observed after affinity purification of the full length and the smaller fragments of CgUlp2 protein, size exclusion chromatography (gel filtration) was performed. The full length, NTD, and CTD of the CgUlp2 protein were observed

to form soluble aggregates, indicating a potential higher oligomeric state or both the NTD and CTD contain a significant amount of unstructured amino acid residues.

Secondary structure prediction of CgUlp2 protein

The PDBsum server was used to predict the secondary structures of the CgUlp2 SUMO protease. The analysis revealed that the N- and C-terminal domains of the CgUlp2 protein consist of unstructured residues, with the C-terminal domain exhibiting significant loop regions. In contrast, the catalytic domain of the CgUlp2 protein predominantly contains both α -helices and β -sheets. Altogether, the absence of a well-defined secondary structure in the N- and C- terminal domains posed challenges in the efficient purification of the full length and these domains. (Figure 23).

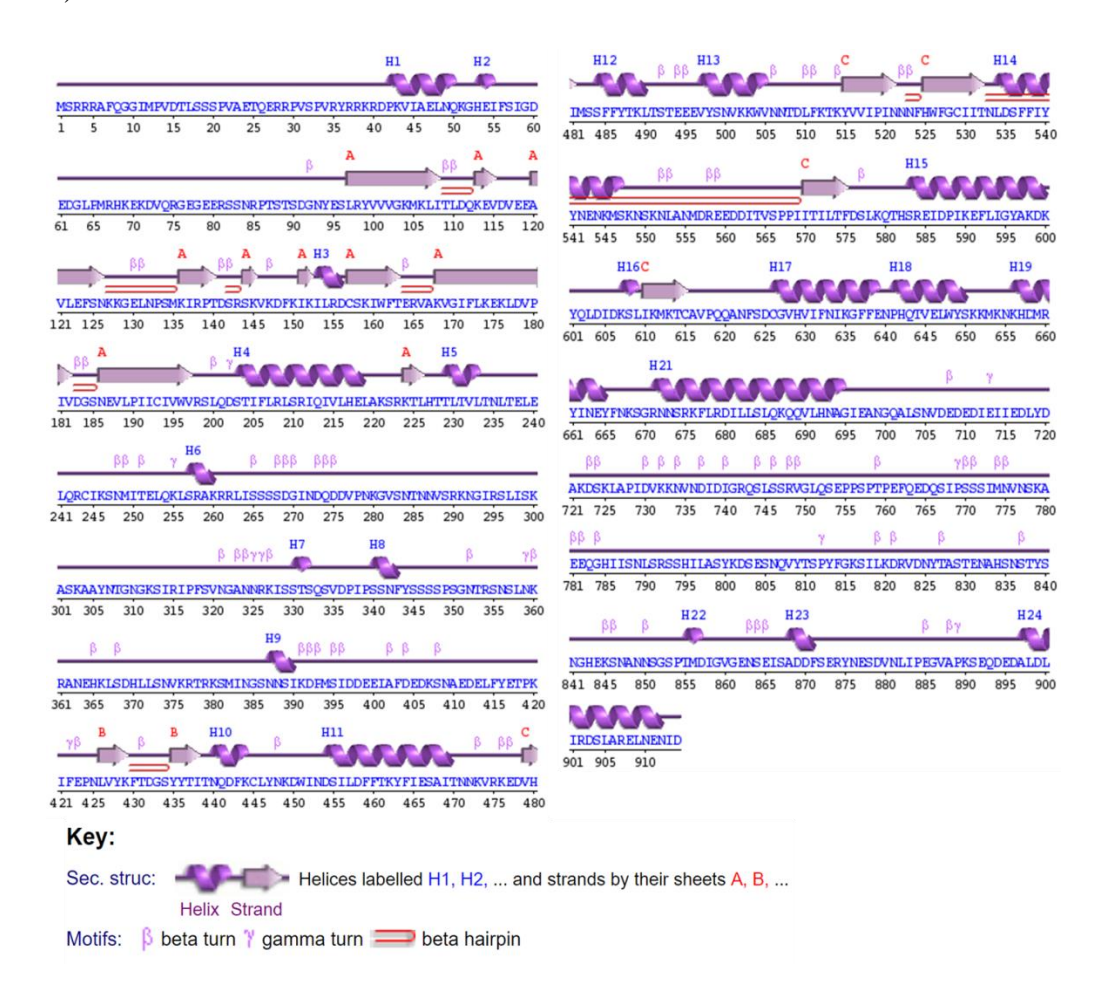


Figure 23. Diagrammatic representation of the CgUlp2 protein secondary structure as shown in PDBsum.

Crystallization of the catalytic domain of CgUlp2 protein

Our major goal is to obtain the crystals of the CgUlp2 protein for structural studies. To that end, since purification of full-length, N- and C- terminal domains of the CgUlp2 protein have low yield and soluble aggregates, we focused on the catalytic domain of this protein. The catalytic domain of the CgUlp2 protein was successfully purified (Figure 24A-B). This protein was concentrated to 12 mg/ml and utilized in experiments to crystallize. The preliminary screening was carried out using the sitting-drop vapor-diffusion technique. Microcrystals were developed in a variety of conditions (Figure 24C). Unfortunately, we didn't get good crystals of this protein upon optimization in various buffer conditions for X-ray diffraction to obtain a high-resolution structure of the protein.

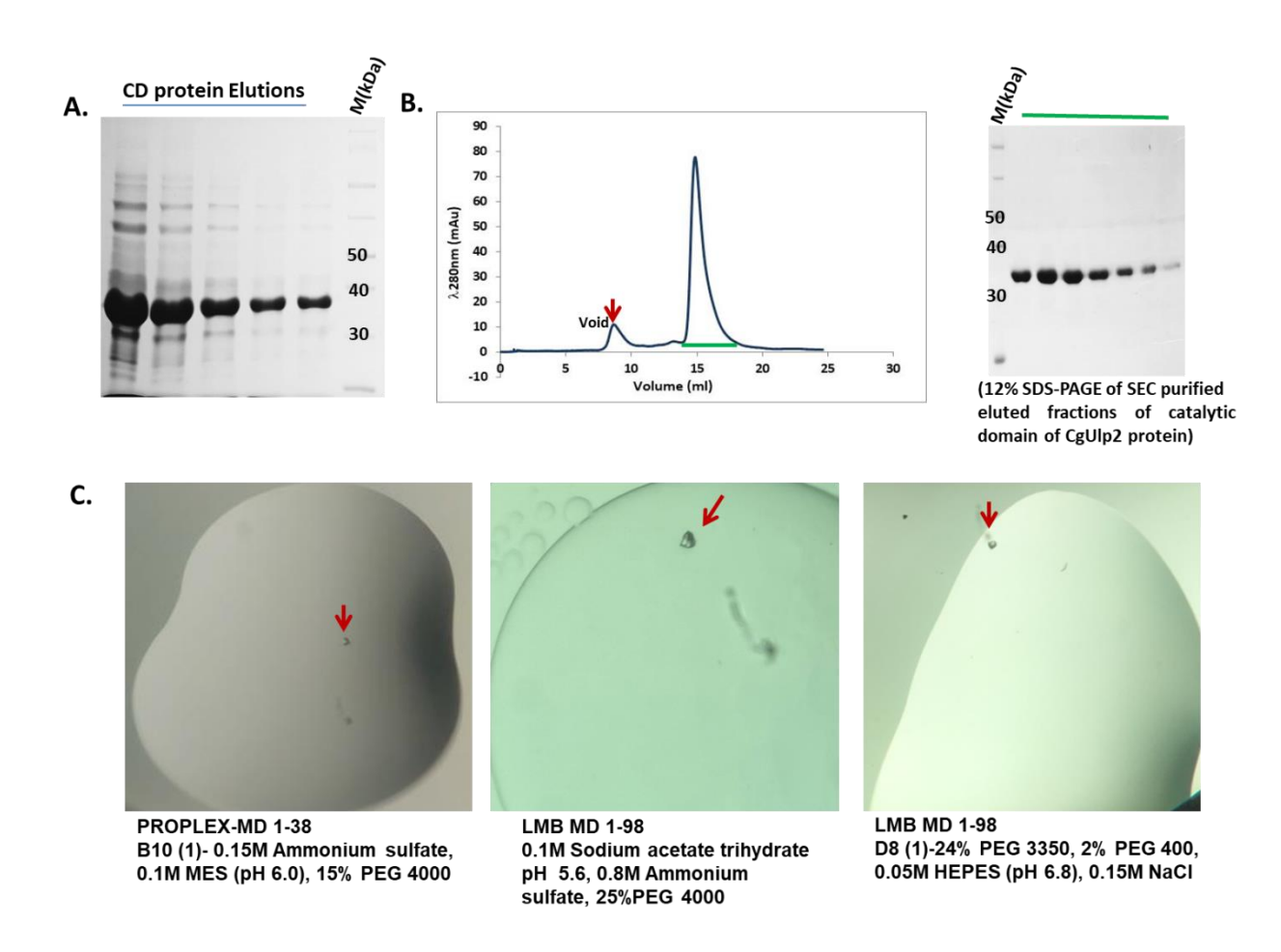


Figure 24. Purification and crystallization screening of the catalytic domain of CgUlp2 protein. A. 12% SDS-PAGE of the affinity purification of CD_CgUlp2 protein. B. Gel filtration

chromatographic elution profile of CD_CgUlp2 protein. C. Catalytic domain of CgUlp2 protein's crystal hits were shown in the above-mentioned buffer conditions.

Biophysical characterization of the SUMO protease CgUlp2 protein

1. Oligomeric state

SEC-MALS (Size exclusion chromatography-multiangle light scattering) was used to determine the oligomerization of CD_CgUlp2, with the column coupled to both multiangle and dynamic light scattering detectors. Multiangle light scattering facilitated the determination of weight-averaged molar masses, while dynamic light scattering provided information on translational diffusion coefficients (DT). The analysis revealed an average molecular weight of 36.2 kDa for the catalytic domain of the CgUlp2 protein, indicating that CD_CgUlp2 exists as a monomeric protein (Figure 25).

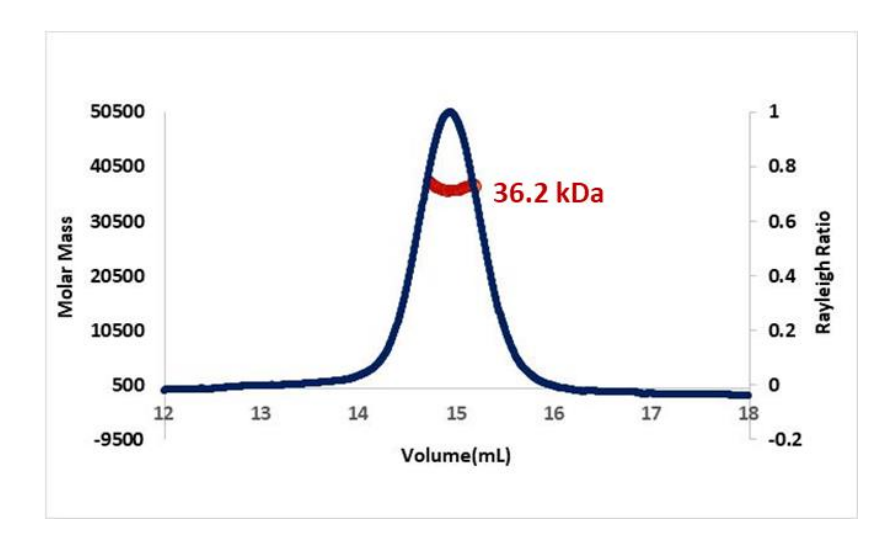


Figure 25. SEC-MALS profile showing the molecular weight of catalytic domain of CgUlp2 protein.

2. Steady-state fluorescence measurements

A Cary Eclipse fluorescence spectrometer was used to assess the intrinsic fluorescence of the protein. The protein solution, with a concentration of 0.2 mg/ml, was subjected to excitation at 295 nm, and the emission was measured within the wavelength range of 310-400 nm at 25°C . Both the excitation and emission slit widths were set to 10.0 nm. The spectra were recorded at a rate of 100 nm/min. The signal created by the buffer solution was used to remove background

emission. The CD_CgUlp2 protein intrinsic fluorescence spectrum had a maximum of 347 nm, indicating that tryptophan (W) residues were exposed to the surrounding environment (Figure 26A).

Further to know if there are any buried tryptophan residues, we performed the fluorescence experiments under the denaturing conditions. In the first case, we used denaturants on the CD_CgUlp2 protein. The CD_CgUlp2 protein samples, purified via SEC, were prepared at a concentration of 0.2 mg/ml and incubated with diverse concentrations of denaturants (ranging from 1.0 to 5.0 M for GdnHCl and from 0 to 6.0 M for urea) at pH 7.0 and 25 °C for a duration of 24 hours. In this analysis, fluorescence data obtained from scans of the native CD_CgUlp2, as well as those denatured with GdnHCl and urea, were used. In fluorescence measurements, the peak values observed for the CD_CgUlp2 protein in the presence of different denaturant concentrations were relatively similar to those of the native protein (Figure 26B-C).

In the second case, we used pH-induced denaturation on the CD_CgUlp2 protein. SEC purified CD_CgUlp2 protein samples were subjected to treatment in different pH buffers for 24 hours at 25°C. Buffers ranging from Glycine–HCl (pH 1-3), sodium acetate (pH 4), citrate–phosphate buffer (pH 5), potassium phosphate buffer (pH 6-7), Tris–HCl (pH 8–9), and glycine–NaOH (pH 10-12) were utilized at a concentration of 100 mM. Blank samples containing only the respective pH buffers without the protein were used to rectify the values. After 24 hours, the intrinsic fluorescence spectrum of CD_CgUlp2 protein was more or less identical to native protein in the pH range of 5.0–9.0, albeit with a slight left shift in fluorescence intensity observed at extreme acidic and alkaline pH values. This left shift of the intrinsic fluorescence spectrum indicates protein compactness. As a result, the protein was stable in the pH range of 5.0 to 9.0. (Figure 26D-E). Collectively, these findings suggest that the tryptophan residues located within the catalytic domain of CgUlp2 SUMO protease are exposed on the protein surface and exhibit stability across a range of ambient pH levels.

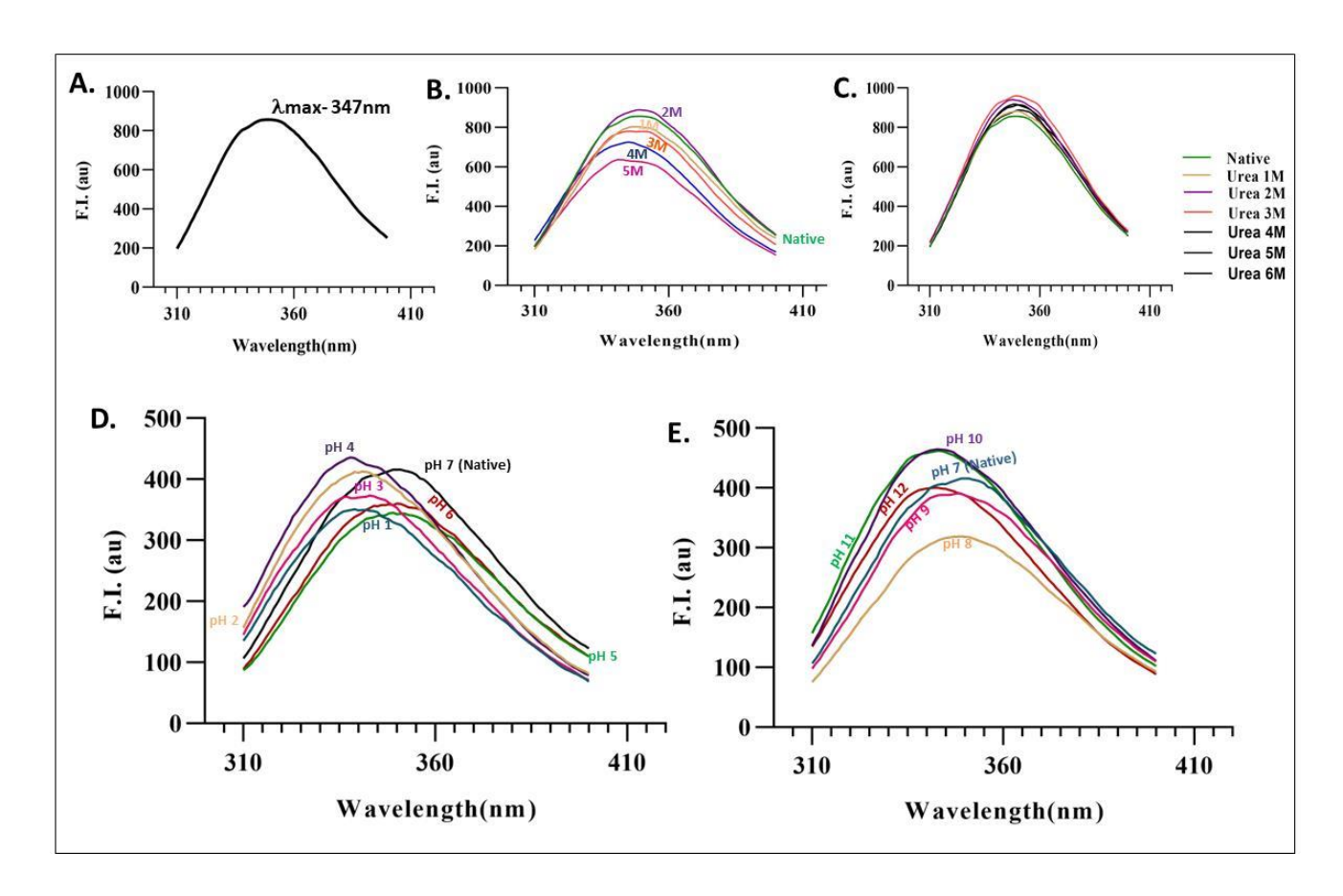


Figure 26. Fluorescence spectrum of the catalytic domain of CgUlp2. A. Tryptophan environment in native condition, **B-C**. GdnHcl and Urea mediated denaturation profile, **D-E**. pHinduced denaturation profile.

Secondary structure characterization by Circular dichroism (CD) spectroscopy

Far-UV CD spectra of the purified catalytic domain of CgUlp2 protein were recorded using a Jasco J-815-150S spectropolarimeter linked to a PTC343 Peltier unit circulating water bath set at 28°C. Spectra were acquired in a rectangular quartz cell with a 1mm path length over the range of 195-250 nm at a scan speed of 100 nm/min, a response time of 1 sec, and a slit width of 1 nm. A protein concentration of 0.3 mg/ml was maintained for all of the samples, and the average of

three scanned spectra was used to create each spectrum. CDPro software was used to calculate the relative amount of various secondary structural elements.

The far-UV CD spectrum of the native catalytic domain of the CgUlp2 protein exhibited negative ellipticity minima at 209 nm with a shoulder at 218 nm, along with positive maxima at 198 (Fig. 27A). The secondary structure components were estimated as 58.3 percent α -helix, 7.5 percent β -sheet, 17.7 percent turns, and 16.5 percent unordered using the CONTINLL tool of CDPro software.

During thermal denaturation, far-UV CD spectroscopy revealed a gradual decrease in negative ellipticity, indicating changes in secondary structure. Tm values of 45.8° C (R2 = 0.972) and 46.1° C (R2 = 0.978) were calculated using a sigmoidal fit analysis of the change in ellipticity at 209 and 218 nm (Fig. 27B). At and above 45° C, there was a significant alteration that resulted in the loss of structure. Proteins with an isodichroic point of about 203 nm also imply a two-state population (α -helix, random coil) (Fig. 27C). In summary, the catalytic domain of the CgUlp2 protein exhibited the presence of both the secondary structures, namely, α -helix, and β -sheet, with α -helix being the predominant form. However, these secondary structures were diminished under elevated temperatures.

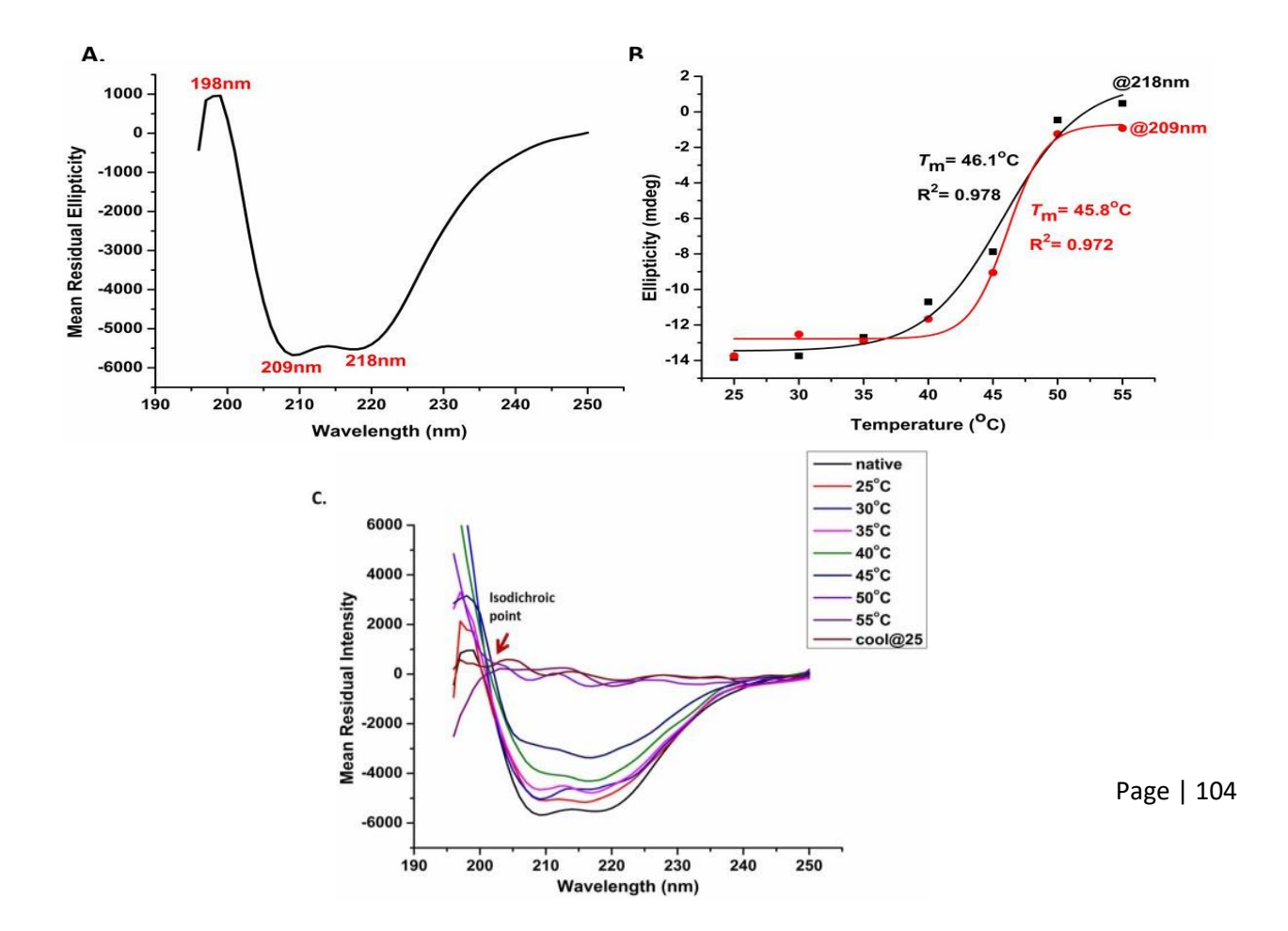


Figure 27. Secondary structure characterization of the catalytic domain of CgUlp2 protein (A) Far-UV CD spectrum (300 μ g/ml at pH 7.5), (B) Sigmoidal fit analysis of the change in ellipticity at 209 nm and 218nm following thermal denaturation at pH 7.5, (C) Far-UV CD spectra of the catalytic domain (0.3 mg/ml) incubated at various temperatures for 5 minutes.

Homology model of the catalytic domain of Ulp2 (CD_Ulp2) protein of various pathogenic fungi

ScUlp2 and HsUlp2 catalytic domains are currently the only crystal structures available in the protein data bank (PDB). Due to limited sequence similarity between the catalytic domains of CgUlp2 and HsUlp2 (PDB Id: 3EAY), which was only 29%, template 3EAY could not be used. Therefore, the catalytic domain of *S. cerevisiae* Ulp2 (PDB Id: 5LNB) with a higher sequence identity of 58.57 percent and 96 percent sequence coverage, was selected as the template for building a homology model of the catalytic domain of the CgUlp2 protein using SWISS-MODEL. The resulting models were subjected to energy minimization and refinement processes using GalaxyWeb and PROCHECK.

The quality of the models was assessed using PDBsum, which evaluated them based on Ramachandran plots. PDBsum was used to examine secondary structural elements of the homology models that were created. The model demonstrates that the CgUlp2 SUMO protease catalytic domain has both secondary structures (helices and sheets), with α -helices in the majority (Figure 28A). The Ramachandran plot analysis indicated that the resulting model conformed to the requirements for favored and allowed regions (Figure 28B, Table 8).

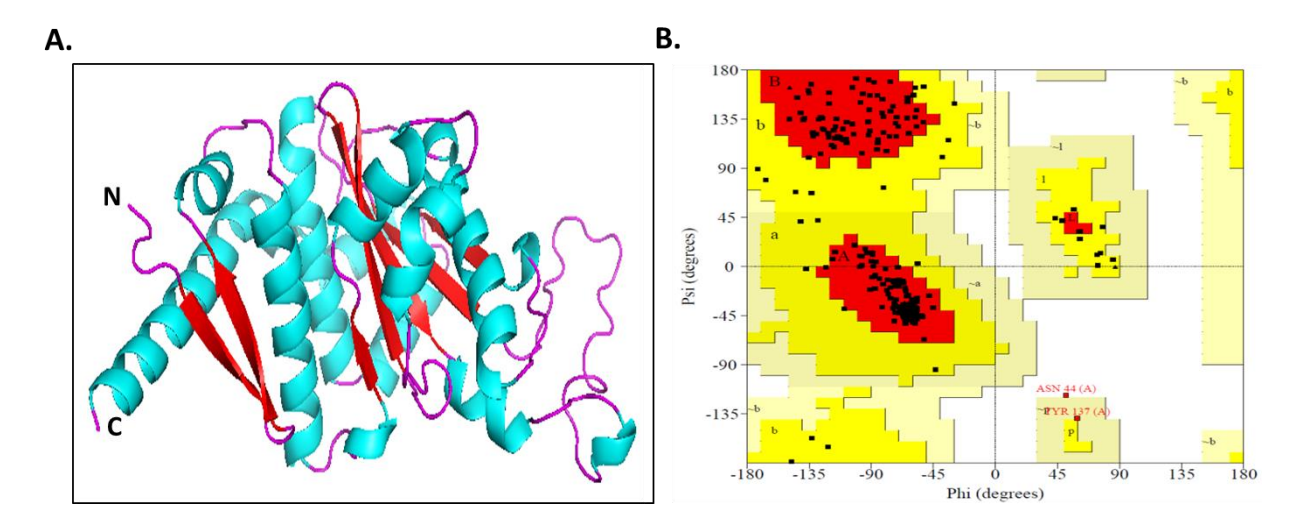


Figure 28. Homology model of CD_CgUlp2 protein. (**A**) Cartoon representation of the homology model of CgUlp2 SUMO protease catalytic domain built using *S. cerevisiae* Ulp2 protein (PDB ID: 5LNB) as a template. (**B**) Ramachandran plot for model validation.

Table 8. Ramachandran plot statistics for the homology model of CD_CgUlp2 protein (after refinement)

	No. of Residues	Percentage
Most favored + additionally allowed regions	211	99
Generously allowed regions	2	0.9
Disallowed regions	0	0

Furthermore, using ScUlp2 as a template, we performed homology modeling for the catalytic domain of Ulp2 proteins from several fungal species (for example, C. albicans (CaUlp2), C. auris (CauUlp2), A. nidulans (AnUlp2) and C. neoformans (CnUlp2)). After energy minimization and refining, the models were validated by Ramachandran plot (RCP). With C. glabrata, the catalytic domain of Ulp2 protein of C. albicans and C. auris has both secondary structures (helices and sheets) with 99.2% RCP. With an additional large unstructured region, A. nidulans and C. neoformans catalytic domains have α -helices and β -sheets with 96.5% and 91.8% RCP (Figure 29A). To identify pan-antifungal targets, we superimposed the catalytic domain of C. glabrata (CgUlp2), C. albicans (CaUlp2), C. auris (CaUlp2), A. nidulans

(AnUlp2) and *C. neoformans* (CnUlp2) with *S. cerevisiae* (CD_ScUlp2) and *Homo sapiens* (CD_HsUlp2). We observed that α-helices and β-sheets of all these fungal species overlapped with CD_ScUlp2 with the exception that CD_ScUlp2 -helices at the C-terminus were missing in CD_CnUlp2 (Figure 29B). While there was conservation among the fungal proteins, the β-sheets of these organisms did not overlap with CD_HsUlp2 and had less similarity with the human protein (Figure 29C). Since the overlap with human Ulp2 is much less based on homology models, the catalytic domain of the Ulp2 protein could serve as a non-toxic antifungal target.

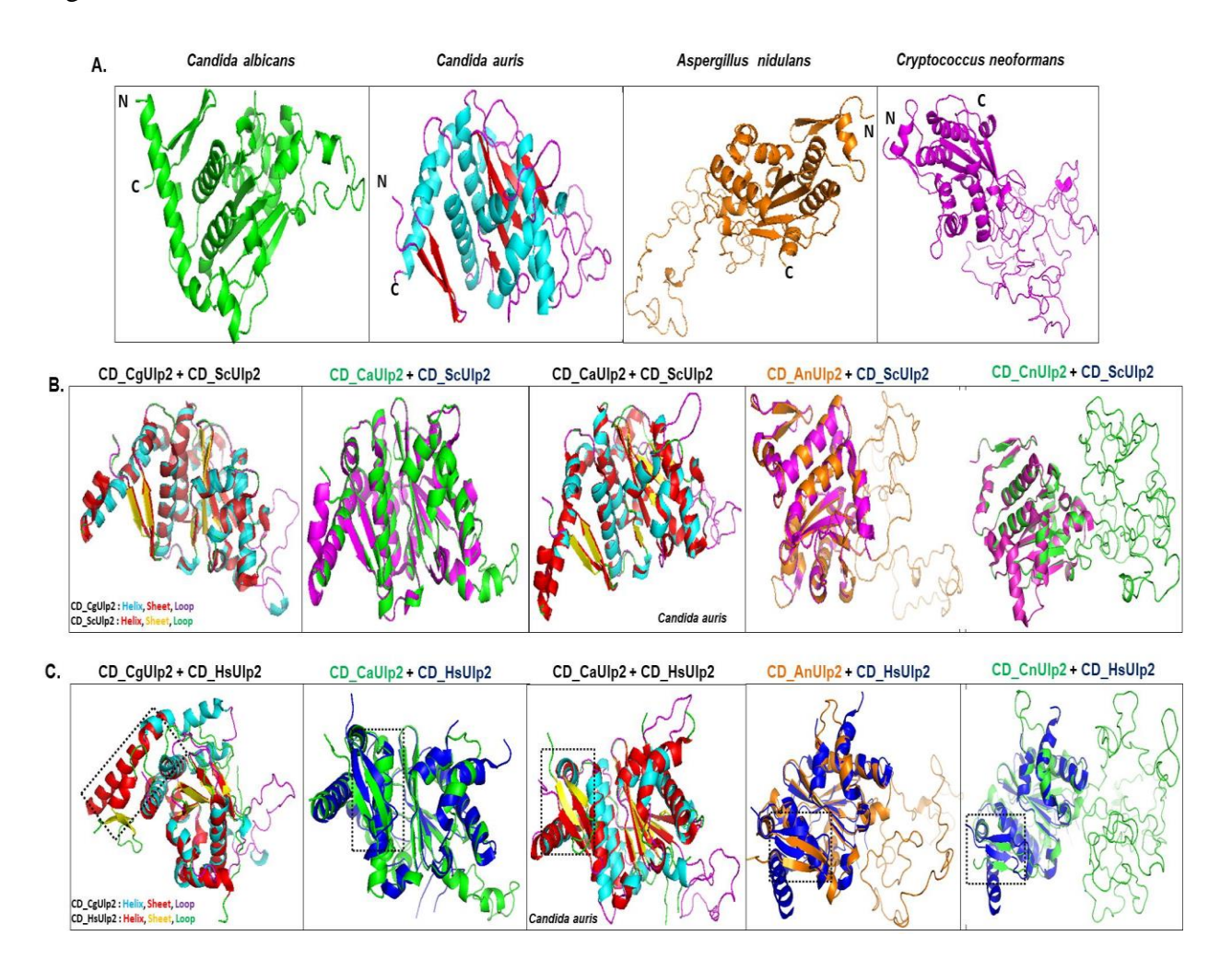


Figure 29. Homology modeling of the catalytic domain of Ulp2 protein of various pathogenic fungi. A. Cartoon representation of homology models of Ulp2 SUMO protease catalytic domain of *C. albicans* (CaUlp2), *C. auris* (CauUlp2), *A. nidulans* (AnUlp2) and *C. neoformans* (CnUlp2) using *S. cerevisiae* Ulp2 protein as a template. **B.** Superimposition of

CD_Ulp2 protein of various pathogenic fungi with CD_ScUlp2. C. Superimposition of CD_Ulp2 protein of various pathogenic fungi with CD_HsUlp2. Non-overlapping β-sheets among the catalytic domain of CgUlp2, CaUlp2, CauUlp2, AnUlp2, and CnUlp2 are represented by a black dotted box.

CgUlp2 protein has conserved catalytic triad residues

Based on sequence alignment and active center similarities with the catalytic domain of Ulp2 protein for both the S. cerevisiae (PDB Id: 5LNB) and H. sapiens (PDB Id: 3EAY), key catalytic residues were identified for CgUlp2 protein. We identified His525, Asp576, and Cys626 as the potential catalytic triad residues by aligning the sequences of ScUlp2, CgUlp2, and HsUlp2 proteins (Figure 30A). In the CD CgUlp2 model, these residues were found in β-sheet (His525), loop (Asp576), and α-helix (Cys626) respectively (Figure 30B). To validate the conserved catalytic triad, we mutated Cys to Ser at position 626 by site-directed mutagenesis. Complementation with the C626S mutant of CgUlp2 showed that it was similar to Cgulp2\Delta single mutant under various stress conditions (Figure 30C). This indicates that the C626S could be catalytically inactive. We further confirmed this by checking the SUMOylation pattern of this mutant. We used an α-FLAG antibody to perform a western blot on whole cell lysates from the C. glabrata WT, $Cgulp2\Delta$, $Cgulp2\Delta/CgULP2$, and $Cgulp2\Delta/CgULP2(C626S)$ augmented with dual tagged CgSmt3 protein (carrying 6xHis and FLAG epitopes at the N-terminus). Higher molecular weight SUMOylated proteins were not observed after the cysteine was changed to serine, which was similar to the $Cgulp2\Delta$ single mutant (Figure 30D). Altogether, these results show His525, Asp576, and Cys626 as the conserved catalytic triad residues in the CgUlp2 protein.

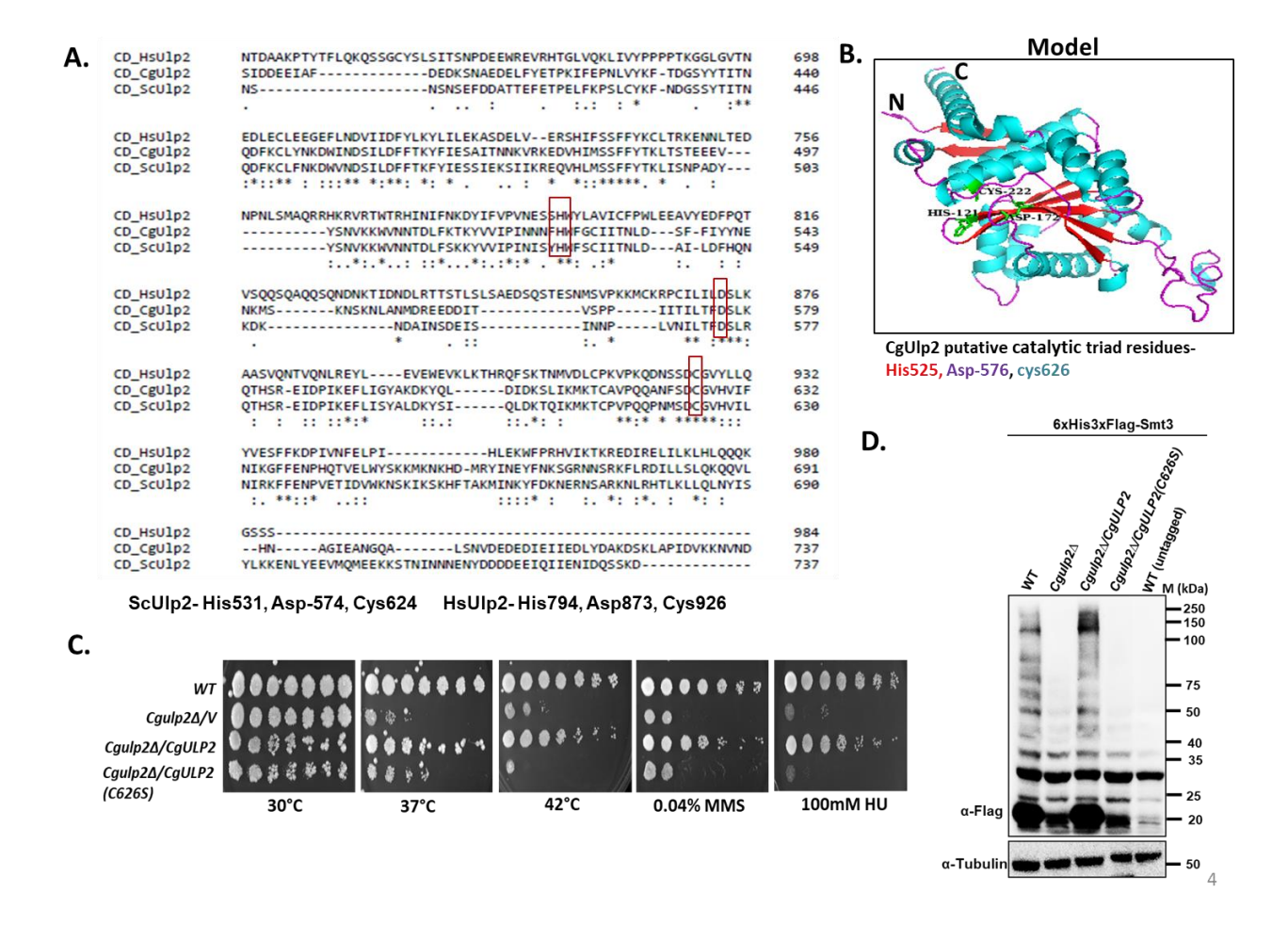


Figure 30. Conserved catalytic triad residues (His-Asp-Cys) of CgUlp2 protein. A. Multiple sequence alignment of the catalytic domain of Ulp2 protein of *S. cerevisiae*, *C. glabarta*, and *H. sapiens* using Clustalw. The catalytic triad was represented in red color rectangular box **B.** The catalytic triad comprised histidine (525), aspartic acid (576), and cysteine (626) residues. PyMOL was used to create the figures. **C.** Growth was examined under various stress conditions to test the complementation of *Cgulp2*Δ phenotype by C626S mutant of CgUlp2 to validate the conserved catalytic triad. On different media, 2μl of 10-fold serial dilutions of 1.0 A600 YPD medium-grown normalized cultures of *C. glabrata* strains were spotted. Plate images were taken after 2 days of incubation at 30°C and 37°C, and 3 days of incubation with Methylmethanesulfonate (MMS), hydroxyurea (HU) at concentrations of 0.04%, and 100 mM, respectively, and 4 days of incubation at 42°C. **D.** Strains were grown in CAA medium and an equal number of cells were taken for whole-cell extracts. Western blot analysis was carried out to examine the SUMOylation status of whole cell extracts using the α-FLAG antibody.

CgUlp2 interacted with CgSmt3 (SUMO) protein directly via SUMO-interacting motifs

As fungi are eukaryotic organisms, it is difficult to identify a drug target because the protein we are targeting must not be present in the host or be sufficiently different from the pathogen protein. As CgUlp2 had the least similarity to the human ortholog among the SUMO pathway enzymes, we hypothesized that it could be a potential antifungal target. We would like to develop SUMOylation inhibitors as a potential antifungal target. We hypothesized that the interaction of the SUMO of polySUMOylated protein with Ulp2 would be essential for Ulp2 function. As a result, we investigated whether Ulp2 and SUMO interact. To do so, we performed the molecular docking of both the catalytic domain of the CgUlp2 and CgSmt3 proteins. A homology model of the CgSmt3 protein was created using the SWISS-MODEL, with a sequence identity of 87.88 percent and 92 percent sequence coverage, utilizing the S. cerevisiae Smt3 protein as a template. Using GalaxyWeb and PROCHECK, the model was subjected to energy minimization and refining. Using the Cluspro 2.0 server, we then performed protein-protein interactions for both of the aforementioned proteins and revealed that CD CgUlp2 and CgSmt3 were primarily interacting hydrophobically at the interfacial regions (Figure 31A). Additionally, we have shown that CD_CgUlp2 ILE 165 (the first amino acid residue of the SUMO-interacting motif) interacts with CgSmt3 ARG 79, and GLU 102 and that CD_CgUlp2 M208, K209, T210, and K248 (the helices) interact hydrophobically with CgSmt3 ILE104 (the loop) (Figure 31B).

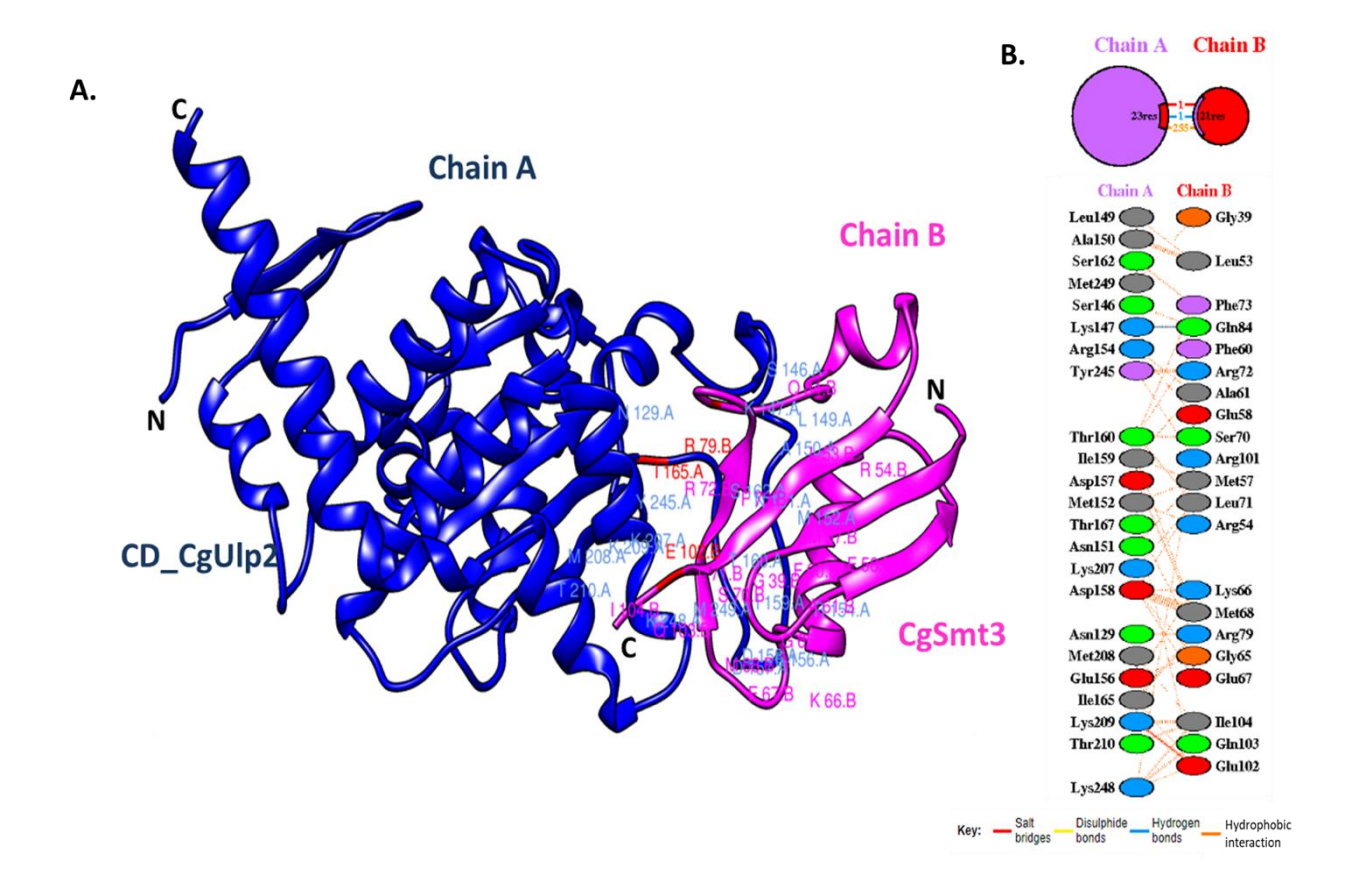


Figure 31. Interaction studies of SUMO protease CgUlp2 and SUMO protein. A. CD_CgUlp2 (Chain A) protein was docked with CgSmt3 (Chain B) protein by using ClusPro 2.0 to identify the interaction between these proteins. Chimera was used to generate the model. B. Diagrammatic illustration showed the amino acid residues of CD_CgUlp2 that interacted with the CgSmt3 protein.

To validate the interaction between both proteins, we used yeast two-hybrid (Y2H) studies to show that this interaction happens physically. Based on the fact that eukaryotic transcriptional activators have two domains-the DNA binding domain (DBD) and the activating domain (AD)—the yeast two-hybrid system was developed. In this test, two proteins of interest (X and Y) are fused to the DNA binding and activating domains of GAL4. Here, the "bait" was DBD- fused to domains of CgUlp2, and the "prey" was GAD-CgSmt3. A functional GAL4 transcription factor is produced when the two proteins physically bind, causing the reporter gene to be expressed under the control of the GAL4 promoter. In our study, we found that all three domains of the CgUlp2 protein interacted physically with the CgSmt3 protein (Figure 32A).

Further, we wanted to see if this interaction was direct through in vitro pull-down experiments. We cloned domains of the CgUlp2 protein and CgSmt3 protein in bacterial expression vectors and these proteins were expressed well (Figure 32B). We cotransformed *E. coli* cells for CTD_CgUlp2 and CgSmt3. We colysed the pellets from two cultures for CD_CgUlp2 and NTD_CgUlp2 pull-down experiments with CgSmt3. The cell lysates were then purified using Ni-NTA resins. When we eluted His-tagged protein (NTD_CgUlp2, CgSmt3) using imidazole then GST tagged proteins (CgSmt3, CD_CgUlp2, and CTD_CgUlp2) was also present in elution fraction which shows that CgUlp2 domains do interact with CgSmt3 directly. Western blot confirms the invitro pull-down results using α-GST and α-His antibodies (Figure 32C).

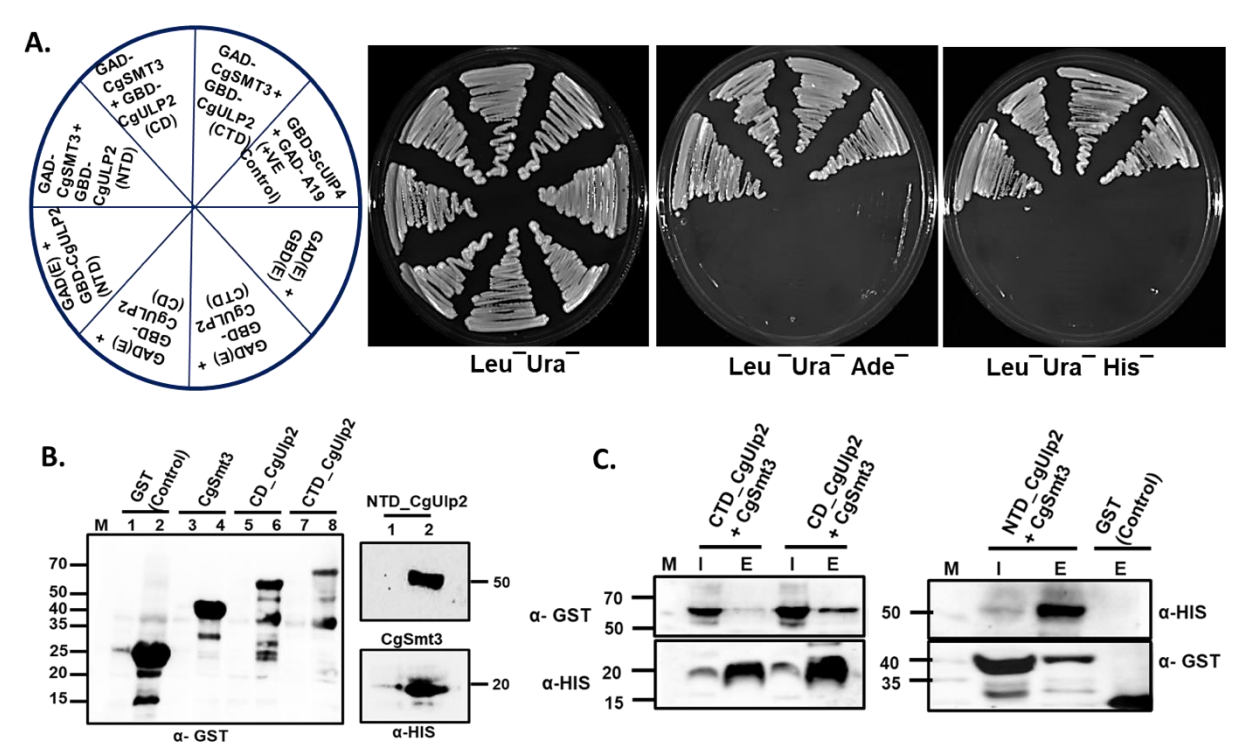


Figure 32. Interaction of domains of CgUlp2 protein with CgSmt3 protein. A. Domains of CgUlp2 protein were shown to have interaction with CgSmt3 protein physically by using a Yeast-two hybrid assay. B. Western blot analyses to show the expression of CgUlp2 domains and CgSmt3 protein constructs in BL21(DE3)-RIL bacterial expression strain using α-HIS and α-GST antibodies. Lane M: Protein marker (kDa), 1, 3, 5, and 7: Uninduced samples and 2, 4, 6, and 8: Induced samples. C. Western blot analyses showing the direct interaction of domains of CgUlp2 and CgSmt3 protein by invitro pull down using α-HIS and α-GST antibody. Lane M, I, and E: Protein marker, Input, and Eluate.

Further, we wanted to test the possibility that the interaction between CgUlp2 domains and CgSmt3 protein was due to the putative SUMO-interacting motif (SIM) present in the CgUlp2 protein. SIM motifs have been previously identified in the C-terminal domain of the Ulp2 protein in *Saccharomyces cerevisiae* ¹³³. We predicted SIM motifs (amino acid residues in N-terminal-IICI, and IQIV; in catalytic domain- IITI, and in the C-terminal domain- IEII) in the CgUlp2 protein using the GPS-SUMO server (Figure 33A). Now, if the predicted SIM motifs in these domains are crucial for the interaction of CgUlp2 with SUMO protein, the interaction with SUMO would be compromised. For this, we successfully generated SIM mutated catalytic domain (I569K) and C-terminal domain (I712T) of CgUlp2 protein which was expressed well under IPTG induction. We performed an in vitro pull-down assay with either Ni-NTA or GST resin beads and found that the SIM mutant of both the domains did not interact with CgSmt3 anymore (Figure 33B-C). It lost the ability to bind to SUMO following the mutation, suggesting that the predicted SIM is essential for binding of CgUlp2 and CgSmt3 protein and also the putative SIMs were actual SIMs present in the Ulp2 protein of *C. glabrata*.

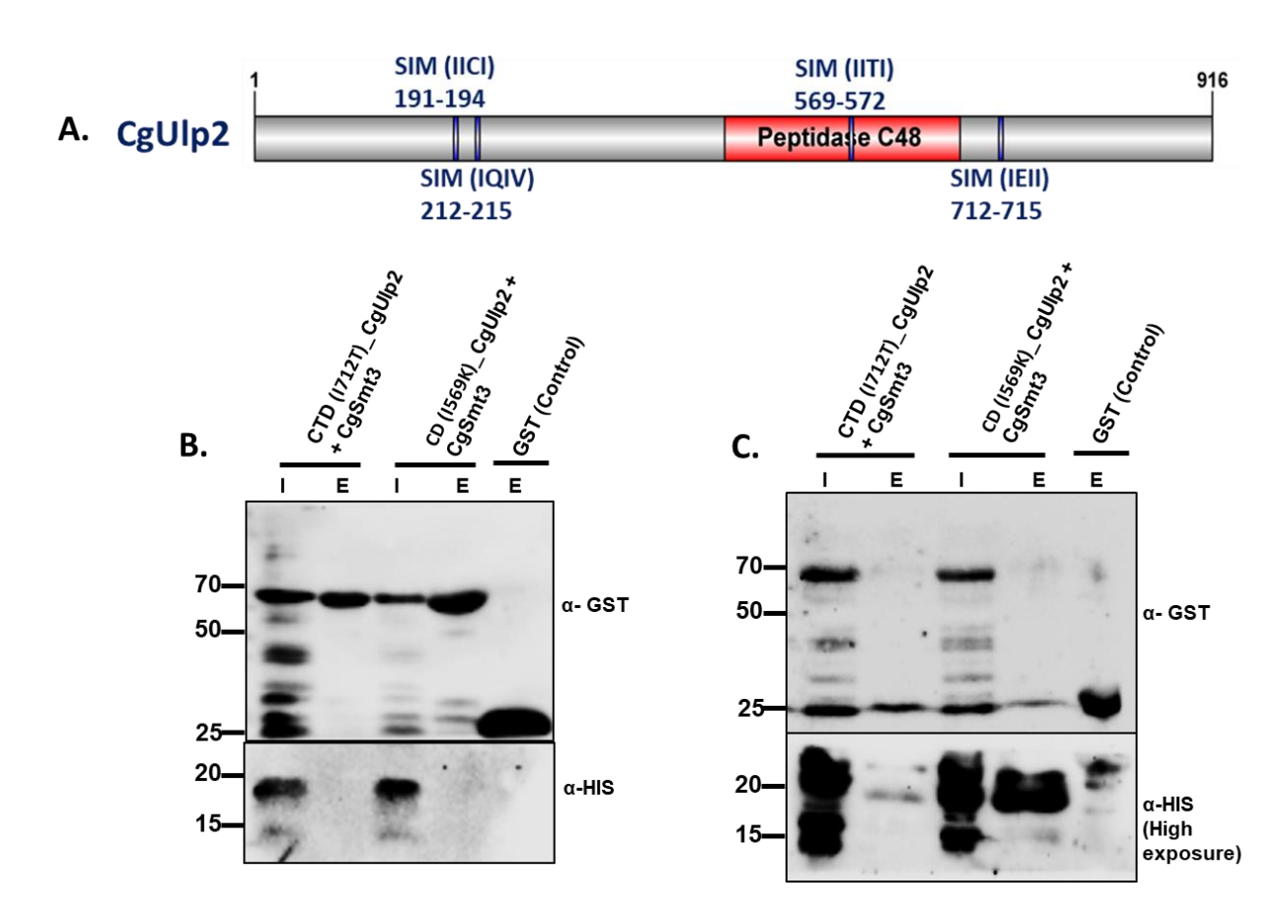


Figure 33. A. CgUlp2 interacted with CgSmt3 by SUMO-interacting motifs. Schematic representation of CgUlp2 protein showing putative SUMO-interacting motifs (SIMs) using GPS-SUMO server. **B-C.** Invitro pull-down was performed either with Glutathione (left side) or Ni-NTA resin beads (right side). Western blot was performed using the α -HIS and α -GST antibodies revealing that the SIM mutant of the CgUlp2 protein did not interact with the CgSmt3 protein. Lane M, I, and E: Protein marker, Input, and Eluate.

Functional characterization of SUMO-CgUlp2 interaction

1. Longer linear SUMO chains have a greater affinity towards the binding of the CgUlp2 protein.

As CgUlp2 targeted polySUMOylated substrates, we then checked the interaction between CgUlp2 protein (WT and SIM mutant) and linear SUMO chains of various lengths (1x-SUMO from *C. glabrata*, 2x-SUMO, and 6x-SUMO from *S. cerevisiae*) of *S. cerevisiae* by performing the binding assay. All the constructs were expressed and purified from bacteria. When the full length of CgUlp2 protein was exposed to a combination of different lengths of linear SUMO chains, we found that it selectively and tightly interacted with 6x-SUMO proteins but not with 2x-SUMO or 1x-SUMO (Figure 34B). This protein was weakly attached to 2x-SUMO while performing with each linear SUMO chain separately (Figure 34A). A similar finding was made with the catalytic domain of CgUlp2 protein (WT). However, this was not the case for the CD_CgUlp2 SIM mutant as it didn't bind to the linear SUMO chains (Figure 34C-D). This indicates that the CgUlp2 protein has a greater affinity to bind to larger linear SUMO chains.

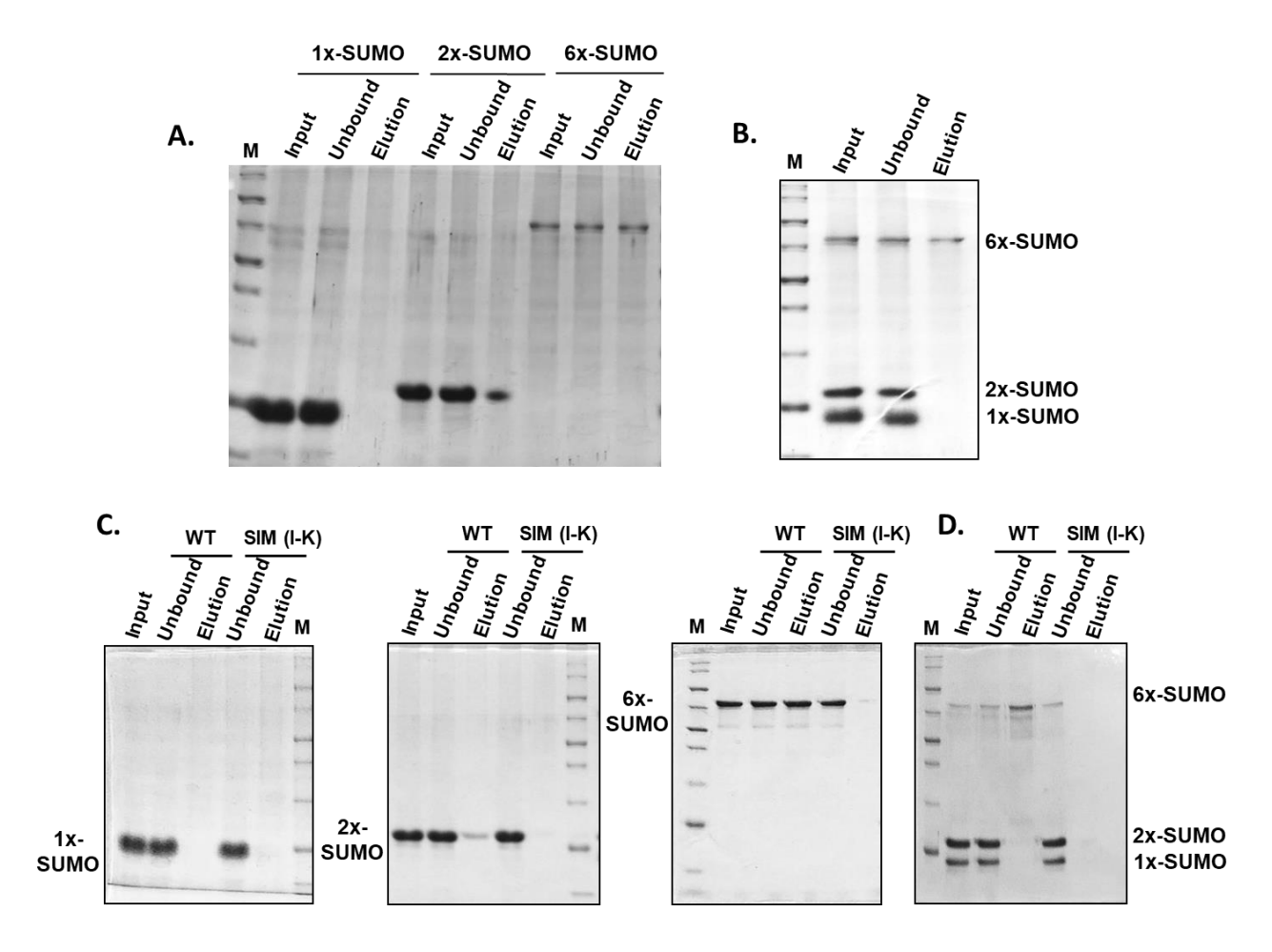


Figure 34. Longer linear SUMO chains are the preferred binding partners of the CgUlp2 protein. Pulldown assay is used to determine if the linear SUMO chains bind to (A) the full length of SUMO protease CgUlp2 individually or (B) in combination, (C) WT or SIM mutant of the catalytic domain of CgUlp2 protein individually or (D) in combination. M- protein marker

2. Enhanced SUMO protease activity induced by the SUMO interacting motif of the CgUlp2 protein

We investigated the effect of full-length and CD_CgUlp2 SIM in modulating Ulp2 SUMO protease activity in vitro to understand the function of CgUlp2 SIM. To do this, we expressed and purified both the full-length (WT) and CD_CgUlp2 (comprising amino acid residues 400-750) variants, including either the WT or SIM mutant, from bacterial sources. Additionally, recombinant 2x-SUMO and 6x-SUMO were purified from bacteria and employed in the assays (Figure 35A). Subsequently, 100 μg of each of these proteins (EDTA-free), whether it be a dimer or hexamer, was added to 50 μl of PBS containing 1 mM DTT and 1 μg of full-length (WT) and

CD_CgUIp2 (WT or SIM mutant) at room temperature. At specified time intervals (0, 15, 30, and 60 minutes) subsequent to the initial addition of each construct, 10 µl aliquots of the reaction were taken for SDS-PAGE analysis. Each fraction was loaded onto a 12% SDS-PAGE gel and subjected to Coomassie staining for visualization. We found that CgUlp2 SUMO protease activity for all the linear SUMO substrates is drastically decreased by the SIM mutant. However, in the case of WT, the impact appeared more pronounced as the SUMO chain length increased. This suggest that CgUlp2 SIM enhances its affinity for longer SUMO chains, enabling it to preferentially cleave such substrates (Figure 35B-C). Thus, our results indicate a preference of the CgUlp2 protein for cleaving longer SUMO chains in vitro.

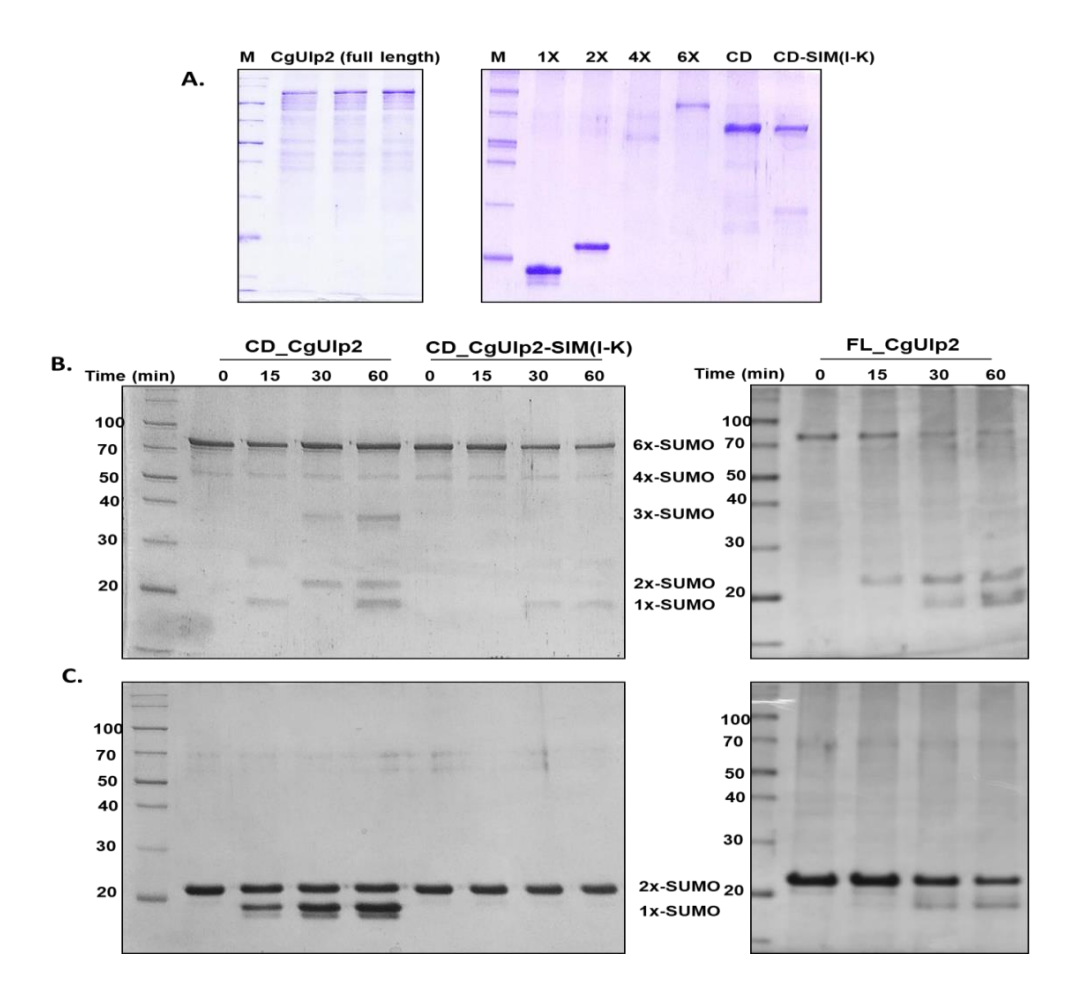


Figure 35. The SUMO protease activity of CgUlp2 targeting linear SUMO chains is encouraged by the CgUlp2 SIM. A. purified full-length (WT), CD (WT and SIM mutant) of CgUlp2 proteins stained with Coomassie. B-C. CgUlp2 enzyme cleavage of 2x, and 6x-SUMO (WT and SIM mutant).

Structure of the SUMO protease CgUlp2 full length with 6x-SUMO protein complex revealed by Negative stain electron microscopy (EM)

As we were getting microcrystals of the catalytic domain of CgUlp2 protein, we could not pursue the X-ray crystallography. In Figure 34, we have shown that the CgUlp2 protein binds tightly to 6x-SUMO and also this protein has 4 SUMO-interacting motifs. So, intending to solve fulllength CgUlp2 protein with the 6x-SUMO complex structure to gain insight into interaction, we analyzed the structure of this complex using electron microscopy. Initially, we purified the CgUlp2•6xSUMO protein complex, confirming the presence of both proteins in the eluted fraction through 10% SDS-PAGE (Figure 36A). Subsequently, the purified protein complex at a concentration of 0.05 mg/mL was adsorbed on EM grids and stained with 2% uranyl acetate. Using approximately 4473 selected particles, single-particle analysis was conducted using CryoSPARC. Figure 36B shows the representative micrograph of purified CgUlp2•6xSUMO complex stained with 2% uranyl acetate. The 2D class averages obtained from this analysis revealed the "globular structures" of the complex (Figure 36C). These 2D classes were further utilized for ab initio 3D reconstruction and refinement, resulting in the generation of the density map (Figure 36D). We obtained the homology models of the CgUlp2 protein using the SWISS model and 6xSUMO using PHYRE and then built a complex model. This modeled complex was subsequently docked into the EM density map (Figure 36E), demonstrating an excellent fit withinthe density and adopting a compact 'globular' shape within it. Overall, the architecture of the CgUlp2•6xSUMO complex exhibited a compact globular structure.

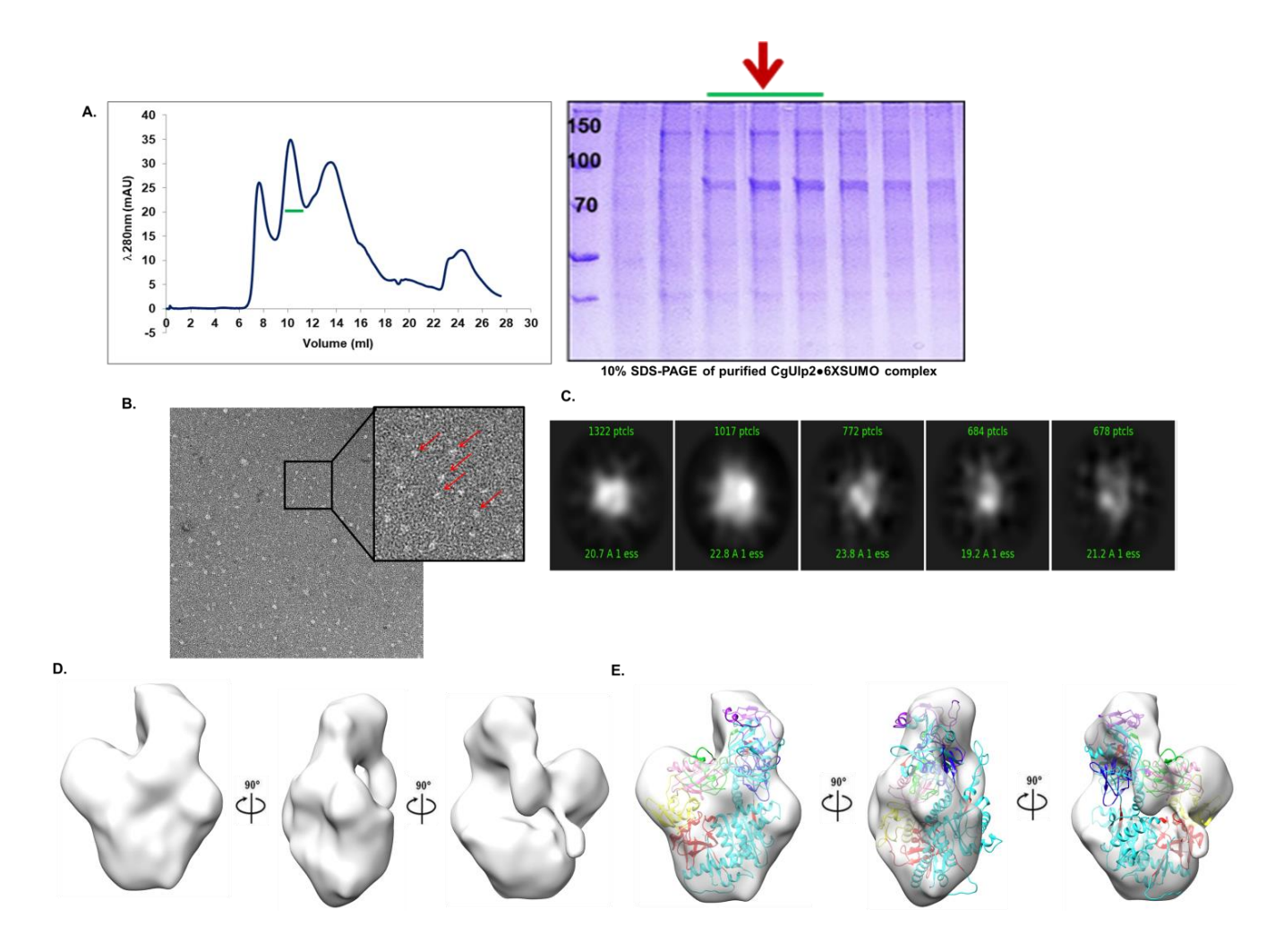


Figure 36. Negative staining EM analysis of CgUlp2•6xSUMO complex complex. A. Gel filtration profile of the CgUlp2•6xSUMO complex followed by 10% SDS-PAGE that showed the purified complex. The fraction of the protein complex indicated in the red arrow was used for the negative staining. B. A representative micrograph of purified CgUlp2•6xSUMO complex stained with 2% uranyl acetate. Representative particles used for the analysis are shown with the red arrow. C. Representative 2D class averages. D. 3D density map obtained for the CgUlp2•6xSUMO complex. E. The density map is fitted with modeled structures of the complex.

Pharmacophore-based virtual screening of CD_CgUlp2-CgSmt3 protein complex for small molecule inhibitors (ligands)

To identify inhibitors that will disrupt the interaction of CD_CgUlp2 and CgSmt3 protein, we have taken an approach of pharmacophore-based virtual screening of this complex. To do this, we used the CD_CgUlp2-CgSmt3 protein complex (shown in Figure 31A) to predict the active site residues of this complex.

Determination of active site on the protein

The active site with the highest druggability for -CD_CgUlp2_CgSmt3 was identified precisely at the docking interface of CD_CgUlp2 and CgSmt3 protein. The amino acid residues that were involved in the active site prediction were mentioned as follows- CD_CgUlp2 (Chain A): 45, 173, 214, 216, 221, 222, 224, 225, 228, 229, 231, 232, 233, 235, 236, 240, 261, 262, 263, 264, 265, 266, 267, 268, 269, 270, 271, 273 and CgSmt3 (Chain B): 33, 37, 39, 40, 41, 24, 43, 44, 45, 46 (Figure 37), with druggability score of 0.80.

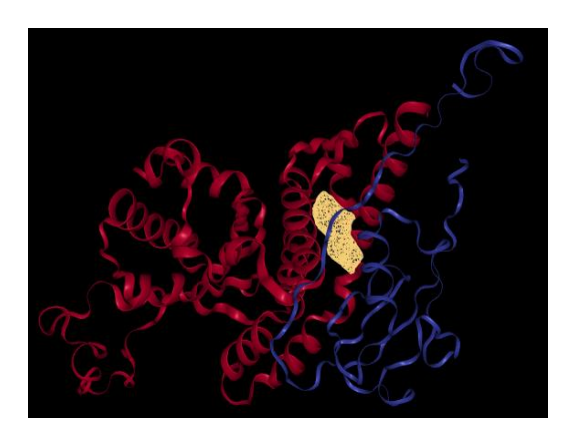


Figure 37. Active site of the CD_CgUlp2_CgSmt3 protein complex. CD_CgUlp2 protein is represented in red color and CgSmt3 protein is represented in blue color along with the docking site shown in the beige color electron cloud.

Virtual screening for ligands with pharmacophore map and binding energy calculations

The pharmacophore map for the CD_CgUlp2_CgSmt3 protein complex was derived using the 'Phase' module of Schrodinger suite ¹²⁰. 7 molecular features were determined for active site on CD_CgUlp2-CgSmt3, consisting of three aromatic rings (R25,R20 and R21), two sites with low

electron (N14 and N16) density and two sites with maximum electron density (D11 and D13) (Figure 38).

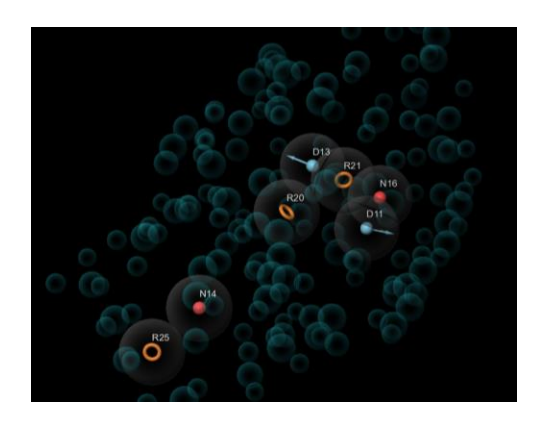


Figure 38. Pharmacophore map of CD_CgUlp2_CgSmt3 protein complex. Protein in the background shows electron density in blue bubbles, with pharmacophore features (R25, R20, R21, N14, N16, D11, and D13).

The Pharmit website was used to search for ligands using the coordinates of these pharmacophore features (listed in Table 9). It used open repositories from NCI, CHEMBL32, Molport, ChemDiv, ChemSpace, MCULE, PubChem, ZINC, and LabNetwork to filter ligands. From thousands of molecules, lead molecules were selected using the RMSD and MM/GBSA scores (Table 10). Apart from this, an independent screening from 2000 FDA drugs was done using a Phase module from Schrodinger, and the top 10 molecules that showed MM/GBSA ≤ 0.002 were carried forward for molecular docking with protein.

Table 9. Coordinates (X, Y, and Z) of pharmacophores for the CD_CgUlp2-CgSmt3 protein complex.

Pharmacophore	X	Y	Z
R25	27.56	19.09	61.89
R21	14.67	27.75	61.12
R20	17.63	25.03	60.56
N14	24.04	20.73	61.74
N16	14.78	30.10	63.50
D11	16.35	29.14	63.98
D13	15.56	27.53	59.18

Molecular docking

Using the Flare suite of CressetUk software, the CD_CgUlp2-CgSmt3 protein complex was used for molecular docking with the ligands that were selected from the FDA database as well as the small ligand database. The top 20 hits were shortlisted based on docking scores \leq -9.0 (Tables 10-11). Out of all these, the top 3 molecules: CHEMBL3936817 (small ligand) from the small ligand database and silymarin and honokiol from FDA screening were selected, as they showed good binding with protein complex.

Table 10. Top hits of lead molecules identified through virtual screening of the CD_CgUlp2-CgSmt3 protein from the small molecules database.

S.No	ID	Source	RMSD	Docking score	MMGBSA
1	CHEMBL1950571	CHEMBL	0.73	-9.891	0.0936113
2	CHEMBL4761817	CHEMBL	0.79	-9.358	-0.018152
3	CHEMBL344827	CHEMBL	0.63	-9.232	-0.02565
4	CHEMBL3936817	CHEMBL	0.621	-9.772	-0.002182
5	MCULE-3584742176	MCULE	0.70	-8.734	-0.000987
6	MCULE-8451610057	MCULE	0.85	-8.724	-0.016537
7	MCULE-1667318895	MCULE	0.76	-8.724	-0.003371
8	MCULE-1330778436	Zinc	0.72	-8.712	-0.0008812
9	ZINC8902579	Zinc	0.79	-8.494	-0.001586
10	CHEMBL7557647	CHEMBL	0.826	-9.156	-0.023766

Table 11. Top hits of lead molecules identified through virtual screening of the CD_CgUlp2-CgSmt3 protein from the FDA database.

S.no	Ligand molecule	Docking Score	MMGBSA
1	Tizanidine hydrochloride	-9.963	-0.018152
2	Silymarin	-9.579	-0.02565
3	Silibinin	-9.465	-0.002182
4	Chlorquinaldol	-9.452	-0.000987
5	Cisatracurium besylate	-9.401	-0.016537
6	Bromfenac sodium	-9.288	-0.003371
7	Broxyquinoline	-9.191	0.0008812
8	Guanabenz acetate	-9.075	-0.001586
9	Ritonavir	-9.051	-0.023766
10	Honokiol	-10.042	-0.0008817

.

We studied the protein-ligand interaction between CD_CgUlp2-CgSmt3 and small ligand (CHEMBL3936817), silymarin, and honokiol. 2D analysis of protein complex with small ligand was shown to have hydrogen bond, electrostatic and hydrophobic interaction with the complex (Figure 39A). With silymarin, it showed hydrogen bonds with Glu260, and Ser265, electrostatic interactions at Lys264, and Glu260, and hydrophobic interactions at Lys264 (Figure 39B). Similarly, with honokiol, it displayed hydrogen bonds with Asn263, Glu42, and Gly232, hydrophobic interactions with Pro214 and Lys264 (Figure 39C). Table 12 shows the details of the interaction of CD_CgUlp2-CgSmt3 with these 3 molecules. Furthermore, 3D analysis of the CD_CgUlp2-CgSmt3 protein complex with all the ligands revealed that the ligand placement was in between the binding site of CD_CgUlp2 (chain A- green) and CgSmt3 (chain B-blue) protein (Figure 39D-F).

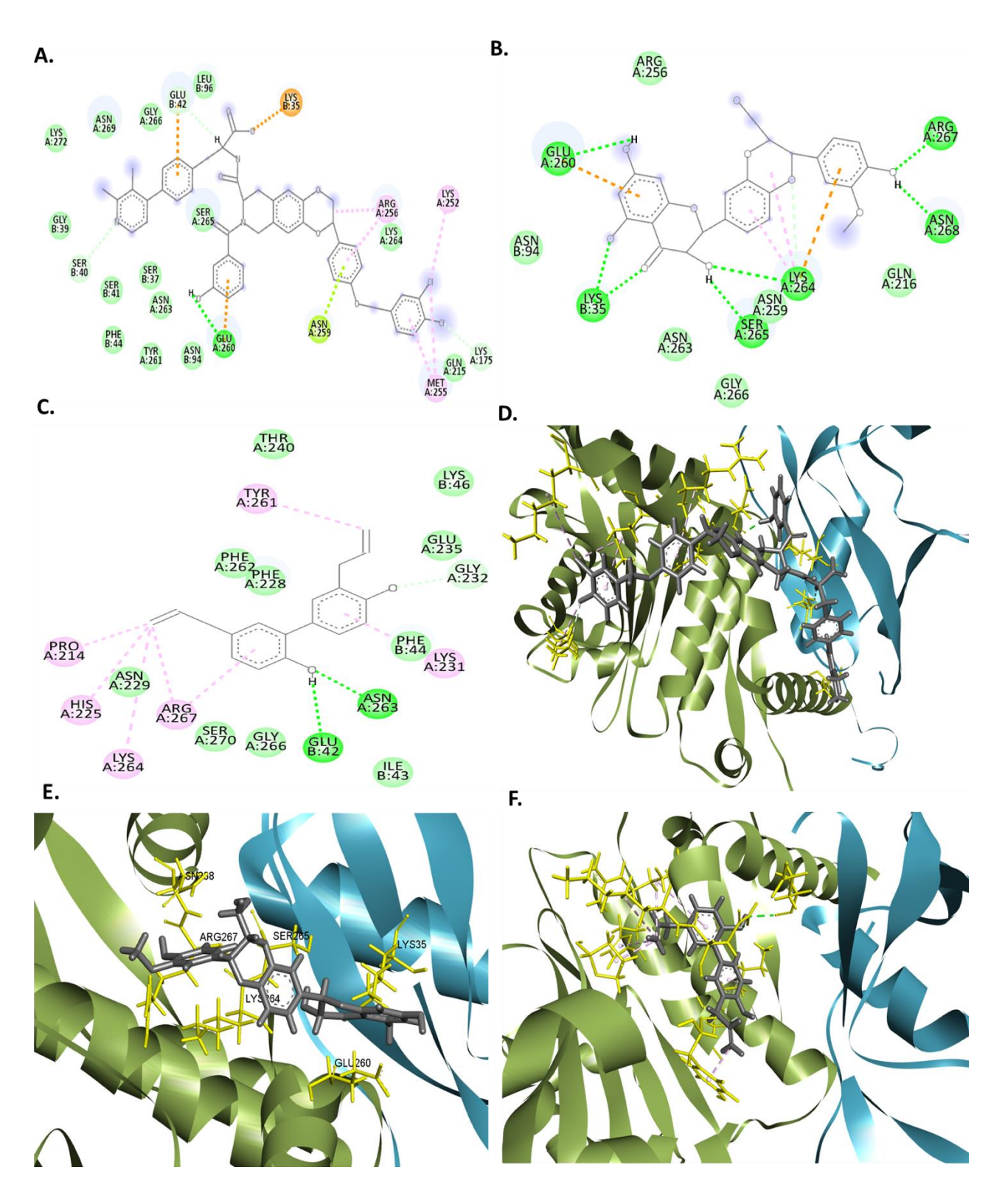


Figure 39. Molecular docking of a CD_CgUlp2-CgSmt3 protein complex with small ligand, silymarin, and honokiol. A-C. 2D images of CD-CgUlp2-CgSmt3 complex with small ligand,

silymarin, and honokiol. **D-F.** 3D images showing CD_CgUlp2 (green) and CgSmt3 (blue) complex with small ligand, silymarin, and honokiol, silymarin (grey). Active site interacting residues (yellow) of CD_CgUlp2- complex interacting with ligand.

Table 12. List of the amino acid residues of CD_CgUlp2 (chain A) and CgSmt3 (chain B) protein complex interacted with lead molecules along with the distance and type of interaction.

	_	otein complex MBL3936817)			-			
Protein complex residues	Distance	Interaction type	Protein complex residues	Distance	Interaction type	Protein complex residues	Distance	Interaction type
B:LYS35	4.72361	Electrostatic	A:LYS264	4.89388	Electrostatic	A:ASN263	1.86	Hydrogen
A:GLU260	1.8272	Hydrogen	A:GLU260	3.32107	Electrostatic	B:GLU42	2.4	Hydrogen
A:LYS175	2.5415	Hydrogen	A:LYS264	2.58325	Hydrogen	A:GLY232	1.78	Hydrogen
B:SER40	2.98157	Hydrogen	A:ARG267	2.02626	Hydrogen	A:PRO214	3.345	Hydrophobic
A:GLU260	2.59799	Hydrogen	A:ARG267	1.99519	Hydrogen	A:LYS264	5	Hydrophobic
B:GLU42	3.7665	Electrostatic	B:LYS35	1.99174	Hydrogen	A:ARG267	4.41	Hydrophobic
A:ASN259	3.24863	Electrostatic	B:LYS35	2.07006	Hydrogen	A:HIS225	4.32	Hydrophobic
A:LYS175	4.06837	Hydrophobic	A:SER265	2.11711	Hydrogen	A:TYR261	3.71	Hydrophobic
A:LYS252	4.20676	Hydrophobic	A:ASN268	1.85512	Hydrogen	A:LYS231	4.413	Hydrophobic
A:MET255	4.8719	Hydrophobic	A:GLU260	3.06052	Hydrogen	A:ARG267	4.99	Hydrophobic
A:ARG256	4.02391	Hydrophobic	A:LYS264	3.07085	Hydrogen			
A:MET255	4.80113	Hydrophobic	A:LYS264	4.70904	Hydrophobic			
			A:LYS264	4.21527	Hydrophobic			
			A:LYS264	4.19883	Hydrophobic			

Molecular Dynamics (MD) Simulation of CD_CgUlp2-CgSmt3 protein complex with and without ligands

To determine the conformational changes and stability, MD simulation on the CD_CgUlp2-CgSmt3 protein complex was carried out for 10 nanoseconds. It took 1.4 ns to reach equilibrium and showed an average RMSD of 0.33 Å. This protein complex showed good stability throughout the time (Figure 40).

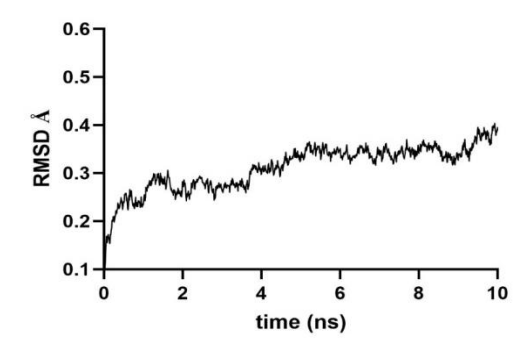


Figure 40. MD simulation of CD_CgUlp2-CDSmt3 protein complex

Further MD simulations were performed with protein complex and lead molecules for 10ns each. The generated trajectories were examined by calculating RMSD and thus, generated RMSD plots.

RMSD of the small ligand (CHEMBL3936817) shown in Figure 41A was more stable, but the average RMSD was 13.6 Å when compared to CD_CgUlp2-CgSmt3 protein complex. This indicates the protein complex was highly unstable with this ligand. In the case of silymarin, RMSD was very high with an average of 0.78 Å as compared to that of a protein complex (0.33 Å). The plot shows that there is no stability throughout the period of 10ns as there is a sharp disturbance with high peaks at 7ns and between 2ns to 4ns (Figure 41B). But with honokiol, RMSD was close to that of the protein complex, but it showed no uniformity and did not seem to equilibrize throughout the 10ns time period. This may indicate certain instability with the complex (Figure 41C). Though the average RMSD is 0.34 Å, which is close to the RMSD of protein, the inability of the complex to stabilize is a concern. Overall, this result demonstrated that the small ligand (CHEMBL3936817) was extremely unstable, followed by silymarin and

honokiol when compared to the CD_CgUlp2-CgSmt3 protein complex, suggesting that these molecules interfere with the interaction between CD_CgUlp2 and CgSmt3 protein.

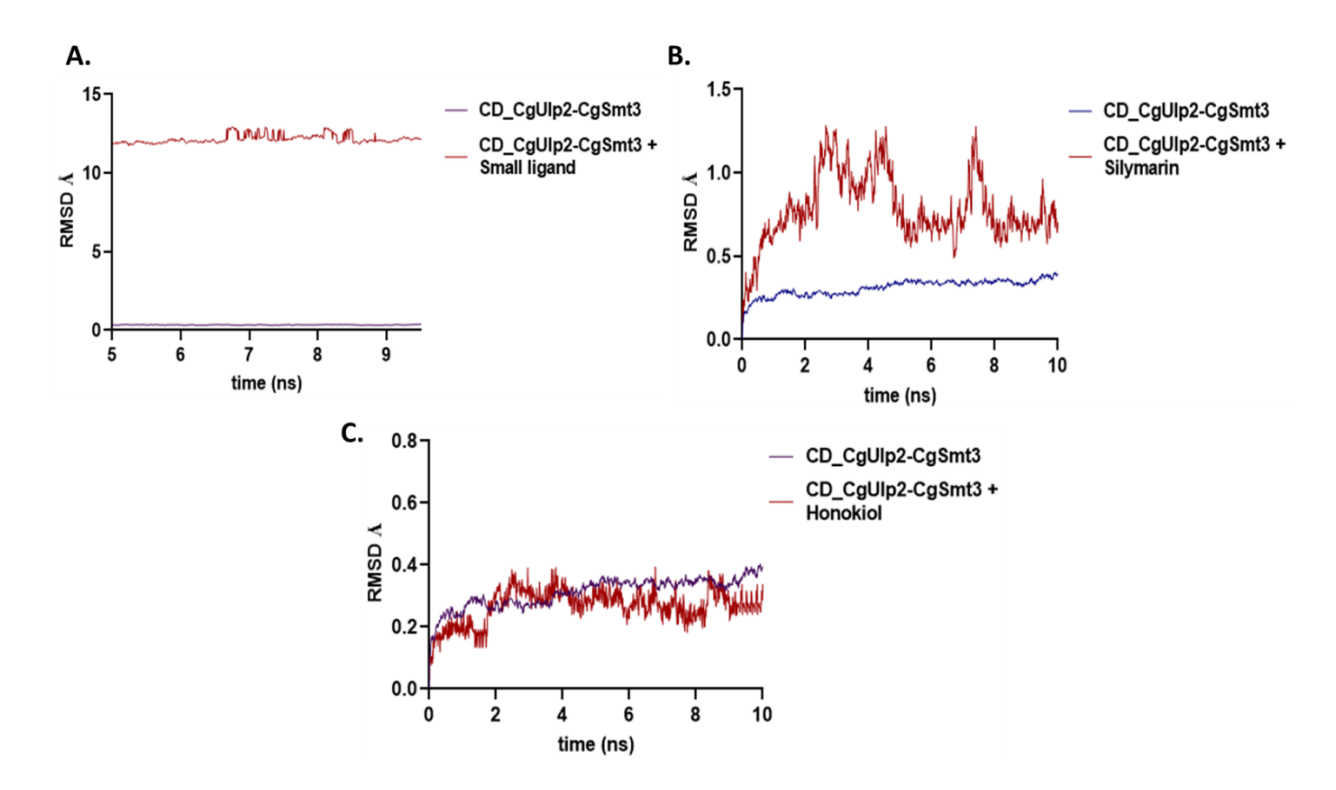


Figure 41. MD simulation of CD_CgUlp2-CDSmt3 protein complex with 3 lead molecules. A-C. RMSD plots of CD_CgUlp2-CgSmt3 (black) with small ligand (A), silymarin (B), and honokiol (C).

6.3 SUMMARY

We conclude this objective with a few key points that are mentioned below.

- The full length, N-terminal domain (NTD), and C-terminal domain (CTD) of CgUlp2 protein were found to be soluble aggregates as it has a large number of unstructured amino acid residues in both NTD and CTD of CgUlp2 protein.
- The catalytic domain of CgUlp2 is monomeric.
- Analysis of the far-UV CD spectrum of the native catalytic domain of CgUlp2 protein revealed the presence of both α -helices and β -sheet, with α -helices constituting approximately 58.3 % of the secondary structure.
- In comparing homology models, the catalytic domain of Ulp2 protein may serve as an antifungal target because it has the least similarities to human proteins.
- Through sequence alignment of ScUlp2, CgUlp2, and HsUlp2 protein, we identified His525, Asps-576, and Cys626 as the putative active site residues forming the catalytic triad. Additionally, mutating Cys626 to serine (C626S) in the full-length CgUlp2 protein resulted in catalytic inactivation.
- In vitro, pull-down analysis showed that CgUlp2 protein interacts directly with CgSmt3 protein through SUMO interacting motifs.

In addition, we have experimentally shown the physical interaction between the domains of the CgUlp2 protein and CgSmt3 using the yeast two-hybrid assay (Y2H). Furthermore, we have established a screening platform based on the Y2H system for identifying small molecules capable of inhibiting Ulp2. These inhibitors aim to disrupt the interaction between the SUMO protease CgUlp2 and the SUMO protein CgSmt3. Based on the pharmacophore-based virtual screening of CD_CgUlp2-CgSmt3 protein complex, 3 lead molecules (small ligand-CHEMBL3936817, silymarin, and honokiol) were identified that disrupt the interaction of CgUlp2 and CgSmt3 protein. Furthermore, we established that CgUlp2 interacts with 6xSUMO in vitro, and this forms a stable complex. So, we are currently attempting to decipher the structure of the CgUlp2•6xSUMO complex in order to gain a better understanding of the interaction between these proteins and to better define the target

for drug discovery. This will make it possible to design molecules that can interfere with the SUMO-deSUMOylase interaction.

CHAPTER 7 DISCUSSION

Fungal infections are a global health problem. Estimates say over 150 million severe cases of fungal infections occur worldwide, resulting in approximately 1.7 million deaths per year ¹³⁴. A key reason for deaths is that many fungi are tolerant to very high levels of antifungals or, sometimes, entirely resistant to antifungals, leading to increased mortality levels. This led WHO to release a first-ever Fungal priority pathogens list (FFPL), highlighting the importance of fungal infections and antifungal resistance (ISBN 978-92-4-006024-1). *Candida glabrata* is listed as a high-priority pathogen due to its innate resistance to antifungals and as one of the key causative agents of candidiasis. Currently, available antifungals fall into three main categories: azoles, echinocandins, and polyenes. All these drugs target either the cell wall or cell membrane. Therefore our project started with the idea of exploring new targets for developing antifungals.

There is limited research on drugs that target post-translational modifications, but such drugs could be highly effective. So, our investigation focused on SUMOylation, a type of post-translational modification, in order to find new targets. SUMOylation of proteins serves as a crucial regulator in a variety of cellular activities, encompassing gene transcription, cell cycle control, DNA replication, and repair. SUMO protein, belonging to the family of ubiquitin-like modifiers, is present in all eukaryotic organisms, from yeast to humans. SUMO is covalently attached to other proteins, modifying their functions. Notably, SUMOylation is a reversible phenomenon, with deSUMOylating enzymes responsible for removing SUMO from target proteins. Apart from monoSUMOylation which alters protein properties, polySUMOylation, the sequential addition of SUMO molecules to target proteins, holds significance in maintaining protein homeostasis. These polySUMOylated proteins undergo ubiquitination facilitated by a group of ubiquitin ligases and are subsequently directed for proteasomal degradation, a process known as SUMO-targeted ubiquitin ligases (STUbLs). This method of controlling protein homeostasis (proteostasis) is key to several physiological processes including DNA repair, and cell cycle regulation.

Previous studies conducted in our lab have demonstrated the critical role of the SUMOylation machinery in *C. glabrata*. In particular, the *CgULP2* gene, which is a deSUMOylase with specificity to both mono and polySUMO, was shown to be particularly critical for pathogenicity and was speculated to have the potential to be a promising target for the development of drugs against *C. glabrata* ^{90,116}.

In this thesis, we have explored the idea that Ulp2 contributed to pathogenicity via its capacity to deSUMOylate polySUMOylated proteins and thus protect proteins from being polyubiquitinated and degraded. This degradation of polySUMOylated protein is attributed to the STUbL pathway. So, in the first part of the work, we identified the STUbL pathway across the fungal kingdom, focusing on pathogenic fungi. We found that the pathway is conserved and all fungi have at least one STUbL. Focusing on *C. glabrata*, we identified that like *S. cerevisiae*, *C. glabrata* has three STUbLs, namely, Slx5, Slx8, and Uls1. In order to test the significance of these STUbLs in *C. glabrata* physiology and pathology, we generated deletions of these, and deletions in combination with the Ulp2. Our studies show that while loss of these STUbLs leads to reduced capacity to infect and survive in macrophages, proliferate in RPMI, or form biofilms, they are not particularly affected by stress conditions in YPD. This suggests that the STUbL pathway might be particularly important in the host or in conditions mimicking the host environment.

Our genetic and biochemical investigations of these mutants revealed that loss of CgUlp2 indeed leads to loss of proteins, potentially activating the STUbL pathway. Interestingly, we found that Cgslx8 loss in the background of Cgulp2 loss was particularly detrimental and the double delete strains were very sick and sensitive to several forms of stress. They also had elevated protein degradation. On the contrary, the Cgulp2Cguls1 double deletes could rescue some of the stress sensitivities of the Cgulp2 loss suggesting that Uls1 could probably be the main STUbL for the Ulp2 targets. This provided us with a genetic handle to investigate the targets of STUbLs that were involved in pathogenicity.

We identified downstream pathways that were affected in the mutants of STUbLs and CgUlp2 by performing quantitative mass spectrometry. The analysis unveiled a significant impact on the ubiquitin-proteosome pathway, ribosomal biogenesis, purine nucleotide biosynthesis pathway, and mitochondrial function in the $Cgulp2\Delta Cgslx8\Delta$ double mutant. This effect was more

pronounced than in the $Cgulp2\Delta$ single mutant. The combination of reduced protein synthesis, enhanced proteasomal pathway, and potentially upregulated CgUls1 collectively contributes to the increased protein loss and slow growth of $Cgulp2\Delta Cgslx8\Delta$ cells at 30°C. Conversely, the $Cgulp2\Delta Cguls1\Delta$ double mutant exhibited opposite trends, with a decreased level in the ubiquitin-proteosome pathway and an increased level or up to the level of wild-type in the purine nucleotide biosynthesis pathway and mitochondrial function. These changes correlated with the restored growth and accumulation of polySUMOylated protein in the $Cgulp2\Delta Cguls1\Delta$ mutant. Our study underscores the importance of STUbLs as essential regulators of protein homeostasis. Along with CgULP2, they play a pivotal role in the pathophysiology of C. glabrata. Further work on the pathways that are particularly affected would provide a better understanding of the processes involved in establishing a successful infection.

We worked towards establishing methodologies to identify SUMOylated proteins in order to establish the causal relationship and also identify the precise targets to get a better understanding of the process of pathogenicity. We found it quite challenging to establish a method to enrich/isolate SUMOylated proteins. Despite having had considerable success in identifying SUMOylated proteins in *S. cerevisiae*, we found those methods were not efficient in *C. glabrata*. Following multiple efforts, we successfully developed a technique for identifying targets of SUMOylation that play a role in contributing the pathogenicity of *C. glabrata*, employing tandem SUMO-interacting motifs (SIMs). This method can now be used to determine the SUMOylation targets influencing infection in this organism.

This work was initiated with the intention of identifying new targets for antifungals. We zeroed in on CgUlp2 as a potential strong candidate as loss of *Cgulp2* compromises the pathogenicity properties. Also, the protein sequence is least conserved with respect to humans among the SUMO pathway components. We aimed to purify the protein and derive atomic resolution structures to design drugs that can target this pathway by rational design. Despite attempts to purify large quantities of CgUlp2 for high-resolution structural studies, soluble purified CgUlp2 protein proved elusive due to numerous unstructured regions in N- and C-terminal domains. Crystallization efforts focused on the catalytic domain of the CgUlp2 protein were unsuccessful for X-ray diffraction after several attempts. Meanwhile, we characterized the protein and performed a homology model of the catalytic domain of the CgUlp2 protein. This domain was

identified as monomeric, displaying both α -helix and β -sheet secondary structures, with α -helix predominance. Furthermore, we identified His525, Asp576, and Cys626 as the conserved catalytic triad residues in the CgUlp2 protein.

Since Ulp2 activity would be dependent on recognizing polySUMOylated protein, we investigated the potential for Ulp2 and SUMO to interact. Our findings highlight a direct interaction between CgUlp2 and CgSmt3 (SUMO) proteins, facilitated by SUMO interacting motifs. Further, our results demonstrate the ability of CgUlp2 to interact with polySUMOylated (6xSUMO) substrates, forming a stable complex. To gain insights into this interaction, we aimed to elucidate the structure of the full-length CgUlp2 with the 6xSUMO. We conducted negative staining of the CgUlp2-6xSUMO protein complex, and subsequent data processing using CryoSPARC unveiled its overall architecture as a compact globular structure. In future, elucidation of this structure will allow the designing of drug molecules that target fungal-specific features of this structure thus avoiding toxicity to humans. Since the structure of this complex has not been established in any system, it will also provide valuable information on the mechanistic aspects of this interaction.

In parallel, using computational approaches including homology modeling of the catalytic domain of CgUlp2 and CgSmt3 proteins we conducted molecular docking studies to understand the interaction between these proteins. Our analysis revealed that the interaction between the two proteins was predominantly through hydrophobic interactions at the interfacial regions. Subsequently, we proceeded with the pharmacophore-based virtual screening of the CD_CgUlp2-CgSmt3 protein complex to identify lead molecules capable of interfering with their interaction. Through this virtual screening, we successfully identified three promising lead molecules: small ligand-CHEMBL3936817, silymarin, and honokiol. Our next step involves conducting preliminary assays to evaluate the efficacy of these molecules in disrupting the interaction between CD_CgUlp2 and CgSmt3 proteins, thereby testing their potential as novel drugs against fungal infections.

FUTURE PROSPECTS

Our ongoing efforts involve elucidating the structure of the CgUlp2•6xSUMO complex using cryo-electron microscopy. A comprehensive understanding of this complex structure will enable the development of compounds capable of disrupting the SUMO-deSUMOylase interaction. Once the structure of this complex is determined, a comparative analysis with the human Ulp2 will be conducted to identify differences, facilitating effective drug targets. Notably, STUbL mutants impede pathogen replication within macrophages, reducing survivability, indicating their potential as targets for designing antifungal drugs.

The mass spectrometric analysis has provided us with multiple pathways that are particularly affected in these mutants. This data can be used to study the role of these pathways in pathogenesis, providing us with a molecular understanding of the mechanisms involved in establishing a successful infection. The method established for identifying SUMOylated proteins can now be used for specifically interrogating which proteins in the pathways identified are direct targets of SUMO-meditated protein homeostasis. Additionally, our identification of downstream pathways for both CgUlp2 and STUbLs opens avenues for developing combinatorial drugs, enhancing their effectiveness as targets. In sum, the work presented in this thesis has opened several avenues to better understand the pathogenesis mechanisms of *Candida glabrata* with a view to develop much-needed new antifungals.

APPENDIX

9.1 LIST OF PLASMIDS USED IN THE STUDY

Plasmid	Description of the plasmid	Source
no.		
CKM 225	pGEX-4T1, Bacterial expression vector having GST tag	Lab collection
CKM 289	pGBDU-C1, Yeast two-hybrid bait vector	Lab collection
CKM 292	pGAD-C1, Yeast two-hybrid prey vector	Lab collection
CKM 294	pBS, pBluescript vector for blunt-end cloning (blue-white	Lab collection
	screening)	
CKM 364	pGRB2.2, a CEN-ARS plasmid of C. glabrata carrying S.	Dr. Rupinder
	cerevisiae URA3 as a selection marker. MCS sites are flanked	Kaur (CDFD)
	by S. cerevisiae PGK1 promoter at one end and by 3' UTR of	
	HIS3 at the other end.	
CKM 379	CgSMT3 cloned in pGRB2.2 as BamH1/Xho1 fragment	Lab collection
CKM 382	CgULP2 cloned in pGRB2.2 as BamH1/Sal1 fragment	Lab collection
CKM 391	CgULP2 cloned in pBEVY-L as BamH1/Sal1 fragment	Lab collection
CKM 402	pCN-PDC1, a high expression promoter with nat1 gene	Dr. Rupinder
		Kaur (CDFD)
CKM 405	6XHIS3XFLAG tagged CgSMT3 at the N-terminus of pCN-	Lab collection
	PDC1vector (6XHIS3xFLAG in Xba1/BamH1, CgSMT3 in	
	BamH1/Xho1)	
CKM 431	6XHIS3XFLAG tagged CgULP2 in pGRB2.2 (6XHIS3xFLAG	Lab collection
	in Xba1/BamH1, CgULP2 in BamH1/Sal1 site)	
CKM 468	6XHIS3XFLAG tagged <i>CgSMT3</i> in pGRB2.2 (6XHIS3xFLAG	Lab collection
	in Xba1/BamH1, CgSMT3 in BamH1/Xho1 site)	
CKM 476	3XFLAG tagged CgSMT3 in pGRB2.2 (3XFLAG in	Lab collection
	Xba1/BamH1, CgSMT3 in BamH1/Xho1 site)	
CKM 661	Full length CgULP2 subcloned in BamH1/Sal1 site of pET28a	This study
	from CKM 391	
CKM 686	NAT cassette cloned in pCR2.1 plasmid	Dr. Rupinder
		Kaur (CDFD)

CKM 687	FLP1, FLP1 containing plasmid under EPA1 promoter to	Dr. Rupinder
	excise NAT cassette	Kaur (CDFD)
CKM 689	C-terminal domain (CTD) of CgULP2 cloned in EcoRV	This study
	digested pBS vector	
CKM 690	Catalytic domain (CD) of CgULP2 cloned in EcoRV digested	This study
	pBS vector	
CKM 691	CTD_CgULP2 subcloned in BamH1/Sal1 site of pGEX4T1	This study
	from CKM 689	
CKM 692	CD_CgULP2 subcloned in BamH1/Sal1 site of pGEX4T1 from	This study
	CKM 690	
CKM 693	N-terminal domain (NTD) of CgULP2 cloned in pET28a as	This study
	BamH1/Sal1 fragment	
CKM 694	CD_CgULP2 subcloned in BamH1/Sal1 site of pET28a from	This study
	CKM 690	
CKM 695	CTD_CgULP2 subcloned in BamH1/Sal1 site of pET28a from	This study
	CKM 689	
CKM 717	CgSLX5 (1.5 kb) cloned in EcoRV digested pBS vector	This study
CKM 718	CgSLX8 (633 bps) cloned in EcoRV digested pBS vector	This study
CKM 719	CgSLX5 subcloned in BamHI/XhoI site of pGRB2.2 from	This study
	CKM 717	
CKM 720	CgSLX8 subcloned in BamHI/XhoI site of pGRB2.2 from	This study
	CKM 718	
CKM 721	CgSMT3 cloned in pGAD-C1 as BamH1/Pst1 fragment	This study
CKM 733	CgULS1 (4.2 kb) cloned in EcoRV digested pBS vector	This study
CKM 737	CgSMT3 subcloned in BamH1/Xho1 site of pET28a from CKM	This study
	379	
CKM 738	CgULP2 (C626S), Cysteine residue was replaced with serine at	This study
	the position of 626 in the full length of CgULP2 that was	
	cloned in pGRB2.2	
CKM 741	CgULS1 subcloned in BamHI/XhoI site of pGRB2.2 from	This study

	CKM 733	
CKM 742	CgSMT3 subcloned in BamH1/Xho1 site of pGEX4T1 from	This study
	CKM 379	
CKM 743	SIM (72 bps)-pET28a, 72 bps of SIM motif directly cloned in	This study
	pET28a with Nde1/BamH1 sites	
CKM 744	SIM (154 bps)-pET28a, 154 bps of SIM motif cloned in	This study
	BamH1/Sac1 site of pET28a using SIM (72 bps) as template	
CKM 745	SIM (308 bps)-pET28a, 308 bps of SIM motif cloned in	This study
	Sac1/HindIII site of pET28a using SIM (154 bps) as a template	
CKM 754	CD_CgULP2(I569K)-pGEX4T1, Isoleucine was replaced with	This study
	lysine at the position of 569 in the catalytic domain of <i>CgULP2</i>	
	that was cloned in pGEX4T1	
CKM 755	CTD_CgULP2(I712T)-pGEX4T1, Isoleucine was replaced with	This study
	threonine at the position of 712 in the C-terminal domain of	
	CgULP2 that was cloned in pGEX4T1	
CKM 758	6XHIS3XFLAG tagged CgULS1 under its native promoter	This study
	(500 bps) in pGRB2.2	
CKM 793	CgADE5,7 cloned in EcoRV digested pBS vector	This study
CKM 794	3XFLAG-CgADE5,7- pGRB2.2, Replace CgSMT3 from CKM	This study
	476 and cloned CgADE5,7 with BamHI/XhoI sites in frame	
	with 3XFLAG in pGRB2.2 vector	
CKM 726	CD_CgULP2 cloned in BamH1/Sal1 site of pGBD-C1	This study
CKM 728	CTD_CgULP2 cloned in BamH1/Sal1 site of pGBD-C1	This study
CKM 736	NTD_CgULP2 cloned in BamH1/Sal1 site of pGBD-C1	This study
CKM 806	pET28a, Bacterial expression vector having His tag	Lab collection

9.2 LIST OF PRIMERS USED IN THE STUDY

Primer sequences	Description		
For generation of deletion strains			
TATCCTCTGCCTGCAATG	CgSLX5 5'UTR Forward		
gcgtcgacctgcagcgtacgTCTGTCTCCTCTGGGGCTAA	CgSLX5 5'UTR Reverse		
cgacggtgtcggtctcgtagGGGAGTGTCCACGACAACA	CgSLX5 3'UTR Forward		
AGGCACATTCCACAATCTCC	CgSLX5 3'UTR Reverse		
CGAACAAGAGCGATGACAGA	CgSLX5 Internal check		
	Forward		
CCCGATTCCTAACTCAACTCC	CgSLX5 Internal check		
	Reverse		
GATCGGACATCCCGTCTTTA	CgSLX5 5' Integration		
	check Forward		
GGATCCATGCATAGCGAAAC	CgSLX5 3' Integration		
	check Reverse		
TCCTGACAAGAGCTGGACCT	CgSLX8 5'UTR Forward		
gcgtcgacctgcagcgtacg CCACCTCGCACACATAATTG	CgSLX8 5'UTR Reverse		
cgacggtgtcggtctcgtagTGTCCGTTTTTCAGGGATTC	CgSLX8 3'UTR Forward		
ATGTGTGGGAAAGGGACAGA	CgSLX8 3'UTR Reverse		
AGGTCTGGTGGAAACCAGTG	CgSLX8 5' Integration		
	check Forward		
GGCACAAGAAGGCATTTT	CgSLX8 3' Integration		
	check Reverse		
AAGCTGGACAACATTGATTGC	CgULS1 5'UTR Forward		
gcgtcgacctgcagcgtacgGCAGGGTCCTATAGTGACAACC	CgULS1 5'UTR Reverse		
cgacggtgtcggtctcgtagTGAGATTCATGAAAGCATTGTT	CgULS1 3'UTR Forward		
CATTTCAAAGAATTTTGGATGC	CgULS1 3'UTR Reverse		
TTGACGGTGTTCCTATTTTGG	CgULS1 Internal check		
	Forward		
TTCCTTTTGGACCGCTTCTA	CgULS1 Internal check		

	Reverse
AACCAATGGAAAGCAGATGG	CgULS1 5' Integration
	check Forward
TCCTTGTGCACCACTAGAAGG	CgULS1 3' Integration
	check Reverse
For amplification of nat1 cassette for C. gla	brata gene disruption
CGTACGCTGCAGGTCGACGCcttccgctgctaggcgc	5' NAT half Forward
TCTGTTCCAACCAGAATAAG	5' NAT half Reverse
GTCTACTACTTTGGATGATACTGC	3' NAT half Forward
ctacgagaccgacaccgtcgGGCCGCTGACGAAGT	3' NAT half Reverse
TGCGCACGTCAAGACTGTCAAGG	5' Integration check
	Forward
TGTGAATGCTGGTCGCTATACTGC	3' Integration check
	Forward
For gene cloning	
AATGGATCCATGAAACGGGATGGT	CgSLX5 Forward
GCGCTCGAGTTAGAAATATACTTCTCTCAT	CgSLX5 Reverse
GCCGGATCCATGGCTAAATCTGAG	CgSLX8 Forward
GAGCTCGAGTCAGGTCTTCTTCTG	CgSLX8 Reverse
GCGGGATCCATGCCAAAAGTTACA	CgULS1 Forward
GCGCTCGAGTCATAATGAATTTAGTCCG	CgULS1 Reverse
GGCGAGCTCGTTAATCACAAGTCAT	CgULS1 Promoter Forward
AATTCTAGATTGCCATCTGCGATGG	CgULS1 Promoter Reverse
GGCGGATCCATGTTGAACATTCTAG	CgADE5,7 Gene Forward
GGACTCGAGTTAGTATAGGTTGCTGG	CgADE5,7 Gene Reverse
TAGTGGATCCATGTCTGACACTAACG	CgSMT3 Forward
TAGTCTCGAGCTAGTACGCACCACCG	CgSMT3 Reverse
GGATCCAATAGTATGTCGCGGAG	CgULP2 (Full length)
	Forward
GTCGACCTAATGAGTATCGATATTTTC	CgULP2 (Full length)

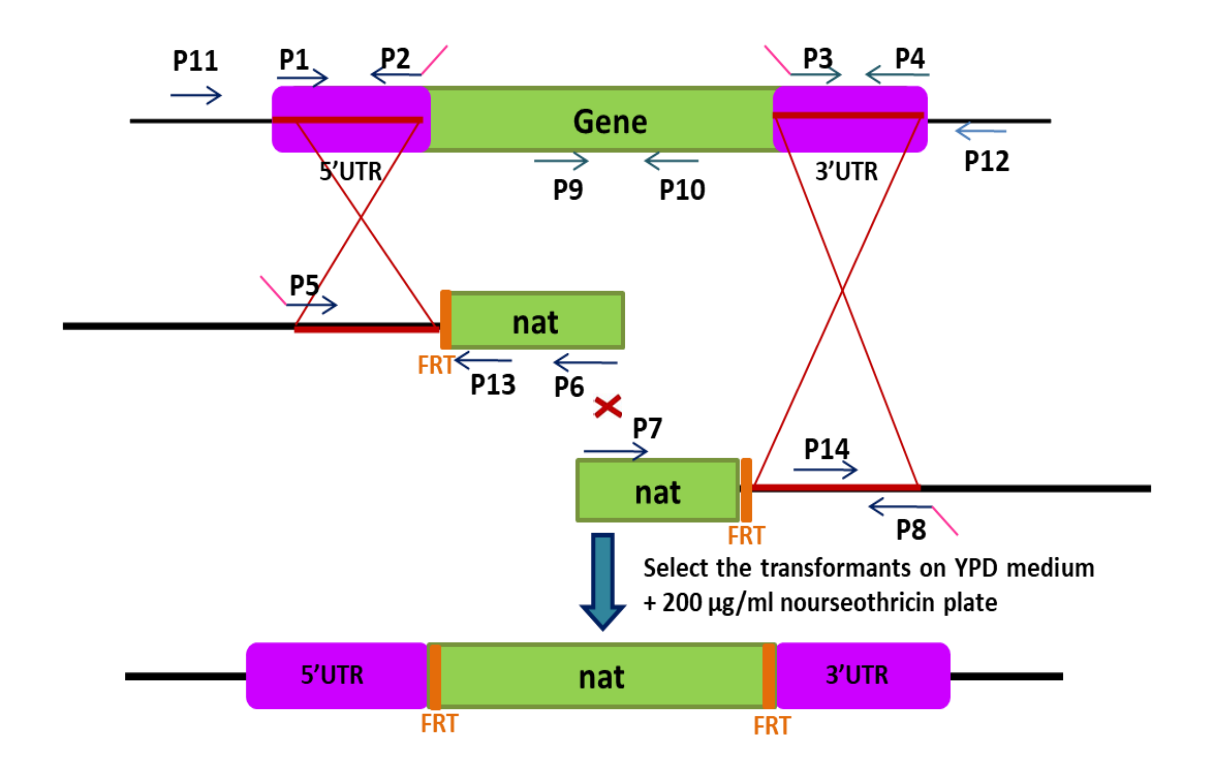
	Reverse
AATGGATCCATGTCGCGGAGG	CgULP2 (N-terminal
	domain) Forward
AATGTCGACCATCCTCTTTCCGCA	CgULP2 (N-terminal
	domain) Reverse
AGTGGATCCATGGAGGACAAAAGC	CgULP2 (Catalytic
	domain) Forward
AGTGTCGACAATGCTTGTCCATTGG	CgULP2 (Catalytic
	domain) Reverse
AATGGATCCATGACGCATAGCAGAGAA	CgULP2 (C-terminal
	domain) Forward
CGGGTCGACCTAATGAGTATCGATATTTTC	CgULP2 (C-terminal
For cloning of tandem SUMO-Interacting	domain) Reverse
CGGCATATGATGGTAGTGATCGTAGACGG	SIM 1, 2 Forward
ATAGGATCCCCACCGCCTCCTCC	SIM 1, 2 Reverse
CGGGGATCCGTAGTGATCGTAGACGG	SIM 3, 4 Forward
ATAGAGCTCCCACCGCCTCCTCC	SIM 3, 4 Reverse
CGGGAGCTCGTAGTGATCGTAGACGG	SIM 5-8 Forward
ATAAAGCTTCTACCCACCGCCTCCTCC	SIM 5-8 Reverse
For qRT-PCR	
AAGGCGGTATAATGCCTGTG	CgULP2 Forward
CTCACCTTCACCACGCTGTA	CgULP2 Reverse
GTGGTGGACGAGGAGGATAA	CgSLX5 Forward
GCACTAAATTCCCACCCAGA	CgSLX5 Reverse
GACACCCGAGACCATCAACT	CgSLX8 Forward
GAACAAGCATTCGCAACAGA	CgSLX8 Reverse
GGCAAATGAGCTCAAAAAGC	CgULS1 Forward
CTTTAGCGGCCTGTGTCTTC	CgULS1 Reverse
GTAACATCGTTATGTCCGGTGGTAC	CgACT1 Forward
CCAAGATAGAACCACCAATCCAGAC	CgACT1 Reverse

For Site-directed mutagenesis			
CAGGCAAACTTTAGTGATTCTGGTGTCCATGTGATTTTC	CgULP2(C626S) Forward		
GAAAATCACATGGACACCAGAATCACTAAAGTTTGCCTG	CgULP2(C626S) Reverse		
CAGTTAGTCCACCAAAAATTACGATACTCACGTTTGATTC	CD (I569K) Forward		
GAATCAAACGTGAGTATCGTAATTTTTGGTGGACTAACTG	CD (I569K) Reverse		
GAAGATGAGGATACTGAAATAATTGAAGATTTATAT	CTD (I712T) Forward		
ATATAAATCTTCAATTATTTCAGTATCCTCATCTTC	CTD (I712T) Reverse		

9.3 LIST OF STRAINS USED IN THE STUDY

Yeast	Genotype	Reference
strain		
YRK 19	ura3∆::Tn903 G418 ^R	Dr. Rupinder Kaur
	(WT Ura- strain)	(CDFD)
YRK 971	YRK 19 except Cgulp2Δ::nat1	Dr. Rupinder Kaur
		(CDFD)
KRC 6	Smt3::hyg/CKM405	Lab collection
KRC 30	YRK 19 except Cgslx8Δ::nat1	This study
KRC 33	YRK 19 except Cguls1∆::nat1	This study
KRC 36	YRK 19 except Cgulp2Δ::nat1/CKM 687	This study
KRC 42	YRK 19 except Cgulp2ΔCguls1Δ::nat1	This study
KRC 45	YRK 19 except Cgslx5∆::nat1	This study
KRC 46	YRK 19 except Cgslx5∆Cguls1∆::nat1	This study
KRC 47	YRK 19 except Cgslx5ΔCgslx8Δ::nat1	This study
KRC 50	YRK 19 except Cgslx5Δ::nat1/CKM 687	This study
KRC 53	YRK 19 except Cgulp2ΔCgslx8Δ::nat1	This study

9.4 SCHEMATIC REPRESENTATION OF SINGLE DELETION STRAINS GENERATED FOR THIS STUDY



Full-length single deletion knockout of STUbLs (*CgSLX5*, *CgSLX8*, and *CgULS1*) was carried out by employing a homologous recombination-based strategy using a cassette encoding the nourseothricin acetyltransferase (*NAT1*) gene.

The primers used for amplifying the deletion cassette using *NAT* as the template and for screening the deletion strains are listed in Appendix 8.2.

9.5 DETAILS OF RECOMBINANT DNA CONSTRUCTS GENERATED FOR THIS STUDY

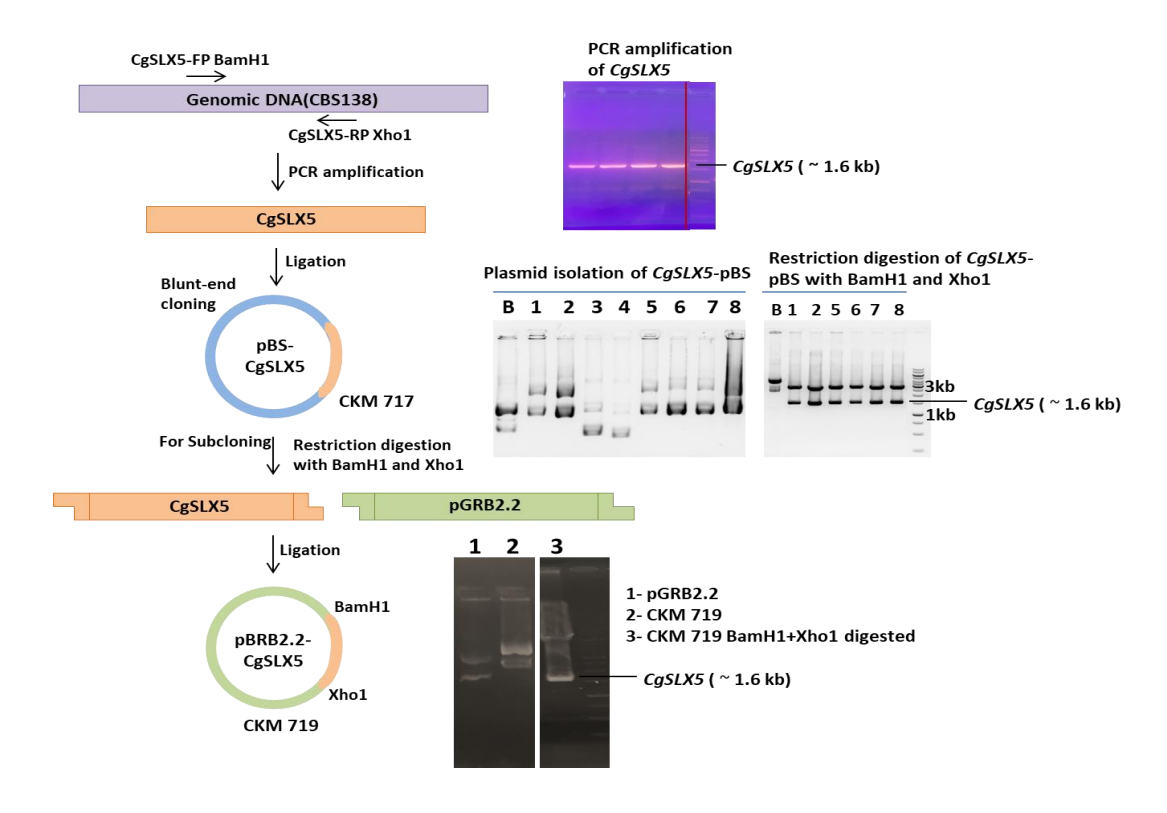
Generating *CgSLX5* in pGRB2.2 (CKM 719)

In order to clone *CgSLX5* in pGRB2.2, genomic DNA from YRK19 (*C. glabrata* WT strain-CBS138) was used as a template for amplifying the *CgSLX5* gene. The following primers were used for the amplification:

CgSLX5 FP Forward primer from START codon of CgSLX5 with BamH1 site AATGGATCCATGAAACGGGATGGT

CgSLX5 RP Reverse primer from up to STOP codon of CgSLX5 with Xho1 site GCGCTCGAGTTAGAAATATACTTCTCAT

The ~1.6 kb PCR product obtained was ligated into pBlueScript vector. This clone was digested with BamH1 and Xho1 restriction enzymes to generate the fragment for ligation into pGRB2.2 vector. The clone was confirmed by restriction digestion. This clone (CKM 719) was used for the complementation assay (Refer to **Figure 6E**).



Schematic showing cloning generation of CKM 719

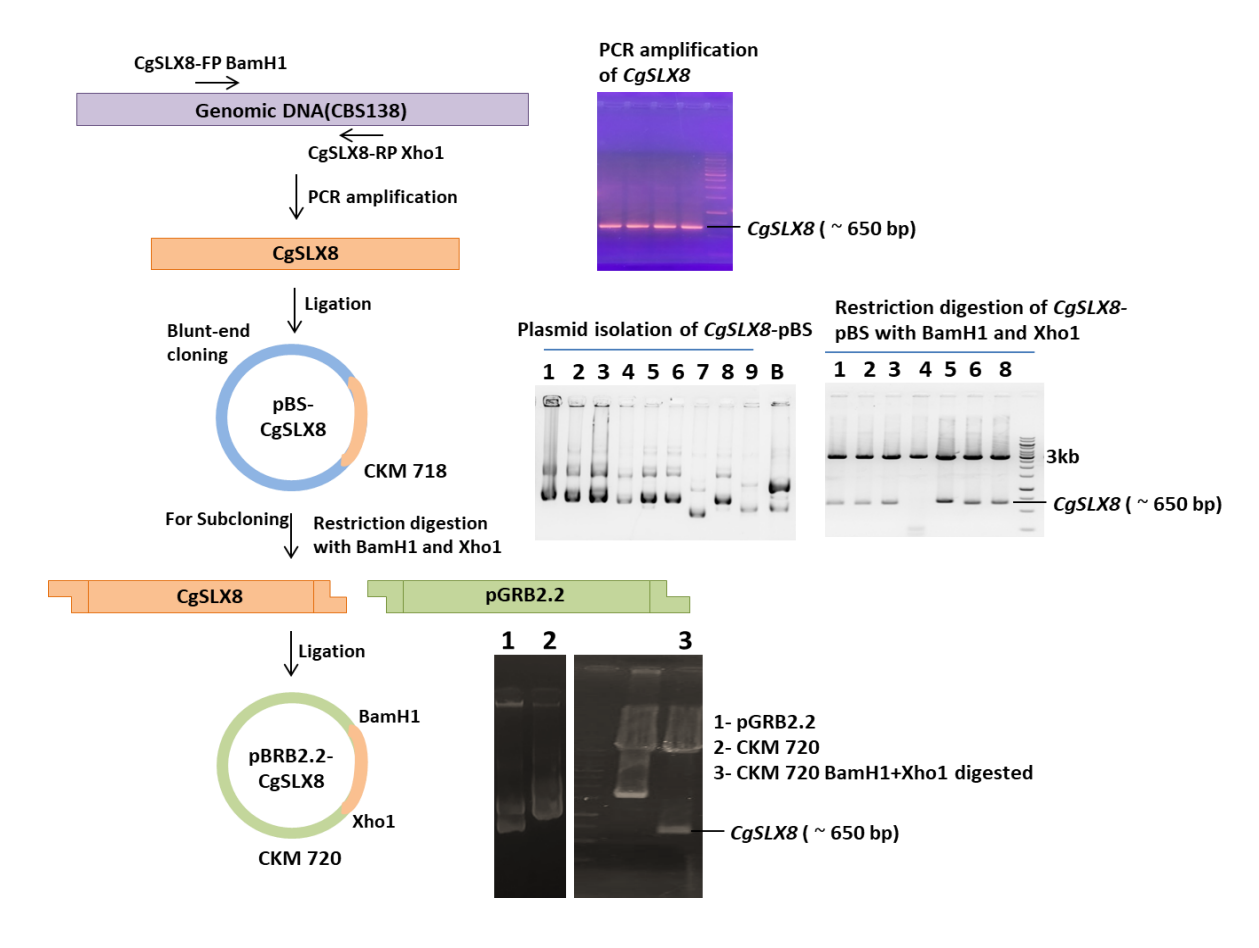
Generating *CgSLX8* in pGRB2.2 (CKM 720)

To clone *CgSLX8* into pGRB2.2, genomic DNA from YRK19 (*C. glabrata* WT strain-CBS138) was used as a template for amplifying the *CgSLX8* gene. The following primers were employed for the amplification:

CgSLX8 FP Forward primer from START codon of CgSLX8 with BamH1 site GCCGGATCCATGGCTAAATCTGAG

CgSLX8 RP Reverse primer from upto STOP codon of CgSLX8 with Xho1 site GAGCTCGAGTCAGGTCTTCTTCTG

The ~650 bp PCR product obtained was ligated into pBlueScript vector. This clone was digested with BamH1 and Xho1 restriction enzymes to generate the fragment for ligation in to pGRB2.2 vector. The clone was confirmed by restriction digestion. This clone (CKM 720) was used for the complementation assay (Refer to **Figure 6E**).



Schematic showing cloning generation of CKM 719

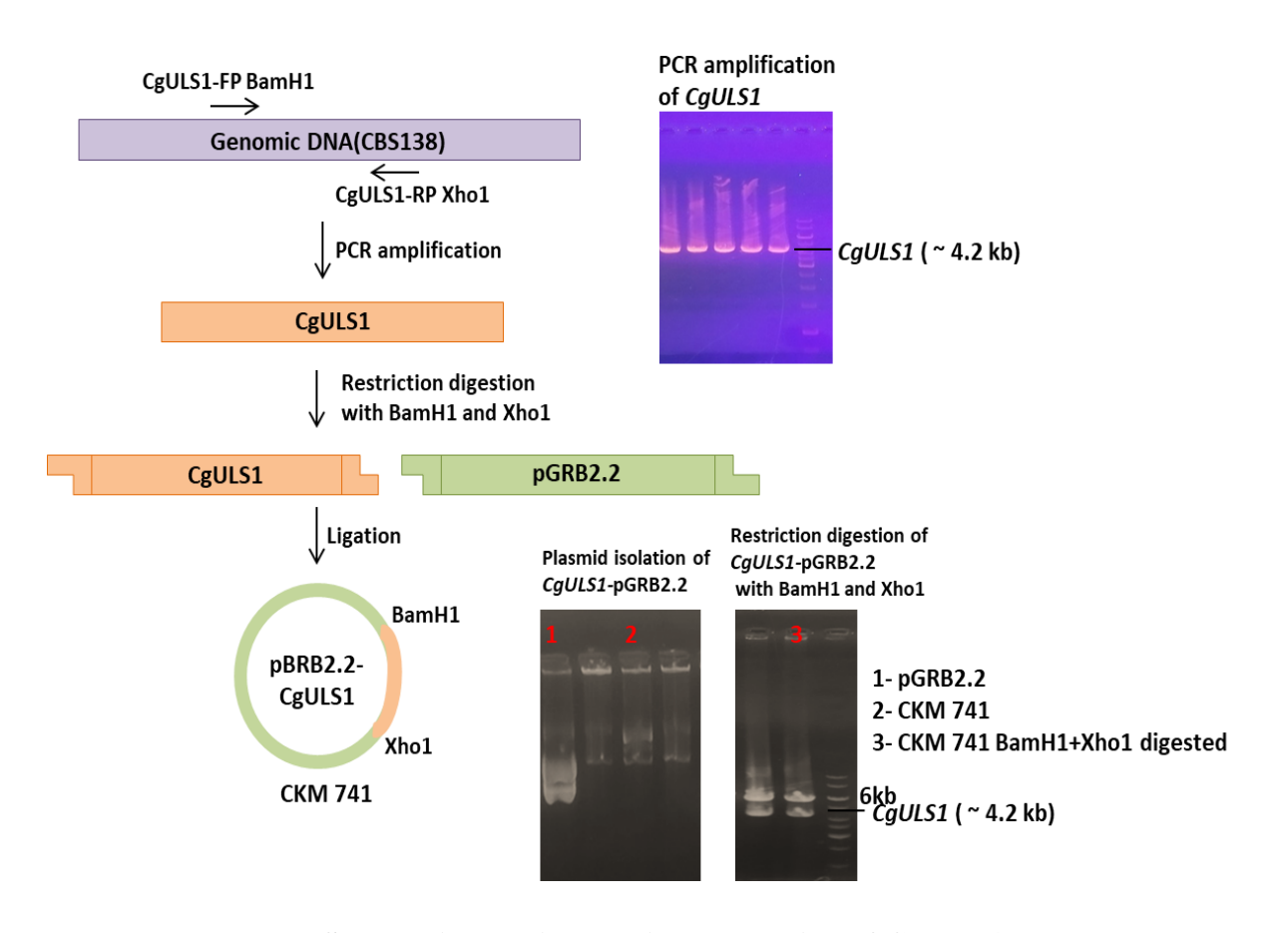
Generating *CgULS1* in pGRB2.2 (CKM 741)

In order to clone *CgULS1* in pGRB2.2, genomic DNA from YRK19 (*C. glabrata* WT strain-CBS138) was used as a template for amplifying the *CgULS1* gene. The following primers were used for the amplification:

CgULS1 FP Forward primer from START codon of CgULS1 with BamH1 site GCGGGATCCATGCCAAAAGTTACA

CgULS1 RP Reverse primer from upto STOP codon of CgULS1 with Xho1 site GCGCTCGAGTCATAATGAATTTAGTCCG

The ~4.2 kb PCR product was obtained and digested with BamH1 and Xho1 restriction enzymes to ligate in to pGRB2.2 vector. The clone was confirmed by restriction digestion. This clone (CKM 741) was used for the complementation assay (Refer to **Figure 6E**).

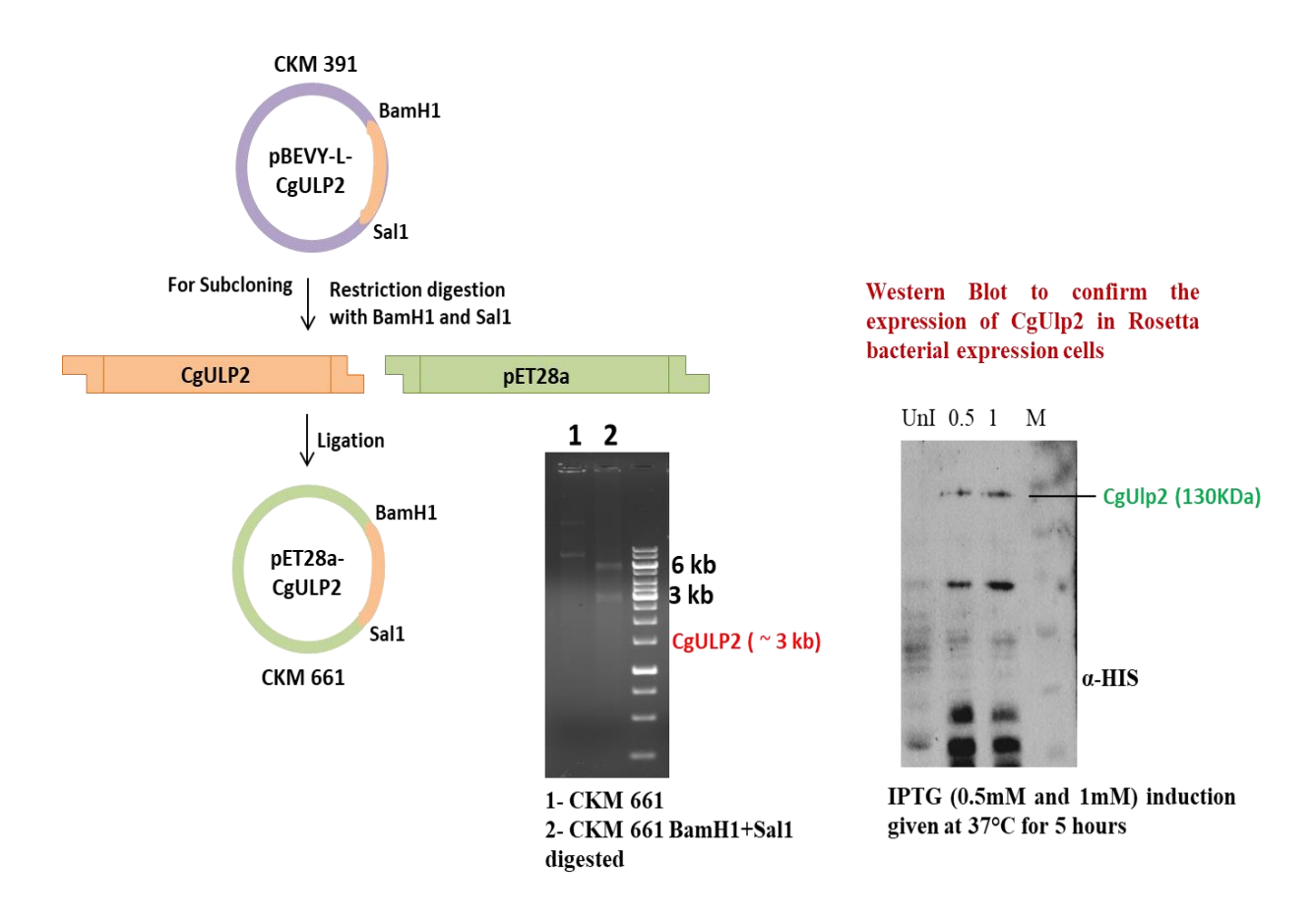


Schematic showing cloning generation of CKM 741

Generating CgULP2 in pET28a (CKM 661)

The *CgULP2* gene was subcloned from the CKM 391 (*CgULP2*-pBEVY-L). *CgULP2* was digested with BamH1 and Sal1 restriction enzymes to generate ~3kb fragment for ligation into pET28a vector. The clone was confirmed by restriction digestion and sequencing.

The CgULP2 protein was expressed in the Rosetta bacterial expression strain using IPTG concentrations of 0.5 mM and 1 mM at 37°C for 5 hours. The expression of CgULP2 protein was confirmed by using an α -HIS antibody. Purification of the CgULP2 protein was attempted (Refer to **Figure 22B**).



Schematic showing cloning generation of CKM 661

Generating N-terminal domain (NTD) of the CgULP2 in pET28a (CKM 693)

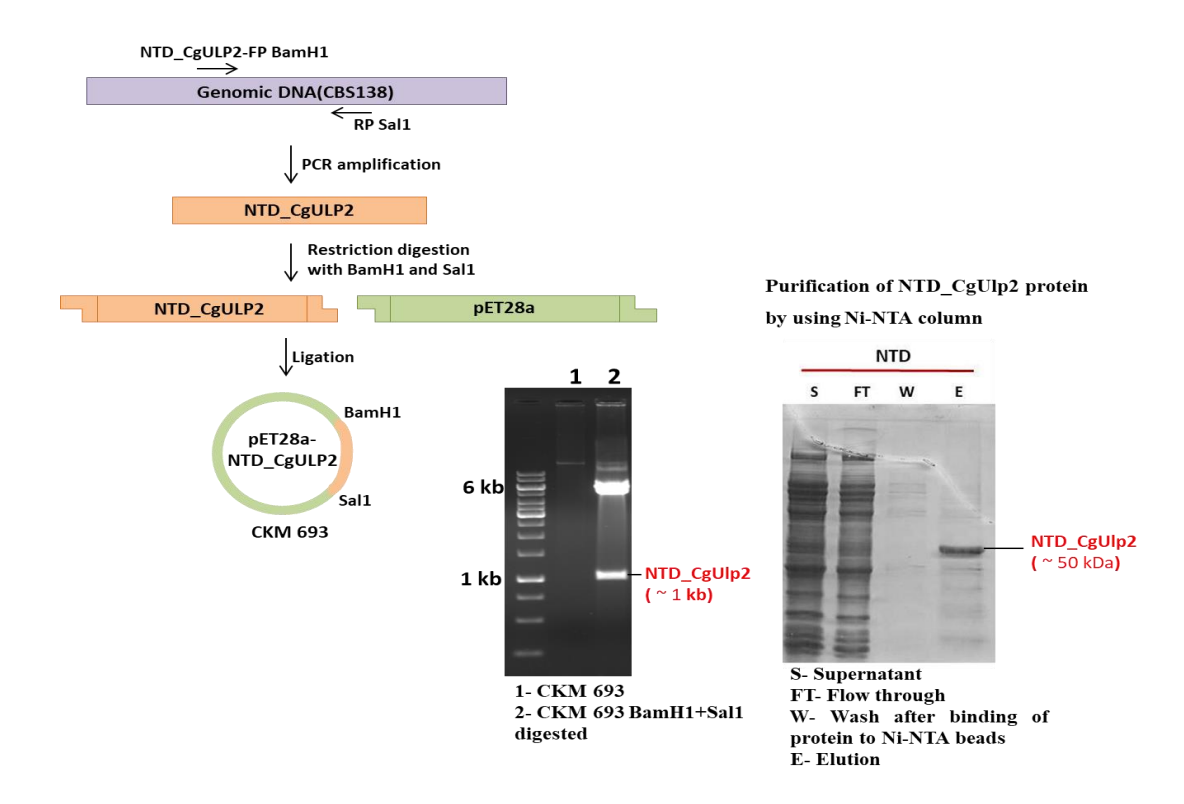
In order to clone NTD_CgULP2 in pET28a, genomic DNA from YRK19 (C. glabrata WT strain-CBS138) was used as a template for amplifying the NTD_CgULP2 gene. The following primers were used for the amplification:

NTD_CgULP2 FP Forward primer from START codon of NTD_CgULP2 with BamH1 site AATGGATCCATGTCGCGGAGG

NTD_CgULP2 RP Reverse primer from up to STOP codon of NTD_CgULP2 with Sal1 site AATGTCGACCATCCTCTTTCCGCA

The ~1kb PCR product was obtained and was digested with BamH1 and Sal1 restriction enzymes to ligate into pET28a vector. The clone was confirmed by restriction digestion and sequencing.

The NTD_CgULP2 protein was expressed in the BL21(DE3)-RIL bacterial expression strain using an IPTG concentration of 0.4 mM at 22°C for 16 hours. The expression of NTD_CgULP2 protein was confirmed by using α -HIS antibody (Refer to **Figure 32B**). Purification of the NTD_CgULP2 protein was attempted.



Schematic showing cloning generation of CKM 693

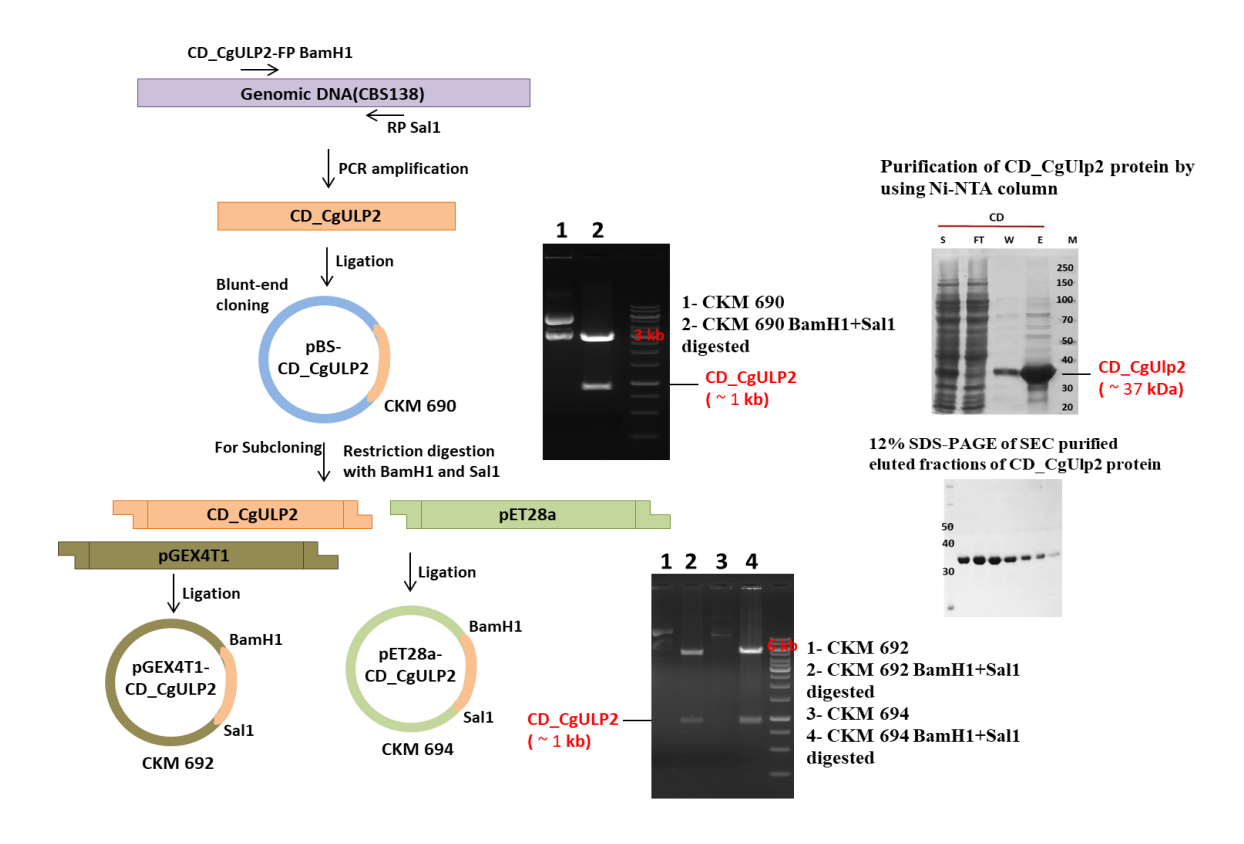
Generating catalytic domain (CD) of the CgULP2 in pGEX4T1 (CKM 692) and pET28a (CKM 694)

In order to clone CD_CgULP2 in pGEX4T1 and pET28a, genomic DNA from YRK19 (*C. glabrata* WT strain-CBS138) was used as template for amplifying the CD_CgULP2 gene. The following primers were used for the amplification:

CD_*CgULP2* FP Forward primer from START codon of CD_*CgULP2* with BamH1 site AGTGGATCCATGGAGGACAAAGC

CD_*CgULP2* RP Reverse primer from up to STOP codon of CD_*CgULP2* with Sal1 site AGTGTCGACAATGCTTGTCCATTGG

The ~1kb PCR product obtained was ligated into pBlueScript vector. This clone was digested with BamH1 and Sal1 restriction enzymes to ligate into pGEX4T1 and pET28a vector. The clone was confirmed by restriction digestion and sequencing. The CD_CgULP2 protein was expressed in the BL21(DE3)-RIL bacterial expression strain using an IPTG concentration of 0.4 mM at 22°C for 16 hours. The expression of CD_CgULP2 protein was confirmed by using α -GST antibody (Refer to **Figure 32B**). CD_CgULP2 protein was purified well (Figure 24A).



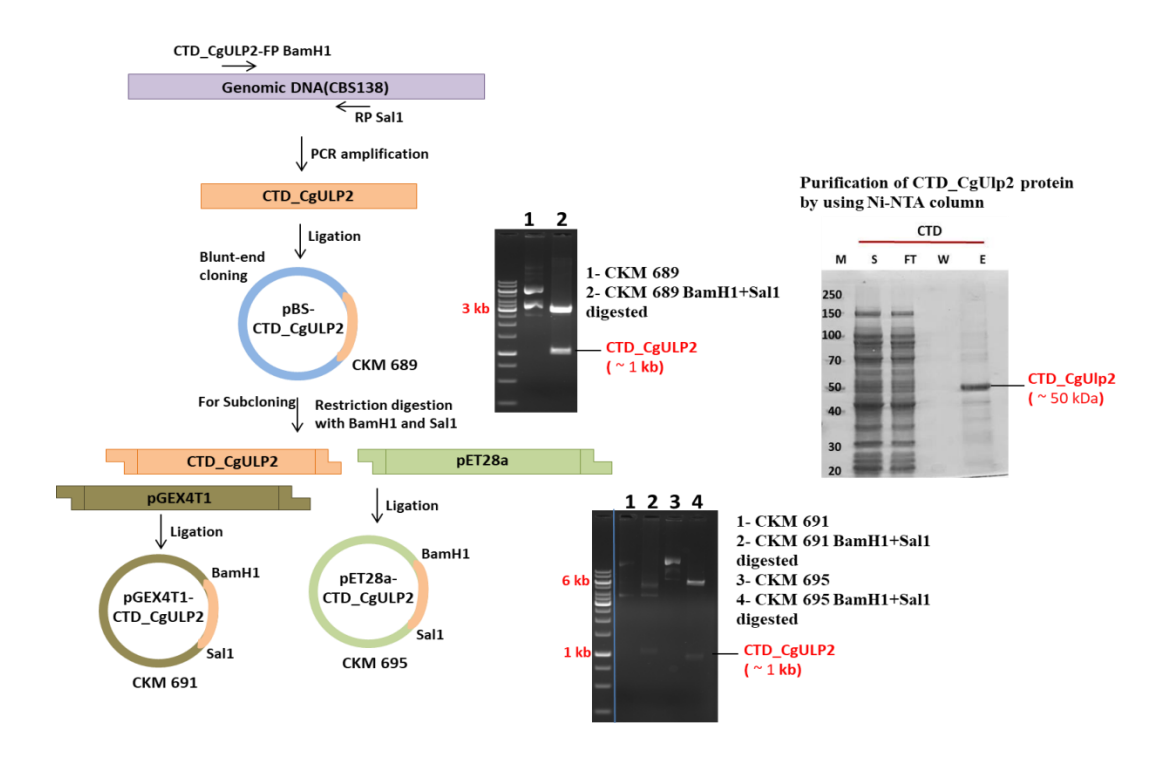
Schematic showing cloning generation of CKM 692, and CKM 694 Generating C-terminal domain (CTD) of the *CgULP2* in pGEX4T1 (CKM 691) and pET28a (CKM 695)

In order to clone CTD_CgULP2 in pGEX4T1 and pET28a, genomic DNA from YRK19 (*C. glabrata* WT strain-CBS138) was used as a template for amplifying the CTD_CgULP2 gene. The following primers were used for the amplification:

CTD_CgULP2 FP Forward primer from START codon of CTD_CgULP2 with BamH1 site AATGGATCCATGACGCATAGCAGAGAA

CTD_*CgULP2* RP Reverse primer from upto STOP codon of CTD_*CgULP2* with Sal1 site CGGGTCGACCTAATGAGTATCGATATTTTC

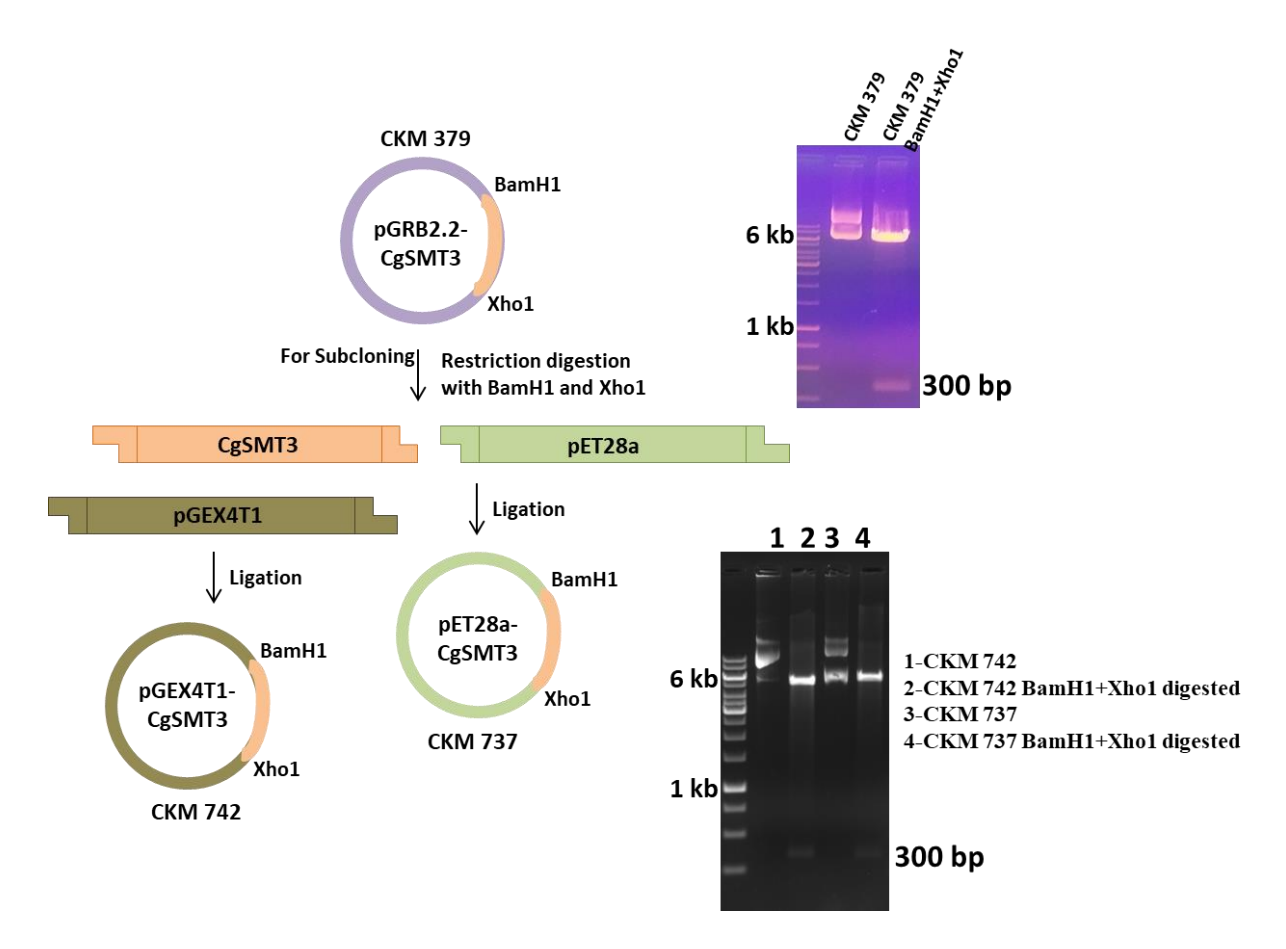
The ~1kb PCR product obtained was ligated into pBlueScript vector. This clone was digested with BamH1 and Sal1 restriction enzymes to ligate into pGEX4T1 and pET28a vector. The clone was confirmed by restriction digestion and sequencing. The CTD_CgULP2 protein was expressed in the BL21(DE3)-RIL bacterial expression strain using an IPTG concentration of 0.4 mM at 22°C for 16 hours. The expression of CTD_CgULP2 protein was confirmed by using α -GST antibody (Refer to **Figure 32B**).



Schematic showing cloning generation of CKM 691, and CKM 695

Generating CgSMT3 in pGEX4T1 (CKM 742) and pET28a (CKM 737)

The CgSMT3 gene was subcloned from the CKM 379 (CgSMT3-pGRB2.2). CgSMT3 was digested with BamH1 and Xho1 restriction enzymes to generate ~300 bp fragment for ligation into pGEX4T1 and pET28a vector. The clone was confirmed by restriction digestion and the expression of CgSMT3 protein was confirmed by western blot using α -HIS and α -GST antibodies (Refer to **Figure 32B**).



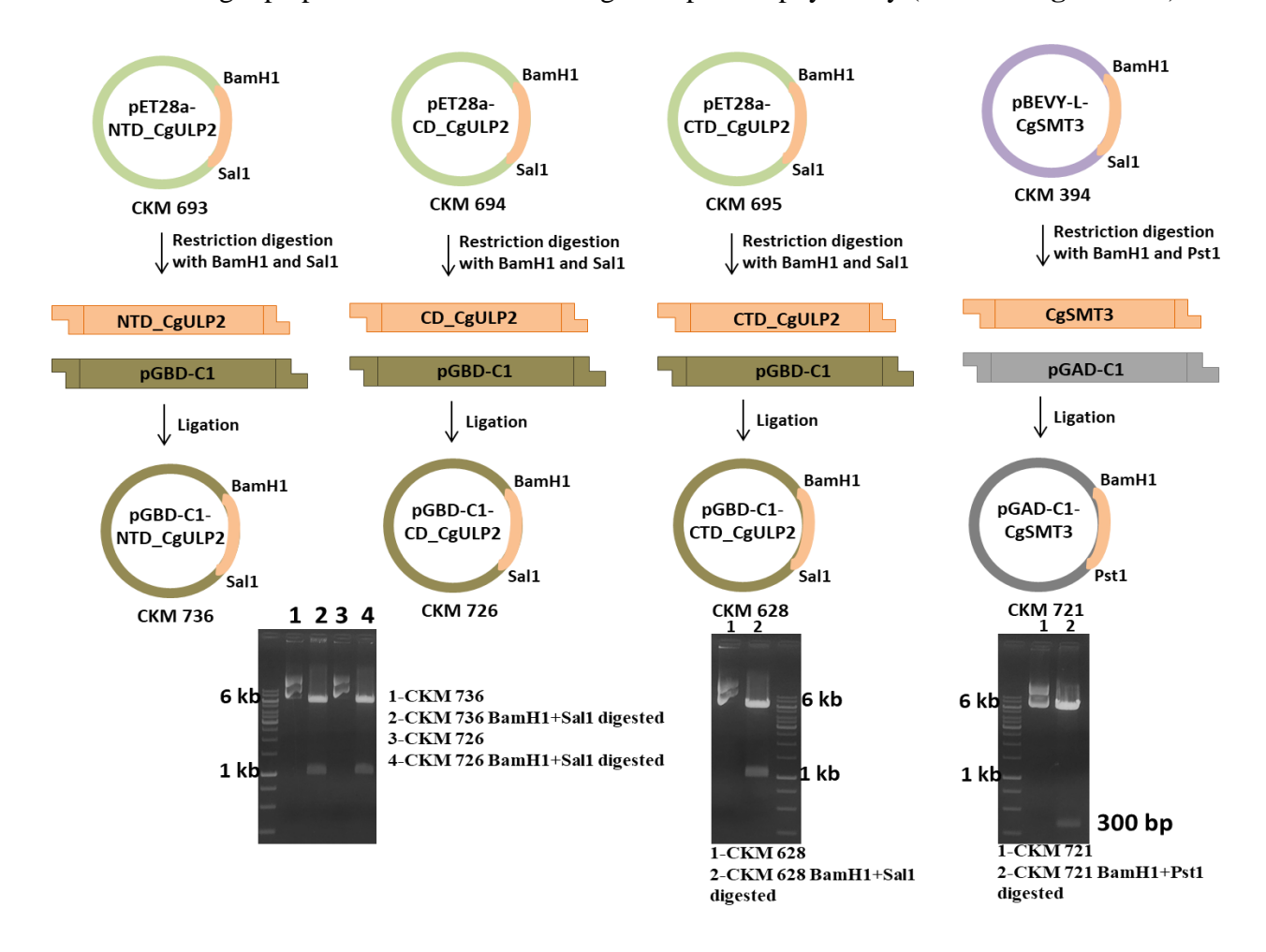
Schematic showing cloning generation of CKM 742, and CKM 737

Generating CgULP2 in pGBDU-C1 and CgSMT3 in pGAD-C1 for Yeast-two hybrid assay

N-terminal, catalytic domain, and C-terminal domain of the *CgULP2* cloned in pGBDU-C1 vector was used as bait and *CgSMT3* cloned in pGAD-C1 was used as prey for yeast two-hybrid screen. The respective gene was subcloned from the CKM 693 (NTD_CgULP2- pET28a), 694 (CD_CgULP2- pET28a), 695 (CTD_CgULP2- pET28a) and 394 (CgSMT3- pBEVY-L)

All the domains of the *CgULP2* were digested with BamH1 and Sal1 restriction enzymes to generate ~1 kb fragment for ligation into pGBDU-C1 vector. *CgSMT3* was digested with BamH1 and Pst1 restriction enzymes to generate ~300 bp fragments for ligation into pGAD-C1 vector. The clone was confirmed by restriction digestion.

Domains of CgUlp2 protein interacted with CgSmt3 protein physically (Refer to Figure 32A).



Schematic showing cloning generation of CKM 736, CKM 726, CKM 628, and CKM 721

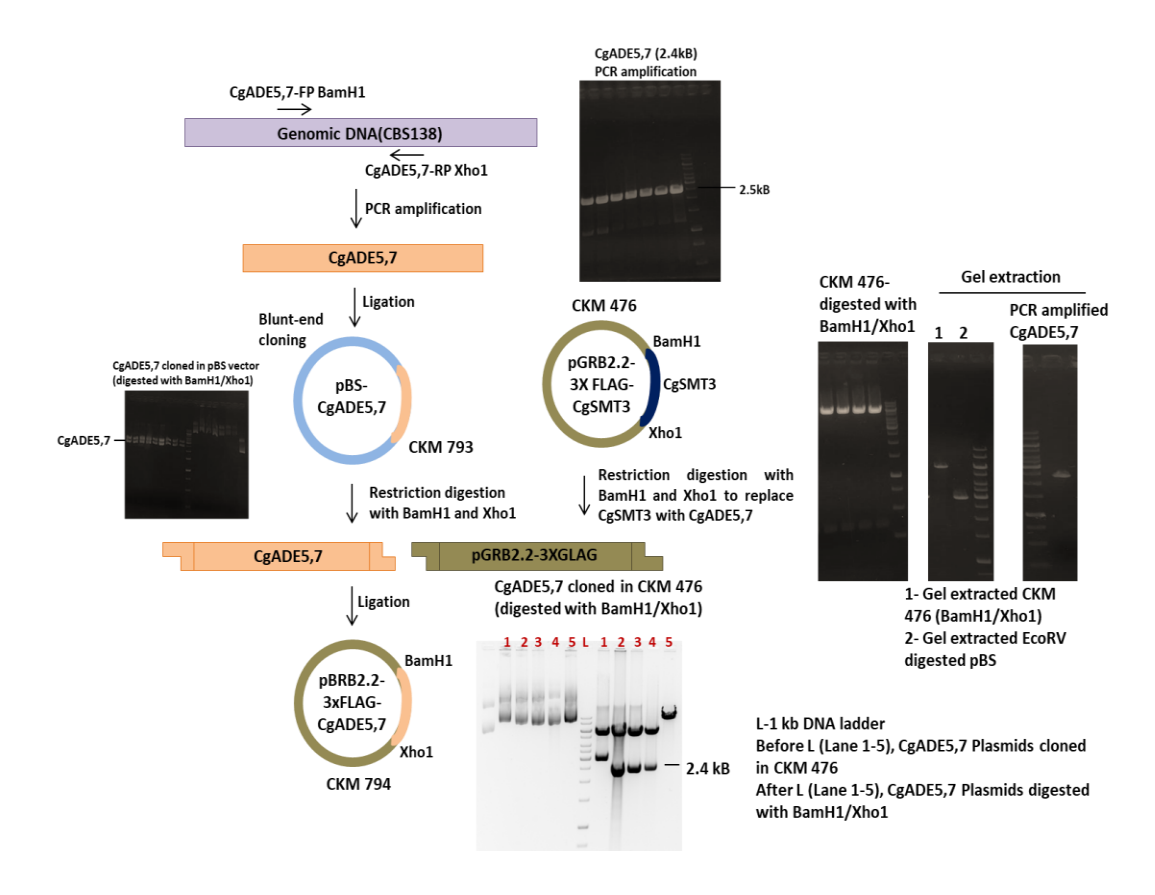
Generating *CgADE5*,7 in 3xFLAG-pGRB2.2 (CKM 794)

In order to clone *CgADE5*,7 with a 3xFLAG tag into pGRB2.2, genomic DNA from YRK19 (*C. glabrata* WT strain-CBS138) was used as a template for amplifying the *CgADE5*,7 gene. The following primers were used for the amplification:

CgADE5,7 FP Forward primer from START codon of CgADE5,7 with BamH1 site GGCGGATCCATGTTGAACATTCTAG

CgADE5,7 RP Reverse primer from up to STOP codon of CgADE5,7 with Xho1 site GGACTCGAGTTAGTATAGGTTGCTGG

The ~2.4 kb product obtained was ligated into pBlueScript vector. This clone was digested with BamH1 and Xho1 restriction enzymes to generate the fragment for ligation into 3xFLAG-tagged pGRB2.2 vector. The clone was confirmed by restriction digestion. The expression of *CgADE5*,7 protein was confirmed by western blot using an α -FLAG antibody (Refer to **Figure 16C**).



Schematic showing cloning generation of CKM 794

9.6 LISTS OF SIGNIFICANT PROTEINS IDENTIFIED BY QUANTITATIVE MASS SPECTROMETRY FOR EACH MUTANT

A list of 107 significantly upregulated proteins and 90 significantly downregulated proteins were identified in the $Cgulp2\Delta$ mutant in comparison with the wild type.

Cgulp2∆					
Upregula	nted Proteins	Downregula	nted Proteins		
Protein name	log2 fold change	Protein name	log2 fold change		
CgCca1	1.357	CgGlo3	-0.089		
CgCdc48	0.114	CgLaa1	-0.104		
CgAcl4	0.325	CgHpr1	-0.302		
CgAdh6	0.715	CgPho86	-0.439		
CgAro3	0.172	CgHsp10	-0.361		
CgAsk10	0.101	CgNic96	-1.211		
CgCat2	0.088	CgEnt5	-0.303		
CgCdc10	0.105	CgSky1	-0.203		
CgCog1	0.311	CgTom6	-0.478		
CgCox1	0.180	CgVps54	-0.411		
CgCpr6	0.174	CgMge1	-0.203		
CgCuz1	0.356	CgRho1	-0.165		
CgCys3	0.197	CgErp3	-0.409		
CgDnf1	0.088	CgMtr2	-0.090		
CgDph2	0.211	CgNup188	-0.359		
CgDph6	0.374	CgGnp1	-0.444		
CgEcm15	0.108	CgAfg3	-0.471		
CgEfm1	0.156	CgTim8	-0.298		
CgEnp2	0.334	CgTim44	-0.232		
CgFmn1	0.161	CgDjp1	-0.450		
CgFub1	0.311	CgVps10	-2.374		
CgGcn1	0.062	CgSod1	-0.416		

CgHam1	0.160	CgTif6	-0.397
CgHch1	0.161	CgGef1	-0.388
CgHom3	0.243	CgDnf2	-0.140
CgKrr1	0.196	CgMmt1	-0.322
CgLat1	0.122	CgGln1	-0.169
CgLcb4	0.309	CgCsg2	-0.241
CgLsg1	0.165	CgHtb1	-0.324
CgMas1	0.300	CgIxr1	-0.356
CgMed1	0.263	CgHmo1	-0.312
CgMeh1	0.385	CgMcm6	-0.099
CgMet12	0.262	CgPat1	-0.309
CgMet18	0.171	CgHtz1	-0.339
CgMeu1	0.139	CgHhf2	-0.331
CgMrp17	0.273	CgSmt3	-0.380
CgMrp21	0.167	CgAsk1	-0.291
CgMsh2	0.327	CgHhoA	-0.250
CgMtc2	0.342	CgCin8	-0.162
CgNar1	0.168	CgSmc1	-0.300
CgNat1	0.103	CgHtb2	-0.324
CgNnt1	0.417	CgFpr1	-0.144
CgNop15	0.964	CgShm2	-0.393
CgNus1	0.146	CgGcd11	-0.082
CgNut2	0.114	CgNet1	-0.175
CgPan1	0.201	CgGpi17	-0.128
CgPbr1	0.216	CgTps2	-0.350
CgPop3	0.162	CgHir2	-0.457
CgPre3	0.566	CgAde5,7	-0.160
CgPrp45	0.434	CgTfb5	-0.190
CgPrt1	0.148	CgAdk1	-0.105
CgPse1	0.149	CgYHR020W	-0.112
CgPus7	0.143	CgPsa1	-0.367

CgRet1	0.337	CgFlc1	-0.137
CgRet3	0.110	CgFcy2	-0.499
CgRio2	0.250	CgHxt1	-0.424
CgRna1	0.171	CgPtr2	-0.528
CgRpa34	0.229	CgAtp3	-0.651
CgRpn1	0.207	CgCus1	-0.367
CgRpn11	0.080	CgHsm3	-0.652
CgRpn12	0.185	CgSin4	-0.373
CgRpn5	0.293	CgTef1	-0.116
CgRpn6	0.315	CgHal5	-0.188
CgRpn8	0.304	CgClu1	-0.331
CgRpt2	0.106	CgPin4	-0.302
CgSdh5	0.333	CgBem1	-0.144
CgSdt1	0.213	CgChz1	-0.195
CgSec5	0.047	CgPom33	-0.239
CgSec72	0.090	CgYbp1	-0.087
CgSfl1	0.254	CgRps14B	-0.231
CgSis2	1.036	CgRpl19A	-0.323
CgSrb6	0.326	CgRps16A	-1.449
CgSrp14	0.164	CgRps21A	-0.187
CgSto1	0.098	CgRpl4B	-0.122
CgSua7	0.453	CgRpl13A	-0.152
CgSup45	0.140	CgRps25A	-0.197
CgTaf9	0.174	CgTup1	-0.487
CgTfb4	0.235	CgSws2	-0.155
CgTml25	0.256	CgMrp10	-0.006
CgTmt1	0.430	CgRsm18	-0.128
CgTom71	0.173	CgMrm1	-0.143
CgTrp3	0.272	CgMae1	-0.171
CgUtp9	0.369	CgMrx3	-0.170
CgUtr1	0.268	CgUsa1	-0.957

CgVps75	0.157	CgHpc2	-0.574
CgYar1	0.170	CgEcm21	-0.557
CgYdj1	0.179	CgFet4	-0.484
CgYhm2	0.460	CgSlk19	-0.272
CgYJR015W	0.217	CgCox12	-0.000
CgYKR011C	0.178		
CgYKR018C	0.301		
CgYLR287C	0.174		
CgYML082W	0.284		
CgYMR099C	0.048		
CgYpk3	0.213		
CgYps1	0.389		
CgCwp1.1	0.755		
CgEcm4	0.224		
CgExg1	0.430		
CgGas1	0.179		
CgGsh1	0.134		
CgLap3	0.149		
CgLrs4	0.429		
CgPir3	1.041		
CgPre5	0.156		
CgTrx3	0.410		

A list of 87 significantly upregulated proteins and 130 significantly downregulated proteins were identified in the $Cgslx8\Delta$ mutant in comparison with the wild type.

$Cgslx\delta\Delta$					
Upregulated	Proteins		Downregula	ated Proteins	
Protein name	log2 fold	Protein name	log2 fold	Protein name	log2 fold
	change		change		change
CgLap3	0.068	CgVps10	-2.310	CgYDR415C	-0.287
CgVig9	0.074	CgGcn5	-1.744	CgMss116	-0.286
CgRet3	0.081	CgRps16A	-1.438	CgApe3	-0.280
CgRvb1	0.082	CgEsp1	-1.415	CgPex5	-0.273
CgOye2	0.108	CgAtp3	-1.223	CgMcp2	-0.270
CgOla1	0.109	CgArg5,6	-1.120	CgSsa3	-0.260
CgCdc60	0.111	CgPpz2	-1.028	CgMam3	-0.257
CgCdc10	0.112	CgTog1	-1.011	CgUtp5	-0.256
CgPup3	0.131	CgMrx3	-0.989	CgSky1	-0.253
CgSec26	0.137	CgHpc2	-0.939	CgClu1	-0.249
CgSec17	0.144	CgCtk2	-0.932	CgRmd1	-0.248
CgRer1	0.148	CgSec3	-0.916	CgYNL320W	-0.246
CgGas1	0.150	CgEcm21	-0.865	CgYLR126C	-0.244
CgFpt1	0.153	CgMak10	-0.823	CgGar1	-0.228
CgHom3	0.153	CgSit1	-0.823	CgBig1	-0.225
CgSec4	0.155	CgHsm3	-0.807	CgYro2	-0.223
CgRps0B	0.155	CgSrc1	-0.783	CgVph2	-0.220
CgNat1	0.157	CgRtn1	-0.779	CgMrpL27	-0.214
CgPmi40	0.157	CgTrm5	-0.774	CgMic26	-0.210
CgTao3	0.160	CgRfc4	-0.745	CgAco1	-0.206
CgTfb4	0.161	CgKin4	-0.736	CgRpl21A	-0.205
CgUfo1	0.168	CgHxt2	-0.728	CgRpn1	-0.204
CgGrx8	0.171	CgTfb6	-0.720	CgSnq2	-0.197
CgRps20	0.173	CgDug3	-0.706	CgCaf20	-0.195

CgKar2	0.174	CgCti6	-0.694	CgOtu1	-0.194
CgSrp14	0.176	CgMix17	-0.688	CgCdc33	-0.191
CgTub3	0.176	CgHal5	-0.684	CgRsm28	-0.183
CgCcp1	0.177	CgErg7	-0.666	CgUrb2	-0.180
CgCdc12	0.178	CgRsm22	-0.653	CgSec13	-0.174
CgFmn1	0.179	CgSdh6	-0.646	CgSwh1	-0.173
CgArc15	0.181	CgMhp1	-0.646	CgLsb3	-0.162
CgKre2	0.184	CgPep8	-0.644	CgYpt1	-0.137
CgExg2	0.186	CgFzo1	-0.643	CgBil1	-0.136
CgPbr1	0.188	CgMsf1	-0.642	CgTim44	-0.134
CgCdc8	0.194	CgSmt3	-0.628	CgZrg17	-0.133
CgCuz1	0.200	CgUsa1	-0.627	CgRpt6	-0.128
CgOst3	0.202	CgYOR283W	-0.607	CgDid4	-0.124
CgSub2	0.202	CgMrpl15	-0.576	CgTim21	-0.119
CgEpt1	0.212	CgBck1	-0.571	CgVhs3	-0.108
CgRpa34	0.217	CgPex23B	-0.567	CgMbf1	-0.098
CgLap2	0.217	CgShq1	-0.562	CgYbp1	-0.095
CgYps1	0.218	CgDog2	-0.558	CgPtc5	-0.080
CgPyp1	0.220	CgFet4	-0.546	CgYMR099C	-0.062
CgVma2	0.221	CgTfb5	-0.546		
CgRnr1	0.221	CgRps17B	-0.542		
CgDpm1	0.222	CgHnt2	-0.538		
CgAcs2	0.225	CgYGR237C	-0.538		
CgMed1	0.231	CgMiy1	-0.536		
CgMvd1	0.236	CgUra4	-0.535		
CgDph5	0.243	CgCpa2	-0.523		
CgHho1	0.251	CgRot2	-0.509		
CgSec7	0.266	CgYta12	-0.506		
CgYMR027W	0.268	CgDur1:2	-0.500		
CgCox1	0.270	CgLcb4	-0.493		
CgCpr1	0.271	CgMia40	-0.490		

CgRgt1	0.298	CgGip2	-0.485
CgMet12	0.309	CgCgi121	-0.471
CgHmg1	0.309	CgRpl19A	-0.451
CgSdd2	0.311	CgSod1	-0.450
CgCog1	0.335	CgBud16	-0.449
CgVti1	0.335	CgErc1	-0.445
CgMtd1	0.339	CgCmc1	-0.442
CgAsk1	0.340	CgMic60	-0.420
CgSw14	0.344	CgAdh6	-0.409
CgErg5	0.362	CgPap1	-0.406
CgGlm6	0.364	CgSfb3	-0.406
CgYkt6	0.368	CgGsp1	-0.398
CgLsm3	0.370	CgSpt15	-0.392
CgTaf9	0.370	CgDnf2	-0.375
CgRad51	0.382	CgPho81	-0.373
CgEhd3	0.402	CgHir2	-0.370
CgScd6	0.418	CgSdh8	-0.368
CgDog2	0.419	CgCus1	-0.364
CgCta1	0.419	CgGrr1	-0.351
CgTom14	0.420	CgSte13	-0.345
CgScs7	0.471	CgPtk1	-0.335
CgRpl31A	0.476	CgPro2	-0.334
CgPff1	0.525	CgMam33	-0.331
CgTdh3	0.595	CgNab2	-0.328
CgPil1	0.605	CgOsh7	-0.326
CgEnt2	0.633	CgNar1	-0.324
CgSrb6	0.646	CgTuf1	-0.324
CgAqy1	1.078	CgRtp1	-0.319
CgCca1	1.178	CgSfk1	-0.313
CgUra3	1.933	CgSpn1	-0.311
CgPck1	2.169	CgYey2	-0.293

A list of 148 significantly upregulated proteins and 241 significantly downregulated proteins were identified in the Cguls 1Δ mutant in comparison with the wild type.

$Cguls1\Delta$					
Upregulated	Proteins		Downregula	ted Proteins	
Protein name	log2 fold	Protein name	log2 fold	Protein name	log2 fold
	change		change		change
CgVas1	0.048	CgYbp1	-0.112	CgNup188	-0.458
CgCdc10	0.062	CgRts3	-0.220	CgTsl1	-0.178
CgRps28B	0.083	CgYBR137W	-0.394	CgSws2	-0.408
CgZpr1	0.153	CgGga1	-0.270	CgYJL068C	-0.289
CgSub2	0.158	CgBbc1	-0.340	CgAim22	-0.257
CgMft1	0.221	CgMam3	-0.270	CgAat2	-0.284
CgOla1	0.338	CgSdd3	-0.139	CgPim1	-0.324
CgMet12	0.413	CgPre6	-0.163	CgVps10	-2.900
CgHom2	0.222	CgErg7	-0.339	CgAim9	-0.287
CgAro4	0.421	CgMam33	-0.730	CgGip2	-0.391
CgCdc8	0.366	CgYro2	-0.291	CgRsm18	-0.558
CgCam1	0.169	CgMrm1	-0.211	CgTim44	-0.222
CgMnt3	0.113	CgCdc48	-0.193	CgVid28	-0.342
CgYBR242W	0.637	CgYDL124W	-0.129	CgYta12	-0.364
CgRps20	0.234	CgEcm21	-1.004	CgSdh1	-0.826
CgHts1	0.247	CgMpm1	-0.310	CgCox6	-0.166
CgMpd2	0.176	CgPep8	-0.343	CgHsh49	-0.224
CgWrs1	0.173	CgDcs1	-0.112	CgRsm23	-0.305
CgMcd4	0.182	CgCoq1	-0.287	CgMrps35	-0.292
CgGln4	0.128	CgSod1	-0.713	CgNif3	-0.657
CgBcp1	0.196	CgOsh2	-0.339	CgLaa1	-0.134
CgAro3	0.300	CgGre2	-0.799	CgHal5	-0.412
CgEpt1	0.153	CgSdh8	-0.309	CgVps35	-0.314
CgPyp1	0.175	CgTae1	-0.494	CgPtc2	-0.092

CgYML119W	0.221	CgOxa1	-0.477	CgCsg2	-0.319
CgVig9	0.112	CgYey2	-0.308	CgSec13	-0.176
CgEbp2	0.298	CgShm1	-0.206	CgPup2	-0.156
CgRpl43A	0.204	CgFmp52	-0.439	CgRps16A	-1.207
CgCyb5	0.413	CgRpn1	-0.229	CgAfg3	-0.459
CgSsh1	0.165	CgDid2	-0.162	CgPtk1	-0.334
CgUtp9	0.265	CgCmc1	-0.667	CgMsf1	-0.534
CgRps19A	0.152	CgAdd66	-0.156	CgCoa1	-0.615
CgYMR027W	0.188	CgMss51	-0.322	CgSte23	-0.168
CgOpi3	0.840	CgYMR196W	-0.683	CgGlr1	-0.312
CgRpl42B	0.150	CgDyn1	-0.480	CgMrp21	-0.203
CgRpp0	0.174	CgImg1	-0.313	CgMnp1	-0.429
CgKre2	0.206	CgMas1	-0.230	CgNam8	-0.252
CgSpe3	0.101	CgAtp4	-0.456	CgDpl1	-0.240
CgFes1	0.308	CgLeu2	-0.343	CgTuf1	-0.415
CgPcf11	0.122	CgRib4	-0.384	CgDnf2	-0.390
CgAsc1	0.193	CgMrx3	-0.574	CgZrg17	-0.245
CgYFR006W	0.211	CgNpy1	-0.440	CgMrps12	-0.377
CgSec4	0.146	CgFzo1	-0.593	CgMic60	-0.580
CgRpl25	0.320	CgCub1	-0.122	CgApe3	-0.358
CgRpa34	0.385	CgMrpl35	-0.568	CgPhm3	-0.231
CgPrp45	0.271	CgTom70	-0.452	CgTps2	-0.418
CgMsh3	0.192	CgMtc1	-0.219	CgRsm28	-0.394
CgRpc34	0.207	CgMrpl37	-0.328	CgSsa3	-0.564
CgPnc1	0.651	CgHxt2	-0.598	CgEsp1	-2.179
CgRet1	0.248	CgRpt2	-0.148	CgIdh1	-0.267
CgOye2	0.222	CgBpl1	-0.183	CgYLR345W	-0.250
CgArc1	0.219	CgBcy1	-0.293	CgPex23	-0.215
CgYar1	0.175	CgExg1	-0.355	CgEno1	-0.526
CgRsn1	0.553	CgDsk2	-0.327	CgYGR237C	-0.374
CgAro2	0.133	CgCus1	-0.310	CgMic26	-0.202

CgShm2	0.208	CgTpm2	-0.491	CgRmd9	-0.371
CgRpl22A	0.256	CgUsa1	-0.992	CgIrc24	-0.417
CgSui2	0.235	CgPdx1	-0.447	CgMss116	-0.308
CgDpm1	0.404	CgYKR070W	-0.610	CgMss4	-0.295
CgTef1	0.162	CgEcm4	-0.425	CgEde1	-0.287
CgScm4	0.619	CgImp2	-0.542	CgMrpl40	-0.412
CgMsh2	0.162	CgMrps16	-0.201	CgKsp1	-0.353
CgErg11	0.510	CgSte13	-0.443	CgCym1	-0.331
CgRps22A	0.417	CgDnf1	-0.065	CgMef1	-0.171
CgUra3	1.752	CgYPL113C	-0.474	CgNut1	-0.226
CgHht1	0.314	CgMcm6	-0.051	CgGtb1	-0.157
CgErg5	0.597	CgYMR099C	-0.047	CgHir1	-0.125
CgCta1	0.476	CgPex11	-0.254	CgTrx3	-0.304
CgThs1	0.109	CgHfd1	-0.213	CgAco1	-0.365
CgEfm7	0.622	CgTim21	-0.204	CgRad7	-0.214
CgExg2	0.090	CgPho88	-0.131	CgPho4	-0.346
CgRps6A	0.157	CgPex5	-0.423	CgYPR127W	-0.463
CgTaf9	0.299	CgHis4	-0.489	CgGcv1	-0.555
CgRna1	0.282	CgSam2	-0.311	CgMia40	-0.588
CgRpl33A	0.309	CgCuz1	-0.495	CgSdo1	-0.686
CgPff1	0.340	CgXrn1	-0.236	CgMtr2	-0.237
CgYDR391C	0.304	CgHpc2	-0.482	CgCpa2	-0.735
CgBos1	0.696	CgLpd1	-0.429	CgYJR096W	-0.546
CgCaf20	0.196	CgLip5	-0.554	CgMxr1	-0.195
CgPdr13	0.363	CgPhb1	-0.546	CgMsc3	-0.186
CgSup45	0.178	CgPan1	-0.088	CgMic10	-0.402
CgRps23A	0.139	CgMbf1	-0.110	CgMxr2	-0.482
CgMls1	1.268	CgSlc1	-0.350	CgNdi1	-0.247
CgNop15	0.820	CgGrr1	-0.251	CgCin8	-0.154
CgCnb1	0.238	CgPmc1	-0.458	CgMrpl27	-0.388
CgRpl10	0.191	CgTog1	-1.027	CgPre4	-0.174

CgSes1	0.164	CgTim8	-0.278	CgCmc2	-0.373
CgSec26	0.100	CgVma4	-0.170	CgShp1	-0.305
CgPrt1	0.168	CgAtp3	-1.279	CgPex23B	-0.348
CgKti12	0.292	CgCbp3	-0.368	CgMrp1	-0.311
CgTrm2	0.297	CgLsb3	-0.212	CgChc1	-0.184
CgYNL134C	0.317	CgTpo4	-0.813	CgSdh6	-0.689
CgMcm4	0.478	CgMdh1	-0.476	CgCox1	-0.153
CgSlx9	0.369	CgLcb4	-0.384		
CgCat2	0.094	CgIdh2	-0.304		
CgTop1	0.160	CgYGL082W	-0.354		
CgHom3	0.092	CgNam9	-0.383		
CgTdh3	1.286	CgPpa2	-0.412		
CgFaa1	0.193	CgYnk1	-0.317		
CgRex4	0.553	CgMrpl15	-0.567		
CgHmt1	0.105	CgGdi1	-0.362		
CgArf2	0.122	CgAro8	-0.116		
CgFap7	0.503	CgUbp6	-0.278		
CgErp5	0.157	CgCbf3D	-0.278		
CgPby1	0.292	CgSfk1	-0.249		
CgBap2	0.216	CgAro1	-0.093		
CgDys1	0.125	CgRcf2	-0.656		
CgPck1	3.277	CgMrps8	-0.348		
CgRps9A	0.286	CgHsp78	-0.347		
CgRli1	0.224	CgClu1	-0.389		
CgApt1	0.284	CgEht1	-0.120		
CgCct3	0.222	CgAlg2	-0.299		
CgNop6	0.265	CgDur1:2	-0.667		
CgCct7	0.083	CgBem1	-0.154		
CgKap123	0.240	CgYNL320W	-0.306		
CgAsk10	0.236	CgMrpl4	-0.557		
CgPil1	0.942	CgBig1	-0.170		

CgLap2	0.171	CgVhs3	-0.158	
CgGrs1	0.129	CgAim45	-0.388	
CgRpl26A	0.189	CgMrps9	-0.250	
CgGas1	0.220	CgYhb1	-0.554	
CgZuo1	0.177	CgGts1	-0.301	
CgErg8	0.428	CgIsn1	-0.301	
CgScs7	0.283	CgAim41	-0.437	
CgFyv7	0.279	CgGsf2	-0.295	
CgHam1	0.357	CgGcv2	-0.140	
CgLia1	0.647	CgOtu1	-0.260	
CgCpr1	0.216	CgSpc2	-0.167	
CgRnr4	0.221	CgRga1	-0.441	
CgMeu1	0.230	CgNvj2	-0.255	
CgGcn1	0.064	CgZrc1	-0.230	
CgMed1	0.180	CgPdb1	-0.563	
CgRpl31A	0.317	CgPyc2	-0.303	
CgNat1	0.244	CgYHR112C	-0.294	
CgPop2	0.118	CgYme1	-0.250	
CgGpn2	0.286	CgSto1	-0.118	
CgAcs2	0.261	CgHse1	-0.541	
CgFpt1	0.194	CgAtp20	-0.539	
CgDph5	0.281	CgRps5	-0.192	
CgRer1	0.149	CgMrp10	-0.494	
CgRpl4B	0.160	CgMix17	-0.920	
CgAqy1	1.397	CgLat1	-0.254	
CgDed81	0.153	CgTps1	-0.609	
CgCdc12	0.137	CgCpr6	-0.137	
CgAto3	1.442	CgPnp1	-0.178	
CgPmi40	0.135	CgPtc5	-0.095	
CgRpl37A	0.158	CgUfd1	-0.154	
CgCca1	1.356	CgZwf1	-0.419	

A list of 277 significantly upregulated proteins and 184 significantly downregulated proteins were identified in the $Cgulp2\Delta Cgslx8\Delta$ mutant in comparison with the wild type.

$Cgulp2\Delta Cgslx8\Delta$							
	Upregulate	ed Proteins		Downregulate	d Proteins		
Protein name	log2 fold	Protein name	log2 fold	Protein name	log2 fold		
	change		change		change		
CgRfc3	0.062	CgPan6	0.382	CgAco1	-0.538		
CgSto1	0.086	CgMdj1	0.383	CgAde2	-0.390		
CgCmr1	0.088	CgPre5	0.394	CgAat2	-0.219		
CgHcr1	0.098	CgRib4	0.395	CgAbf2	-0.302		
CgCdc60	0.099	CgRds1	0.399	CgAch1	-0.573		
CgRet2	0.111	CgRad7	0.401	CgAde1	-0.353		
CgCop1	0.113	CgExg2	0.408	CgAde12	-0.274		
CgTfg2	0.114	CgGpn2	0.410	CgAde3	-0.126		
CgCys4	0.117	CgGsh1	0.410	CgAde4	-0.277		
CgSly1	0.118	CgRpn5	0.417	CgAde5,7	-0.295		
CgTom71	0.119	CgRpn8	0.423	CgAdp1	-0.157		
CgCdc10	0.120	CgSrv2	0.426	CgApd1	-0.287		
CgErp2	0.121	CgAqy1	0.429	CgApt1	-0.065		
CgLsb3	0.121	CgEfm3	0.430	CgArg5,6	-0.648		
CgSec7	0.122	CgCpr1	0.433	CgAsc1	-0.239		
CgMxr1	0.124	CgCym1	0.435	CgAtp19	-1.546		
CgYbp1	0.131	CgFmp27	0.435	CgAtp20	-1.174		
CgCam1	0.132	CgVmr1	0.441	CgAtp3	-1.184		
CgYMR155W	0.136	CgPfs2	0.441	CgAtp4	-0.721		
CgPop2	0.136	CgRpn2	0.442	CgBat1	-0.235		
CgTaf4	0.138	CgSnf1	0.443	CgBat2	-0.754		
CgCpr6	0.139	CgMet18	0.443	CgCbp3	-0.121		
CgPob3	0.140	CgZrt3	0.443	CgCcp1	-0.308		
CgDst1	0.142	CgPre1	0.447	CgCcw22	-0.327		

CgPhb1	0.142	CgUtp20	0.451	CgCit1	-0.519
CgInp51	0.144	CgTmt1	0.452	CgClu1	-0.487
CgInm1	0.146	CgYdc1	0.45	CgCox1	-1.451
CgRer1	0.146	CgCdc48	0.453	CgCox2	-1.066
CgRgd1	0.147	CgMcy1	0.455	CgCox4	-0.928
CgBsc6	0.151	CgCnb1	0.458	CgCox5B	-0.660
CgLcb1	0.155	CgSpt10	0.460	CgCox6	-1.134
CgVps25	0.156	CgRba50	0.468	CgCox8	-0.887
CgGbp2	0.159	CgPre10	0.473	CgCta1	-0.273
CgGyl1	0.162	CgDys1	0.475	CgCyt1	-0.373
CgYpt1	0.163	CgNnt1	0.475	CgDed81	-0.141
CgCne1	0.166	CgYML082W	0.476	CgDid4	-0.185
CgSpt5	0.166	CgZwf1	0.481	CgDsk2	-0.685
CgNut2	0.169	CgRib1	0.482	CgEcm21	-0.873
CgCsg2	0.171	CgPre7	0.492	CgEht1	-0.333
CgSte23	0.171	CgYop1	0.497	CgErg20	-0.163
CgSrp54	0.173	CgTrx3	0.499	CgEsp1	-2.868
CgSec4	0.174	CgSed4	0.505	CgFcy21	-0.581
CgYFR006W	0.175	CgYme2	0.515	CgFet4	-1.348
CgMeu1	0.177	CgCdc8	0.515	CgFhn1	-0.557
CgSgv1	0.177	CgSca7	0.516	CgFpr1	-0.168
CgOsm1	0.179	CgYcf1	0.518	CgFpt1	-0.236
CgSrp101	0.179	CgYDR248C	0.521	CgFzo1	-0.483
CgLap2	0.180	CgRpn12	0.522	CgGcd11	-0.157
CgHir1	0.181	CgInm2	0.524	CgGcv1	-0.839
CgHch1	0.186	CgYKR018C	0.525	CgGcv2	-0.701
CgCat2	0.188	CgCwp2	0.527	CgGip2	-0.291
CgRpn7	0.193	CgPyp1	0.530	CgGlm6	-0.269
CgTaf3	0.193	CgLys4	0.536	CgGln1	-0.303
CgEmc2	0.194	CgMbf1	0.538	CgGln4	-0.445
CgKes1	0.196	CgTmn2	0.538	CgGlo3	-0.130

CgPbr1	0.196	CgGsf2	0.549	CgHal5	-0.511
CgGas1	0.197	CgPam17	0.549	CgHir2	-0.366
CgUbr1	0.199	CgCuz1	0.550	CgHis4	-0.670
CgMrx18	0.200	CgSft2	0.556	CgHmt1	-0.200
CgCaj1	0.200	CgZta1	0.563	CgHrp1	-0.408
CgDpb4	0.202	CgNpy1	0.565	CgHsh49	-0.200
CgTfb5	0.202	CgCtf18	0.567	CgHtb2	-0.206
CgRpd3	0.202	CgShq1	0.578	CgIdh1	-0.254
CgNma1	0.203	CgMet30	0.586	CgImg1	-0.679
CgYGR130C	0.203	CgIfa38	0.586	CgKin4	-0.244
CgUbx4	0.203	CgSak1	0.587	CgLat1	-0.279
CgAos1	0.205	CgJem1	0.588	CgLip5	-0.584
CgDpm1	0.209	CgGrx8	0.594	CgLpd1	-0.292
CgInp51	0.209	CgPre8	0.600	CgLpx2	-0.249
CgKre2	0.212	CgRfs1	0.601	CgMae1	-0.501
CgClp1	0.213	CgMp65	0.627	CgMdh1	-0.380
CgCin8	0.214	CgScs7	0.630	CgMic10	-0.604
CgRpb2	0.215	CgOye2	0.633	CgMic60	-0.529
CgPim1	0.215	CgFmp52	0.645	CgMmt1	-0.371
CgMgm1	0.219	CgInp53	0.653	CgMrm1	-1.249
CgAro3	0.220	CgUfo1	0.655	CgMrp1	-0.321
CgXrn1	0.221	CgYps1	0.668	CgMrp10	-0.581
CgRet3	0.221	CgFub1	0.703	CgMrp17	-0.261
CgSec14	0.224	CgBos1	0.754	CgMrp21	-0.388
CgSte50	0.227	CgHlj1	0.762	CgMrpl10	-0.451
CgPlp1	0.228	CgNop15	0.778	CgMrpl13	-0.318
CgEug1	0.232	CgErv1	0.780	CgMrpl15	-0.451
CgVma2	0.232	CgSnq2	0.830	CgMrpl20	-0.524
CgPup2	0.232	CgPup1	0.865	CgMrpl22	-0.812
CgPup3	0.233	CgRex4	0.892	CgMrpl27	-0.539
CgSec24	0.236	CgApe1	0.896	CgMrpl37	-0.225

CgTaf7	0.236	CgPdr16	0.955	CgMrpl40	-0.845
CgYMR027W	0.236	CgAdh6	0.971	CgMrps12	-0.870
CgNpa3	0.238	CgHfd1	1.000	CgMrps16	-0.791
CgKel3	0.240	CgPir3	1.254	CgMrps18	-0.603
CgCak1	0.243	CgAdh6	1.302	CgMrps35	-0.645
CgYER152C	0.244	CgPdh1	1.369	CgMrps8	-0.413
CgMpd2	0.246	CgCca1	1.422	CgMrps9	-1.226
CgRnr4	0.246	CgYML131W	1.561	CgMrx3	-0.453
CgYMR099C	0.249	CgPup1	2.332	CgMsc3	-0.278
CgGlo4	0.250			CgMss51	-0.196
CgPff1	0.251			CgMtd1	-0.452
CgYDL124W	0.251			CgNam9	-0.715
CgAro1	0.252			CgNdi1	-0.270
CgBna3	0.252			CgNup85	-0.181
CgZds1	0.253			CgOxa1	-0.182
CgUbp6	0.261			CgPdb1	-0.697
CgSnf4	0.263			CgPds5	-0.366
CgIst3	0.264			CgPex23B	-0.338
CgReh1	0.266			CgPnc1	-0.327
CgSfl1	0.267			CgPyc2	-0.427
CgErg6	0.267			CgQcr7	-1.285
CgPrp45	0.268			CgRcf2	-0.650
CgYap3	0.271			CgRck2	-0.440
CgYme1	0.271			CgRod1	-0.497
CgTma23	0.272			CgRpl10	-0.190
CgPho88	0.275			CgRpl19A	-0.207
CgLap3	0.276			CgRpl22A	-0.189
CgGlr1	0.276			CgRpl26A	-0.232
CgArp2	0.277			CgRpl42B	-0.267
CgPre6	0.282			CgRpp0	-0.171
CgYDR391C	0.283			CgRpp1A	-0.224

CgRpt6	0.283		CgRps0	-0.106
CgRpt3	0.285		CgRps14B	-0.173
CgFun30	0.285		CgRps19A	-0.176
CgGas1	0.289		CgRps21	-0.279
CgSrm1	0.289		CgRps25A	-0.291
CgPtk2	0.290		CgRps9A	-0.301
CgHbs1	0.293		CgRsm18	-1.767
CgTml25	0.295		CgRsm23	-0.427
CgSec66	0.296		CgRsm28	-1.020
CgSsd1	0.296		CgScm4	-0.443
CgUbp1	0.296		CgSdh6	-0.751
CgRpn11	0.296		CgSdo1	-0.699
CgSec62	0.296		CgShm1	-0.425
CgSsl2	0.298		CgShm2	-0.423
CgMak3	0.299		CgSmt3	-0.462
CgPdr17	0.300		CgSrc1	-0.527
CgTfb4	0.302		CgSso2	-0.309
CgVrg4	0.303		CgSws2	-1.239
Cg V1g4 CgHrd3	0.306		Cg5ws2 CgTef1	-0.078
	0.300		_	-0.078
CgAge2			CgThr4	
CgSdt1`	0.310		CgTif3	-0.160
CgTaf2	0.310		CgTim17	-0.263
CgCub1	0.311		CgTim21	-0.273
CgBol2	0.313		CgTim44	-0.078
CgBsd2	0.314		CgTog1	-1.306
CgRvb2	0.317		CgTpo4	-0.579
CgKar2	0.318		CgTps2	-0.413
CgYar1	0.320		CgTrp4	-0.093
CgOrc5	0.321		CgTuf1	-0.286
CgRpt5	0.324		CgTup1	-0.093
CgKre5	0.324		CgTwf1	-0.964

CgCue4	0.324		CgUra4	-0.158
CgYPL247C	0.327		CgUsa1	-0.894
CgTcb3	0.327		CgUtp5	-0.166
CgPga3	0.327		CgVas1	-0.100
	0.327			-0.043
CgRpn1	0.329		CgVps10	-0.622
CgYnd1			CgYBR242W	
CgSec27	0.331		CgYhm2	-0.896
CgGpi12	0.333		CgYHR020W	-0.194
CgRpn9	0.333		CgYLR456W	-0.151
CgUfd1	0.334		CgYnk1	-0.291
CgCdc43	0.334		CgZrg17	-0.104
CgPre4	0.337		CgCox12	-0.891
CgRtp1	0.340		CgDur1:2	-0.726
CgEcm15	0.342		CgEno1	-0.470
CgCog1	0.345		CgGsp1	-0.373
CgRpt2	0.347		CgHtb2	-0.175
CgMas1	0.350		CgIdh2	-0.252
CgRsc3	0.350		CgOla1	-0.138
CgYPR127W	0.354		CgPho4	-0.291
CgRpn6	0.354		CgRpl13A	-0.251
CgCcr4	0.356		CgRpl36A	-0.139
CgPre9	0.358		CgRpl4B	-0.191
CgEfm1	0.358		CgRps13	-0.180
CgApe4	0.362		CgRps16	-0.206
CgHem12	0.363		CgRps16SA	-1.506
CgVma4	0.364		CgRps17B	-0.252
CgYBR137W	0.365		CgRps28B	-0.130
CgYDR476C	0.368		CgRps6A	-0.170
CgAto3	0.369		CgSdh1	-0.669
CgAim2	0.373		CgSsa3	-0.383
CgRpt4	0.374		CgTps1	-0.404
			U 1	

CgMed1	0.375		CgUbp3	-0.178
CgSmd2	0.377		CgVig9	-0.108
CgYIL108W	0.378		CgYhb1	-0.629

A list of 300 significantly upregulated proteins and 134 significantly downregulated proteins were identified in the $Cgulp2\Delta Cguls1\Delta$ mutant in comparison with the wild type.

Cgulp2∆Cguls1∆								
	Upregulate	Downregulated Proteins						
Protein name	log2 fold	Protein name	log2 fold	Protein name	log2 fold			
	change		change		change			
CgYMR099C	0.049	CgMdh1	0.275	CgVps10	-2.153			
CgImd4	0.058	CgRpc34	0.277	CgRps16	-1.521			
CgSec27	0.079	CgDis3	0.280	CgEsp1	-1.191			
CgSec72	0.084	CgYta12	0.280	CgDsk2	-1.171			
CgSec26	0.086	CgCdc24	0.280	CgTwf	-0.928			
CgOsm1	0.089	CgCym1	0.281	CgUsa1	-0.911			
CgPtc5	0.102	CgRrp8	0.281	CgYpi1	-0.772			
CgArf2	0.103	CgRai1	0.282	CgFet4	-0.665			
CgLcb1	0.103	CgPdr13	0.282	CgSmt3	-0.656			
CgPhb1	0.107	CgYpt1	0.283	CgTps2	-0.619			
CgCys4	0.114	CgBud22	0.285	CgSod1	-0.614			
CgSui1	0.120	CgIdh1	0.287	CgSdo1	-0.584			
CgBig1	0.121	CgVrg4	0.289	CgPsa1	-0.580			
CgTom71	0.121	CgSec62	0.289	CgYMR196W	-0.565			
CgTsh1	0.124	CgSfl1	0.290	CgLip5	-0.556			
CgGcn1	0.126	CgUtp22	0.290	CgYBR238C	-0.536			
CgMet12	0.127	CgHir1	0.291	CgTup1	-0.531			
CgCwh43	0.127	CgLip1	0.293	CgIxr1	-0.471			
CgSly1	0.131	CgInp51	0.293	CgFcy21	-0.470			
CgSec31	0.132	CgSec66	0.295	CgRpl28	-0.456			

CgLap2	0.136	CgSdt1	0.295	CgPnc1	-0.455
CgRvb1	0.136	CgRqc2	0.296	CgHtb2	-0.454
CgSrp14	0.140	CgMak3	0.297	CgClu1	-0.447
CgArc1	0.142	CgGly1	0.297	CgShm2	-0.440
CgNat1	0.145	CgPdr16	0.298	CgHmo1	-0.438
CgShs1	0.146	CgRio2	0.299	CgHis4	-0.433
CgHom3	0.149	CgYDR391C	0.301	CgGln1	-0.421
CgCog3	0.149	CgBet3	0.305	CgRpl19A	-0.419
CgCdc10	0.151	CgGsh1	0.305	CAGL0A02299g	-0.403
CgSla2	0.153	CgMrp17	0.305	CgDap1	-0.388
CgKap123	0.155	CgDph2	0.306	CgHtb2	-0.380
CgYMR027W	0.155	CgSmm1	0.308	CgSlf1	-0.360
CgRna1	0.160	CgYGR130C	0.315	CgMaf1	-0.354
CgUbx4	0.160	CgMcd4	0.316	CgCcw22	-0.338
CgHom2	0.162	CgNup53	0.316	CgSlc1	-0.331
CgMnp1	0.164	CgExg1	0.317	CgHem1	-0.321
CgTif35	0.167	CgPga3	0.318	CgTpm2	-0.321
CgTrp3	0.167	CgNip7	0.318	CgCta1	-0.318
CgCbp3	0.168	CgGpn3	0.320	CgBmt3	-0.318
CgNus1	0.169	CgCue4	0.320	CgMtd1	-0.317
CgMyo4	0.169	CgNar1	0.322	CgRpl31	-0.316
CgSnq2	0.171	CgBre1	0.324	CgPin4	-0.301
CgElp3	0.171	CgMed1	0.325	CgRps21	-0.299
CgPdx1	0.176	CgIml2	0.325	CgRps17B	-0.290
CgExg2	0.178	CgBmt2	0.325	CgHhoA	-0.289
CgCdc37	0.178	CgTaf7	0.326	CgPir5	-0.286
CgKin4	0.178	CgHsp78	0.327	CgRpl25	-0.284
CgMbf1	0.179	CgVps75	0.328	CgYGL082W	-0.281
CgMft1	0.180	CgPfs2	0.328	CgScm4	-0.281
CgMkt1	0.181	CgTaf3	0.329	CgRpl23B	-0.279
CgGas1	0.181	CgCox17	0.331	CgRpp1A	-0.271

CgRrt12	0.182	CgYJL193W	0.332	CgRpl4B	-0.268
CgYER152C	0.183	CgMix17	0.334	CgRpl13A	-0.265
CgCdc34	0.184	CgMeh1	0.338	CgRpl42B	-0.262
CgRer1	0.185	CgNop2	0.341	CgRps25A	-0.253
CgPpg1	0.185	CgMak21	0.344	CgYLR456W	-0.252
CgYDL124W	0.186	CgPet54	0.345	CgEpl26A	-0.251
CgGcd1	0.193	CgIst3	0.346	CgRpl27B	-0.243
CgAim2	0.193	CgSte50	0.348	CgRps14B	-0.242
CgSto1	0.194	CgYpt7	0.348	CgHal5	-0.240
CgTfg2	0.194	CgMis1	0.349	CgGlt1	-0.239
CgKel3	0.194	CgHpm1	0.349	CgRpl11A	-0.232
CgSgv1	0.196	CgNop6	0.349	CgRbl2	-0.229
CgTif5	0.197	CgRpc17	0.350	CgRps16	-0.220
CgYar1	0.199	CgHbs1	0.350	CgNam8	-0.211
CgMpd2	0.200	CgUtp23	0.350	CgTif3	-0.208
CgSrp54	0.200	CgPrp43	0.354	CgAdp1	-0.208
CgMrps9	0.201	CgKap104	0.359	CgVph2	-0.208
CgMet18	0.203	CgNar1	0.359	CgRpl36A	-0.206
CgSrm1	0.203	CgRet1	0.361	CgAsc1	-0.203
CgZpr1	0.203	CgApe4	0.361	CgRps4B	-0.199
CgRrp40	0.207	CgAcl4	0.365	CgFpr1	-0.199
CgMgm1	0.207	CgRpa135	0.366	CgRpl10	-0.198
CgPmt7	0.209	CgErc1	0.369	CgChz1	-0.196
CgGin4	0.209	CgUra6	0.369	CgRpl15A	-0.192
CgLsg1	0.210	CgTfb4	0.370	CgTup1	-0.191
CgErp2	0.210	CgSit1	0.371	CgReb1	-0.190
CgSnu71	0.211	CgUtp13	0.374	CgMnt3	-0.186
CgRmd9	0.211	CgEcm4	0.378	CgTim13	-0.184
CgTaf9	0.212	CgHrr25	0.380	CgAdk1	-0.181
CgCat2	0.214	CgSdh5	0.380	CgRpl34B	-0.179
CgNew1	0.215	CgCog1	0.381	CgRps6A	-0.176

CgSup45	0.215	CgRqc1	0.383	CgRps13	-0.170
CgOxa1	0.218	CgSsl2	0.390	CgRps19A	-0.167
CgGyl1	0.220	CgFub1	0.390	CgRpl14A	-0.163
CgMrps16	0.222	CgYdj1	0.395	CgVig9	-0.157
CgGpi12	0.222	CgUtp9	0.396	CgMam3	-0.157
CgHch1	0.222	CgBud16	0.396	CgRpl37A	-0.156
CgMrs6	0.223	CgLap3	0.402	CgAbf2	-0.154
CgYNL195C	0.224	CgNrd1	0.404	CgDur1:2	-0.150
CgNip1	0.224	CgYps1	0.411	CgRpp0	-0.149
CgRet3	0.225	CgNoc2	0.412	CgGcv1	-0.144
CgInp51	0.227	CgNop16	0.413	CgArc15	-0.143
CgYLR287C	0.230	CgFyv7	0.413	CgYHR020W	-0.136
CgNot3	0.230	CgLcb4	0.418	CgAcs2	-0.133
CgCam1	0.231	CgCnb1	0.419	CgGlo3	-0.130
CgRvb2	0.231	CgTma64	0.420	CgGsp1	-0.128
CgMsh6	0.233	CgNmd3	0.421	CgVsh3	-0.123
CgPrp45	0.233	CgRci37	0.421	CgEde1	-0.107
CgArt10	0.233	CgOaf1	0.422	CgApt1	-0.097
CgPob3	0.236	CgYML082W	0.424	CgToa2	-0.094
CgZta1	0.236	CgUtp11	0.424	CgGcd11	-0.083
CgYta7	0.236	CgNep1	0.424	CgTef1	-0.082
CgGcn20	0.238	CgPbr1	0.424	CgMcm6	-0.048
CgLat1	0.238	CgKri1	0.425	CgErp5	-0.039
CgPex5	0.239	CgYDR248C	0.425	CgDef1	-0.038
CgVma4	0.240	CgSdh6	0.426	CgCuz1	-0.647
CgZds1	0.241	CgUpa2	0.428	CgPre2	-0.509
CgVma3	0.244	CgMrpl10	0.429	CgPre3	-0.566
CgIls1	0.245	CgShq1	0.432	CgPre5	-0.232
CgClp1	0.246	CgTrx3	0.432	CgPre7	-0.311
CgCdc8	0.246	CgBol2	0.434	CgPre8	-0.299
CgCdc53	0.246	CgMrpl22	0.434	CgRup1	-0.177

CgBsc6	0.246	CgYhm2	0.435	CgPup1	-0.577
CgRpp1	0.246	CgGpx2	0.436	CgPup3	-0.125
CgTrp2	0.247	CgSua7	0.437	CgRpn1	-0.387
CgMeu1	0.248	CgPam17	0.438	CgRpn2	-0.321
CgNup85	0.249	CgDbp10	0.440	CgRpn5	-0.477
CgRpo31	0.250	CgGpn2	0.440	CgRpn6	-0.403
CgTrm44	0.250	CgMct1	0.452	CgRpn9	-0.343
CgMas1	0.251	CgCpr6	0.454	CgRpn8	-0.288
CgPus7	0.252	CgHis1	0.455	CgRpn11	-0.135
CgUra4	0.253	CgRrp12	0.461	CgRpn12	-0.361
CgDld2	0.253	CgDsd1	0.469	CgRpt2	-0.210
CgArg5,6	0.253	CgRex4	0.469	CgRpt4	-0.286
CgAos1	0.253	CgNog1	0.477	CgRpt6	-0.126
CgRcl1	0.254	CgAsf1	0.480	CgUfo1	-0.416
CgTml25	0.255	CgSlx9	0.481	CgUfd1	-0.228
CgEpt1	0.256	CgKgd1	0.486	CgCdc48	-0.251
CgMrpl4	0.262	CgSpt10	0.491	CgMeh1	-0.333
CgMtr2	0.263	CgMxr2	0.502	CgMdj1	-0.417
CgPse1	0.266	CgMrx12	0.502	CgPim1	-0.209
CgPsp2	0.269	CgEfm7	0.505		
CgCak1	0.269	CgBud21	0.510		
CgDpm1	0.269	CgNma111	0.521		
CgNpa3	0.270	CgLys12	0.527		
CgNcs6	0.271	CgAyr1	0.528		
CgTma23	0.273	CgTmn2	0.535		
CgNup82	0.273	CgAtp3	0.669		
CgPan1	0.274	CgRpc25	0.537		
CgSnf1	0.275	CgEar1	0.540		
CgTmt1	0.726	CgNap1	0.541		
CgNre1	0.819	CgLrs4	0.546		
CgAdh6	0.837	CgVti1	0.557		

CgNop15	1.038	CgAde5,7	0.150	
CgPir3	1.178	CgSed4	0.562	
CgCwp2	1.293	CgUtp20	0.580	
CgCha1	1.351	CgLys4	0.609	
CgCca1	1.531	CgPpz2	0.620	
CgUpt6	0.479			

9.7 LIST OF PUBLICATIONS

• **Gupta, D.;** Garapati, H. S.; Kakumanu, A. V. S.; Shukla, R.; Mishra, K. SUMOylation in Fungi: A Potential Target for Intervention. *Comput Struct Biotechnol J* **2020**, *18*, 3484–3493. https://doi.org/10.1016/j.csbj.2020.10.037.

REFERENCES

- (1) Case, N. T.; Berman, J.; Blehert, D. S.; Cramer, R. A.; Cuomo, C.; Currie, C. R.; Ene, I. V.; Fisher, M. C.; Fritz-Laylin, L. K.; Gerstein, A. C.; Glass, N. L.; Gow, N. A. R.; Gurr, S. J.; Hittinger, C. T.; Hohl, T. M.; Iliev, I. D.; James, T. Y.; Jin, H.; Klein, B. S.; Kronstad, J. W.; Lorch, J. M.; McGovern, V.; Mitchell, A. P.; Segre, J. A.; Shapiro, R. S.; Sheppard, D. C.; Sil, A.; Stajich, J. E.; Stukenbrock, E. E.; Taylor, J. W.; Thompson, D.; Wright, G. D.; Heitman, J.; Cowen, L. E. The Future of Fungi: Threats and Opportunities. *G3 (Bethesda)* 2022, *12* (11), jkac224. https://doi.org/10.1093/g3journal/jkac224.
- (2) Case, N. T.; Heitman, J.; Cowen, L. E. The Rise of Fungi: A Report on the CIFAR Program Fungal Kingdom: Threats & Opportunities Inaugural Meeting. *G3 (Bethesda)* **2020**, *10* (6), 1837–1842. https://doi.org/10.1534/g3.120.401271.
- (3) Fisher, M. C.; Gurr, S. J.; Cuomo, C. A.; Blehert, D. S.; Jin, H.; Stukenbrock, E. H.; Stajich, J. E.; Kahmann, R.; Boone, C.; Denning, D. W.; Gow, N. A. R.; Klein, B. S.; Kronstad, J. W.; Sheppard, D. C.; Taylor, J. W.; Wright, G. D.; Heitman, J.; Casadevall, A.; Cowen, L. E. Threats Posed by the Fungal Kingdom to Humans, Wildlife, and Agriculture. *mBio* **2020**, *11* (3), e00449-20. https://doi.org/10.1128/mBio.00449-20.
- (4) Bergeron, A.; Porcher, R.; Sulahian, A.; de Bazelaire, C.; Chagnon, K.; Raffoux, E.; Vekhoff, A.; Cornet, M.; Isnard, F.; Brethon, B.; Lacroix, C.; Poirot, J. L.; Bouges, C.; Derouin, F.; Tazi, A.; Ribaud, P. The Strategy for the Diagnosis of Invasive Pulmonary Aspergillosis Should Depend on Both the Underlying Condition and the Leukocyte Count of Patients with Hematologic Malignancies. *Blood* 2012, *119* (8), 1831–1837; quiz 1956. https://doi.org/10.1182/blood-2011-04-351601.
- (5) Bermas, A.; Geddes-McAlister, J. Combatting the Evolution of Antifungal Resistance in *Cryptococcus Neoformans. Molecular Microbiology* **2020**, *114* (5), 721–734. https://doi.org/10.1111/mmi.14565.
- (6) Fridkin, S. K.; Jarvis, W. R. Epidemiology of Nosocomial Fungal Infections. *Clin Microbiol Rev* **1996**, *9* (4), 499–511. https://doi.org/10.1128/CMR.9.4.499.
- (7) Lamoth, F.; Lockhart, S. R.; Berkow, E. L.; Calandra, T. Changes in the Epidemiological Landscape of Invasive Candidiasis. *J Antimicrob Chemother* **2018**, *73* (suppl_1), i4–i13. https://doi.org/10.1093/jac/dkx444.

- (8) Revie, N. M.; Iyer, K. R.; Robbins, N.; Cowen, L. E. Antifungal Drug Resistance: Evolution, Mechanisms and Impact. *Curr Opin Microbiol* **2018**, *45*, 70–76. https://doi.org/10.1016/j.mib.2018.02.005.
- (9) Armstrong-James, D.; Brown, G. D.; Netea, M. G.; Zelante, T.; Gresnigt, M. S.; van de Veerdonk, F. L.; Levitz, S. M. Immunotherapeutic Approaches to Treatment of Fungal Diseases. *Lancet Infect Dis* 2017, 17 (12), e393–e402. https://doi.org/10.1016/S1473-3099(17)30442-5.
- (10) Crous, P. W.; Groenewald, J. Z.; Slippers, B.; Wingfield, M. J. Global Food and Fibre Security Threatened by Current Inefficiencies in Fungal Identification. *Philos Trans R Soc Lond B Biol Sci* **2016**, *371* (1709), 20160024. https://doi.org/10.1098/rstb.2016.0024.
- (11) Fisher, M. C.; Hawkins, N. J.; Sanglard, D.; Gurr, S. J. Worldwide Emergence of Resistance to Antifungal Drugs Challenges Human Health and Food Security. *Science* **2018**, *360* (6390), 739–742. https://doi.org/10.1126/science.aap7999.
- (12) Lim, Y.-J.; Kim, K.-T.; Lee, Y.-H. SUMOylation Is Required for Fungal Development and Pathogenicity in the Rice Blast Fungus Magnaporthe Oryzae. *Mol Plant Pathol* **2018**, *19* (9), 2134–2148. https://doi.org/10.1111/mpp.12687.
- (13) Singh, R. P.; Hodson, D. P.; Huerta-Espino, J.; Jin, Y.; Bhavani, S.; Njau, P.; Herrera-Foessel, S.; Singh, P. K.; Singh, S.; Govindan, V. The Emergence of Ug99 Races of the Stem Rust Fungus Is a Threat to World Wheat Production. *Annu Rev Phytopathol* **2011**, *49*, 465–481. https://doi.org/10.1146/annurev-phyto-072910-095423.
- (14) Fisher, M. C.; Henk, D. A.; Briggs, C. J.; Brownstein, J. S.; Madoff, L. C.; McCraw, S. L.; Gurr, S. J. Emerging Fungal Threats to Animal, Plant and Ecosystem Health. *Nature* **2012**, 484 (7393), 186–194. https://doi.org/10.1038/nature10947.
- (15) Strange, R. N.; Scott, P. R. Plant Disease: A Threat to Global Food Security. *Annu Rev Phytopathol* **2005**, *43*, 83–116. https://doi.org/10.1146/annurev.phyto.43.113004.133839.
- (16) Beernaert, L. A.; Pasmans, F.; Van Waeyenberghe, L.; Haesebrouck, F.; Martel, A. *Aspergillus* Infections in Birds: A Review. *Avian Pathology* **2010**, *39* (5), 325–331. https://doi.org/10.1080/03079457.2010.506210.
- (17) Seyedmousavi, S.; Bosco, S. D. M. G.; De Hoog, S.; Ebel, F.; Elad, D.; Gomes, R. R.; Jacobsen, I. D.; Jensen, H. E.; Martel, A.; Mignon, B.; Pasmans, F.; Piecková, E.; Rodrigues, A. M.; Singh, K.; Vicente, V. A.; Wibbelt, G.; Wiederhold, N. P.; Guillot, J.

- Fungal Infections in Animals: A Patchwork of Different Situations. *Medical Mycology* **2018**, *56* (suppl_1), S165–S187. https://doi.org/10.1093/mmy/myx104.
- (18) Almeida, F.; Rodrigues, M. L.; Coelho, C. The Still Underestimated Problem of Fungal Diseases Worldwide. *Front Microbiol* **2019**, *10*, 214. https://doi.org/10.3389/fmicb.2019.00214.
- (19) Scorzoni, L.; De Paula E Silva, A. C. A.; Marcos, C. M.; Assato, P. A.; De Melo, W. C. M. A.; De Oliveira, H. C.; Costa-Orlandi, C. B.; Mendes-Giannini, M. J. S.; Fusco-Almeida, A. M. Antifungal Therapy: New Advances in the Understanding and Treatment of Mycosis. *Front. Microbiol.* 2017, 08. https://doi.org/10.3389/fmicb.2017.00036.
- (20) Cowen, L. E.; Sanglard, D.; Howard, S. J.; Rogers, P. D.; Perlin, D. S. Mechanisms of Antifungal Drug Resistance. *Cold Spring Harb Perspect Med* **2014**, *5* (7), a019752. https://doi.org/10.1101/cshperspect.a019752.
- (21) Fisher, M. C.; Alastruey-Izquierdo, A.; Berman, J.; Bicanic, T.; Bignell, E. M.; Bowyer, P.; Bromley, M.; Brüggemann, R.; Garber, G.; Cornely, O. A.; Gurr, S. J.; Harrison, T. S.; Kuijper, E.; Rhodes, J.; Sheppard, D. C.; Warris, A.; White, P. L.; Xu, J.; Zwaan, B.; Verweij, P. E. Tackling the Emerging Threat of Antifungal Resistance to Human Health. *Nat Rev Microbiol* **2022**, *20* (9), 557–571. https://doi.org/10.1038/s41579-022-00720-1.
- (22) Perlin, D. S. Echinocandin Resistance in Candida. *Clin Infect Dis* **2015**, *61 Suppl 6* (Suppl 6), S612-617. https://doi.org/10.1093/cid/civ791.
- (23) Perlin, D. S. Mechanisms of Echinocandin Antifungal Drug Resistance. *Ann N Y Acad Sci* **2015**, *1354* (1), 1–11. https://doi.org/10.1111/nyas.12831.
- (24) Hossain, C. M.; Ryan, L. K.; Gera, M.; Choudhuri, S.; Lyle, N.; Ali, K. A.; Diamond, G. Antifungals and Drug Resistance. *Encyclopedia* **2022**, 2 (4), 1722–1737. https://doi.org/10.3390/encyclopedia2040118.
- (25) Moran, M.; Guzman, J.; Ropars, A.-L.; McDonald, A.; Jameson, N.; Omune, B.; Ryan, S.; Wu, L. Neglected Disease Research and Development: How Much Are We Really Spending? *PLoS Med* **2009**, *6* (2), e1000030. https://doi.org/10.1371/journal.pmed.1000030.
- (26) Hassan, Y.; Chew, S. Y.; Than, L. T. L. Candida Glabrata: Pathogenicity and Resistance Mechanisms for Adaptation and Survival. *Journal of Fungi.* 2021. https://doi.org/10.3390/jof7080667.

- (27) Kumar, K.; Askari, F.; Sahu, M. S.; Kaur, R. Candida Glabrata: A Lot More Than Meets the Eye. *Microorganisms* **2019**, *7* (2), 39. https://doi.org/10.3390/microorganisms7020039.
- (28) de Groot, P. W. J.; Bader, O.; de Boer, A. D.; Weig, M.; Chauhan, N. Adhesins in Human Fungal Pathogens: Glue with Plenty of Stick. *Eukaryot Cell* **2013**, *12* (4), 470–481. https://doi.org/10.1128/EC.00364-12.
- (29) Rodrigues, C. F.; Silva, S.; Henriques, M. Candida Glabrata: A Review of Its Features and Resistance. *Eur J Clin Microbiol Infect Dis* **2014**, *33* (5), 673–688. https://doi.org/10.1007/s10096-013-2009-3.
- (30) Reithofer, V.; Fernández-Pereira, J.; Alvarado, M.; de Groot, P.; Essen, L.-O. A Novel Class of Candida Glabrata Cell Wall Proteins with β-Helix Fold Mediates Adhesion in Clinical Isolates. *PLoS Pathog* 2021, 17 (12), e1009980. https://doi.org/10.1371/journal.ppat.1009980.
- (31) Seider, K.; Brunke, S.; Schild, L.; Jablonowski, N.; Wilson, D.; Majer, O.; Barz, D.; Haas, A.; Kuchler, K.; Schaller, M.; Hube, B. The Facultative Intracellular Pathogen Candida Glabrata Subverts Macrophage Cytokine Production and Phagolysosome Maturation. *J Immunol* **2011**, *187* (6), 3072–3086. https://doi.org/10.4049/jimmunol.1003730.
- (32) Galocha, M.; Pais, P.; Cavalheiro, M.; Pereira, D.; Viana, R.; Teixeira, M. C. Divergent Approaches to Virulence in C. Albicans and C. Glabrata: Two Sides of the Same Coin. *IJMS* **2019**, *20* (9), 2345. https://doi.org/10.3390/ijms20092345.
- (33) Csank, C.; Haynes, K. Candida Glabrata Displays Pseudohyphal Growth. *FEMS Microbiol Lett* **2000**, *189* (1), 115–120. https://doi.org/10.1111/j.1574-6968.2000.tb09216.x.
- (34) Rasheed, M.; Battu, A.; Kaur, R. Host-Pathogen Interaction in Candida Glabrata Infection: Current Knowledge and Implications for Antifungal Therapy. *Expert Rev Anti Infect Ther* **2020**, *18* (11), 1093–1103. https://doi.org/10.1080/14787210.2020.1792773.
- (35) Pristov, K. E.; Ghannoum, M. A. Resistance of Candida to Azoles and Echinocandins Worldwide. *Clin Microbiol Infect* **2019**, 25 (7), 792–798. https://doi.org/10.1016/j.cmi.2019.03.028.
- (36) Johnson, E. S. Protein Modification by SUMO. *Annu Rev Biochem* **2004**, *73*, 355–382. https://doi.org/10.1146/annurev.biochem.73.011303.074118.
- (37) Wang, Y.; Dasso, M. SUMOylation and deSUMOylation at a Glance. *Journal of Cell Science* **2009**, *122* (23), 4249–4252. https://doi.org/10.1242/jcs.050542.

- (38) Johnson, E. S. The Ubiquitin-like Protein Smt3p Is Activated for Conjugation to Other Proteins by an Aos1p/Uba2p Heterodimer. *The EMBO Journal* **1997**, *16* (18), 5509–5519. https://doi.org/10.1093/emboj/16.18.5509.
- (39) Lois, L. M.; Lima, C. D. Structures of the SUMO E1 Provide Mechanistic Insights into SUMO Activation and E2 Recruitment to E1. *EMBO J* **2005**, 24 (3), 439–451. https://doi.org/10.1038/sj.emboj.7600552.
- (40) Hay, R. T. SUMO: A History of Modification. *Mol Cell* **2005**, *18* (1), 1–12. https://doi.org/10.1016/j.molcel.2005.03.012.
- (41) Sahu, M. S.; Patra, S.; Kumar, K.; Kaur, R. SUMOylation in Human Pathogenic Fungi: Role in Physiology and Virulence. *J Fungi (Basel)* **2020**, *6* (1), 32. https://doi.org/10.3390/jof6010032.
- (42) Gareau, J. R.; Lima, C. D. The SUMO Pathway: Emerging Mechanisms That Shape Specificity, Conjugation and Recognition. *Nat Rev Mol Cell Biol* **2010**, *11* (12), 861–871. https://doi.org/10.1038/nrm3011.
- (43) Dieckhoff, P.; Bolte, M.; Sancak, Y.; Braus, G. H.; Irniger, S. Smt3/SUMO and Ubc9 Are Required for Efficient APC/C-Mediated Proteolysis in Budding Yeast. *Mol Microbiol* 2004, 51 (5), 1375–1387. https://doi.org/10.1046/j.1365-2958.2003.03910.x.
- (44) Johnson, E. S.; Blobel, G. Ubc9p Is the Conjugating Enzyme for the Ubiquitin-like Protein Smt3p. *Journal of Biological Chemistry* **1997**, 272 (43), 26799–26802. https://doi.org/10.1074/jbc.272.43.26799.
- (45) Johnson, E. S.; Gupta, A. A. An E3-like Factor That Promotes SUMO Conjugation to the Yeast Septins. *Cell* **2001**, *106* (6), 735–744. https://doi.org/10.1016/S0092-8674(01)00491-3.
- (46) Kagey, M. H.; Melhuish, T. A.; Wotton, D. The Polycomb Protein Pc2 Is a SUMO E3. *Cell* **2003**, *113* (1), 127–137. https://doi.org/10.1016/S0092-8674(03)00159-4.
- (47) Kahyo, T.; Nishida, T.; Yasuda, H. Involvement of PIAS1 in the Sumoylation of Tumor Suppressor P53. *Molecular Cell* **2001**, 8 (3), 713–718. https://doi.org/10.1016/S1097-2765(01)00349-5.
- (48) Pichler, A.; Gast, A.; Seeler, J. S.; Dejean, A.; Melchior, F. The Nucleoporin RanBP2 Has SUMO1 E3 Ligase Activity. *Cell* **2002**, *108* (1), 109–120. https://doi.org/10.1016/S0092-8674(01)00633-X.

- (49) Geiss-Friedlander, R.; Melchior, F. Concepts in Sumoylation: A Decade On. *Nat Rev Mol Cell Biol* **2007**, *8* (12), 947–956. https://doi.org/10.1038/nrm2293.
- (50) Gasser, S. M.; Stutz, F. SUMO in the Regulation of DNA Repair and Transcription at Nuclear Pores. FEBS Letters 2023, 597 (22), 2833–2850. https://doi.org/10.1002/1873-3468.14751.
- (51) Hannan, A.; Abraham, N. M.; Goyal, S.; Jamir, I.; Priyakumar, U. D.; Mishra, K. Sumoylation of Sir2 Differentially Regulates Transcriptional Silencing in Yeast. *Nucleic Acids Res* **2015**, gkv842. https://doi.org/10.1093/nar/gkv842.
- (52) Newman, H. A.; Meluh, P. B.; Lu, J.; Vidal, J.; Carson, C.; Lagesse, E.; Gray, J. J.; Boeke, J. D.; Matunis, M. J. A High Throughput Mutagenic Analysis of Yeast Sumo Structure and Function. *PLoS Genet* 2017, 13 (2), e1006612. https://doi.org/10.1371/journal.pgen.1006612.
- (53) Eckhoff, J.; Dohmen, R. J. In Vitro Studies Reveal a Sequential Mode of Chain Processing by the Yeast SUMO (Small Ubiquitin-Related Modifier)-Specific Protease Ulp2. *J Biol Chem* **2015**, 290 (19), 12268–12281. https://doi.org/10.1074/jbc.M114.622217.
- (54) Jansen, N. S.; Vertegaal, A. C. O. A Chain of Events: Regulating Target Proteins by SUMO Polymers. *Trends in Biochemical Sciences* **2021**, *46* (2), 113–123. https://doi.org/10.1016/j.tibs.2020.09.002.
- (55) Yang, M.; Hsu, C.-T.; Ting, C.-Y.; Liu, L. F.; Hwang, J. Assembly of a Polymeric Chain of SUMO1 on Human Topoisomerase I in Vitro. *Journal of Biological Chemistry* **2006**, *281* (12), 8264–8274. https://doi.org/10.1074/jbc.M510364200.
- (56) Wang, W.; Matunis, M. J. Paralogue-Specific Roles of SUMO1 and SUMO2/3 in Protein Quality Control and Associated Diseases. *Cells* **2023**, *13* (1), 8. https://doi.org/10.3390/cells13010008.
- (57) Boulanger, M.; Chakraborty, M.; Tempé, D.; Piechaczyk, M.; Bossis, G. SUMO and Transcriptional Regulation: The Lessons of Large-Scale Proteomic, Modifomic and Genomic Studies. *Molecules* **2021**, *26* (4), 828. https://doi.org/10.3390/molecules26040828.
- (58) Flotho, A.; Melchior, F. Sumoylation: A Regulatory Protein Modification in Health and Disease. *Annu. Rev. Biochem.* **2013**, 82 (1), 357–385. https://doi.org/10.1146/annurev-biochem-061909-093311.

- (59) Zhao, Q.; Ma, Y.; Li, Z.; Zhang, K.; Zheng, M.; Zhang, S. The Function of SUMOylation and Its Role in the Development of Cancer Cells under Stress Conditions: A Systematic Review. *Stem Cells Int* **2020**, *2020*, 8835714. https://doi.org/10.1155/2020/8835714.
- (60) Liu, C.; Li, Z.; Xing, J.; Yang, J.; Wang, Z.; Zhang, H.; Chen, D.; Peng, Y.-L.; Chen, X.-L. Global Analysis of Sumoylation Function Reveals Novel Insights into Development and Appressorium-Mediated Infection of the Rice Blast Fungus. *New Phytol* **2018**, *219* (3), 1031–1047. https://doi.org/10.1111/nph.15141.
- (61) Eifler, K.; Vertegaal, A. C. O. SUMOylation-Mediated Regulation of Cell Cycle Progression and Cancer. *Trends Biochem Sci* **2015**, *40* (12), 779–793. https://doi.org/10.1016/j.tibs.2015.09.006.
- (62) Galanty, Y.; Belotserkovskaya, R.; Coates, J.; Jackson, S. P. RNF4, a SUMO-Targeted Ubiquitin E3 Ligase, Promotes DNA Double-Strand Break Repair. *Genes Dev* **2012**, *26* (11), 1179–1195. https://doi.org/10.1101/gad.188284.112.
- (63) Tatham, M. H.; Geoffroy, M.-C.; Shen, L.; Plechanovova, A.; Hattersley, N.; Jaffray, E. G.; Palvimo, J. J.; Hay, R. T. RNF4 Is a Poly-SUMO-Specific E3 Ubiquitin Ligase Required for Arsenic-Induced PML Degradation. *Nat Cell Biol* 2008, 10 (5), 538–546. https://doi.org/10.1038/ncb1716.
- (64) Rodriguez, M. S.; Dargemont, C.; Hay, R. T. SUMO-1 Conjugation in Vivo Requires Both a Consensus Modification Motif and Nuclear Targeting. *Journal of Biological Chemistry* **2001**, *276* (16), 12654–12659. https://doi.org/10.1074/jbc.M009476200.
- (65) Sapetschnig, A.; Rischitor, G.; Braun, H.; Doll, A.; Schergaut, M.; Melchior, F.; Suske, G. Transcription Factor Sp3 Is Silenced through SUMO Modification by PIAS1. *EMBO J* **2002**, *21* (19), 5206–5215. https://doi.org/10.1093/emboj/cdf510.
- (66) Bernier-Villamor, V.; Sampson, D. A.; Matunis, M. J.; Lima, C. D. Structural Basis for E2-Mediated SUMO Conjugation Revealed by a Complex between Ubiquitin-Conjugating Enzyme Ubc9 and RanGAP1. *Cell* **2002**, *108* (3), 345–356. https://doi.org/10.1016/S0092-8674(02)00630-X.
- (67) Lin, D.; Tatham, M. H.; Yu, B.; Kim, S.; Hay, R. T.; Chen, Y. Identification of a Substrate Recognition Site on Ubc9. *J Biol Chem* 2002, 277 (24), 21740–21748. https://doi.org/10.1074/jbc.M108418200.

- (68) Reverter, D.; Lima, C. D. Insights into E3 Ligase Activity Revealed by a SUMO-RanGAP1-Ubc9-Nup358 Complex. *Nature* **2005**, *435* (7042), 687–692. https://doi.org/10.1038/nature03588.
- (69) Pichler, A.; Knipscheer, P.; Oberhofer, E.; van Dijk, W. J.; Körner, R.; Olsen, J. V.; Jentsch, S.; Melchior, F.; Sixma, T. K. SUMO Modification of the Ubiquitin-Conjugating Enzyme E2-25K. *Nat Struct Mol Biol* **2005**, *12* (3), 264–269. https://doi.org/10.1038/nsmb903.
- (70) Yang, S.-H.; Galanis, A.; Witty, J.; Sharrocks, A. D. An Extended Consensus Motif Enhances the Specificity of Substrate Modification by SUMO. *EMBO J* **2006**, *25* (21), 5083–5093. https://doi.org/10.1038/sj.emboj.7601383.
- (71) Mohideen, F.; Capili, A. D.; Bilimoria, P. M.; Yamada, T.; Bonni, A.; Lima, C. D. A Molecular Basis for Phosphorylation-Dependent SUMO Conjugation by the E2 UBC9. *Nat Struct Mol Biol* **2009**, *16* (9), 945–952. https://doi.org/10.1038/nsmb.1648.
- (72) Hietakangas, V.; Anckar, J.; Blomster, H. A.; Fujimoto, M.; Palvimo, J. J.; Nakai, A.; Sistonen, L. PDSM, a Motif for Phosphorylation-Dependent SUMO Modification. *Proc Natl Acad Sci U S A* **2006**, *103* (1), 45–50. https://doi.org/10.1073/pnas.0503698102.
- (73) Matic, I.; Schimmel, J.; Hendriks, I. A.; Van Santen, M. A.; Van De Rijke, F.; Van Dam, H.; Gnad, F.; Mann, M.; Vertegaal, A. C. O. Site-Specific Identification of SUMO-2 Targets in Cells Reveals an Inverted SUMOylation Motif and a Hydrophobic Cluster SUMOylation Motif. *Molecular Cell* 2010, 39 (4), 641–652. https://doi.org/10.1016/j.molcel.2010.07.026.
- (74) Minty, A.; Dumont, X.; Kaghad, M.; Caput, D. Covalent Modification of P73α by SUMO 1. Journal of Biological Chemistry 2000, 275 (46), 36316–36323.
 https://doi.org/10.1074/jbc.M004293200.
- (75) Hecker, C.-M.; Rabiller, M.; Haglund, K.; Bayer, P.; Dikic, I. Specification of SUMO1-and SUMO2-Interacting Motifs. *J Biol Chem* **2006**, *281* (23), 16117–16127. https://doi.org/10.1074/jbc.M512757200.
- (76) Kerscher, O. SUMO Junction-What's Your Function? New Insights through SUMO-Interacting Motifs. *EMBO Rep* **2007**, 8 (6), 550–555. https://doi.org/10.1038/sj.embor.7400980.

- (77) Meulmeester, E.; Kunze, M.; Hsiao, H. H.; Urlaub, H.; Melchior, F. Mechanism and Consequences for Paralog-Specific Sumoylation of Ubiquitin-Specific Protease 25. *Molecular Cell* **2008**, *30* (5), 610–619. https://doi.org/10.1016/j.molcel.2008.03.021.
- (78) Praefcke, G. J. K.; Hofmann, K.; Dohmen, R. J. SUMO Playing Tag with Ubiquitin. *Trends Biochem Sci* **2012**, *37* (1), 23–31. https://doi.org/10.1016/j.tibs.2011.09.002.
- (79) Sriramachandran, A. M.; Dohmen, R. J. SUMO-Targeted Ubiquitin Ligases. *Biochim Biophys Acta* **2014**, *1843* (1), 75–85. https://doi.org/10.1016/j.bbamcr.2013.08.022.
- (80) Grabbe, C.; Dikic, I. Functional Roles of Ubiquitin-like Domain (ULD) and Ubiquitin-Binding Domain (UBD) Containing Proteins. *Chem Rev* **2009**, *109* (4), 1481–1494. https://doi.org/10.1021/cr800413p.
- (81) Li, S. J.; Hochstrasser, M. The Yeast ULP2 (SMT4) Gene Encodes a Novel Protease Specific for the Ubiquitin-like Smt3 Protein. *Mol Cell Biol* **2000**, *20* (7), 2367–2377. https://doi.org/10.1128/MCB.20.7.2367-2377.2000.
- (82) Bylebyl, G. R.; Belichenko, I.; Johnson, E. S. The SUMO Isopeptidase Ulp2 Prevents Accumulation of SUMO Chains in Yeast. *J Biol Chem* **2003**, 278 (45), 44113–44120. https://doi.org/10.1074/jbc.M308357200.
- (83) Mukhopadhyay, D.; Dasso, M. Modification in Reverse: The SUMO Proteases. *Trends Biochem Sci* **2007**, *32* (6), 286–295. https://doi.org/10.1016/j.tibs.2007.05.002.
- (84) Yeh, E. T. H. SUMOylation and De-SUMOylation: Wrestling with Life's Processes. *J Biol Chem* **2009**, 284 (13), 8223–8227. https://doi.org/10.1074/jbc.R800050200.
- (85) Shin, E. J.; Shin, H. M.; Nam, E.; Kim, W. S.; Kim, J.-H.; Oh, B.-H.; Yun, Y. DeSUMOylating Isopeptidase: A Second Class of SUMO Protease. *EMBO Rep* **2012**, *13* (4), 339–346. https://doi.org/10.1038/embor.2012.3.
- (86) Bailey, D.; O'Hare, P. Characterization of the Localization and Proteolytic Activity of the SUMO-Specific Protease, SENP1. *J Biol Chem* **2004**, 279 (1), 692–703. https://doi.org/10.1074/jbc.M306195200.
- (87) Castro, P. H.; Couto, D.; Freitas, S.; Verde, N.; Macho, A. P.; Huguet, S.; Botella, M. A.; Ruiz-Albert, J.; Tavares, R. M.; Bejarano, E. R.; Azevedo, H. SUMO Proteases ULP1c and ULP1d Are Required for Development and Osmotic Stress Responses in Arabidopsis Thaliana. *Plant Mol Biol* **2016**, *92* (1–2), 143–159. https://doi.org/10.1007/s11103-016-0500-9.

- (88) Kong, X.; Luo, X.; Qu, G.-P.; Liu, P.; Jin, J. B. Arabidopsis SUMO Protease ASP1 Positively Regulates Flowering Time Partially through Regulating FLC Stability. *J Integr Plant Biol* **2017**, *59* (1), 15–29. https://doi.org/10.1111/jipb.12509.
- (89) Park, H. J.; Kim, W.-Y.; Park, H. C.; Lee, S. Y.; Bohnert, H. J.; Yun, D.-J. SUMO and SUMOylation in Plants. *Mol Cells* **2011**, *32* (4), 305–316. https://doi.org/10.1007/s10059-011-0122-7.
- (90) Gujjula, R.; Veeraiah, S.; Kumar, K.; Thakur, S. S.; Mishra, K.; Kaur, R. Identification of Components of the SUMOylation Machinery in Candida Glabrata. *Journal of Biological Chemistry* **2016**, *291* (37). https://doi.org/10.1074/jbc.M115.706044.
- (91) Leach, M. D.; Stead, D. A.; Argo, E.; Brown, A. J. P. Identification of Sumoylation Targets, Combined with Inactivation of SMT3, Reveals the Impact of Sumoylation upon Growth, Morphology, and Stress Resistance in the Pathogen Candida Albicans. *Mol Biol Cell* **2011**, 22 (5), 687–702. https://doi.org/10.1091/mbc.E10-07-0632.
- (92) Islam, A.; Tebbji, F.; Mallick, J.; Regan, H.; Dumeaux, V.; Omran, R. P.; Whiteway, M. Mms21: A Putative SUMO E3 Ligase in Candida Albicans That Negatively Regulates Invasiveness and Filamentation, and Is Required for the Genotoxic and Cellular Stress Response. *Genetics* 2019, 211 (2), 579–595. https://doi.org/10.1534/genetics.118.301769.
- (93) Tunnicliffe, G.; Schomberg, L.; Walsh, S.; Tinwell, B.; Harrison, T.; Chua, F. Airway and Parenchymal Manifestations of Pulmonary Aspergillosis. *Respir Med* **2013**, *107* (8), 1113–1123. https://doi.org/10.1016/j.rmed.2013.03.016.
- (94) Nie, X.; Yu, S.; Qiu, M.; Wang, X.; Wang, Y.; Bai, Y.; Zhang, F.; Wang, S. Aspergillus Flavus SUMO Contributes to Fungal Virulence and Toxin Attributes. *J Agric Food Chem* **2016**, *64* (35), 6772–6782. https://doi.org/10.1021/acs.jafc.6b02199.
- (95) Bratton, E. W.; El Husseini, N.; Chastain, C. A.; Lee, M. S.; Poole, C.; Stürmer, T.; Juliano, J. J.; Weber, D. J.; Perfect, J. R. Comparison and Temporal Trends of Three Groups with Cryptococcosis: HIV-Infected, Solid Organ Transplant, and HIV-Negative/Non-Transplant. *PLoS One* 2012, 7 (8), e43582. https://doi.org/10.1371/journal.pone.0043582.
- (96) Perfect, J. R.; Dismukes, W. E.; Dromer, F.; Goldman, D. L.; Graybill, J. R.; Hamill, R. J.; Harrison, T. S.; Larsen, R. A.; Lortholary, O.; Nguyen, M.-H.; Pappas, P. G.; Powderly, W. G.; Singh, N.; Sobel, J. D.; Sorrell, T. C. Clinical Practice Guidelines for the Management

- of Cryptococcal Disease: 2010 Update by the Infectious Diseases Society of America. *Clinical Infectious Diseases* **2010**, *50* (3), 291–322. https://doi.org/10.1086/649858.
- (97) Mayer, F. L.; Sánchez-León, E.; Kronstad, J. W. A Chemical Genetic Screen Reveals a Role for Proteostasis in Capsule and Biofilm Formation by Cryptococcus Neoformans. *Microb Cell* **2018**, *5* (11), 495–510. https://doi.org/10.15698/mic2018.11.656.
- (98) Harting, R.; Bayram, O.; Laubinger, K.; Valerius, O.; Braus, G. H. Interplay of the Fungal Sumoylation Network for Control of Multicellular Development. *Mol Microbiol* **2013**, *90* (5), 1125–1145. https://doi.org/10.1111/mmi.12421.
- (99) Horio, T.; Szewczyk, E.; Oakley, C. E.; Osmani, A. H.; Osmani, S. A.; Oakley, B. R. SUMOlock Reveals a More Complete Aspergillus Nidulans SUMOylome. *Fungal Genet Biol* **2019**, *127*, 50–59. https://doi.org/10.1016/j.fgb.2019.03.002.
- (100) Wong, K. H.; Todd, R. B.; Oakley, B. R.; Oakley, C. E.; Hynes, M. J.; Davis, M. A. Sumoylation in Aspergillus Nidulans: sumO Inactivation, Overexpression and Live-Cell Imaging. *Fungal Genet Biol* **2008**, *45* (5), 728–737. https://doi.org/10.1016/j.fgb.2007.12.009.
- (101) Kim, S.; Park, S.-Y.; Kim, K. S.; Rho, H.-S.; Chi, M.-H.; Choi, J.; Park, J.; Kong, S.; Park, J.; Goh, J.; Lee, Y.-H. Homeobox Transcription Factors Are Required for Conidiation and Appressorium Development in the Rice Blast Fungus Magnaporthe Oryzae. *PLoS Genet* 2009, 5 (12), e1000757. https://doi.org/10.1371/journal.pgen.1000757.
- (102) Weisshaar, S. R.; Keusekotten, K.; Krause, A.; Horst, C.; Springer, H. M.; Göttsche, K.; Dohmen, R. J.; Praefcke, G. J. K. Arsenic Trioxide Stimulates SUMO-2/3 Modification Leading to RNF4-Dependent Proteolytic Targeting of PML. *FEBS Lett* 2008, 582 (21–22), 3174–3178. https://doi.org/10.1016/j.febslet.2008.08.008.
- (103) Sun, H.; Leverson, J. D.; Hunter, T. Conserved Function of RNF4 Family Proteins in Eukaryotes: Targeting a Ubiquitin Ligase to SUMOylated Proteins. *EMBO J* **2007**, *26* (18), 4102–4112. https://doi.org/10.1038/sj.emboj.7601839.
- (104) Prudden, J.; Pebernard, S.; Raffa, G.; Slavin, D. A.; Perry, J. J. P.; Tainer, J. A.; McGowan, C. H.; Boddy, M. N. SUMO-Targeted Ubiquitin Ligases in Genome Stability. EMBO J 2007, 26 (18), 4089–4101. https://doi.org/10.1038/sj.emboj.7601838.

- (105) Xie, Y.; Kerscher, O.; Kroetz, M. B.; McConchie, H. F.; Sung, P.; Hochstrasser, M. The Yeast Hex3.Slx8 Heterodimer Is a Ubiquitin Ligase Stimulated by Substrate Sumoylation. *J Biol Chem* **2007**, 282 (47), 34176–34184. https://doi.org/10.1074/jbc.M706025200.
- (106) Køhler, J. B.; Tammsalu, T.; Jørgensen, M. M.; Steen, N.; Hay, R. T.; Thon, G. Targeting of SUMO Substrates to a Cdc48-Ufd1-Npl4 Segregase and STUbL Pathway in Fission Yeast. *Nat Commun* **2015**, *6*, 8827. https://doi.org/10.1038/ncomms9827.
- (107) Westerbeck, J. W.; Pasupala, N.; Guillotte, M.; Szymanski, E.; Matson, B. C.; Esteban, C.; Kerscher, O. A SUMO-Targeted Ubiquitin Ligase Is Involved in the Degradation of the Nuclear Pool of the SUMO E3 Ligase Siz1. *Mol Biol Cell* 2014, 25 (1), 1–16. https://doi.org/10.1091/mbc.E13-05-0291.
- (108) Borden, K. L.; Boddy, M. N.; Lally, J.; O'Reilly, N. J.; Martin, S.; Howe, K.; Solomon, E.; Freemont, P. S. The Solution Structure of the RING Finger Domain from the Acute Promyelocytic Leukaemia Proto-Oncoprotein PML. *EMBO J* 1995, 14 (7), 1532–1541. https://doi.org/10.1002/j.1460-2075.1995.tb07139.x.
- (109) Saurin, A. J.; Borden, K. L.; Boddy, M. N.; Freemont, P. S. Does This Have a Familiar RING? *Trends Biochem Sci* **1996**, *21* (6), 208–214.
- (110) Hannich, J. T.; Lewis, A.; Kroetz, M. B.; Li, S.-J.; Heide, H.; Emili, A.; Hochstrasser, M. Defining the SUMO-Modified Proteome by Multiple Approaches in Saccharomyces Cerevisiae. *J Biol Chem* **2005**, 280 (6), 4102–4110. https://doi.org/10.1074/jbc.M413209200.
- (111) Uzunova, K.; Göttsche, K.; Miteva, M.; Weisshaar, S. R.; Glanemann, C.; Schnellhardt, M.; Niessen, M.; Scheel, H.; Hofmann, K.; Johnson, E. S.; Praefcke, G. J. K.; Dohmen, R. J. Ubiquitin-Dependent Proteolytic Control of SUMO Conjugates. *J Biol Chem* 2007, 282 (47), 34167–34175. https://doi.org/10.1074/jbc.M706505200.
- (112) Lallemand-Breitenbach, V.; Jeanne, M.; Benhenda, S.; Nasr, R.; Lei, M.; Peres, L.; Zhou, J.; Zhu, J.; Raught, B.; de Thé, H. Arsenic Degrades PML or PML-RARalpha through a SUMO-Triggered RNF4/Ubiquitin-Mediated Pathway. *Nat Cell Biol* 2008, 10 (5), 547–555. https://doi.org/10.1038/ncb1717.
- (113) Wang, Z.; Jones, G. M.; Prelich, G. Genetic Analysis Connects SLX5 and SLX8 to the SUMO Pathway in Saccharomyces Cerevisiae. *Genetics* **2006**, *172* (3), 1499–1509. https://doi.org/10.1534/genetics.105.052811.

- (114) Perry, J. J. P.; Tainer, J. A.; Boddy, M. N. A SIM-Ultaneous Role for SUMO and Ubiquitin. *Trends Biochem Sci* **2008**, *33* (5), 201–208. https://doi.org/10.1016/j.tibs.2008.02.001.
- (115) Pero, R.; Lembo, F.; Di Vizio, D.; Boccia, A.; Chieffi, P.; Fedele, M.; Pierantoni, G. M.; Rossi, P.; Iuliano, R.; Santoro, M.; Viglietto, G.; Bruni, C. B.; Fusco, A.; Chiariotti, L. RNF4 Is a Growth Inhibitor Expressed in Germ Cells but Not in Human Testicular Tumors. *Am J Pathol* **2001**, *159* (4), 1225–1230. https://doi.org/10.1016/S0002-9440(10)62508-4.
- (116) Gupta, D.; Garapati, H. S.; Kakumanu, A. V. S.; Shukla, R.; Mishra, K. SUMOylation in Fungi: A Potential Target for Intervention. *Comput Struct Biotechnol J* **2020**, *18*, 3484–3493. https://doi.org/10.1016/j.csbj.2020.10.037.
- (117) Sambrook, J.; Russell, D. W. The Inoue Method for Preparation and Transformation of Competent e. Coli: "Ultra-Competent" Cells. *CSH Protoc* **2006**, *2006* (1), pdb.prot3944. https://doi.org/10.1101/pdb.prot3944.
- (118) Da Silva-Ferrada, E.; Xolalpa, W.; Lang, V.; Aillet, F.; Martin-Ruiz, I.; de la Cruz-Herrera, C. F.; Lopitz-Otsoa, F.; Carracedo, A.; Goldenberg, S. J.; Rivas, C.; England, P.; Rodríguez, M. S. Analysis of SUMOylated Proteins Using SUMO-Traps. *Sci Rep* **2013**, *3*, 1690. https://doi.org/10.1038/srep01690.
- (119) Volkamer, A.; Kuhn, D.; Rippmann, F.; Rarey, M. DoGSiteScorer: A Web Server for Automatic Binding Site Prediction, Analysis and Druggability Assessment. *Bioinformatics* 2012, 28 (15), 2074–2075. https://doi.org/10.1093/bioinformatics/bts310.
- (120) Dixon, S. L.; Smondyrev, A. M.; Rao, S. N. PHASE: A Novel Approach to Pharmacophore Modeling and 3D Database Searching. *Chem Biol Drug Des* **2006**, *67* (5), 370–372. https://doi.org/10.1111/j.1747-0285.2006.00384.x.
- (121) Sunseri, J.; Koes, D. R. Pharmit: Interactive Exploration of Chemical Space. *Nucleic Acids Res* **2016**, *44* (W1), W442-448. https://doi.org/10.1093/nar/gkw287.
- (122) M., J.; Archontis, G. MM-GB(PB)SA Calculations of Protein-Ligand Binding Free Energies. In *Molecular Dynamics Studies of Synthetic and Biological Macromolecules*; Wang, L., Ed.; InTech, 2012. https://doi.org/10.5772/37107.
- (123) Xie, Y.; Rubenstein, E. M.; Matt, T.; Hochstrasser, M. SUMO-Independent in Vivo Activity of a SUMO-Targeted Ubiquitin Ligase toward a Short-Lived Transcription Factor. *Genes Dev.* **2010**, *24* (9), 893–903. https://doi.org/10.1101/gad.1906510.

- (124) Nagai, S.; Dubrana, K.; Tsai-Pflugfelder, M.; Davidson, M. B.; Roberts, T. M.; Brown, G. W.; Varela, E.; Hediger, F.; Gasser, S. M.; Krogan, N. J. Functional Targeting of DNA Damage to a Nuclear Pore-Associated SUMO-Dependent Ubiquitin Ligase. *Science* 2008, 322 (5901), 597–602. https://doi.org/10.1126/science.1162790.
- (125) Tan, W.; Wang, Z.; Prelich, G. Physical and Genetic Interactions Between Uls1 and the Slx5–Slx8 SUMO-Targeted Ubiquitin Ligase. *G3 Genes/Genomes/Genetics* **2013**, *3* (4), 771–780. https://doi.org/10.1534/g3.113.005827.
- (126) Keiten-Schmitz, J.; Wagner, K.; Piller, T.; Kaulich, M.; Alberti, S.; Müller, S. The Nuclear SUMO-Targeted Ubiquitin Quality Control Network Regulates the Dynamics of Cytoplasmic Stress Granules. *Molecular Cell* **2020**, 79 (1), 54-67.e7. https://doi.org/10.1016/j.molcel.2020.05.017.
- (127) Altschul, S. F.; Gish, W.; Miller, W.; Myers, E. W.; Lipman, D. J. Basic Local Alignment Search Tool. *Journal of Molecular Biology* **1990**, *215* (3), 403–410. https://doi.org/10.1016/S0022-2836(05)80360-2.
- (128) Cao, C.; Cao, Z.; Yu, P.; Zhao, Y. Genome-Wide Identification for Genes Involved in Sodium Dodecyl Sulfate Toxicity in Saccharomyces Cerevisiae. *BMC Microbiol* **2020**, *20* (1), 34. https://doi.org/10.1186/s12866-020-1721-2.
- (129) Harriott, M. M.; Lilly, E. A.; Rodriguez, T. E.; Fidel, P. L.; Noverr, M. C. Candida Albicans Forms Biofilms on the Vaginal Mucosa. *Microbiology (Reading)* **2010**, *156* (Pt 12), 3635–3644. https://doi.org/10.1099/mic.0.039354-0.
- (130) Tanaka, K. The Proteasome: Overview of Structure and Functions. *Proc. Jpn. Acad., Ser. B* **2009**, *85* (1), 12–36. https://doi.org/10.2183/pjab.85.12.
- (131) Chandel, N. S. Nucleotide Metabolism. *Cold Spring Harb Perspect Biol* **2021**, *13* (7), a040592. https://doi.org/10.1101/cshperspect.a040592.
- (132) Pedley, A. M.; Benkovic, S. J. A New View into the Regulation of Purine Metabolism: The Purinosome. *Trends in Biochemical Sciences* **2017**, *42* (2), 141–154. https://doi.org/10.1016/j.tibs.2016.09.009.
- (133) De Albuquerque, C. P.; Suhandynata, R. T.; Carlson, C. R.; Yuan, W.-T.; Zhou, H. Binding to Small Ubiquitin-like Modifier and the Nucleolar Protein Csm1 Regulates Substrate Specificity of the Ulp2 Protease. *Journal of Biological Chemistry* **2018**, *293* (31), 12105–12119. https://doi.org/10.1074/jbc.RA118.003022.

(134) Bongomin, F.; Gago, S.; Oladele, R.; Denning, D. Global and Multi-National Prevalence of Fungal Diseases—Estimate Precision. *JoF* **2017**, *3* (4), 57. https://doi.org/10.3390/jof3040057.

SUMO-mediated protein homeostasis in Candida glabrata

by Dipika Gupta

Librarian

Indira Gandhi Memorial Library UNIVERSITY OF HYDERABAD

Central University P.O. HYDERABAD-500 046.

Submission date: 08-Apr-2024 03:50PM (UTC+0530)

Submission ID: 2343380174

File name: Dipika_Gupta.docx (557.27K)

Word count: 24256 Character count: 135925 The similarity of over 5% comes from Dipika's published paper in CSJB. The student paper is the report on this work submitted to the funding agency and was plagiarism checked as an assignment and hence was stored in database, the rest are terms used in methods, scientific description of the phenomenon etc that do not have alternate phrases.

SUMO-mediated protein homeostasis in Candida glabrata Kishnavei Mhra Prof. KRISHNAVENI MISHRA ORIGINALITY REPORT Department of Biochemistry School of Life Sciences University of Hyderabad Hyderabad-500046. (TS), INDIA 17% SIMILARITY INDEX INTERNET SOURCES STUDENT PAPERS PRIMARY SOURCES www.ncbi.nlm.nih.gov Internet Source Submitted to University of Hyderabad, Hyderabad Student Paper kups.ub.uni-koeln.de Internet Source docksci.com Internet Source dspace.uohyd.ac.in Internet Source www.jbc.org Internet Source Claudio Ponte de Albuquerque, Raymond T. Suhandynata, Christopher R. Carlson, Wei-Tsung Yuan, Huilin Zhou. "Binding to small ubiquitin-like modifier and the nucleolar

protein Csm1 regulates substrate specificity

of the Ulp2 protease", Journal of Biological

Chemistry, 2018

- Dipika Gupta, Hita Sony Garapati, Kakumanu <1% 8 V.S. Akhil, Renu Shukla, Krishnaveni Mishra. "SUMOylation in fungi: a potential target for intervention", Computational and Structural Biotechnology Journal, 2020 Publication Dipika Gupta, Hita Sony Garapati, Akhil V.S. <1% Kakumanu, Renu Shukla, Krishnaveni Mishra. "SUMOylation in fungi: A potential target for intervention", Computational and Structural Biotechnology Journal, 2020 **Publication** Pankaj Kumar Madheshiya, Ekta Shukla, <1% 10 Jyotsana Singh, Shrankhla Bawaria, Mohammad Yusuf Ansari, Radha Chauhan. "Insights into the role of Nup62 and Nup93 in assembling cytoplasmic ring and central transport channel of the nuclear pore complex", Cold Spring Harbor Laboratory, 2022 **Publication** www.nature.com **Internet Source**
- Ameya D. Bendre, C. G. Suresh,
 Dhanasekaran Shanmugam, Sureshkumar
 Ramasamy. "Structural insights into the
 unique inhibitory mechanism of Kunitz type

trypsin inhibitor from . ", Journal of Biomolecular Structure and Dynamics, 2018 Publication

13	archive.org Internet Source	<1%
14	othes.univie.ac.at Internet Source	<1%
15	www.frontiersin.org Internet Source	<1%
16	ddd.uab.cat Internet Source	<1%
17	"SUMO Regulation of Cellular Processes", Springer Science and Business Media LLC, 2017 Publication	<1%
18	purehost.bath.ac.uk Internet Source	<1%
19	era.ed.ac.uk Internet Source	<1%
20	Akib Nisar, Devangi K. Ajabia, Sanskruthi B. Agrawal, Sanjana Varma, Bhushan P. Chaudhari, Rashmi S. Tupe. "Mechanistic insight into differential interactions of iron oxide nanoparticles with native, glycated albumin and their effect on erythrocytes	<1%

parameters", International Journal of Biological Macromolecules, 2022 Publication

21	Submitted to Polytechnic University of the Philippines - Sta. Mesa Student Paper	<1%
22	academic.oup.com Internet Source	<1%
23	Jiahui Zhang, Panfeng Tao, Natalie T. Deuitch, Xiaomin Yu, Ivona Askentijevich, Qing Zhou. "Proteasome-Associated Syndromes: Updates on Genetics, Clinical Manifestations, Pathogenesis, and Treatment", Journal of Clinical Immunology, 2024 Publication	<1%
24	dmg.nott.ac.uk Internet Source	<1%
25	mrc.ac.ir Internet Source	<1%
26	jcs.biologists.org Internet Source	<1%
27	openaccesspub.org Internet Source	<1%
28	Submitted to Regional Centre for Biotechnology Student Paper	<1%

29	Submitted to University of Aberdeen Student Paper	<1%
30	"Antimicrobial Drug Resistance", Springer Science and Business Media LLC, 2017 Publication	<1%
31	www.escholar.manchester.ac.uk Internet Source	<1%
32	Wai Wa Ray Chan, Wen Li, Raymond Chuen Chung Chang, Kwok-Fai Lau. "ARF6-Rac1 signaling-mediated neurite outgrowth is potentiated by the neuronal adaptor FE65 through orchestrating ARF6 and ELMO1", The FASEB Journal, 2020 Publication	<1%
33	Dipan Roy, Ari Sadanandom. "SUMO mediated regulation of transcription factors as a mechanism for transducing environmental cues into cellular signaling in plants", Cellular and Molecular Life Sciences, 2021 Publication	<1%
34	academicworks.cuny.edu Internet Source	<1%
35	edoc.ub.uni-muenchen.de Internet Source	<1%
36	www.biorxiv.org	

Internet Source

<1% Submitted to Fakultet elektrotehnike i 37 računarstva / Faculty of Electrical Engineering and Computing Student Paper cdr.lib.unc.edu <1% 38 Internet Source labtestsonline.org 39 Internet Source oparu.uni-ulm.de 40 Internet Source theses.ncl.ac.uk 41 Internet Source www.omicsdi.org 42 Internet Source Maruti Nandan Rai, Chirag Parsania, Rikky 43 Rai, Niranjan Shirgaonkar, Kaeling Tan, Koon Ho Wong. "Temporal transcriptional response of during macrophage infection reveals a multifaceted transcriptional regulator CgXbp1 important for macrophage response and drug resistance ", Cold Spring Harbor Laboratory, 2021 **Publication**

44	Internet Source	<1%
45	dspace.ncl.res.in:8080 Internet Source	<1%
46	research-repository.griffith.edu.au Internet Source	<1%
47	www.researchsquare.com Internet Source	<1%
48	123dok.net Internet Source	<1%
49	cyberleninka.org Internet Source	<1%
50	kops.uni-konstanz.de Internet Source	<1%
51	scholarshare.temple.edu Internet Source	<1%
52	www.science.gov Internet Source	<1%
53	Submitted to University of Adelaide Student Paper	<1%
54	Submitted to West Coast University Student Paper	<1%
55	archive.nnl.gov.np Internet Source	<1%

56	patents.justia.com Internet Source	<1%
57	Sitrarasu Vijaya Prabhu, Sanjeev Kumar Singh. "Atom-based 3D-QSAR, induced fit docking, and molecular dynamics simulations study of thieno[2,3-b]pyridines negative allosteric modulators of mGluR5", Journal of Receptors and Signal Transduction, 2018 Publication	<1%
58	elifesciences.org Internet Source	<1%
59	link.springer.com Internet Source	<1%
60	open.library.ubc.ca Internet Source	<1%
61	pubs.acs.org Internet Source	<1%
62	www.embopress.org Internet Source	<1%
63	Submitted to University of Central Florida Student Paper	<1%
64	Submitted to University of Stellenbosch, South Africa Student Paper	<1%
65	pdffox.com Internet Source	

Exclude quotes On Exclude bibliography On Exclude matches

< 14 words